IAEA-TECDOC-1154

Irradiation damage in graphite due to fast neutrons in fission and fusion systems

INTERNATIONAL ATOMIC ENERGY AGENCY IAEA

September 2000

The originating Section of this publication in the IAEA was:

Nuclear Power Technology Development Section
International Atomic Energy Agency
Wagramer Strasse 5
P.O. Box 100
A-1400 Vienna, Austria

IRRADIATION DAMAGE IN GRAPHITE DUE TO
FAST NEUTRONS IN FISSION AND FUSION SYSTEMS

IAEA, VIENNA, 2000
IAEA-TECDOC-1154
ISSN 1011–4289

Printed by the IAEA in Austria
September 2000

FOREWORD

Gas cooled reactors have been in operation for the production of electricity for over forty years, encompassing a total of 56 units operated in seven countries. The predominant experience has been with carbon dioxide cooled reactors (52 units), with the majority operated in the United Kingdom. In addition, four prototype helium cooled power plants were operated in the USA and Germany. The United Kingdom has no plans for further construction of carbon dioxide units, and the last helium cooled unit was shut down in 1990. However, there has been an increasing interest in modular helium cooled reactors during the 1990s as a possible future nuclear option.

Graphite is a primary material for the construction of gas cooled reactor cores, serving as a low absorption neutron moderator and providing a high temperature, high strength structure. Commercial gas cooled reactor cores (both carbon dioxide cooled and helium cooled) utilize large quantities of graphite. The structural behaviour of graphite (strength, dimensional stability, susceptibility to cracking, etc.) is a complex function of the source material, manufacturing process, chemical environment, and temperature and irradiation history.

A large body of data on graphite structural performance has accumulated from operation of commercial gas cooled reactors, beginning in the 1950s and continuing to the present. The IAEA is supporting a project to collect graphite data and archive it in a retrievable form as an International Database on Irradiated Nuclear Graphite Properties, with limited general access and more detailed access by participating Member States. Because of the large size of the database, the complexity of the phenomena and the number of variables involved, a general understanding of graphite behaviour is essential to the understanding and use of the data.

Research into the subject of radiation damage in graphite began in the early 1940s as a part of the development of nuclear weapons and nuclear power. Since that time many graphite moderated nuclear fission reactors have been built and many varieties of graphite developed. In recent years the scale of research on the effects of fission neutrons has been much reduced and many of the active researchers have retired. However, new programmes are being formulated related to the use of graphite, particularly in the form of carbon–carbon composites in fusion systems and of modular helium cooled reactors, and these developments should be assisted by the existing fission related database. It is possible to engineer the properties of graphite to a remarkable degree, and also the response to neutron irradiation. The objective of this report is to summarize the vast amount of information that has been accumulated and the understanding that has been gained for the use of those concerned with such materials in the future.

The primary contributor to the technical information contained in this report was B.T. Kelly of United Kingdom Atomic Energy Authority (UKAEA). Additional material was produced by B.J. Marsden, K. Hall, D.G. Martin, A. Harper and A. Blanchard, also of the UKAEA. B.J. Marsden was also responsible for assembling the total report. The IAEA officer responsible for this publication was J. Kendall of the Division of Nuclear Power.

EDITORIAL NOTE

The use of particular designations of countries or territories does not imply any judgement by the publisher, the IAEA, as to the legal status of such countries or territories, of their authorities and institutions or of the delimitation of their boundaries.

The mention of names of specific companies or products (whether or not indicated as registered) does not imply any intention to infringe proprietary rights, nor should it be construed as an endorsement or recommendation on the part of the IAEA.

CONTENTS

CHAPTER 1

FUNDAMENTALS OF RADIATION DAMAGE IN GRAPHITE DUE TO ENERGETIC NEUTRONS

Study of the basic processes which produce the property and dimensional changes known as radiation damage due to energetic neutrons is necessary for two distinct reasons:

(i) The number and distribution of displaced atoms and transmutation products are required for theories of the development of the defect structure and prediction of the consequent property and dimensional changes.
(ii) The use of graphite components in fission and fusion reactor systems requires predictions of dimensional and physical property changes using data obtained under different conditions of neutron spectrum and temperature.

The source neutrons produced by nuclear fission extend over a wide range of energies, from a small fraction of an eV to ~10 MeV, with a mean energy of ~2 MeV. The fusion of tritium and deuterium atoms, which is likely to be the basis of fusion power generation systems, produces source neutrons with energies of 14.1 MeV. In every practical case the source neutron spectra are degraded by elastic and inelastic scattering in the reactor structure and it is necessary to consider spatially varying neutron spectra. The neutron flux with energies in the range E_n to $E_n + dE_n$ is defined to be $\phi(E_n)\, dE_n$ at a field point $\tilde{R}$.

In this chapter we consider the simplest model of the process of atomic displacement in graphite in fission neutron spectra, the comparison of calculated displacement rates with experiment, and the extension of these ideas to fusion neutron systems. Transmutation does not play any significant role in property and dimensional changes of graphite in fission neutron systems, but this is not certain for the higher energies of fusion neutrons.

The neutron induced fissions of the isotopes of uranium and plutonium which are of practical importance produce on average ~3 neutrons/fission with an energy distribution which may, for example, be described by the Watt-Cranberg expression:

$$X(E_n)\, dE_n = K \exp(-AE_n) \sinh(BE_n)^{1/2}\, dE_n \tag{1.1}$$

where K, A and B are constants. The current values of these parameters are:

$A = 1.0123\ \text{MeV}^{-1}$
$B = 2.189\ \text{MeV}^{-1}$
$K = 0.453$

with a mean energy of

$E = (3 + B/2A)/2A = 2.0158$ MeV

In both the fission and fusion cases the neutron spectra in particular materials may be calculated using modern Monte Carlo or diffusion theory based computer codes.

Space Group: $C6/mc(D_{6h}^4)$
Unit cell:
$a = 2.4612 \pm 0.0001$A
$c = 6.7079 \pm 0.0007$A
Volume = 35.190 A^3
Atoms per unit cell = 4
Crystal density = 2.266 g/cm^3

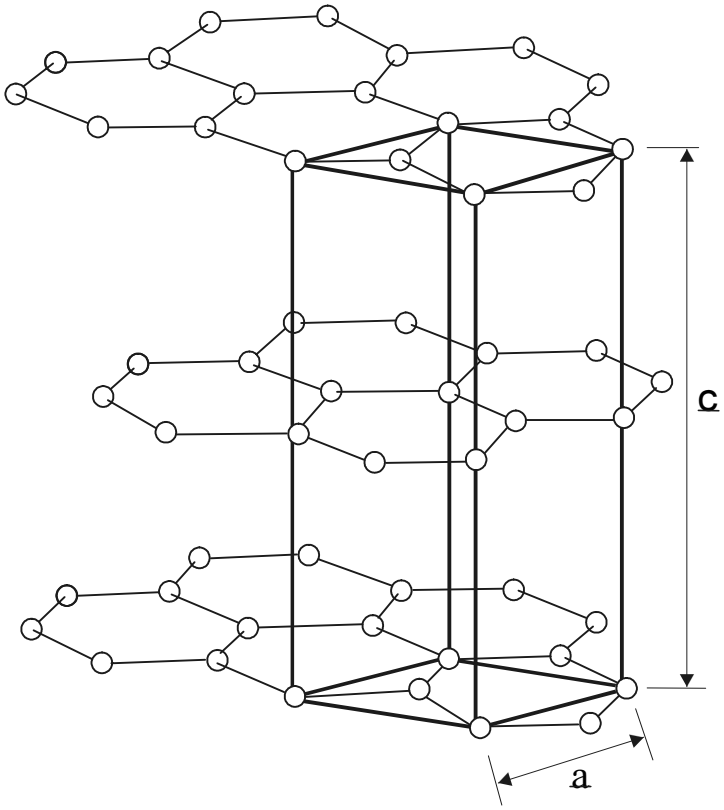

FIG. 1.1. Unit cell of graphite.

The process of creation of crystal lattice defects, which produce the changes in properties and dimensions of graphite, is due to the scattering of the energetic neutrons by the nuclei of the carbon atoms either elastically or inelastically. The binding energy of a carbon atom in the graphite crystal lattice is ~7 eV and it is reasonable to suppose that the transferred energy from the neutron to the nucleus which will irreversibly displace the lattice atom from its site (primary displacements) will be a few times this value, and may be expected to depend upon the direction in which the struck atom is propelled. This energy is denoted by E_d and is assumed to be a function of Q, the angle between the direction of motion and the crystallite hexagonal axis. In fact, the two pairs of atoms in the unit cell do not have identical environments (see Fig. 1.1) and this may complicate the variation of E_d. The maximum energy which can be transferred to a nucleus of atomic weight A by a neutron of energy E_n in a purely elastic collision is:

$$\Delta E_n = \frac{4A}{(A+1)^2} E_n \tag{1.2}$$

which for $^{12}C_6$ is:

$$\Delta E_n = 0.284 E_n \tag{1.3}$$

Equation (1.3) shows that a large proportion of neutron energy is transferred in a collision between a neutron and a carbon nucleus (which, together with its low cross-section for neutron absorption, accounts for its use as a reactor moderator). In both fission and fusion systems, neutrons with energies greater than about 100 eV produce displacements, and the displaced atoms with greater energies produce further displacements in collisions with other carbon atoms in a cascade. Neutron–nucleus collisions may be treated as elastic for neutron energies up to

5.5 MeV in carbon. The cross-section for the (n, a) reaction becomes appreciable for neutron energies above ~9 MeV, and it is also necessary to account for anisotropic scattering.

The energy E_d required to produce displaced atoms and the consequent vacant lattice sites in graphite can be measured using radiation of well-defined energy and interaction and finding the minimum energy necessary to produce a measurable property change. The first measurement was due to Eggen (1950) using electrons of controlled energy (~1 MeV) and finding the minimum energy to give a change in the electrical resistivity in a polycrystalline graphite; he found E_d = 24.7 ± 0.9 eV, presumably the lowest value. The variation of E_d with Q can be obtained using highly oriented graphite samples, such as natural graphite flakes or highly oriented pyrolytic graphite, bombarded at various angles to the hexagonal axis. Lucas and Mitchell (1964) measured the effect of electron irradiation with energies between 0.3 and 2 MeV on the electrical resistivity of natural graphite crystals — the displacement energy was found by fitting curves of damage rate as a function of electron energy. The value of 60 eV obtained presumably corresponds to the value for Q = 0 (i.e. beam parallel to the hexagonal axis). Ohr et al. (1972) observed the onset of visible damage in transmission electron microscopy and obtained a value of E_d = 24 eV for Q = 0, for sample temperatures in the range 300–600°C. Montet (1967) and Montet and Myers (1971) determined the minimum electron energy to create sites which could subsequently be etched to become visible in the electron microscope. Values of 33 eV and 31 eV were obtained for the beam parallel to the hexagonal axis. Rotation of the beam about the hexagonal axis gave the same values for E_d until Q = 60°, when the value increased reaching a value of 60 eV at an angle Q = 80°. Iwata and Nihira (1966, 1971) bombarded highly oriented pyrolytic graphite with electrons at 6, 80 and 285K. In each case the initial rate of change of electrical resistivity parallel to the deposition plane was measured and the results fitted using a model which allowed for secondary displacements caused by the primary displaced atom. The displacement energy as a function of Q was expressed as:

$$E_d = A\cos^2 Q + B\sin^2 Q + C(1 - \cos 4Q) \tag{1.4}$$

where A, B and C are constants. Values of A varied from 23–32 eV and B from 30–42 eV, increasing with irradiation temperature. C varied between 0 and –2 eV. Evidence was obtained for different values of E_d for different atoms in the unit cell.

The situation regarding the displacement energy and its variation with crystallographic direction is not satisfactory. Thrower and Mayer (1978) concluded that a value of 40 eV is appropriate for irradiation in an isotropic electron flux. The value of E_d currently used in the United Kingdom is 60 eV, which is certainly too high. However the calculated atomic displacement rates are essentially inversely dependent on E_d, so that relative damage rates are independent of E_d (Wright, 1962), which is the situation of practical interest where data taken in one neutron spectrum are required to predict effects occurring in a different spectrum. The value of the displacement energy is important in comparison of theoretical models of the radiation damage process with data. It is possible that E_d depends upon the temperature, increasing with temperature, and this needs to be included in theoretical models (Iwata and Nihira, 1966, 1971).

A number of theoretical models have been used to estimate the number of atomic displacements produced by a collision of a neutron of energy E_n and a carbon nucleus, which then permits calculations of the number of atomic displacements in a neutron spectrum, knowing the cross-sections for energy transfer. The most comprehensive calculations, which also consider

TABLE 1.1. GROUP-AVERAGED VALUES OF THE GRAPHITE SCATTERING CROSS-SECTION AND THE THOMPSON AND WRIGHT DISPLACEMENT WEIGHTING FUNCTION

Neutron Energy Group	Upper Energy (MeV)	ENDF-IV Elastic Scattering Cross-Section for Graphite (barns)	Thompson and Wright Displacement Weighting Function
1	14.9	0.771	548.4
2	13.5	0.785	540.6
3	12.2	0.842	532.7
4	11.1	0.673	524.7
5	10.0	0.665	516.5
6	9.05	0.773	508.2
7	8.19	1.43	499.8
8	7.41	0.740	491.5
9	6.70	0.969	482.9
10	6.07	0.924	474.1
11	5.49	1.12	465.3
12	4.97	1.41	456.3
13	4.49	1.95	447.2
14	4.07	2.15	437.6
15	3.68	2.57	428.2
16	3.33	1.80	418.7
17	3.01	2.21	409.1
18	2.73	1.65	399.4
19	2.47	1.60	389.6
20	2.23	1.90	379.7
21	2.02	1.73	369.6
22	1.83	1.85	359.4
23	1.65	1.97	349.1
24	1.50	2.10	338.7
25	1.35	2.23	328.2
26	1.22	2.35	317.6
27	1.11	2.49	306.9
28	1.00	2.62	296.1

TABLE 1.1. (cont.)

Neutron Energy Group	Upper Energy (MeV)	ENDF-IV Elastic Scattering Cross-Section for Graphite (barns)	Thompson and Wright Displacement Weighting Function
29	0.907	2.75	285.2
30	0.821	2.87	274.2
31	0.743	2.99	262.9
32	0.672	3.11	251.5
33	0.608	3.22	240.5
34	0.550	3.32	229.2
35	0.498	3.43	218.1
36	0.450	3.52	207.3
37	0.408	3.62	196.7
38	0.369	3.70	186.3
39	0.334	3.78	176.1
40	0.302	3.86	166.2
41	0.273	3.93	156.5
42	0.247	4.00	147.0
43	0.223	4.06	137.8
44	0.202	4.12	128.8
45	0.183	4.17	120.0
46	0.166	4.22	111.5
47	0.150	4.26	103.2
48	0.136	4.30	95.2
49	0.123	4.34	87.4
50	0.111	4.40	74.8
51	0.0865	4.47	61.2
52	0.0674	4.53	49.7
53	0.0525	4.57	40.2
54	0.0409	4.61	32.3
55	0.0318	4.63	25.9
56	0.0248	4.65	20.7
57	0.0193	4.67	16.5
58	0.0150	4.68	13.1
59	0.0117	4.69	10.3

TABLE 1.1. (cont.)

Neutron Energy Group	Upper Energy (MeV)	ENDF-IV Elastic Scattering Cross-Section for Graphite (barns)	Thompson and Wright Displacement Weighting Function
60	0.00912	4.70	8.0
61	0.00710	4.71	6.2
62	0.00553	4.71	4.8
63	0.00431	4.71	3.7
64	0.00335	4.72	2.9
65	0.00261	4.72	2.3
66	0.00203	4.72	1.8
67	0.00158	4.72	1.4
68	0.00123	4.72	1.1
69	0.000961	4.72	0.8
70	0.000749	4.73	0.6
71	0.000583	4.73	0.5
72	0.000454	4.73	0.4
73	0.000353	4.73	0.3
74	0.000275	4.73	0.2
75	0.000214	4.73	0.1

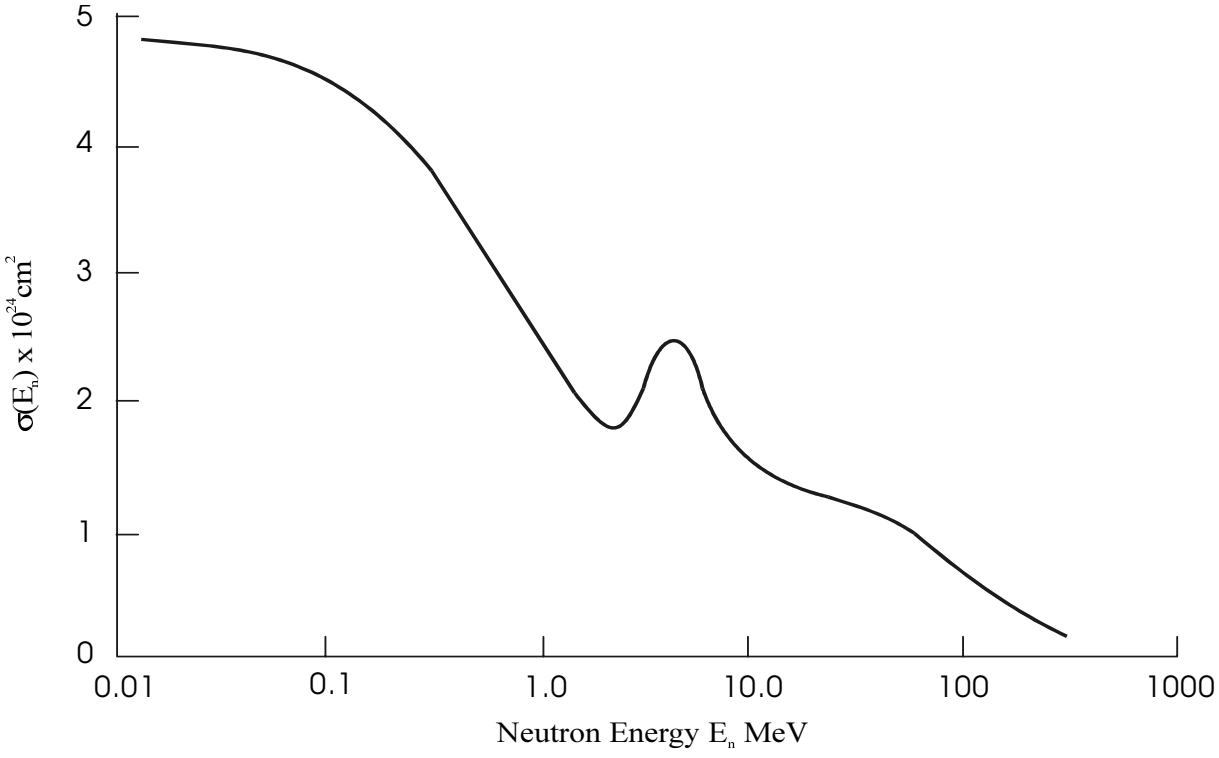

FIG. 1.2. Neutron elastic scattering cross-section.

the spatial distribution of atomic displacements, have been presented by De Halas (1962) and Simmons (1965). We follow the latter in most of the ensuing discussion.

The rate of atomic displacement in a neutron spectrum $\phi(E_n)$ is given by:

$$\frac{dN}{dt} = \iint \phi(E_n)\Omega(E_n, E_p)\nu(E_p)dE_n dE_p \tag{1.5}$$

where N is the fraction of atoms displaced, W (E_n, E_p) is the cross-section for a neutron of energy E_n to produce a carbon atom recoil with energy E_p, and $\nu(E_p)$ is the number of atomic displacements due to a knock-on primary displacement of energy E_p. If $\overline{\nu}(E_n)$ is the average number of displacements produced by a collision with a neutron of energy E_n, then Equation (1.5) can be written:

$$\frac{dN}{dt} = \int \phi(E_n)\sigma(E_n)\overline{\nu}(E_n)dE_n \tag{1.6}$$

where s (E_n) is the elastic scattering cross-section of the carbon nucleus for neutrons, illustrated in Fig. 1.2 and listed in Table 1.1. This assumption is satisfactory for fission neutrons, where the mean energy of the source neutrons is ~2 MeV and only a very small proportion have energies greater than 10 MeV. The source neutrons in deuterium–tritium systems have an energy of 14.1 MeV and thus it is necessary to account for anisotropic and inelastic scattering.

The first model used to estimate the atomic displacement rate in fission systems was due to Kinchin and Pease (1955). It is assumed that the primary neutron–carbon atom collisions are isotropic, each collision transferring the average energy transfer, that is:

$$\Delta E_n = E_p = \frac{1}{2}\left[\frac{4A}{(A+1)^2}\right]E_n = \frac{1}{2}\alpha E_n \qquad \text{say,} \tag{1.7}$$

where A is the atomic weight of carbon. It is a good approximation for the energies relevant to fission reactors. The primary knock-on carbon atom loses energy by two separate mechanisms, the first by collisions with other carbon atoms and the second to the electrons. The latter is dominant at the higher knock-on energies because the majority of the knock-on atoms are ionised. The degree of ionisation decreases with the velocity of the atom until the rate of energy loss is dominated by atom–atom collisions. Kinchin and Pease, as an approximation, assume that for moving atom energies greater than L_c, all of the energy loss above L_c is electronic in character, while for lower energies it is solely due to atom–atom collisions. A rough estimate for L_c is A keV. The atom–atom collisions may be treated to a first approximation as between billiard balls with equal masses undergoing isotropic scattering in the centre of mass system for a monatomic lattice. These assumptions lead to:

$$\frac{L_c}{2E_d} \quad \text{.....} \quad E_p \geq L_c$$

$$\frac{E_p}{2E_d} \quad \text{.....} \quad 2E_d \leq E_p \leq L_c$$

$$\nu(E_p) = \tag{1.8}$$

$$1 \quad \text{.....} \quad E_d \leq E_p \leq 2E_d$$

$$0 \quad \text{.....} \quad 0 \leq E_p \leq E_d$$

which in turn leads to:

$$\frac{L_c}{E_d}\left[1 - \frac{L_c}{\alpha E_n}\right] \quad \text{.....} \quad E_n \geq \frac{2L_c}{\alpha}$$

$$\frac{\alpha E_n}{4E_d} \quad \text{.....} \quad \frac{4E_d}{\alpha} \leq E_n \leq \frac{2L_c}{\alpha}$$

$$\bar{\nu}(E_n) = \tag{1.9}$$

$$1 \quad \text{.....} \quad \frac{2E_d}{\alpha} \leq E_n \leq \frac{4E_d}{\alpha}$$

$$0 \quad \text{.....} \quad E_n \leq \frac{2E_d}{\alpha}$$

The Kinchin-Pease formulae were used by Wright (1962) to calculate the atomic displacement rates in a number of reactor neutron spectra, obtained using Monte Carlo methods, for varying values of L_c. A comparison of these results with relative measured rates of change of graphite properties in the reactor locations for which the spectra had been obtained indicated a value of L_c = 25 keV, but the relative damage rates are very insensitive to the value. A complete theory of radiation damage requires knowledge of the spatial distribution of displaced atoms as well as their numbers. This aspect has been considered by Simmons (1965) as follows.

A detailed treatment of a collision between a moving carbon atom and a lattice atom performing thermal vibrations would need to account for the interactions between the electrons and nuclei of the moving atoms and the lattice atoms. As an approximation, collisions between free atoms interacting with a potential $V(r)$, where r is the separation, are considered with a separate treatment of the electronic energy loss. The approximation should be adequate provided that the mean distance between displacement collisions is large compared to the interatomic distances in the crystal lattice, which is satisfied in the case of graphite.

The potential chosen for collisions between similar atoms was that due to Bohr:

$$V(r) = \frac{Z^2 e^2}{r} \exp\left(-\frac{r}{a}\right) \tag{1.10}$$

Z is the atomic number of the atom involved in the collisions, e is the electronic charge and a is the "screening radius". The parameter values for carbon atoms are:

$$Z^2 e^2 = 520 \times 10^{-8} \text{ cm. EV}$$

$$a = 0.207 \times 10^{-8} \text{ cm}$$

The classical collision diameter is defined as:

$$b = \frac{2Z^2 e^2}{T_1} = \frac{1040 \times 10^{-8}}{T_1} \quad \text{cm} \tag{1.11}$$

where T_1 is the kinetic energy of the moving atom before the collision. The collisions are most conveniently considered in relative co-ordinates where the centre of mass is at rest. If q is the angle of deflection in this co-ordinate system, then the energy transferred to the struck atom is

$$T_2 = T_1 \sin^2\left(\frac{\theta}{2}\right) \tag{1.12}$$

Classical theory is adequate for the calculation of atomic displacements, and thus the differential collision cross-section may be written

$$d\sigma_a = 2\pi p\, dp \tag{1.13}$$

where p is the "impact parameter", defined as the perpendicular distance from the centre of the struck atom to the line of motion of the moving atom. A relationship between p and a and hence p and T_2 can be obtained. The differential cross-section can then be expressed as

$$d\sigma_a = W_a(T_2)\, dT_2 \tag{1.14}$$

At energies $T_1 > \sim 50$ keV the scattering follows the Rutherford law (valid for $\theta > b/a$)

$$d\sigma_a = \frac{\pi Z^4 e^4}{T_2^2 T_1} dT_2 \tag{1.15}$$

The appropriate value of Equation (1.15) for carbon atoms is

$$d\sigma_a = \frac{8.46 \times 10^{-11}}{T_2^2 T_1} dT_2 \quad \text{cm}^2 \tag{1.16}$$

with T_1 and T_2 in electron volts.

TABLE 1.2. LOW AND MEDIUM ENERGY ATOMIC COLLISIONS

Energy of Moving Atom T_1 (eV)	Energy Transferred T_2 (eV)	$W_a(T_2)$ [cm^2 eV^{-1}]	Energy of Moving Atom T_1 (eV)	Energy Transferred T_2 (eV)	$W_a(T_2)$ [cm^2 eV^{-1}]
500	25	1.5×10^{-18}	10 000	25	7.2×10^{-19}
	100	3.0×10^{-19}		2000	1.0×10^{-21}
	200	1.3×10^{-19}		4000	2.9×10^{-22}
	300	8.0×10^{-20}		6000	1.4×10^{-22}
	400	5.6×10^{-20}		8000	8.1×10^{-23}
	500	4.2×10^{-20}		10 000	5.4×10^{-23}
1000	25	1.3×10^{-18}	25 000	25	5.2×10^{-19}
	200	1.0×10^{-19}		5000	1.0×10^{-22}
	400	3.9×10^{-20}		10 000	2.6×10^{-23}
	600	2.2×10^{-20}		15 000	1.2×10^{-23}
	800	1.5×10^{-20}		20 000	6.8×10^{-24}
	1000	1.1×10^{-20}		25 000	4.3×10^{-24}
2500	25	1.0×10^{-18}	50 000	25	4.0×10^{-19}
	500	1.9×10^{-20}		10 000	1.5×10^{-23}
	1000	6.8×10^{-21}		20 000	3.8×10^{-24}
	1500	3.6×10^{-21}		30 000	1.7×10^{-24}
	2000	2.2×10^{-21}		40 000	9.4×10^{-25}
	2500	1.6×10^{-21}		50 000	6.0×10^{-25}
5000	25	8.3×10^{-19}			
	1000	4.6×10^{-21}			
	2000	1.5×10^{-21}			
	3000	7.4×10^{-22}			
	4000	4.5×10^{-22}			
	5000	3.0×10^{-22}			

The lower energy collisions were treated using the results of Everhart et al. (1955) who employed classical theory and the Bohr potential (Equation (1.10)) to calculate the differential cross-sections. Table I.2 presents Simmons' results based on their calculations.

Equation (1.15) and Table 1.2 show that at high energies the probability is greater that the energy transferred is a small fraction of the initial energy of the moving atom, while at lower energies there is a tendency towards an equal distribution between moving and struck atoms. Simmons (1965) reviewed the theories then available. Qualitatively, the moving atom can be regarded as a charged particle with average charge qZe where q depends upon the relative values of the cross-sections for electron capture and loss (ignoring the loss of energy by charge exchange amounting to ~20% for the slower moving atoms). Knipp and Teller (1941) have estimated q from a statistical model of the atom rather then attempt the computation of the capture and loss electron cross-sections. The work gives a relationship between q and $(v / v_0)Z^{2/3}$ where $v_0 = 2\pi e^2/h$ is the velocity of an electron in the hydrogen atom ground state. It was found that q varies from 0.6 at 10^5 eV to ~2 at 10^6 eV. The energy loss per atom for $v > v_o$

TABLE 1.3. DETAILS OF DISPLACEMENT COLLISIONS IN GRAPHITE

Energy T_1 of Moving Atom (eV)	Energy lost/Collision of Primary Knock-on (eV)			Mean Path between Displacement Collisions** (cm) × 10^8	Approximate Range of Primary Knock-on (cm) × 10^8
	Energy lost to lattice vibrations T_L	Energy transfe-rred T_2	R*		
500	11	136	-	9.8	-
1000	12	196	-	11.0	67
5000	13	368	200	18.0	210
10 000	14	415	405	22.5	250
50 000	18	424	1600	45.2	1300
100 000	22	382	3100	64.6	2350
500 000	39	297	15 140	173.0	7900
1 000 000	50	282	32 800	285.0	13 650

R* is the amount of energy lost by electronic excitation between successive displacement collisions.

** The mean free path is calculated from $(N_0\ s_d)^{-1}$ where N_0 is the number of carbon atoms/unit volume and s_d is the cross-section for displacement of a moving atom of energy T_1.

and $v>qZv_o$ may then be obtained using the relationship due to Mott and Massey (1949). However, data were available on the rate of energy loss of carbon ions in graphite due to Porat and Ramavataram (1961) and Ormrod and Duckworth (1963). The two sets of data join smoothly and this was used by Simmons to calculate the ranges of moving atoms of various energies. The energy of the moving atom at which the rate of energy loss due to collisions is equal to that due to the electronic system was found to be ~12 keV (which is an estimate for L_c in the Kinchin-Pease model). The number of displaced atoms was assumed to be given by Equation (1.8), and the energy lost to lattice vibrations T_L is estimated as that transferred in collisions which transfer energy less than E_d The results of these calculations are given in Table 1.3.

The calculations permit visualisation of the events following the creation of a primary knock-on. Table 1.3 shows that when the primary energy is between 10^3 eV and 10^6 eV the mean distance between displacement collisions is large compared to the interatomic spacing, and over this range of energy the average energy of the secondary knock-on is less than 500 eV. As a consequence, the damage produced by the primary knock-on consists of separate groups of displaced atoms. This is illustrated in Fig. 1.3. It is a reasonable approximation to assume that individual displacements occur at random in theoretical models of the creation of the more complex defects formed from the displacements.

Each of the groups contains less than an average of ten displacements, and is known as "displacement groups". The range of the primary knock-on atom varies from about 10^{-6} cm at

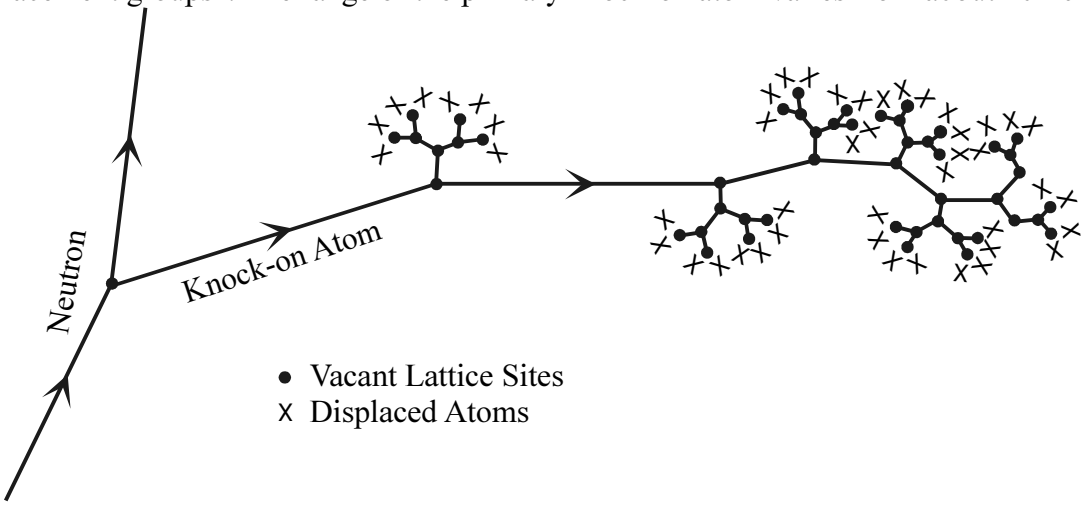

FIG. 1.3. Distribution of displaced atoms and vacant lattice sites.

10^{3} eV to 10^{-4}cm at 10^{6} eV. When the primary energy falls below ~ 500 eV each knock-onproduces one displacement group. The collisions within the displacement groups can be regarded as separate events until the energy falls to about 100 eV, at which the collision separation becomes comparable with the interatomic spacing. At this point some interstitial atoms will spontaneously recombine with vacancies and some multiple vacancies may be produced. Computer studies (see later) show that multiplication of the total number of displaced atoms by a constant factor allows for the first of these effects. No attempts have been made to estimate the fraction of multiple vacancies.

The lattice structure of graphite favours channelling of displaced atoms into the large interlayer spacing and this will have the effect of spreading the displacement groups over a larger volume and increase the probability of collisions with atoms in interstitial positions. It has also been suggested that focused collisions may occur in $\{11\bar{2}0\}$ lattice directions. The lack of high quality

single crystals of any size has precluded detailed experimental studies of channelling and focusing effects.

Simmons provided a method of calculating the number of atomic displacements in carbon and their spatial distribution in fission reactor neutron spectra. Calculations of the atomic displacements in fusion reactor spectra are, as already noted, more difficult because of the higher energy source neutrons, but in fact for many realistic spectra in such systems substantial degradation in energy has occurred and the methods may with some care be adequate in these cases.

Examination of the neutron cross-section as a function of energy in the Evaluated Nuclear Data File (ENDF) (see Fig. 1.2 and Table 1.1 for values) shows that the elastic scattering cross-

section for neutrons in carbon is the same as the total scattering cross-section for neutrons of energies up to 2 MeV (the energy of the peak in the fission spectrum) and the scattering is isotropic in the centre of mass system up to an energy of 0.1 MeV. For neutron energies of greater than 2 MeV the scattering cross-section shows many resonances and the effects of inelastic and anisotropic scattering become important. It is clear that relative atomic displacement rates in different fission reactor spectra will be quite accurate.

Prior to consideration of improved methods of calculating atomic displacement rates for fission and fusion reactor spectra, it is necessary to compare the results with experiment and decide whether they are useful. The fundamental technological reason for such calculations is, after all, the prediction to acceptable accuracy of the dimensional changes and property changes of graphite in different neutron spectra.

The changes in a graphite property P_i may be written

$$R_i = \frac{1}{P_i}\frac{dP_i}{dt} \propto \int_0^\infty \phi(E_n)\,\psi_i(E_n)\,dE_n \tag{1.17}$$

where $\psi_i(E_n)$ is a weighting function for the effect of a flux of neutrons of energy E_n on the property P_i. If ψ_i is independent of property then the damaging power, that is the ability to change properties, becomes unique and an extremely useful concept. (In principle ψ_i may include transmutation as well as classical atomic displacement effects.) It can readily be imagined that ψ_i could depend upon the property considered, obvious possibilities being the number of displaced atoms, the number of displacement groups or perhaps the number of closely spaced groups. Fortunately, as we shall see, in fission neutron systems the number of displaced atoms is an adequate approximation to relate the damaging power of different neutron spectra.

If the distribution of the displaced atoms were truly random then Equation (1.17) would be sufficient to characterise the damaging power of the spectrum of neutrons. However the distribution of displacements is not truly random and, following Simmons, it is necessary to consider more carefully the meaning of "damaging power". If identical specimens of graphite are irradiated for the same time at the same temperature in two different neutron spectra, and then show identical property changes, then the damaging powers of the two spectra are the same, even if the neutron spectra are different. This definition of damaging power is useful only if the equality of the property changes is maintained whatever the duration or temperature of irradiation.

If the damaging power may be represented by Equation (1.17) then it must be possible to write the damage flux

$$\phi_d = \frac{R}{\sigma_d} \tag{1.18}$$

where s_d is a normalising factor, which may be chosen quite arbitrarily. In Simmons (1965) s_d is defined with respect to the source neutron flux due to fission, i.e.

$$\sigma_d \propto \int_0^\infty \phi(E_n)\,\sigma(E_n)\,\bar{\nu}(E_n)\,dE_n \tag{1.19}$$

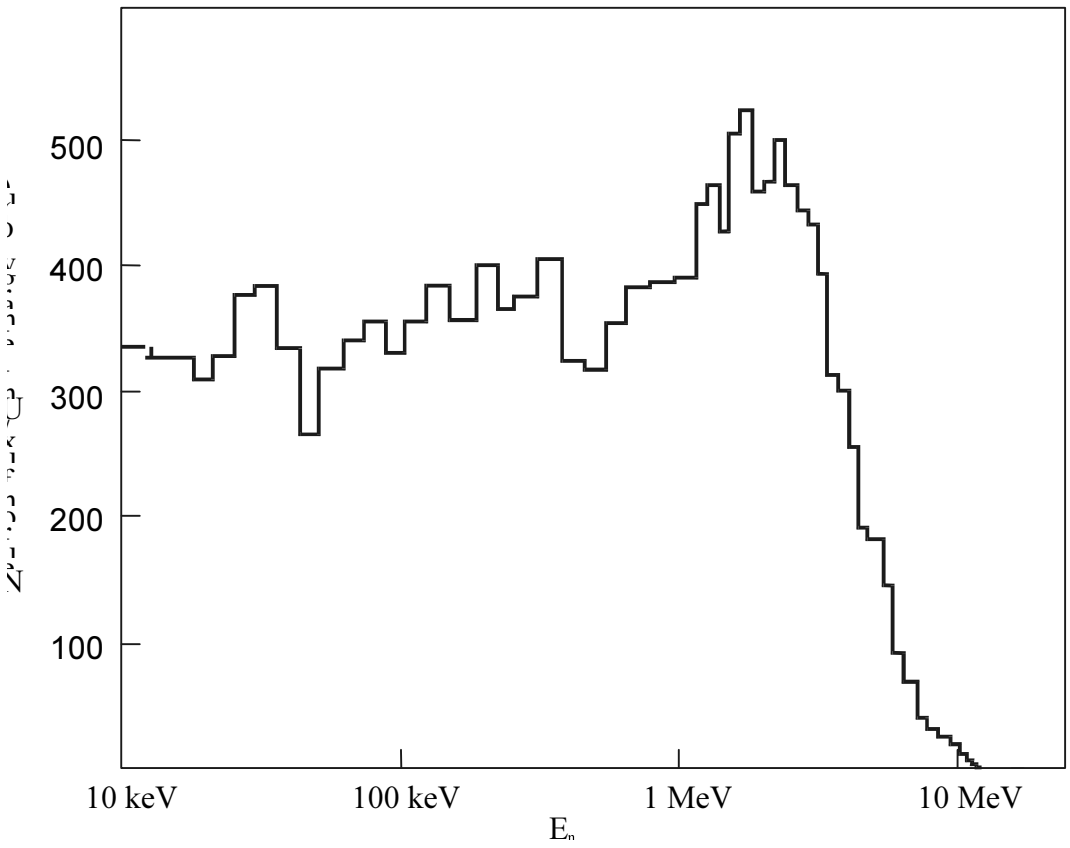

FIG. 1.4. Spectrum in MK. III fuel element in DIDO (the standard position for the DIDO equivalent dose).

That is, ϕ_d is the equivalent fission flux for displacement. However the most generally used normalisation is the neutron spectrum in a Mk III hollow fuel element in the DIDO Materials Test Reactor at the Atomic Energy Research Establishment, Harwell, UK. (The reactor is no longer operational.) The spectrum is shown in Fig. 1.4 and the model used for $\bar{\nu}(E_n)$ is due to Thompson and Wright (1965), discussed later.

The calculated damage ratios in different neutron spectra have been compared with measured rates of property change in many experiments, beginning with the work of Bell et al. (1962), who used changes in the electrical resistivity of a standard block of graphite irradiated at about room temperature. There is evidence that similar methods were in use in the USA in the late 1940's (Primak, 1956). Bell et al. noted that in fact the property changes depend on three variables; that is the damage flux ϕ_d, the irradiation temperature T_i K and the irradiation time t sec. Determination of the damaging power of two reactor spectra is then difficult, because it would be necessary to adjust the reactor powers to give the same property changes after the same irradiation time. It has often been assumed that the property changes just depend upon the irradiation dose and temperature and thus having measured property changes as a function of dose at a particular temperature in one reactor, measurements to a convenient dose at the same temperature yield the damaging power in another reactor. It is known that if two identical graphite samples are irradiated to the same damage dose but taking different times, that is one quickly and the other more slowly, then in general the property changes are not identical; the sample irradiated quickly showing the larger changes. This is a flux level effect — it occurs because the damage depends upon the dose, but the thermal processes to which the defects are

subject depend upon the temperature and the time. The slower irradiation allows more time for the thermal processes to occur. These effects can only be avoided by carrying out experiments at similar displacement rates. In practice the concept was introduced of an "equivalent temperature" q K which would be required in a flux producing a standard displacement rate A_s sec^{-1} to produce the same observed property changes as a function of damage dose as those observed at a temperature T_i K, displacement rate A sec^{-1}. The two temperatures are related by:

$$\frac{1}{\theta} - \frac{1}{T_i} = \left(\frac{k}{E}\right) \ln\left(\frac{A}{A_s}\right) = \left(\frac{k}{E}\right) \ln\left(\frac{\phi_d}{\phi_s}\right) \tag{1.20}$$

where k is Boltzmann's constant and E is an activation energy.

Equation (1.20) can be obtained using an argument due to G H Kinchin (unpublished) as follows. During irradiation the displaced atoms pass through a sequence of configurations which depend upon the rate of displacement and the diffusion rate (thermally activated). If the damage flux is increased then it is necessary, to obtain the same final damage state, to increase the diffusion rate in the same ratio by increasing the temperature as given by Equation (1.20). The Equation may be derived from a wide range of kinetic models of damage accumulation. The argument is not entirely satisfactory and begins to break down for ratios of A/A_s greater than about 20. The activation energy E must be determined experimentally. Given this value all data can be reduced to a function of two variables only; that is the damage dose and the temperature obtained from Equation (1.20) appropriate to irradiation at the standard rate.

Bell et al. (1962) made the first direct determination of the activation energy E using electrical resistivity changes in a standard block of graphite. The dose and temperature dependence of the electrical resistance changes was determined using a temperature controlled irradiation facility in the graphite moderated reactor BEPO located at the Atomic Energy Research Establishment, Harwell. The dose was measured using the activation reaction ^{58}Ni (n,p) ^{58}Co, which is sensitive to neutrons with energies greater than ~1 MeV. The changes in the electrical resistivity were expressed as

$$\frac{\Delta\rho}{\rho} = 0.162\left[1 - 0.00514\left(T - 273\right)\right] \times \left[\gamma_{Ni} \times 10^{-16}\right]^{0.75} \tag{1.21}$$

where γ_{Ni} is the nickel dose. Electrical resistivity changes were then measured in a single reactor position at high and low reactor power in the PLUTO Materials Testing Reactor, also at Harwell. (Actually reactor powers of 300 kW and 7.5 MW were employed.) The resulting data permitted the apparent irradiation temperatures for identical real irradiations to be determined and hence a value of E, as well as the relative damaging powers of the two spectra. The value obtained for E was 1.58 eV. Bridge et al. (1963) using the DR-3 Materials Testing Reactor at Risø, Denmark, measured changes in dimensions, crystal lattice parameter changes, Young's modulus, electrical resistivity and thermal conductivity as a function of dose for irradiation temperatures between 150 and 220°C (dose measured using the ^{58}Ni (n,p) ^{58}Co reaction) in a hollow fuel element with reactor powers of 1 MW and 10 MW. The flux level effect was clearly visible and yielded a value of E = 1.2 eV ± 0.1 eV for all properties.

TABLE 1.4. VARIATION OF DAMAGE FLUX/NICKEL FLUX RATIONORMALISED TO UNITY IN BEPO TE-10

Experimental Position	Reactor Moderator	(ϕ_d/ϕ_{Ni}) Experimental	(ϕ_d/ϕ_{Ni}) Calculated
BEPO TE -10 Exp. Hole	Graphite	1.00 (Definition)	1.00
BEPO HFE	Graphite	0.43	0.43
BEPO Empty Fuel	Graphite	1.00	1.00
Channel	D_2O	0.59	0.52
PLUTO RFE*	D_2O	0.49	0.49
PLUTO HFE**	D_2O	0.51	0.52
DR-3 RFE*	D_2O	0.49	0.49
DR-3 HFE**	H_2O	0.39	-
Herald RFE			

* Denotes similar positions - results should be identical.

** Denotes similar positions.

HFE denotes hollow fuel element and RFE denotes replacement fuel element.

The value of E would be expected, on very general grounds, to increase with irradiation temperature. Two attempts have been made to determine the value of E appropriate to higher temperatures (Brocklehurst, Kelly and Gilchrist, 1981; Kennedy and Eatherly, 1981). The first authors found that different values apparently applied to different properties, which strictly contradicts the theory, while the latter authors essentially found no effect - that is the work was inconclusive. This probably reflects the difficulties of close temperature control in high temperature irradiations (see later).

Given knowledge of the effects of flux level (displacement rate), the relative damaging powers of different reactor spectra can be determined and compared with the calculations of relative damage rate. Table I.4 shows calculations due to Simmons, using the Kinchin-Pease model with L_c = 25 keV and neutron spectra calculated by Monte Carlo methods for the reactor facilities in which electrical resistivity data had been obtained. (The variation of the calculated displacement rate to nickel activation ratio relative to the standard position is only weakly dependent on L_c in the Kinchin-Pease model, but comparison of calculated ratios with the experimental data for the BEPO and PLUTO data showed that the best value for L_c was 25 keV.) The data are normalised to a value of unity for the ratio of ϕ_d/ϕ_{Ni} in the TE-10 position in the moderator of BEPO. ϕ_{Ni} is the flux measured using the reaction ^{58}Ni (n,p) ^{58}Co with a cross-section of 0.107×10^{-24} cm^2.

The studies of relative damage rate so far described showed that calculated relative displacement rates were in good agreement with measured relative rates of property change, and were therefore of practical use. The first proposals for an improved model were made by Thompson and Wright (1965). The energy E_D out of an initial energy E_p which produces displacements was calculated in the form

$$E_D = \int_0^{E_p} \frac{\left(\frac{dE}{dx}\right)_c}{\left\{\left(\frac{dE}{dx}\right)_c + \left(\frac{dE}{dx}\right)_e\right\}} dE \qquad (1.22)$$

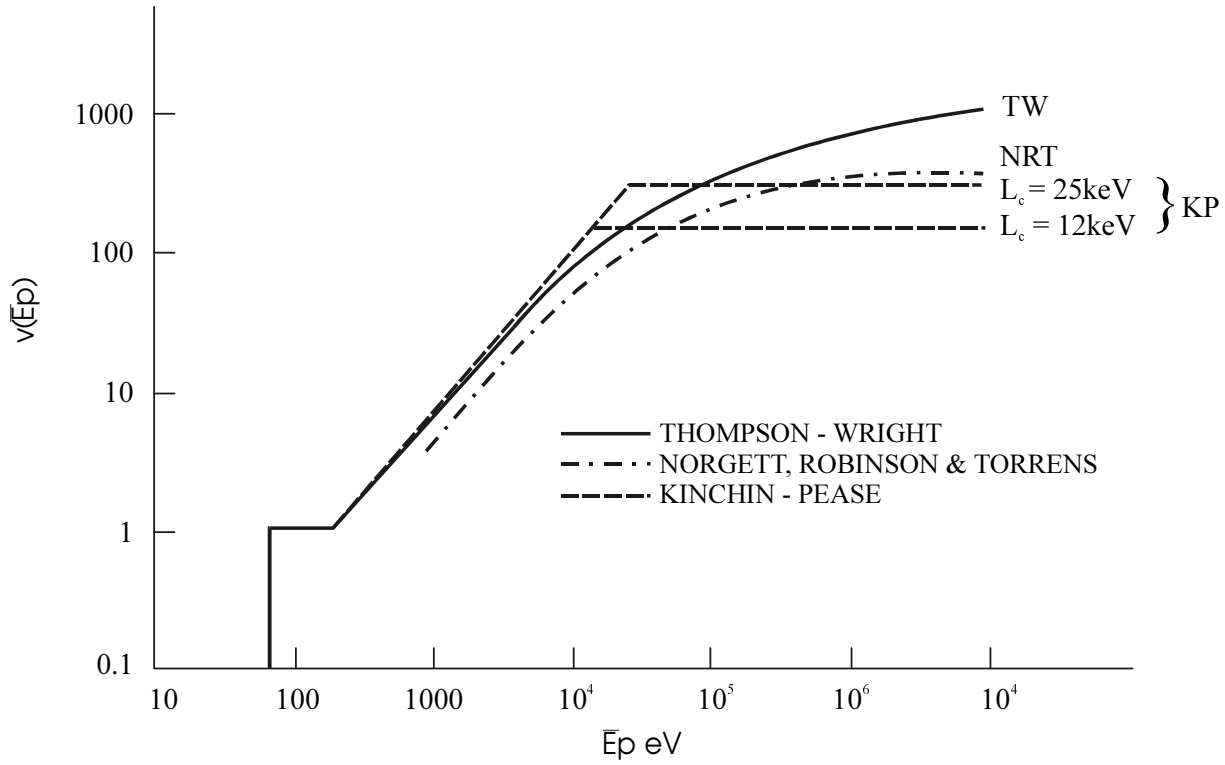

FIG. 1.5. Comparision of primary displacement functions.

where

$(dE/dx)_c$ is the rate of energy loss/unit path length due to collisions.

$(dE/dx)_e$ is the rate of energy loss/unit path length due to electronic processes.

The number of displaced atoms produced on average by a knock-on of energy E_p is now given by

$$\bar{\nu}(E_p) = \begin{cases} \dfrac{E_D}{2E_d} & \text{for } E_D > 2E_d \\ 1 & \text{for } E_d \le E_D \le 2E_d \end{cases} \qquad (1.23)$$

with E_d = 60 eV, following Lucas and Mitchell (1964). The electronic energy losses were taken from the experimental data due to Ormrod and Duckworth (1963) and Porat and Ramavataram (1961).

The average number of displacements for a primary knock-on of energy E_p, $\bar{\nu}1(E_p)$, is shown in Fig. 1.5 for the Kinchin-Pease model with two values of L_c, 12k eV and 25 keV, together with the Thompson-Wright model, all using E_d = 60 eV.

The new method did not make any significant difference to the calculated ratios of displacement rate to activation rate normalised to a standard position; the values are shown in

Table 1.5, now normalised to unity in the spectrum associated with the DIDO hollow fuel element shown

TABLE 1.5. COMPARISON OF CALCULATED AND MEASURED GRAPHITE DAMAGE RATES USING THE THOMPSON-WRIGHT MODEL

Location	Calculated	Measured/Standard	Reference
DIDO hollow fuel element	1.00	1.00	By definition
PLUTO empty lattice position	0.975	1.22	Bell et al. (1962)
DR-3 empty lattice position	0.975	0.90	Bridge et al. (1963)
BR-2, Mol, hollow fuel element	1.00	0.90	
HFR-Petten core	1.02	1.0	Zijp and Rieffe (1972)
BEPO TE-10 hole	2.31	2.04	
1. Empty fuel channel	2.36	2.04	Bell et al. (1962)
2. Hollow fuel channel	0.98	0.87	
Windscale AGR			
1. Replaced fuel stringer B	2.70	2.28	
Replaced fuel stringer D	2.71	2.03	
2. Loop stringer	2.60	2.08	
3. Loop control stringer	2.60	2.51	Gray and Thorne (1968)
4. Fuel element — inner ring	1.18	1.06	
Fuel element —outer ring	1.39	1.06	
Calder x-hole	2.12	2.10	
Dounreay Fast Reactor core	0.46	0.50	Martin and Price (1967)

in Fig. 1.4. All doses can be expressed as “DIDO Equivalent Dose”; that is the dose measured by the ^{58}Ni (n,p) ^{58}Co reaction in the hollow fuel element spectrum, using a cross-section of 0.107×10^{-24} cm^2, which would give the same number of displacements as the sample spectrum. A number of authors have calculated the hollow fuel element spectrum and the ratio of displacement rate to nickel activation rate for the spectrum. The original Thompson-Wright calculation gave 1.313×10^{-21} atoms/atom/n.cm^{-2} which is normally used, but other authors have obtained values ranging from 1.178×10^{-21} to 1.136×10^{-21} atoms/atom/n.cm^{-2}. A DIDO Equivalent Dose of 7.62×10^{20}n.cm^{-2} corresponds to every atom being displaced once (in modern notation 1dpa). The calculations of DIDO Equivalent Temperature for this facility assume a flux measured by the nickel activation reaction of 4×10^{13} n.cm^{-2}.s^{-1}, corresponding to a displacement rate $A_s = 5.25 \times 10^{-8}$ atoms/atom/s. The damage doses are generally expressed in these units for experiments carried out in the UK, Japan and Germany, but in the USA it was noted that for thermal reactor spectra the relative damage rates could be accurately estimated by

taking the neutron flux with energy above some value E_n. Two values have been used: E_n = 0.18 MeV and E_n = 0.05 MeV (sometimes written as 50 keV). Direct comparison of data shows that

1 n/cm^2 (DIDO Equivalent Dose) = 2.0 n/cm^2 (E_n > 0.05 MeV)
1 n/cm^2 (DIDO Equivalent Dose) = 1.5 n/cm^2 (E_n > 0.18 MeV)

A variety of damage dose units were used before the theoretical studies and experimental studies described here. Table 1.6 shows the conversion factors between these units.

TABLE 1.6. CONVERSION OF VARIOUS GRAPHITE DAMAGE DOSE UNITS TO EQUIVALENT DIDO NICKEL DOSE

Dose or flux units and original source	Multiply by
Equivalent DIDO nickel dose (EDND or DNE) UKAEA	1.0
Equivalent fission dose (33) UKAEA	0.547
Calder equivalent dose (MWd/Ate) UKAEA	1.0887×10^{17}
[1]BEPO equivalent dose UKAEA	0.123 (Morgan gives 0.0962 ± 0.01)
Neutron dose n.cm^{-2} (E_n > 0.05 MeV) USA	0.5
Neutron dose n.cm^{-2} (E_n > 0.18 MeV) USA	0.67
Neutron dose n.cm^{-2} (E_n > 1.0 MeV) USA	0.9

MWd/Ate(USA) - Hanford Irradiations, USA. Morgan (1974a) gives values for 1MWd/Ate of 4.56×10^{16} n.cm^{-2} (E_n > 0.18 MeV) originally due to Nightingale (1962) and 5.18×10^{16} n.cm^{-2} (E_n > 0.18 MeV) due to De Halas; that is multiply by 3.26×10^{16} to give EDND.

Note that 1 n.cm^{-2} (EDND) = 1.313×10^{-21} displacements/atom = 148.4 displacements/cm^3 for 1.13×10^{23} atoms/cm^3.

Early design studies of graphite moderated reactors required estimates of the variation of damage dose distribution in the structure, and these were obtained experimentally. In the United Kingdom, Kinchin determined the relative damage rates at a variety of positions in the core and reflector of BEPO (using electrical resistivity measurements). The results were analysed to given the relative damage as a function of distance from a line source of fission neutrons in a graphite medium of fixed density. The curve obtained is illustrated in Fig. 1.6. The damage rate in a reactor could then be obtained by summing the contributions from each fuel channel, allowing for the power distributions (see Bell et al., 1962). Similar methods were developed in the USA, but have not been reported in detail (Primak, 1956). Wright (1965) showed that the empirical curve due to Kinchin was well reproduced by calculations of the variation of the neutron

[1]Note that early UK studies were reported using BEPO Equivalent Doses (BED) rather than the Equivalent DIDO Nickel Dose now recommended for use. The BEPO Equivalent Dose was the thermal neutron dose in a standard position in BEPO which gives the observed damage. The thermal flux is readily perturbed and is not really suitable for the purpose.

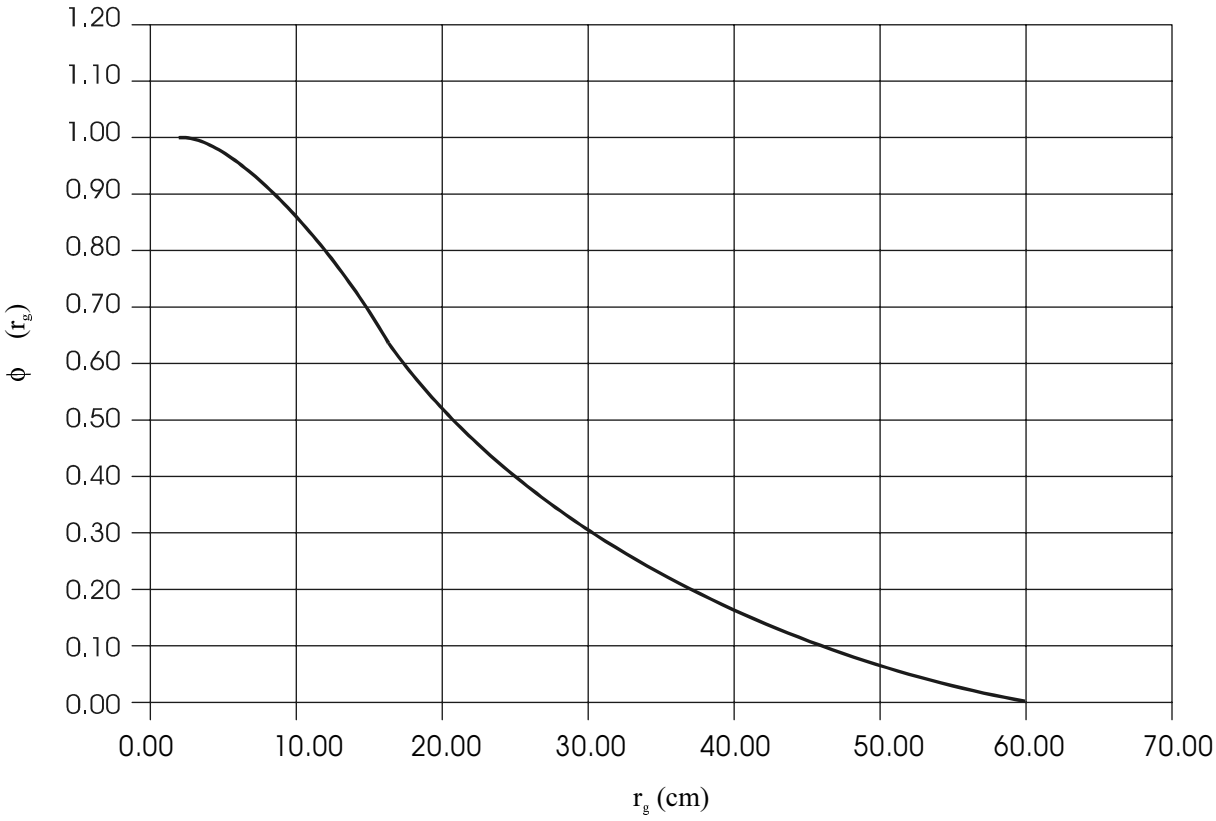

FIG. 1.6. Variation of graphite damage flux with distance through graphite.

spectrum with distance from a line source of fission neutrons in graphite combined with the Thompson-Wright model. The results can be fitted by

$$\phi_d \propto \frac{1}{r}\left\{A_1 \exp(-\lambda_1 r) - A_2 \exp(-\lambda_2 r)\right\} \tag{1.24}$$

where

$A_1 = 1090 \pm 29$ cm, $l_1 = 0.0822 \pm 0.0004$ cm^{-1}
$A_2 = -918 \pm 27$ cm, $l_2 = 0.208 \pm 0.010$ cm^{-1}

for a graphite of density 1.6 g.cm^{-3}, valid for 2 cm < r < 115 cm. Different graphite densities may be allowed for by scaling the radial distance with the relative density, i.e.

$$r_g = 1.6\frac{r}{\rho_g} \tag{1.25}$$

where r_g is the graphite density. These methods are still useful for initial estimates of local damage, but are now superseded by more modern computer based methods.

Morgan (1974b) compared (see Fig. 1.7) the calculated ratios of displacement rate to nickel activation rate normalised to unity in the DIDO Mk III hollow fuel element neutron spectrum, using the Thompson-Wright model, with the experimental measurements. It is clear from Fig. 1.7 that there is a deviation from the theoretical values, the calculated values being too

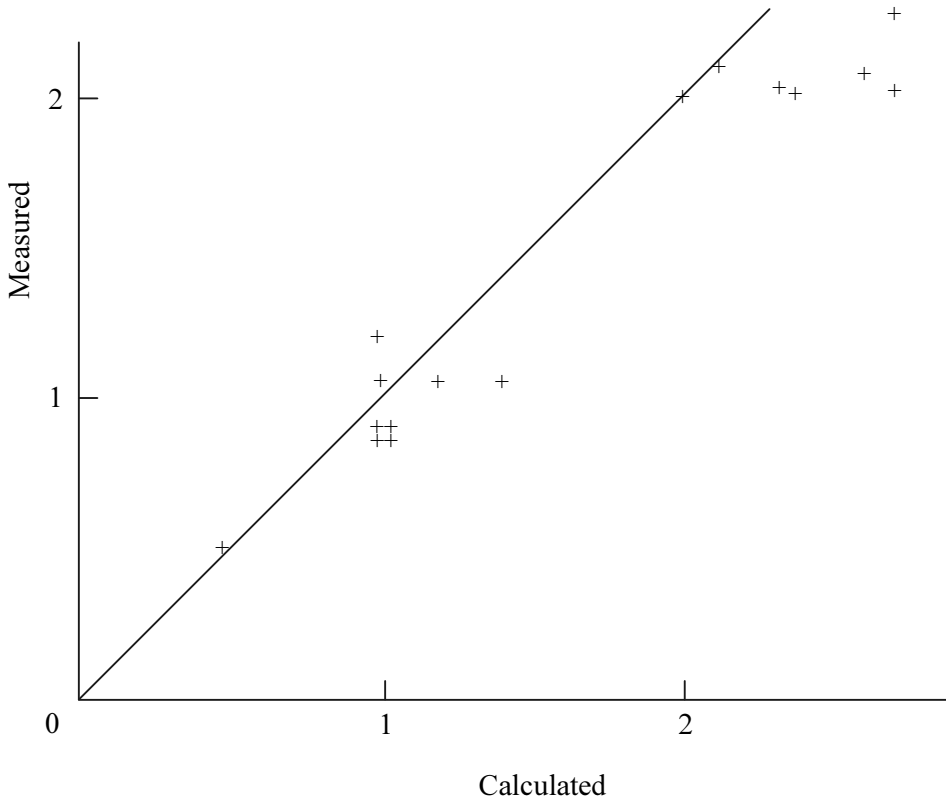

FIG. 1.7. Calculated ratio of damage flux to nickel flux compared with measured rates for graphite damage calibration experiments (Thompson-Wright Model).

high, particularly for values close to 2. This was interpreted by Morgan as showing that a larger fraction of the displacement damage is produced by higher energy neutrons than is implied in the Thompson-Wright model. Morgan proceeded to recalculate the damage function using the neutron cross-sections taken from the third version of the Evaluated Nuclear Data File (ENDF/B III), including the effects of inelastic (n,a) scattering and anisotropic scattering, together with a theoretical treatment of the stopping cross-section of carbon due to Lindhard et al. (1963). Fastrup et al. (1966) demonstrated that the experimentally measured stopping cross-sections (Porat and Ramavataram, 1961; Ormrod and Duckworth, 1963) were in reasonable agreement with the Lindhard theory. The Thompson-Wright model and the Kinchin-Pease model allowed for electronic energy loss in the primary knock-on only, but the Lindhard et al. model more realistically allows for such losses in the secondary and later knock-ons. Lindhard et al. show that, to a good approximation

$$\bar{\nu}\left(E_p\right) = \frac{E_p}{2E_d}\frac{1}{\left[1 + K\,g(\varepsilon)\right]} \tag{1.26}$$

where

$e = E_p/E_l$, where E_l is a constant

and for carbon atoms

$K = 0.12748$

$E_l = 5686.7$ eV

Robinson (1969) parameterised $g(e)$ in the form

$$g(\varepsilon) = 3.4008\varepsilon^{1/6} + 0.40244\varepsilon^{3/4} + \varepsilon \tag{1.27}$$

Morgan compared the normalised displacement cross-sections over the neutron energy range 0.15 MeV to 5 MeV and showed that, as required, the new displacement cross-sections increased more rapidly with energy than in the Thompson-Wright model. Calculations due to Jenkins (1970), who used the ENDF/B nuclear data file and the Thompson-Wright model, apparently showed the opposite effect in this neutron energy range, the lower energy neutrons being relatively more damaging and the high energy neutrons less damaging than the original Thompson-Wright model. The source of the discrepancy must lie in the nuclear data and its treatment. All of the ratios lie within the range 0.9 to 1.2. The displacement cross-section for 14.1 MeV neutrons, the source energy for D-T reactions, obtained by Morgan is 254×10^{-24} cm^2.

It has been demonstrated that for a very general class of scattering potentials for atom-collisions, the mean number of displacements is given by

$$\overline{\nu}\left(E_p\right) = \beta\left(\frac{E_D}{2E_d}\right) \text{ for } E_D >> 2E_d \tag{1.28}$$

where β is known as the "displacement efficiency" and which allows for deviations from hard-sphere scattering and rapid local interstitial-vacancy recombination. Sigmund (1969) demonstrated that the displacement rate is largely determined by the collision cross-section at low energies and that an appropriate value for β is 0.8, independent of material or primary knock-on energy. This factor obviously does not affect relative damage rates. Inclusion of the displacement efficiency in the Lindhard model is known as the Norgett/Robinson/Torrens or NRT model. $\overline{\nu}(E_p)$ calculated using this model is shown in Fig. 1.5. Genthon (1972) showed that the relative damage rates in fission based systems calculated using the Lindhard model were very little different from those calculated using the Thompson-Wright model, the latter being in slightly better agreement with experiment.

The information available on energy loss and the comparison of experimental and theoretical damage rates show that the Lindhard model overestimates the electronic energy loss (and hence underestimates the energy loss due to collisions) at high primary energies. This is apparently true for the Thompson-Wright model also.

The Lindhard model and its developments are clearly more suitable for damage calculations on fusion systems and have been applied by Robinson (1969), Morgan (1974b) and Gabriel et al. (1976). Strictly speaking it is unsatisfactory for carbon recoils with energies greater than 3.2 MeV (or collisions with neutrons of energy greater than ~11 MeV) due to inelastic effects.

Adamson (1987) has examined application of the Lindhard model to 14.1 MeV neutrons and a typical fusion reactor spectrum. The neutron cross-sections for elastic, inelastic and (n,α) reactions were processed from the Fine Group Library (FGL5) at the Atomic Energy Establishment, Winfrith Heath, UK for the 14.1 MeV neutrons. (Actually three energy groups in the range of neutron energies 13.78–14.44 MeV of equal lethargy interval.) The average carbon

atom recoil energies were calculated as well as the displacement cross-sections. It was found the (n,a) reaction contribution was ~25% of the total cross-section. This is because

(i) The recoil energy from the (n,a) reaction is large in relation to that from the scattering reactions (~3 MeV as against 1 MeV) and the fraction of the energy lost in inelastic collisions in the lattice is consequently large.
(ii) The recoil energy from the (n,a) reactions has a significantly smaller mass than the C_6 nucleus, leading to an increased energy loss to electronic processes.

The existence of other reactions such as (n,d), (n,2n) and (n,p) were ignored. Adamson (1987) found that the displacement cross-section for neutrons of average energy 14.1 MeV was 271.1×10^{-24}cm^2, using the same displacement energy of 60 eV. Table 1.7 compares the calculations of Adamson, Robinson, Gabriel et al., Morgan, and Huang and Ghoniem (see later).

TABLE 1.7. COMPARISON OF THE DISPLACEMENT CROSS-SECTION FOR 14.1 MeV NEUTRONS IN GRAPHITE

Source	Reactions included	dpa/n.cm^{-2}
Robinson (1969)	(n,2n)	2.34×10^{-22}
Morgan (1974b)	(n,a)	5.18×10^{-22}
Gabriel et al. (1976)	(n,a)	3.76×10^{-22}
Adamson (1987)	(n,a),(n,n')	2.71×10^{-22}
Huang and Ghoniem (1993)	(n,a),(n,p),(n,γ)	4.9×10^{-22}

Three of the results are similar, but both Morgan's and Huang and Ghoniem's are significantly higher, even when, as here, they have been corrected for the difference in E_d and the displacement efficiency. The reasons for these differences are not clear but must lie in the treatment of the cross-sections. The degradation of the spectrum in real fusion systems due to scattering almost certainly diminishes the differences in comparable dpa calculations.

Huang and Ghoniem (1993) developed a model in which the electronic energy loss treatment was improved. Comparison of the energy losses of carbon ions in carbon with the Lindhard model showed that the losses were overestimated for moving atom energies > MeV. For substantially greater energies (>8 MeV) the Bethe-Bloch theory is appropriate (Bethe, 1930; Bloch, 1933), for which energy loss rates decrease with increasing energy. Huang and Ghoniem show that a good fit to the energy loss data given by Northcliffe and Schilling (1970) may be obtained using an empirical method due to Biersack and Haggmark (1980). These authors propose that the energy loss rate S_e is given by:

$$\frac{1}{S_e} = \left(\frac{1}{S_e}\right)_L + \left(\frac{1}{S_e}\right)_{B-B} \tag{1.29}$$

where $(1/S_e)_L$ is the reciprocal of the energy loss rate obtained from the Lindhard model and $(1/S_e)_{B\text{-}B}$ is the reciprocal of the energy loss rate obtained from the Bethe-Bloch treatment.

Huang and Ghoniem compare the primary carbon recoil spectra in a number of neutron spectra obtained from both fission and fusion systems allowing for (n,a),(n,p) and (n,γ) reactions. There are considerable differences in the spectra for primary energies greater than 1 MeV. The fraction of the primary knock-on energy dissipated in atomic displacements is found to fall

smoothly from unity at an energy of 10^{-4} MeV to 0.03 at an energy of 10 MeV. The displacement cross-section for 14 MeV neutrons estimated from Fig. 8 of the paper is found to be 18×10^{-22} cm^2 for E_d = 16.3 eV, or 4.9×10^{-22} dpa/n.cm^{-2} corrected to E_d = 60eV and β = 0.8 (the latter correction may not be appropriate), roughly in line with the other estimates. The differences merit a careful examination of cross-section data at the higher energies.

The relative damaging power of the high-energy neutrons must eventually be determined experimentally. The only attempt known to the author was made by Gray and Morgan (1979). The problem is difficult because only very low fluxes of mono-energetic neutrons are available and thus it is necessary to use properties which are very sensitive to radiation damage. It was known (see Chapter 5) that the basal shear elastic modulus of highly oriented pyrolytic graphite was extremely sensitive to radiation damage, changes being detectable at neutron doses of ~10^{14} n.cm^{-2}, which can be measured as changes in the sonic velocities in the graphite, with appropriate polarisation and direction. Gray and Morgan irradiated samples in three very different neutron spectra:

(i) The Medical Research Reactor at Brookhaven National Laboratory (USA) which has a typical, well-thermalised fission neutron spectrum, with a peak at ~1.5 MeV.
(ii) The rotating target neutron source at the Lawrence Radiation Laboratory which has a D-T fusion neutron source spectrum which is practically constant at ~15 MeV.
(iii) The deuterium-beryllium neutron source at the University of California (Davis) which produces a neutron spectrum intermediate between (i) and (ii), peaking at about 5.5 MeV, but with a distribution of energies of about one order of magnitude.

Three grades of highly oriented pyrolytic graphite were exposed in each facility at temperatures between 15 and 30°C, together with appropriate flux monitors to measure the neutron dose. Changes in the measured shear modulus as a function of neutron dose with energy >50 keV showed changes increasing in the order 15 MeV >5.5 MeV >1.5 MeV, apparently demonstrating the greater damaging power of the higher energy neutrons.

The relative changes in shear modulus/unit dose were averaged for the three grades of highly oriented material up to fractional changes less than 1.6 in the shear modulus, where changes were linear with dose. The SAND-II computer program is able, given an initial guess, to estimate a neutron spectrum from the activation of an appropriate series of flux monitors or, given relative damage rates in well-differentiated spectra, the damage cross-section as a function of neutron energy. (Note: because this is based on property changes, it need not be the same as the displacement cross-section.) Given atomic displacement models as trial guesses, the damage function generated apparently shows that much greater damage is generated by the high energy neutrons than predicted by the atomic displacement models.

There are therefore two separate pieces of evidence that high-energy neutrons are more damaging than anticipated from displacement models. The Morgan-Gray experiments are however open to three criticisms:

(i) The rate of change of the elastic modulus of graphite is very sensitive to the irradiation temperature (Simmons, 1965) for temperatures close to ambient and no correction has apparently been made for this.

(ii) The damage obtained in irradiation experiments around room temperature anneals significantly at ambient and the observed changes should be corrected to the end of the experiment in each case.
(iii) A very significant displacement rate effect would be expected because of the strong dependence on irradiation temperature.

In a subsequent paper by Gray and Thrower (1979) the annealing of the modulus changes was discussed in detail. It was assumed that a sample with an initial shear modulus C_0 was irradiated to give a new value C_i, which after a long period of time tended to a value $C_¥$ asymptotically. The decay was assumed to be given by

$$C = \left(C_i - C_\infty\right)\exp\left[-\alpha t\right] + C_\infty \qquad (1.30)$$

where a may depend on the irradiation temperature.

The three grades of graphite examined show different values of C_0 and different values of C_i and C_∞, the latter because of exposure to different doses. However, all samples irradiated in the same facility fall on a single curve if plotted as $C/(C_\infty - C_0)$ - this is accounted for by noting that a fixed fraction of the shear modulus changes can be annealed at room temperature, independent of the dose or grade of graphite. The value of C_∞ was taken to be that at the largest value of the time, always greater than 190 days. (This was confirmed by additional annealing studies.) It was found that the fraction of the modulus change which could be annealed at room temperature varied between the three neutron energies - that is 0.40, 0.25 and 0.22 for the 14.8, 5.5 and 1.5 MeV irradiations, corresponding to a values of 3×10^{-3}, 14×10^{-3} and 37×10^{3}/day.

The possibility was examined that mechanical handling of the samples could be a source of changes in the shear modulus and some effects were found. Transmission electron microscopy showed defects, in the form of small interstitial atom clusters $<15 \times 10^{-8}$ cm in diameter, which did not show any change in the process of annealing, thus demonstrating that even smaller defects are involved in the shear modulus changes and the annealing.

The current situation appears to be that it is possible in fission reactor systems to estimate the relative damage rates in different reactor spectra with an accuracy adequate for design - that is data taken in one spectrum can be used to predict behaviour in another, provided that proper consideration is given to the existence of rate effects. The situation with respect to fusion reactor spectra is more complex — quite large differences exist in displacement cross-sections for high energy neutrons estimated by different authors, and thus damage estimates in spectra dominated by source neutrons are not likely to be very accurate. The situation is much better in the substantially degraded spectra which are likely to be found in most of the components of a fusion reactor.

The work of Gray and Morgan (1979) has demonstrated that it is possible to carry out experimental studies of the damage function using available high-energy neutron sources. It is clear that further experimental and theoretical studies are necessary, taking care to control the experimental temperatures and to either control the post-irradiation temperatures to prevent annealing or make post-irradiation measurements which permit correction of properties to the

end of the irradiation. This work needs to be undertaken and should include measurements of the transmutation levels.

The current recommendations for the expression of damage dose, due to the IAEA (1972), are to give the fission neutron dose which will produce the number of displacements estimated for the experiment using the Thompson-Wright damage model. This dose bears a constant relationship to the DIDO Equivalent Dose, which is most generally used (see Table 1.6). It is clear that while the use of dose units based on neutron flux with energies greater than a particular value is not likely to be correct in fusion systems, particularly near the sources, it would be a more modern approach in line with other materials to use a scale expressed in displacements/atom. (It should also be noted that it is quite common in discussion of damage rates in fusion reactor systems to express the neutron flux in terms of the thermal loading, that is in MW/m^2, one unit corresponding to a flux of 4.4×10^{13} $n.cm^{-2}$ of 14.1 MeV neutrons, which using the calculations by Adamson (1987) corresponds to 0.4 displacements/atom/year.)

At this point we turn to the question of the data which are used to evaluate displacement models, and changes which have occurred since the formulation of the Thompson-Wright model and the Lindhard model.

A considerable amount of information has been obtained since the formulation of the Thompson-Wright model on the rate of energy loss of ions in solids. The electronic energy loss data have been summarised by Garnir-Monjoie et al. (1980) in the formula

$$S_e = \left(\frac{dE}{dx}\right)_e = k_2\left(\frac{E}{M}\right)^{k_1}\left[1-\exp\left(-k_3\left(\frac{E}{M}\right)^{-1}\right)\right]^{k_4} \tag{1.31}$$

where for $(dE/dx)_e$ in MeV/(mg.cm^{-2}) and (E/M) in MeV/amu, the constants k_1 to k_4 are given by

$k_1 = 0.5 + 1.8 \times 10^{-3}Z$
$k_2 = 0.8Z + 7.8Z^{1/2} - 3.9$
$k_3 = -2.3 \times 10^{-2}Z + 0.42Z^{1/2} - 0.37$
$k_4 = (2.4 \times 10^{-3}Z^2 + 1.12Z + 0.88)/Z$

Insertion of $Z = 6$ (appropriate to carbon) into Equation (1.31) leads to

$k_1 = 0.51$, $k_2 = 20$, $k_3 = 0.521$, $k_4 = 1.28$

and thence on conversion to units of eV/Å (1Å = 10^{-8}cm) leads to

$$\left(\frac{dE}{dx}\right)_e = 452\left(\frac{E}{12\times10^6}\right)^{0.51}\left[1-\exp\left(-\frac{6.25\times10^6}{E}\right)\right]^{1.28} \tag{1.32}$$

Comparison of the energy loss given by Equation (1.32) with the experimental data used in the Thompson-Wright model shows that it gives lower loss rates, but with a similar energy dependence, while at high energies it is in better agreement with experiment than the Lindhard model. The differences would increase the energy going into atomic displacement, particularly at

high energies where the effect is similar to the analysis of Huang and Ghoniem. However, no detailed evaluation has been made.

The high-energy neutrons characteristic of fusion sources produce transmutation effects to a much greater degree than in fission systems. In particular, transmutation to helium or other elements may have important effects on property changes. The effects of helium generation have been observed directly by Kelly and Mayer (1969), who studied the effects of substitutional doping with ^{10}B and ^{11}B on irradiation damage in a Materials Test Reactor facility with roughly equal thermal and fast neutron flux. In the samples doped with ^{10}B the thermal neutrons produce helium by the ^{10}B (n,a) ^{7}Li reaction and displacement damage due to the helium and lithium recoils. The helium particle production mimics the helium generation due to ^{12}C (n,n')3a reactions (but also produces lithium). Samples of Ticonderoga flake doped with ^{10}B and ^{11}B concentrations in the range 30ppm to 10^4ppm were irradiated at temperatures of 650°C and 900°C. Electron microscope studies of the flakes did not reveal any helium bubbles, but samples containing 1.4%^{10}B irradiated at 650°C showed a huge expansion parallel to the hexagonal axis direction due to the exfoliation of packets of layer planes rather similar to that produced by heating the bromine residue compounds (Martin and Brocklehurst, 1964). These effects were not observed in the ^{11}B samples or the 0.5% ^{10}B samples under the same conditions. The implication of this result may well be that if the helium production rate is high enough and its diffusion rate (presumably parallel to the basal planes) low enough, bubbles will nucleate homogeneously and grow as helium is added, producing eventual exfoliation. Kelly and Mayer estimate that the helium and lithium products of the (n,a) reaction produce 69 and 121 displacements (E_d = 60 eV) for recoil energies of 1.53 MeV and 0.87 MeV respectively.

It is clear that neutron irradiation effects are actually characterised by more than one number, that is at least displacements and helium generation, while currently only the first is considered, and there is no experimental evidence for effects due to the latter. The calculation of displacement rate is less accurate for high-energy neutrons and further experimental studies are desirable.

Recently, experimental data obtained from irradiation of materials for possible use in fusion reactors have had their doses expressed as displacements/atom, calculated using the Thompson-Wright method (Burchell and Eatherly, 1991). The relationship with Equivalent DIDO Nickel Dose is

$$1 \text{ dpa} = 7.62 \times 10^{20} \text{ n/cm}^2 \text{ (EDN)}$$

It is highly desirable that a better absolute displacement rate scale should be achieved, which requires further studies of the displacement energies, particularly the angular and temperature dependencies. The best representation of the electronic energy loss data and neutron cross-sections requires agreement and proper allowance made for inelastic and anisotropic scattering. Calculations for a particular irradiation should also give best estimates of the transmutation rates, particularly the production of helium. It would be sensible for all future data to be expressed on a displacement scale using an agreed set of input data (conditional on transmutation effects being unimportant).

REFERENCES TO CHAPTER 1

ADAMSON, J. (1987), Atomic Displacement Cross-Sections in Graphite for Neutrons of 14 MeV, UKAEA Report AEEW-R 2132.

BELL, J.C, BRIDGE, H., COTTRELL, A.H., GREENOUGH, G.B., REYNOLDS, W.N., SIMMONS, J.H.W. (1962), Phil Trans. Roy. Soc. A, 254, 361.

BETHE, H. (1930), Ann. Physik, 5, 325.

BIERSACK, J.P. and HAGGMARK, L.G. (1980), Nuclear Instruments and Methods, 174, 257.

BIRCH, M. AND BROCKLEHURST, J.E. (1987), A Review of the behaviour of graphite under the conditions appropriate for protection of the first wall of a fusion reactor, UKAEA Report ND-R-1434(S).

BLOCH, F. (1933), Ann. Physik, 16, 285.

BRIDGE, H., GRAY, B. S., KELLY, B.T. and SØRENSEN, H. (1963), Proc. Int. Conf. on Radiation Damage in Reactor Materials, Venice 1962, 3, 531. IAEA Vienna.

BROCKLEHURST, J.E, KELLY, B.T. AND GILCHRIST, K.E. (1981), Extended Abstracts 15th Biennial Conference on Carbon, p546.

BURCHELL, T.D. AND EATHERLY, W.P. (1991), J. Nuclear Materials, 179, 205.

DE HALAS, D. (1962), See Nuclear Graphite (Ed. R.E. Nightingale), Academic Press.

EGGEN, D.T. (1950), Report NAA-SR-69.

EVERHART, E., STONE, G. and CARBONE, R.J. (1955), Phys. Rev., 99, 1287.

FASTRUP, B., HVELPLUND, P. AND SAUTTER, C.A. (1966), Mat. Fys. Medd. Dan.Vid.Selsk.,35,No.10.

GABRIEL, T.A., AMBURGEY, J.D. AND GREENE, N.M. (1976), Nucl. Sci. & Eng., 61, 21.

GARNIR-MONJOIE, F.S., GARNIR, H.P., BAUDINET-ROBINET, Y. AND DUMON, P.D.J. (1980), Physique, 41,599.

GENTHON, J.P. (1972), EUR 4867f, Joint Nuclear Research Centre.

GRAY, B.S. and THORNE, R.P. (1968), J. BRIT. Nuclear Energy Soc., 7, 91.

GRAY, W.J. and MORGAN, W.C. (1979), J. Nuclear Materials, 85 & 86, 237.

GRAY, W.J. and THROWER, P.A. (1979), J. Nuclear Materials, 87, 200.

HUANG, H. and GHONIEM, N. (1993), J. Nuclear Materials, 199, 221.

INTERNATIONAL ATOMIC ENERGY AGENCY. Specialists Meeting on Radiation Damage Units for Graphite, Seattle(1972) (See Morgan, 1974a.).

IWATA, T. and NIHIRA, T. (1966), Physics Letters, 23, 631.

IWATA, T. and NIHIRA, T. (1971), J. Phys. Soc. Japan, 31, 1761.

JENKINS, J.D. (1970), Nucl. Sci. & Eng., 41, 155.

KELLY, A. and MAYER, R.M. (1969), Phil. Mag., 19, 701.

KENNEDY, C.R. and EATHERLY, W.P. (1981), Extended Abstracts 15th Biennial Conference on Carbon, p552.

KINCHIN, G.H. and PEASE, R.S. (1955), Rep. Progress in Physics, 18, 1.

KNIPP, J. and TELLER, E. (1941), PHYS. Rev., 59, 659.

LINDHARD, J., NIELSEN, V., SCHARFF, M. and THOMSEN, P.V. (1963), Mat. Fys. Medd. Dan. Vid. Selsk., 33, No.10.

LUCAS, M.W. and MITCHELL, E.W.J. (1964), Carbon, 1, 345.

MARTIN, W.H. and BROCKLEHURST, J.E. (1964), Carbon, 1, 133.

MARTIN, W.H. and PRICE, A.M. (1967), J. Nuclear Energy, 21, 359.

MONTET, G.L. (1967), Carbon, 5, 19.

MONTET, G.L. and MYERS, G.E. (1971), Carbon, 9, 179.

MORGAN, W.C. (1974a), Nuclear Technology, 21, 50.

MORGAN, W.C. (1974b), J. Nucl. Mater., 51, 209.

MOTT, N.F. and MASSEY, H.S.W. (1949), The Theory of Atomic Collisions. Oxford, p271.
NIGHTINGALE, R.E. (1962), Nuclear Graphite. Academic Press.
NORTHCLIFFE, L.C. and SCHILLING, R.F. (1970), Nuclear Data Tables A7, p233.
OHR, S.M., WOLFENDEN, A. and NOGGLE, T.S. (1972), Electron Microscopy and the Structure of Materials(Ed. G. Thomas). Univ. of California Press.
ORMROD, J.H. and DUCKWORTH, H.E. (1963), Can. J. Phys., 41, 1424.
PORAT, D.I. and RAMAVATARAM, K. (1961), Proc. Phys. Soc., 77, 97.
PRIMAK, W. (1956), Phys. Rev., 103, 1681.
ROBINSON, M.T. (1969), BNES Nuclear Fusion Reactor Conference, Culham.
Paper 4.3, p364.
SIGMUND, P. (1969), Radiation Effects, 1, 15.
SIMMONS, J.H.W. (1965), Radiation Damage in Graphite. Pergamon Press.
THOMPSON, M.W. and WRIGHT, S.B. (1965), J. Nuclear Materials, 16, 146.
THROWER, P.A. and MAYER, R.M. (1978), Phys. Stat. Sol.(a), 47, 11.
WRIGHT, S.B. (1962), Radiation Damage in Solids, 2, 239. IAEA Vienna.
WRIGHT, S.B. (1965), A Calculation of the Carbon-Atom Displacement Rate in the BEPO Core and Reflector, UKAEA Report AERE-M 1548.
ZIJP, W.L. and RIEFFE, H. (1972), CH. RCN-161. Reactor Centrum Nederland,
The Hague, Netherlands

CHAPTER 2

THE STRUCTURE AND MANUFACTURE OF NUCLEAR GRAPHITE

The crystal structure of graphite was one of the first to be determined by X ray methods (see Kelly, 1981). It consists of hexagonal net planes of carbon atoms with nearest neighbour spacing in the planes of 1.42×10^{-8} cm. The net planes are stacked in ..ABABA. sequence with a spacing between the net planes, in perfect crystals, of 3.3535×10^{-8} cm. The crystal structure is shown in Fig. 2.1.

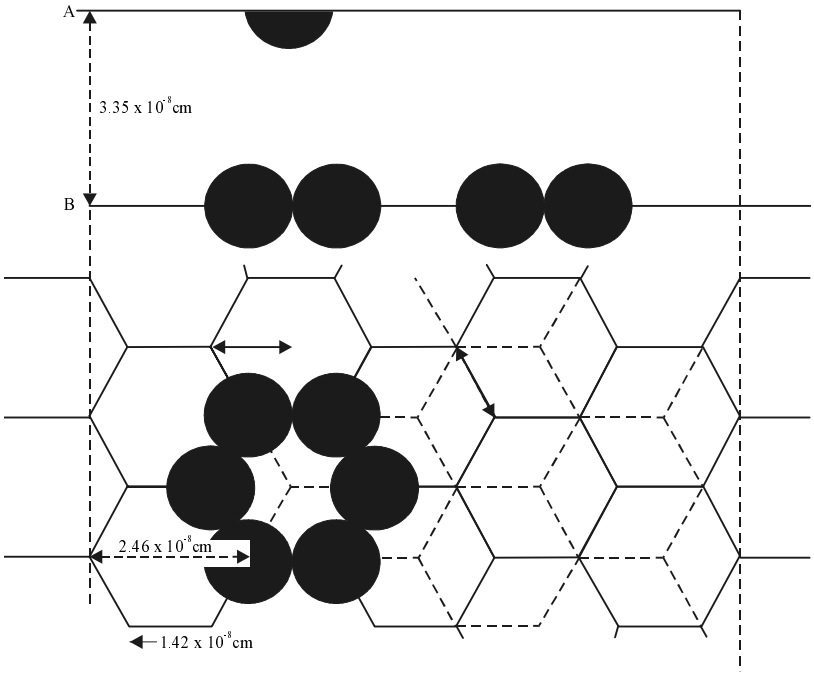

FIG. 2.1. The structure of graphite layer A is displaced relative to layer B by the vector shown. Important lattice directions and planes are marked.

The crystallographic unit cell contains four atoms and has symmetry D_h. The most perfect graphite crystals are found in nature, but these are generally small, perhaps at most ~1 cm across the basal planes and ~1 mm thick. The most common source of such samples for experimental studies is the Lead Hill lead mine at Ticonderoga in New York State, USA — generally known as "Ticonderoga Flake". The flakes are found embedded in a matrix of pyroxene or calcite. Each flake consists of several crystallites delineated by twins. (For a discussion of twinning, see Kennedy (1960).) The crystals may be extracted and purified using alternating treatments with hydrofluoric acid and hydrochloric acid. The final purification is carried out by heating at ~3000°C in flowing chlorine or 1500°C in a vacuum. A particular problem arises with boron which can take up substitutional positions in the graphite lattice and which can be transferred from graphite components in the high temperature furnaces to the flakes undergoing purification.

The majority of graphites of interest in the application to fission and fusion systems are considerably less perfect than single crystals. The imperfection is visible as an increased interlayer spacing (or *d*-spacing) and an increase in the width of the X ray lines and the disappearance of many. The ABAB stacking system is lost, the crystallites becoming “turbostratic” (see later). At the least perfect end of the structural spectrum exhibited by carbons

only the {00*l*} and {*hk*} reflections are found, the former resulting from parallel stacks of layer planes and the latter two-dimensional reflections resulting from the hexagonal structure in the individual layer planes. A major literature exists on the interpretation of the X ray patterns of carbons. The simplest (and technologically useful) interpretation of the patterns is to give the *d*-spacing and the apparent crystal sizes parallel and perpendicular to the basal planes (known as L_a and L_c respectively). The X ray reflections corresponding to three-dimensional ordering appear and develop as the perfection increases. The {00*l*} peaks move to high angles as the *d*-spacing decreases and {*hkl*} peaks appear. For many technical purposes a measurement of the *d*-spacing and the apparent crystallite size is adequate. Virtually all of the carbons and graphites of relevance to the nuclear industry are prepared by heat treatment of carbon-based raw materials (liquid or gas) to give a solid, the perfection of which is then improved by heat treatment at high temperatures, or "graphitising". The degree to which the perfection can be improved depends upon the starting material and in some cases little improvement is obtained by heat treatments up to 3000°C, while in other cases perfection approaching that of small good single crystals can be obtained. The graphitisation process is unusual in that it extends over a very wide range of heat treatment temperatures, although there is some reason to believe that for a given starting material a limiting perfection can be achieved which could only be improved at higher temperatures than currently available (>3000°C).

X ray measurements can yield only a few average measures of perfection and they are generally interpreted using simple models. Warren (1941) formulated a "turbostratic" model based on X ray observations in which it was assumed that the disordered carbons consist of near perfect segments of graphite planes, but without correlation between adjacent layers. The relative displacements of layers may be translations or rotations. This model has been applied to a wide range of materials by Warren (1941), Franklin (1951a, 1951b) and Bacon (1950, 1951). If the parameter *p* is defined as the probability of a stacking error between adjacent planes then according to Wilson (1949) the angular breadth of the {*hkil*} reflections is given by

$$\beta = \frac{\lambda^2 lp}{c^2 \sin 2\theta} \tag{2.1}$$

where λ is the X ray wavelength, *c* the crystallographic unit cell size, and θ the diffraction angle. According to Bacon (1950,1951) $p = c/t$ where *t* is the thickness over which carbon planes are regularly stacked, as defined by Hofmann and Wilm (1936). The latter authors defined *H* as the height over which layers are parallel ($H>>t$). The value of *H* must be obtained from {00*l*} reflections and *t* from {*hkl*} reflections. Hendricks and Teller (1942) obtained a more exact formula relating *p* to the intensity of reflection, that is:

$$I = \frac{1-(1-p)^2}{1+(1-p)^2-2(1-p)\cos \pi l} \tag{2.2}$$

which was applied to $\{11\bar{2}l\}$ lines by Franklin (1951a) and Bacon (1950, 1951) to obtain *p* values. The same formula applies to diffraction lines for which normal and rhombohedral stacking are indistinguishable, that is $h - k = 3n$, where $n = 0,1,2...$. Equation (2.2) fits the diffraction line shapes well and a relationship was found between *p* and the interlayer spacing *d* over a wide range of carbons. For perfect graphite $p = 0$ and $d = 3.3535 \times 10^{-8}$ cm, while for fully turbostratic materials $p = 1$ and $d = 3.440 \times 10^{-8}$ cm. Bacon (1950, 1951) summarised his studies and those of Franklin in the equation

$$d = \left(3.440 - 0.086\left[1 - p\right] - 0.064p\left[1 - p\right]\right) \times 10^{-8} \text{ cm} \qquad (2.3)$$

valid for $p < 0.4$, and

$$d = \left(3.440 - 0.086\left[1 - p^2\right]\right) \times 10^{-8} \text{ cm}$$

valid for $p > 0.4$.

An explanation of these results was proposed based on the assumption that various interlayer spacings were due to various combinations of layer translations, such as

(i) Between two perfectly oriented layers; $d = 3.354 \times 10^{-8}$ cm.
(ii) Between two misoriented layers with adjacent misoriented layers on either side; $d = 3.440 \times 10^{-8}$ cm.
(iii) Between two misoriented layers, one of which is adjacent to an oriented layer; $d = 3.408 \times 10^{-8}$ cm.
(iv) Between two misoriented layers with neighbouring oriented layers; $d = 3.376 \times 10^{-8}$ cm.

It is well known that good crystalline graphites contain a proportion of a rhombohedral phase, that is one in which the hexagonal net planes are stacked in ABC sequence rather than the normal ABAB sequence. The proportion of the rhombohedral phase can be increased by grinding (Bacon 1950, 1951) which also increases p and decreases H.

These studies and the consequent simple correlations between parameters have been replaced in more modern work associated with Ergun, Ruland and Méring. In essence all of these authors postulated that defects in the crystallite were responsible for the X ray patterns. Ergun and Tiensuu (1959) suggested that where it appeared necessary to invoke scattering from amorphous carbon to explain the diffraction pattern of poorly graphitised materials, as in Franklin's (1951a, 1951b) studies of polyvinylidene chloride char, it might be preferable to assume that a proportion of the atoms were tetrahedrally bonded rather than the normal triagonally bonded. It was demonstrated that the diffraction peaks from small tetrahedrally bonded structures can coincide with the two-dimensional graphite layer reflections {10} and {11}. Kakinoki *et al.* (1960) and Kakinoki (1963) reached a similar conclusion.

Analysis of different {00*l*} reflections in carbons of low perfection yields different values for L_c. This was interpreted by Ruland (1968), for instance, as showing that there was a distribution of interlayer spacings. A similar assumption may be made concerning a distribution of the nearest neighbour (in-plane) spacings, assuming that both distributions are Gaussian with mean square deviations Δ^2_{xx} parallel to the layers and Δ^2_{zz} perpendicular to the layers. The value of Δ^2_{zz} is obtained from {00*l*} lines, and with this knowledge Δ^2_{xx} may be obtained from lines with integer values of (*h*-*k*)/3. The fractional number α of rhombohedral stacking faults is obtained from the lines with non-integer values of (*h*-*k*)/3. Ruland (1965) examined carbons derived from three starting materials: acenaphthylene, bifluorenyl and tetrabenzonaphthalene; and also re-examined the earlier work of Franklin (1951a, 1951b), Bacon (1950,1951), Houska and Warren (1954), Maire and Méring (1957), and Méring and Maire (1960). A remarkable correlation was obtained between the average value of the interlayer spacing and Δ^2_{xx} :

$$\bar{d} = \left(3.353 + 0.425\Delta^2_{xx}\right) \times 10^{-8} \text{ cm} \qquad (2.4)$$

A relationship was also found between $\bar{d}$ and Δ^2_{zz}, although the scatter was greater. In this work the value $\bar{d} = 3.44 \times 10^{-8}$ cm had no special significance, it corresponded only to a value of Δ_{xx} which did not perturb the diffraction lines significantly. The correlation obtained between $\bar{d}$ and α indicated that hexagonal layer stacking is preferred only when $\bar{d}$ is less than 3.38×10^{-8} cm. No explanation of these correlations has been attempted. Recently Bragg and co-workers (Tidjani *et al.*, 1986; Aladekomo and Bragg, 1990) have suggested that particular values of the *d*-spacing are preferred which can be observed in the course of graphitisation, grinding and irradiation damage. These spacings, 3.375, 3.40, 3.44 and 3.55×10^{-8} cm, presumably correspond to particular defect states, but no identification of these states has been made.

Maire and Méring (1957) concluded that ordering parallel to the hexagonal axis was due to the interactions with neighbouring layers. The relationship between $\bar{d}$ and p was considered to be due to an intrinsic defect structure of the layer planes, specifically that each layer possessed interstitial carbon atoms bonded to the surfaces. Adjacent layers possess defects which are not correlated and which produce the observed misorientations. A parameter g was defined as the fraction of perfect layer surfaces. This assumption leads to

$$\bar{d} = gd + (1-g)d' \tag{2.5}$$

and

$$\Delta^2_{zz} = 2g(1-g)\varepsilon^2 + 2(1-g)\Delta^2 \tag{2.6}$$

where ε is the average of the difference between the layer spacings in the perfect and imperfect layers and Δ is the root mean square variation of ε. Ruland (1968) notes that the diffraction line shapes are well explained but the model is not very seriously tested.

Combination of the X ray observations which measure a few average parameters with modern transmission electron microscopy in which local parameters are observable reveals that virtually all carbons contain groups of layer planes with varying interlayer spacings and of various size. Increase in perfection occurs by straightening of layer planes and increasing uniformity, but it appears that while the defects are removed, no improvement is obtained in the basic size of layer planes, at least for heat treatment temperatures currently attained. The detailed nature of the defects in the basic layer structure of any particular carbon has not been determined as they are too small for direct observations. However the presence of defects in poorly crystalline carbons does, as we shall see, affect the accumulation of radiation damage under certain conditions.

Essentially all of the graphite employed in fission reactors as moderators and most, but not all, applications of graphite in fusion reactor systems use blocks manufactured from petroleum or pitch cokes. It is possible by variation of the coke, the binder and impregnant materials and the forming and final heat treatment processes to produce a wide range of initial properties and variation of behaviour under irradiation — an ability virtually unique to graphitic materials. Materials of this general type are known as Acheson graphites (after the inventor of the process) and it is produced by selecting an appropriate pitch or petroleum coke. These cokes may be produced industrially or from natural materials (asphalt).

The pitch is heated to a temperature of about 450°C which produces polymerisation and loss of volatiles. The initial liquid solidifies in the course of this process to produce a solid material typically containing ~95% carbon. Further heating increases the loss of volatiles. A

typical raw coke contains ~10% volatiles, 0.1–2.2% ash and 0.1–4.3% sulphur. The coke is broken down at the completion of the formation process and then calcined in large kilns at about 1300 °C to remove excess volatile matter and pre-shrink the coke to prevent excessive dimensional change later in the process. The standard requirement for graphite for use as the moderator in fission reactors is that of low neutron absorption, which implies careful selection of the original coke source to minimise impurities or the employment of a suitable purification process in the manufacture. High neutron cross-sections are associated with boron, europium, vanadium and titanium and in the early days of nuclear graphite production, before the adoption of purification processes, the selection of pure coke was very important. In the United Kingdom, for instance, petroleum coke was obtained from a plant in Holland which produced a very pure (particularly low boron) product with acceptable graphite properties. The use of various purification processes permit a much wider range of cokes to be used, although these processes have been restricted by environmental considerations related to the use of halogens. Following the calcination process the coke is crushed and ground to yield an appropriate particle size distribution for the chosen forming process and size of the final artefact. The largest graphite bodies may have diameters up to 120 cm and lengths of 4–5 m and contain very large coke particles. The usual sizes of graphite bricks for the nuclear industry are 1 m in length and about 20–50 cm in diameter produced by extrusion or moulding with particle sizes up to ~0.1 cm. The more modern cold isostatic pressing technique of manufacture uses much finer particle sizes of a few tens of microns. The selected particle size distribution is mixed with pitch with the appropriate properties to produce a plastic mass suitable for the forming process. The individual coke particles are irregular in shape, the shape being determined in part by the as-formed coke structure, such as the dimensions over which oriented layers of graphene-like structures occur, and the distributions of the wall thickness around bubbles in the coke. It is convenient in the description of the various cokes employed to manufacture conventional nuclear graphites to classify them as follows:

(i) Needle coke

This coke is usually based on the products of the petroleum industry and is widely used in the manufacture of electrodes for the metallurgical industry. Because of its availability and purity it was employed in the manufacture of the first graphite moderator materials in the development of nuclear fission reactors. The grinding process produces, in these cokes, acicular particles in which the planes of carbon atoms tend to lie parallel to the long axis of the particles, giving rise to significant anisotropy. Heat treatment of these cokes to high temperature produces well-crystallised materials with an apparent crystallite size parallel to the basal planes $L_{a,}$ as measured by X rays, of ~800×10^{-8} cm. Thermal conductivity measurements give rather larger values of about 3000×10^{-8} cm. Cokes of this type were employed in the Pile Grade A and Pile Grade B graphites developed in the United Kingdom and the KC and CSF graphites developed in the USA.

(ii) Pitch coke

This coke is produced by heat treatment of the higher molecular weight products of pitch production and leads to much more isometric particles than is the case for needle coke graphites, but with a high degree of internal orientation of graphene layers. The material graphitises well on heat treatment although the perfection is less for a given treatment than in the needle coke. Typical values for the crystallite size are 500×10^{-8} cm obtained by X rays and 2200×10^{-8} cm determined from thermal conductivity.

Two cokes with rather unusual structures have become important in the manufacture of nuclear graphites and are frequently referred to in the literature, these are:

(iii) Gilsonite pitch coke

This coke is prepared from a naturally occurring asphalt found in the Uintah basin of eastern Utah, USA. The ground-up coke, provided the particle size is not too small, has isotropic properties, containing spherical particulates with an onion skin structure, the graphene planes lying perpendicular to the particle radii. The spherical particles are surrounded by randomly oriented material and each particle, following graphitising, has a characteristic central pore. The grinding of the particles to sizes less than ~0.1 cm breaks up the spherical structures and loses the natural isotropy. The degree of final graphitisation of this coke is about the same as in the pitch coke graphites.

(iv) Santa Maria coke

This coke, like Gilsonite coke, leads to isotropic particles but with a quite different internal structure. The spherical structures have graphene layers which are radially oriented. The degree of final graphitisation is slightly less than in the pitch coke materials.

The mix of ground-up coke and pitch is then extruded, moulded or isostatically pressed into the desired shape. These "green" bodies are then baked to carbonise the binder pitch and produce the necessary rigidity in the artefact for handling. The baking, usually at temperatures in the range 750–900°C, is carried out with the artefacts packed in a granular electrically conducting medium, usually coke which permits expansion during heating and gives necessary mechanical support. The thermal conductivity of the contents of the baking furnace is low and the heating cycle may take 30–70 days. The baking cycle may volatilise up to 1/3 of the pitch binder content of the green bodies, which show a loss in density and an increase in permeability.

It is normal to increase the density of the artefact after the baking process by impregnation one or more times with a suitable pitch or other impregnant. Useful increases in density, Young's modulus and strength are obtained, as well as reductions in diffusivity and permeability. A large amount of empirical data exists within the industry for the effects of multiple impregnations with a range of hydrocarbons, both graphitising and non-graphitising. Large reductions in permeability and diffusivity can be obtained using furfuryl alcohol as an impregnant, which is non-graphitising. Pitches suitable for impregnation tend to have lower melting points and smaller benzene and quinoline insoluble fractions than binder pitches. The impregnant carbons must be suitably fluid at the impregnation temperatures. The final graphitisation of the carbon artefacts is carried out at temperatures in the range 2600–3000°C in an Acheson furnace. The carbon bricks are stacked in a conducting coke bed buried under insulating material. In modern

Space Group: $C6/mc(D_{6h}^4)$
Unit cell:
$a = 2.4612 \pm 0.0001$A
$c = 6.7079 \pm 0.0007$A
Volume = 35.190 A^3
Atoms per unit cell = 4
Crystal density = 2.266 g/cm^3

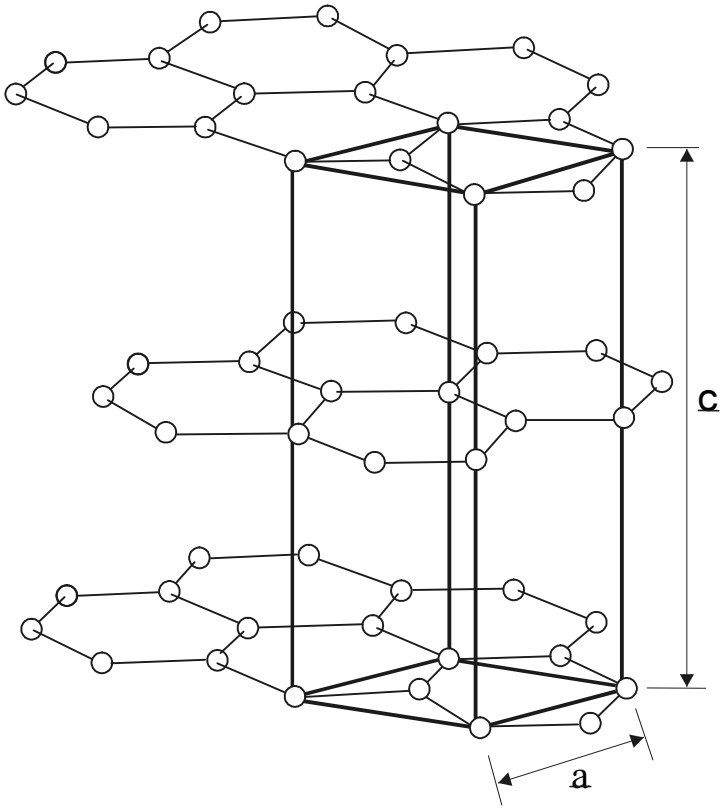

FIG. 2.2. Schematic illustration of graphitising furnace (not to scale).

plants the graphitisation furnaces are smaller with a well-defined firebrick boundary, rather than the poorly defined boundary of insulating sand, and this also permits arrangements for direct pyrometric measurements in the furnace. The older furnace types have often used the total power input as a measure of the final temperature reached. The general furnace arrangement is otherwise similar in that large electric currents are passed through the furnace from water cooled graphite electrodes at the ends of the furnace. Fig. 2.2 shows the cross-section of a furnace.

The heating cycle lasts up to about 15 days, after which the blocks are unpacked from the coke bed. The dimensions of the Acheson furnaces used for graphitising vary widely, but representative values are length 10–60 ft, width 4–12 ft and depth 3–6 ft. The power supply varies between 750 and 7500 kW, leading to a power consumption of 3–5 kWh/lb of graphitised carbon product.

The final products of this process vary considerably, for instance the extrusion process applied to a mix containing needle coke produces graphite bodies with anisotropic properties, the block possessing rotational symmetry about the extrusion axis. The early nuclear graphites, because they were based on already available electrode graphites, were all of this type. The properties of some of these are presented in Table 2.1.

The initial high anisotropy of the graphites used to build nuclear reactors led to many problems in their operation as doses increased, and as radiation effects became more clearly understood it was realised that it was possible to achieve a degree of control over the behaviour of the graphite under irradiation and hence achieve an increased life for graphite moderated reactors with a permanent structure. As we shall see, analysis of the experimental data, obtained

TABLE 2.1. PROPERTIES OF NEEDLE COKE BASED EXTRUDED NUCLEAR GRAPHITES

Country of origin	UK	USA	USA
Designation	Pile Grade A	CSF	KC
Coke	R-coke (Pernis)	Cleves Pet. coke Mid-Continental crude Gulf Oil, Cleves, Ohio Standard, med. hard	Kendal Pet. coke from Bradford, Penn. Refinery
Binder	Ford's pitch	Barrett coal tar pitch	
Impregnant	Catarex pitch	Coal tar pitch	
Final H.T.T.	2800°C	2800°C	2800 °C
Density (g/cm^3)	1.74	1.66	
Open pore volume	0.198		
Closed pore volume	0.01		
Thermal expansion coefficients (K^{-1}) (20–120 °C)			
Parallel to extrusion	0.9×10^{-6}	1.1×10^{-6}	0.9×10^{-6}
Perpendicular to ext.	2.8×10^{-6}	4.8×10^{-6}	5.5×10^{-6}
Electrical Resistivity (ohm-cm)			
Parallel to extrusion	0.62×10^{-3}	0.77×10^{-3}	
Perpendicular to ext.	1.10×10^{-3}	1.33×10^{-3}	
Thermal conductivity (W/m/K)			
Parallel to extrusion	200	167	
Perpendicular to ext.	109	113	
Young's modulus (GN/m^2)			
Parallel to extrusion	11.7	11	
Perpendicular to ext.	5.4	5	
Poisson's ratio	~0.07		
Strength (MN/m^2)			
Tensile Parallel	17		
Perpendicular	11		
Bend Parallel	19		
Perpendicular	12		
Compression Parallel	27		
Perpendicular	27		
Gas transport properties			
Diffusivity	13.6×10^{-3}		
Permeable flow parameters			
B_o (m^2) Parallel	712×10^{-16}		
Perpendicular	147×10^{-16}		
K_o (m) Parallel	108×10^{-9}		
Perpendicular	21×10^{-9}		

principally at that time in the USA and the United Kingdom, indicated that such a material should be as graphitic as possible, isotropic in properties and with an unirradiated thermal expansion coefficient chosen to give the best possible dimensional stability under irradiation (Kelly, Martin and Nettley, 1966; Eatherly, 1992). A variety of methods were used to produce isotropic graphites based on technology already known to the industry. In particular, in the United Kingdom, a specification was issued for a moderator graphite to be used in the Advanced Gas Cooled Reactor (UKAEA, 1965; Hutcheon, 1966) which was to employ a fixed moderator structure with a peak design dose of 1.55×10^{22} n/cm^2 (EDN) at a temperature of about 400°C. It was also necessary to minimise the rate of radiolytic reaction with the carbon dioxide coolant gas chosen for the reactor, which required control of pore structure parameters such as volume and size. A number of graphites were produced to this specification, two of them using the Gilsonite pitch coke already described which naturally leads to isotropic graphite. The properties are summarised in Table 2.2.

TABLE 2.2. PROPERTIES OF ISOTROPIC NUCLEAR GRAPHITES

Country of Origin	UK	USA	USA	USA	Japan
Designation	IMI-24	H-451	AXZ-5Q1	N3M	IG-110
Coke	Gilsonite	Mixed			Petroleum
Final HTT	~2800°C		>2500°C		
Density (g/cm^3)	1.81	1.73	1.5		1.78
Open pore volume	0.11				4.1×10^{-6}
Thermal expansion coefficients (K^{-1}) (20–120°C)	4.3×10^{-6}	4.0×10^{-6}	6.7×10^{-6}	5.0×10^{-6}	
Electrical resistivity (ohm-cm)	0.9×10^{-3}		1.7×10^{-3}		
Thermal conductivity (W/m/K)	131	140	80	180	78
Young's Modulus (GN/m^2)	10.8	8	8	6.5	10.2
Poisson's ratio	0.2	0.1–0.2			0.14
Strength (MN/m^2)					
Tensile	17.5	15	10	41	25.3
Bend	23	20			37.2
Compression	70				76.8
Gas transport properties					
Diffusivity	3×10^{-3}				
Permeable flow parameters					
B_o(m^2)	6.5×10^{-15}				
K_o(m)	5.8×10^{-9}				

An alternative method of producing isotropic graphite was to take an anisotropic graphite such as Pile Grade A, grind it up to an appropriate particle size, mix with pitch binder and mould or extrude and impregnate as in the normal process of manufacture. This technique, remarkably, produced graphite with properties similar to the Gilsonite based materials. In the USA an isotropic nuclear graphite was manufactured using a mixture of cokes, known as H-451. (The Gilsonite based materials were regarded as too expensive for use in a generation of High Temperature Reactors.) The properties of these isotropic graphites are also shown in Table 2.2.

The United Kingdom gas cooled reactors use cylindrical graphite sleeves on each fuel element which are an integral part of the element and hence loaded and unloaded with the fuel element. The performance required from these element sleeves is less arduous (~1/5 of the dose received by the moderator bricks) and it is possible to use pitch coke based graphites which are not quite isotropic, produced by extrusion rather than moulding, but otherwise similar in manufacturing method to the more isotropic conventional materials.

The advent of modern manufacturing techniques using much finer coke particle sizes with cold isostatic pressing in a rubber bag to form the green bodies has permitted manufacture of a wide range of isotropic graphites with very uniform properties and which may be used as moderator materials. As an example the Japanese are building a very high temperature reactor using the IG-110 grade of graphite. These materials provide much higher strengths, based on the fine particle size and much improved quality control. The properties are shown in Table 2.2.

A unique set of isotropic materials is manufactured by a process invented by the POCO company, although the details have never been revealed. These materials are very fine grain, implying an isostatic moulding process, have a high strength and a remarkably high thermal expansion coefficient of about $7–8 \times 10^{-6}°C^{-1}$ at ambient. The volume thermal expansion is very close to that of a graphite single crystal. The coke concerned is probably that known as the Santa Maria material already described (produced by the Pure Oil Company, the original parent company of POCO and known to produce similar but not identical graphites), and because the size of the pieces produced is limited to 50 cm a part of the process is probably related to "green coke" methods in which the removal of volatiles by calcination is deliberately reduced and the volatiles carbonised to assist in the formation of the bulk graphite. This type of graphite has always been regarded as too expensive for use in existing fission reactor systems but it has very good behaviour under irradiation and has been used as protective tiles for the first wall of fusion reactor systems.

The Oak Ridge National Laboratory has developed, in collaboration with the Great Lakes Carbon Co., a material known as Graphnol N3M with the objective of obtaining a long life under irradiation and suitable for use in fusion reactor systems (Kennedy and Eatherly, 1973; Edwards and Starrett, 1981). This material combines the "green coke" methods and pitch overcoating of coke particles of relatively small size. The properties are included in Table 2.2.

The major problems with the use of graphite to very high exposures to fast neutrons are associated with the very large crystal dimensional changes which occur and which show no signs of ceasing (in spite of the prayers and theories of many engineers and scientists!). The crystallite dimensional changes must be accommodated in the structure of the polycrystalline graphite and the mismatch between crystal strains and macroscopic strains eventually lead to the generation of porosity and weakening of the graphite to an unacceptable degree. Simple considerations suggest that this effect can be delayed under a given set of radiation conditions by varying the structure, but not prevented. It would be expected that small grain size, in order to limit the size of initial cracks, and gradual changes in orientation to reduce the local misfit strains would be advantageous. The Graphnol N3M material described was manufactured with these ideas in mind. A clear benefit is obtained for the graphite lifetime for irradiations above ~450°C.

A number of materials are referred to in this work which do not find extensive use in the fusion or fission systems but which are used to provide fundamental data on graphite behaviour. One of the most important of these is highly oriented pyrolytic graphite which is polycrystalline

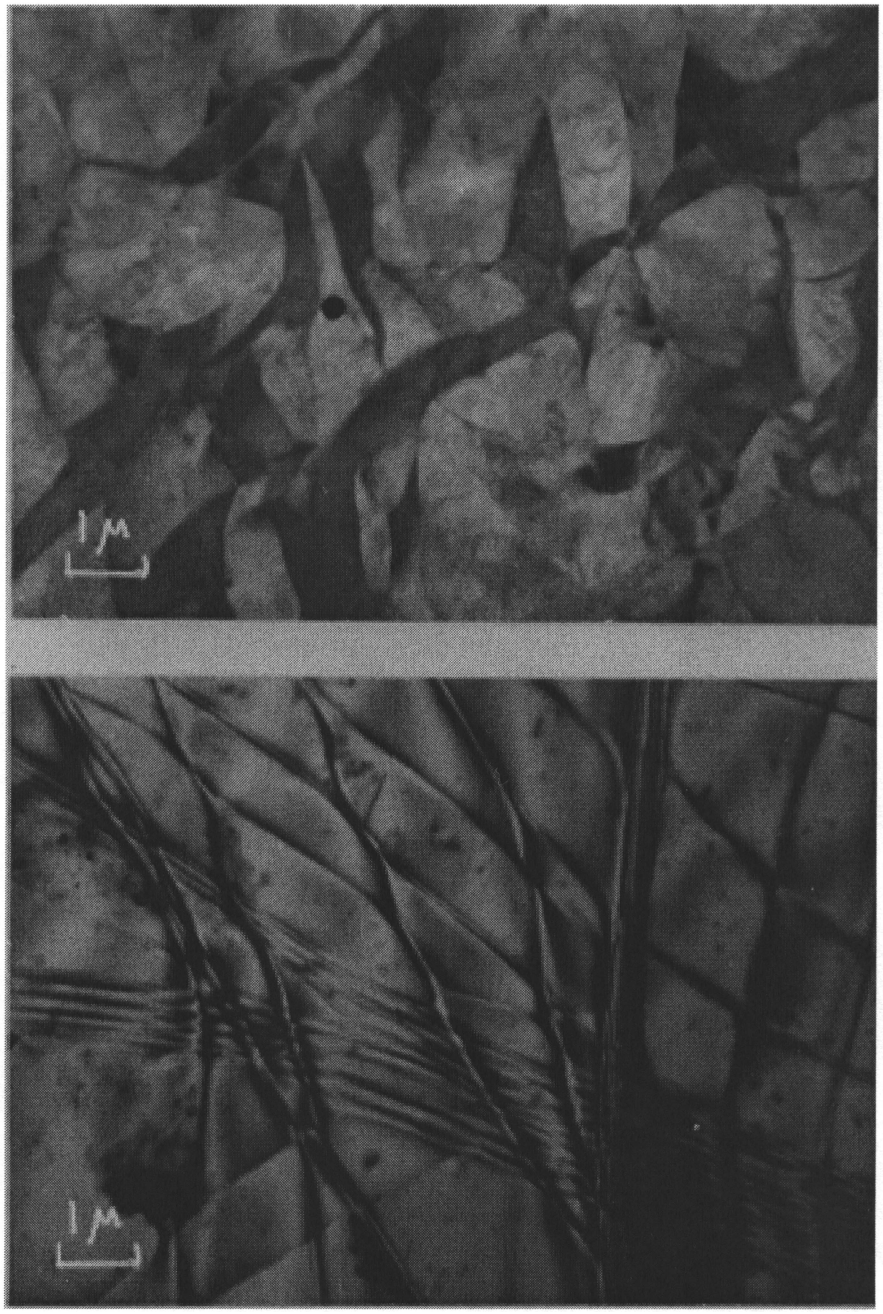

FIG. 2.3. Electron micrographs showing effect of heat treatment.

but possesses near theoretical density and a degree of orientation close to that of a single crystal, such that properties measured in two directions represent basal properties, and in the third direction those perpendicular to the basal planes of the component crystals (Moore, 1973). Highly oriented pyrolytic graphite is prepared by passing a hydrocarbon gas over a heated substrate of polycrystalline graphite. The gas chosen is usually methane and, by a suitable choice of flow rate and substrate temperature, deposits can be produced in the form of overlapping growth cones which are nucleated heterogeneously on the substrate surface. In particular the deposits obtained from methane at ~2000°C have a high density and a high degree of orientation, the basic graphene layers lying parallel to the surface except for some curvature due to the growth cone structure. The material is readily removed from the substrate and may then be treated in a variety of ways to improve the perfection to a controlled degree. In the United Kingdom practically all graphite irradiation experiments contain samples of highly oriented

pyrolytic graphite prepared by deposition at 2000°C–2200°C and then heat treated at 2800°C (Kelly, Martin and Nettley, 1966). The effect of crystallite size variation can be studied by varying the heat treatment temperature up to 3600°C. Alternative methods of varying the perfection of such materials have been devised, such as applying stress perpendicular to the deposition plane during heat treatment or a shear stress parallel to the deposition plane. However, the heat treatment method alone has proven to be best; the other methods improve the average crystallite size and orientation, but apparently introduce some misorientated regions which eventually give rise to some pore generation similar to the normal materials. Figure 2.3 shows the development of the structure with heat treatment temperature as observed with the transmission electron microscope. The β type material was heat treated at 2900°C and the γ type material was heat treated at 3300 to 3600°C. The material properties of highly oriented pyrolytic graphite are summarised in Table 2.3.

TABLE 2.3.PROPERTIES OF HIGHLY ORIENTED PYROLYTIC GRAPHITE

Density (g/cm^3)	2.250 to 2.266
Interlayer spacing (Å)	3.354 to 3.359
Electrical resistivity (ohm-cm)	
a-axis	$3.5 \text{ to } 4.5 \times 10^{-5}$
c-axis	0.15 to 0.25
Thermal conductivity (W/m/K)	
a-axis	1600 to 2000
c-axis	7 to 9
Thermal expansion (K^{-1}) (20–100°C)	
a-axis	-1×10^{-6}
c-axis	25×10^{-6}
Thermo-electric power (μV/K)	
a-axis	-5 to -10
c-axis	4 to 6
Magnetic susceptibility (emu/g)	
a-axis	$-0.2 \text{ to } -1 \times 10^{-6}$
c-axis	$-20 \text{ to } -22 \times 10^{-6}$

REFERENCES TO CHAPTER 2

ALADEKOMO, J.B., BRAGG, R.H. (1990), Carbon, 28, 897.
BACON, G.E. (1950), Acta Cryst., 3, 137.
BACON, G.E. (1951), Acta Cryst., 4, 558.
EATHERLY, W.P. (1992), Carbon 92, Arbeitkreis Kohlenstoff der Deutschen Keramischen Gesellschaft eV, p19.
EDWARDS, R.J., STARRETT H.S. (1981), Ext. Abstr. 15th Conf. Carbon, p508.
ERGUN, S. and TIENSUU, V.H. (1959), Acta Cryst., 12, 1050.
FRANKLIN, R.E. (1951a), Acta Cryst., 4, 253.
FRANKLIN, R.E. (1951b), Comptes Rendus, 232, 232 .
HENDRICKS, S. and TELLER, E. J. (1942), Chem. Phys., 10, 147.
HOFMANN, U. and WILM, D.Z. (1936), Elektrochem., 42, 504.
HOUSKA, C.R. and WARREN, B.E. (1954), J. Applied Physics, 25, 1503.
HUTCHEON, J.M. (1966), Graphite for AGR Power Stations, Paper 4, AGR Symposium, Frankfurt.
KAKINOKI, J. (1963), Proc. Fifth Biennial Carbon Conference, 2, Pergamon Press, New York, p499.
KAKINOKI, J., KATADA, K., HANAWA, T., INO, T. (1960), Acta Cryst., 13, 171.
KELLY, B.T. (1981), Physics of Graphite, Applied Science Publishers, London.
KELLY, B.T., MARTIN, W.H., NETTLEY, P.T. (1966), Phil. Trans. Roy. Soc. A, 260, 37 & 51.
KENNEDY, A.J. (1960), Proc. Phys. Soc., 75, 607.
KENNEDY, C.R. and EATHERLY, W.P. (1973), Ext. Abstr. 11th Conf. Carbon, p304.
MAIRE, J. MÉRING, J. (1957), Proc. Conf. Industrial Carbon and Graphite, London, p204.
MÉRING, J. and MAIRE, J. (1960), J. Chim. Phys., 57, 803.
MOORE, A.W., Chemistry and Physics of Carbon, 11 (Eds. P.L Walker, Jr
And P.A. Thrower),
MARCEL, DEKKER (1973), New York, p69.
RULAND, W. (1965), Acta Cryst., 18, 992.
RULAND, W. (1968), Chemistry and Physics of Carbon, 4 (Ed. P.L. WALKER, Jr), MARCEL, DEKKER, NewYork, p1
TIDJANI, M., LACHTER, J., KABRE, T.S., BRAGG, R.H. (1986), Carbon, 24, 447.
UKAEA. Report on the Life of the Graphite Core of the Advanced Gas Cooled Reactor, Emeléus Graphite Committee, UKAEA Report (1965).
WARREN, B.E. (1941), Phys. Rev. 59, 693.
WILSON, A.J.C. (1949), X ray Optics, Methuen, London.

CHAPTER 3

DIMENSIONAL CHANGES IN GRAPHITE AND THE THERMAL EXPANSION COEFFICIENT

Irradiation of graphite with energetic neutrons over a range of irradiation conditions leads to dimensional changes of considerable magnitude which must be accommodated in reactor design. The behaviour of graphite is regarded as being that of an aggregate of crystallites (including carbon-carbon composites), generally with identical properties. Irradiation experiments with energetic neutrons have been carried out at temperatures from 5 K to 1700 K. In each case it has been observed that the irradiated graphite crystals grow in the direction perpendicular to the basal planes and contract in the direction parallel to them, although the relative magnitudes of the changes depend upon the exposure conditions.

In a free graphite crystal it is possible to define two distinct measures of dimensional changes. The first is the change in the mean interatomic spacing parallel and perpendicular to the hexagonal axis (denoted by $\Delta d/d$ and $\Delta a/a$ respectively) measured by X rays (neglecting for the moment the deduction of the appropriate values from the measurements). The second is the change in dimensions of gauge lengths embedded in each crystallite parallel and perpendicular to the hexagonal axis (denoted by $\Delta X_c/X_c$ and $\Delta X_a/X_a$ respectively). These two measures of the dimensional change do not have to be the same. It is found that for all conditions

$$\frac{\Delta X_c}{X_c} \geq \frac{\Delta d}{d} \text{ and } \left|\frac{\Delta X_a}{X_a}\right| \geq \left|\frac{\Delta a}{a}\right|$$

the relationship between the two measures depending upon the type of lattice defects created in the irradiation. The lattice parameter changes can be measured, given sufficient material, but the crystal strains $\Delta X_c/X_c$ and $\Delta X_a/X_a$ can be measured on single crystals or highly oriented pyrolytic graphite samples, or deduced from the dimensional changes of ordinary polycrystalline graphite using a theoretical relationship between the macroscopic and microscopic dimensional changes.

In this chapter measurements of the changes in crystal lattice parameters and crystal strains are reviewed, followed by the dimensional changes observed in polycrystalline graphites subjected to extensive studies. The theory of the relationship between the macroscopic and microscopic changes is then presented and the application of these relations and their verification considered.

Application of X ray crystallographic methods to the measurement of irradiation damage in graphite was first reviewed by Bacon and Warren (1956) and Bacon (1959,1960). Unirradiated polycrystalline graphites as well as the more perfect crystals and highly oriented pyrolytic graphite show many lines in the diffraction pattern (Fig. 3.1). Exposure to neutron irradiation at about ambient temperature results in the diffraction lines becoming fainter and more diffuse until eventually only the {0002} and $\{10\bar{1}0\}$ lines can be used for measurement. The centres of the {000l} lines are displaced to smaller angles, as illustrated in Fig. 3.2, showing that the average interlayer spacing $\Delta d/d$ has increased, while the $\{10\bar{1}0\}$ line is displaced to larger angles, indicating that $\Delta a/a$ has decreased. (θ_0 is the peak unirradiated intensity position, θ_1 the centre of the half-peak-intensity position after irradiation, and θ_2 the peak intensity position after irradiation.) The lines are very broad and asymmetric at high doses showing that

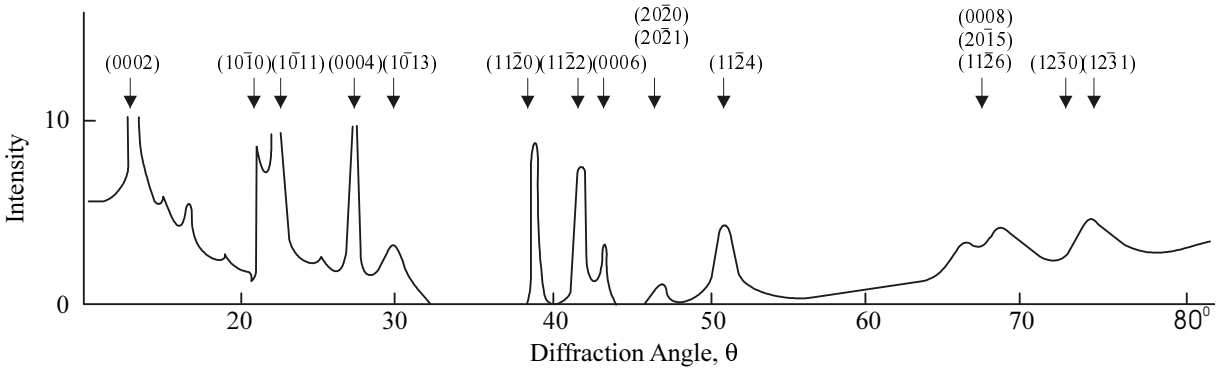

FIG. 3.1. X ray diffraction pattern of artificial graphite in Cu Kα radiation.

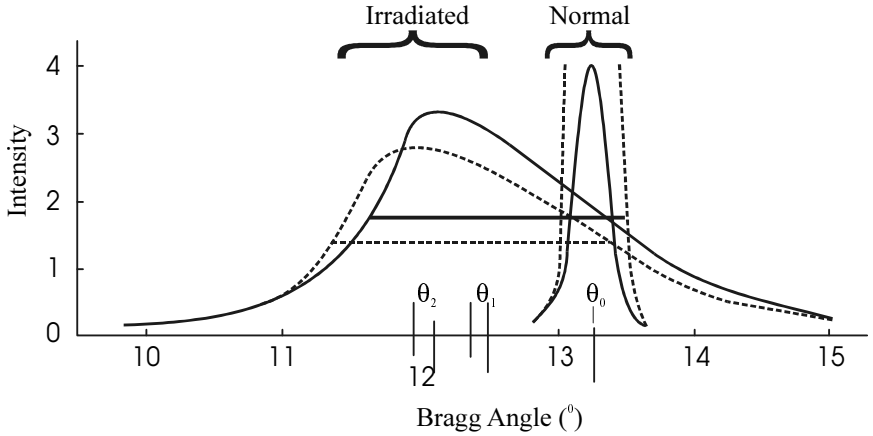

FIG. 3.2. {0002} line shapes for normal and heavily irradiated graphites of differing perfections (p = 0.20 for solid line, p = 0.02 for broken line).

the degree of crystalline order has decreased. Heat treatment of the materials to very high temperature restores the diffraction pattern.

Fundamental studies on a wide variety of properties after irradiation at very low temperatures indicated that, although there was some movement of interstitial atoms below 80 K, there was no significant interstitial-vacancy recombination and thus the number of interstitial atoms is expected to be the same as the number of vacancies. Studies of lattice parameter and dimensional changes at 77 K have been made by Keating (1955), Austerman (1958), Pluchery (1963) and Chinaglia et al. (1965). Maeta et al. (1975) measured changes in the lattice parameter Δd/d following neutron irradiation at 5 K in a fission spectrum. The changes in the d-spacing are not expected to be sensitive to the presence of vacancies and for not too large doses to be proportional to the concentration of interstitial atoms x_i. It was found that the changes in Δd/d were linear with dose, for doses up to 3×10^{17} n.cm^{-2} (instantaneous flux 1.1×10^{13} n.cm^{-2}.s^{-1} , $E_n > 0.1$ MeV), in both virgin and pre-irradiated samples. In this case the volume change of the graphite crystallite is given by

$$\frac{\Delta V}{V} = K\, x_i + 2\left(\frac{S_{13}}{S_{33}}\right)\frac{\Delta d}{d} \qquad (3.1)$$

where K is a constant and S_{13} and S_{33} are the elastic compliances of the crystal at zero dose. The value of x_i was estimated using essentially the model of Norgett, Robinson and Torrens (see Chapter 1) with a displacement energy of 28 ± 2 eV, taken from the work of Iwata and Nihira (1971) at 6 K. The calculation leads to $x_i = 0.92 \pm 0.3 \times 10^{-4}$ for a dose of 1×10^{17} n.cm^{-2} in the fission neutron spectrum. The values of x_i would be reduced by (28/60) using the usual value for E_d of 60 eV. Comparison of the results with the theory using the measured ratio of (S_{13}/S_{33}) of -0.012 leads to $\Delta V/V = 3.3x_i$. Analysis of the thermal expansion coefficients of graphite crystals (Kelly, 1981) leads to a maximum value for (S_{13}/S_{33}) of -0.066, which leads to $\Delta V/V = 3.5x_i$. Significant annealing begins at about 100 K where about 25% of the changes are recovered, thereafter the recovery is steady up to about 400 K where only about 20% of the change remains.

Pluchery (1963), Keating (1955) and Chinaglia et al. (1965) measured lattice parameter changes. The lattice parameter changes measured by Pluchery were essentially linear with dose up to a dose of 3×10^{18} n.cm^{-2}. The ratio ($\Delta a/a$)/($\Delta d/d$) was found to be low, ~ -0.1. Direct measurements of crystal strain by Ayasse and Bonjour (1976) showed that $\Delta X_c/X_c = 1.4\ \Delta d/d$.

Simmons (1965) and Kelly (1981) have reviewed lattice parameter measurements following irradiation at temperatures from 30°C to 1050°C. The changes in $\Delta d/d$ are very large at the lower temperatures, values of up to 15% being recorded (Nightingale, Davidson and Snyder, 1958). The changes in the a-spacing are smaller and the ratio varies with dose and irradiation temperature.

$$\delta' = \frac{\left(\frac{\Delta a}{a}\right)}{\left(\frac{\Delta d}{d}\right)}$$

Irradiation at temperatures at and below ambient give d' = -0.09 approximately, but the distortion of the diffraction pattern quickly becomes too large for accurate determination. The rate of change of $\Delta d/d$ decreases with increasing dose. Detailed data were obtained by Simmons and co-workers for temperatures ³150°C. The results at 150°C showed an increase of about 13% in $\Delta d/d$ at a dose of 1.6×10^{21} n.cm^{-2} (EDN) and it was still increasing at a reducing rate. Data taken in the same series of experiments at 200°C showed changes in $\Delta d/d$ of similar magnitude but taking place more slowly, however the dose dependence was clearly sigmoid. The change $\Delta d/d$ saturates at ~8%, accompanied by a change in $\Delta a/a$ of about -2% at a dose of 2.5×10^{21} n.cm^{-2} (EDN). The results at higher temperatures show saturating changes with dose for both $\Delta d/d$ and $\Delta a/a$, the saturation levels decreasing with increasing irradiation temperature, but with the ratio d' decreasing (magnitude increasing) to about -0.6 at 500°C and then reaching a peak at irradiation temperatures between 1000°C and 1200°C.

The analysis of line widths and shapes in terms of the distribution of lattice parameters in irradiated graphite has not made significant progress since the early work of Chipman and Warren (1952), Warren and Chipman (1953) and Austin and Harrison (1959). Figures 3.3 and 3.4 summarise the results for mean lattice parameter changes with dose.

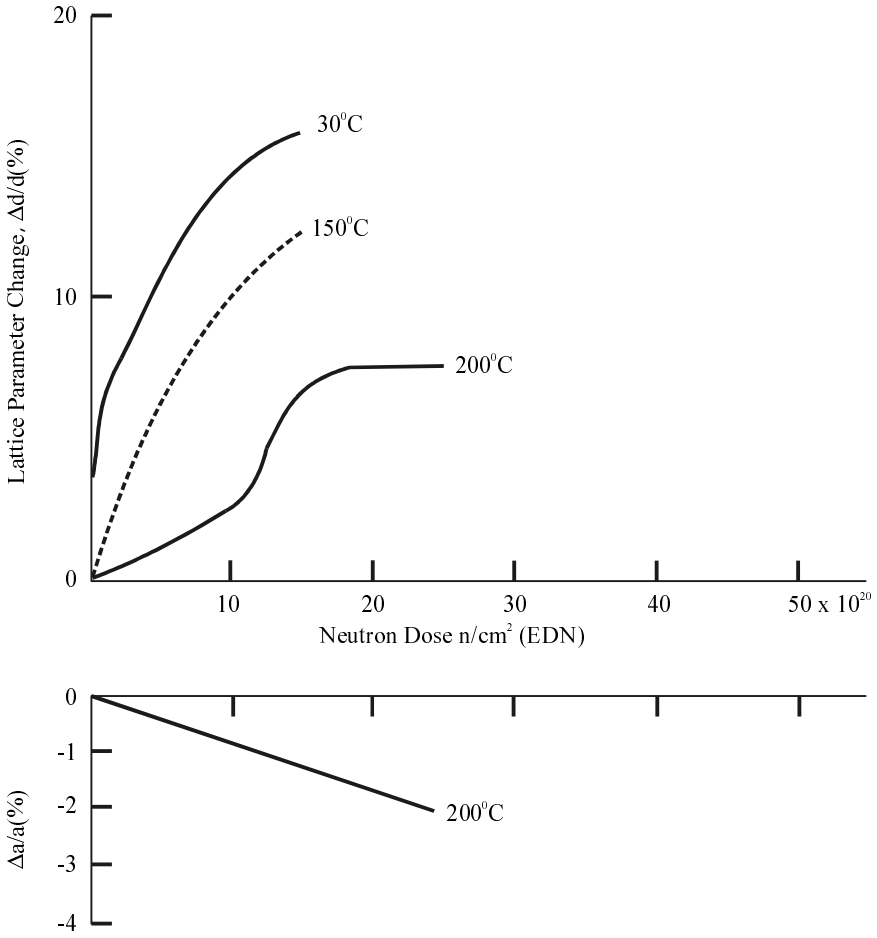

FIG. 3.3. Lattice parameter changes in low temperature irradiations.

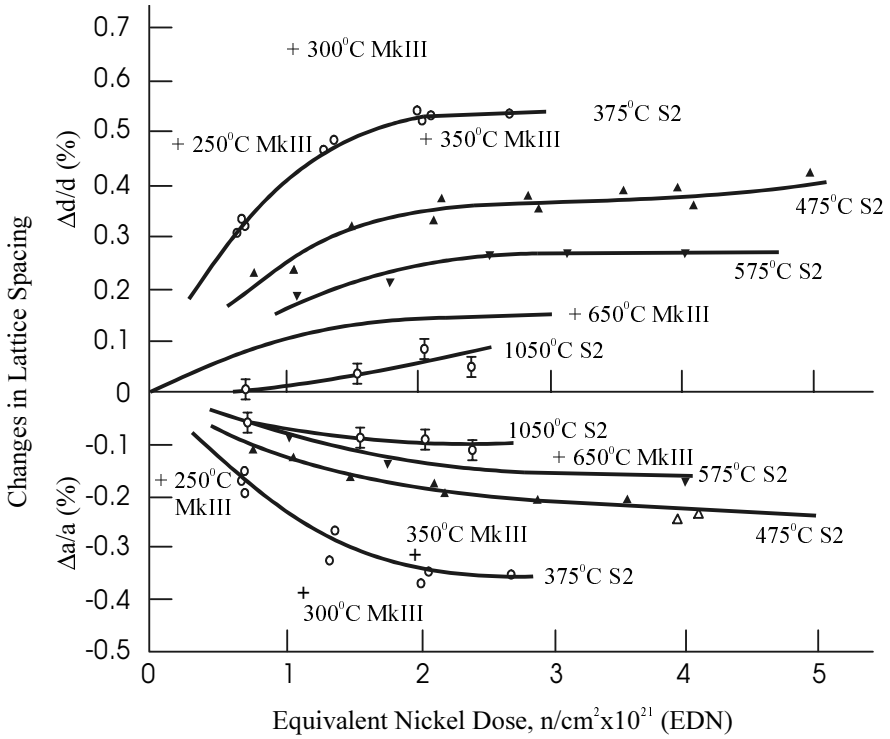

FIG. 3.4. Lattice parameter changes in MTR irradiations.

In a direct analogy with the theory of thermal expansion the presence of crystal lattice defects can be represented as a source of internal pressure, that is

$$\frac{\Delta d}{d} = S_{33}P_c + 2S_{13}P_a$$

$$\frac{\Delta a}{a} = (S_{11} + S_{12})P_a + S_{13}P_c \qquad (3.2)$$

where the S_{ij} are the usual crystal elastic compliances and P_a and P_c are the internal pressures acting parallel and perpendicular to the basal planes. Analyses have been given by Temkin (1970) and Stoneham (1973).

Stoneham considers a block of material with flat orthogonal surfaces. The insertion of an anisotropic defect which produces forces F_i on the lattice atom i distorts the crystal. If the crystal has hexagonal symmetry with the hexagonal axis parallel to one of the cube edges, then it is possible to apply the Betti reciprocity theorem (assuming harmonic forces). Applied external forces P produce displacements U in the solid, while in the absence of applied forces the defect forces F produce surface displacements d_l normal to surfaces l. The reciprocity theorem gives

$$\sum_l \boldsymbol{P}_l \cdot \delta_{\boldsymbol{I}} = \sum_i \boldsymbol{F}_i \cdot \boldsymbol{U}_i \qquad (3.3)$$

If the stresses P are assumed uniform over the surfaces then only mean displacements apply to the left hand side of equation (3.3). The right hand side may be evaluated for various F representing interstitial and vacancy defects.

The analysis of lattice parameter changes in irradiation experiments between 150°C and 650°C for doses up to 5 x 10^{21} n.cm^{-2} (EDN) assumes:

(i) Small interstitial groups of ~ 4 ± 2 atoms, as derived from neutron scattering experiments by Martin and Henson (1964, 1967), produce lattice parameter changes Δd/d.
(ii) Small uncollapsed vacancy groups contribute to the basal lattice parameter changes Δa/a.
(iii) Interstitial loops do not contribute to the lattice parameter changes.
(iv) Collapsed vacancy lines do not contribute to lattice parameter changes.

Equation (3.2) can be written

$$\frac{\Delta d}{d} = K_i x_i + \frac{K_v c_v}{\sigma_v}$$

$$\frac{\Delta a}{a} = K_i \sigma_i x_i + K_v c_v \qquad (3.4)$$

where x_i and c_v are the interstitial and uncollapsed vacancy concentrations, K_i and K_v are "effectiveness" factors for the interstitial and vacancy, and

$$\sigma_i = \frac{(S_{11} + S_{12})P_{ai} + S_{13}P_{ci}}{S_{33}P_{ci} + 2S_{13}P_{ai}}$$

$$\sigma_v = \frac{(S_{11} + S_{12})P_{av} + S_{13}P_{cv}}{S_{33}P_{cv} + 2S_{13}P_{av}} \qquad (3.5)$$

These equations imply that

$$K_i x_i = S_{33}P_{ci} + 2S_{13}P_{ai}$$

$$K_v c_v = (S_{11} + S_{12})P_{av} + S_{13}P_{cv} \qquad (3.6)$$

For an irradiation in which $x_i = c_v$, as might be appropriate for low temperature and low dose irradiations, $d' = s_i$.

Earlier work by Kelly (1972) had shown that $(S_{11} + S_{12})P_{av} \sim -0.14c_v$ and $S_{33}P_{ci} \sim 1 - 5x_i$, suggesting that $K_i >> K_v$. Pluchery's data showed that $d' = -0.086$, which is close to the value for $s_i = S_{13}/S_{33}$ of -0.075 due to Spence (1963) and -0.066 due to Kelly and Walker (1970) and Morgan (1972). Henson and Reynolds (1965) thus assumed $P_{ai} << P_{ci}$ and therefore

$$K_i x_i = S_{33}P_{ci} \qquad (3.7)$$

The values of d' obtained varied from -0.25 to -0.47 which implies that P_{cv} cannot be neglected, contradicting the assumption made by Kelly that $P_{cv} = 0$. A value of $s_2 = -0.56$ was obtained which gave $K_v = -0.11$. The concentrations of defects can then be estimated from the equations

$$x_i = \frac{1}{0.865K_i}\left[\frac{\Delta d}{d} + 1.8\frac{\Delta a}{a}\right]$$

$$c_v = \frac{1}{0.865K_v}\left[\frac{\Delta a}{a} + 0.075\frac{\Delta d}{d}\right] \qquad (3.8)$$

The concentrations of defects calculated from these changes are compatible with those obtained by other methods, but there are some changes in interpretation. A comparison with the stored energy in the graphite shows that the apparent energy per vacancy decreases with increasing concentration, from 7 eV to 1 eV. Henson, Perks and Simmons (1968) showed that the derived concentrations of vacancies would lead to excessive concentrations of collapsed vacancy lines. Both observations can be rationalised to some degree by assuming that the collapsed vacancy lines do cause lattice parameter changes (negative) and thus the observed changes in $\Delta a/a$ contain contributions from point vacancies and vacancy lines. If this is the case the interpretation of other property changes, such as thermal conductivity, must also be modified.

The first attempt to compare the crystal lattice parameter changes observed by X rays with the direct dimensional changes of the crystals was made by Simmons (1959) who obtained a relationship between the unirradiated thermal expansion coefficients of a series of graphites and the initial rates of dimensional change on irradiation at temperatures of 30, 80 and 180°C.

Simmons obtained a theoretical relationship between the thermal expansion coefficient and the dimensional change rate (following earlier attempts, summarised by Kelly, 1981) as follows:

Dimensional change rate with dose in direction x:

$$\frac{dG_x}{d\gamma} = A_x \frac{1}{X_c}\frac{dX_c}{d\gamma} + \left(1 - A_x\right)\frac{1}{X_a}\frac{dX_a}{d\gamma} \tag{3.9}$$

Thermal expansion coefficient in direction x:

$$\alpha_x = A_x\alpha_c + \left(1 - A_x\right)\alpha_a \tag{3.10}$$

Given the thermal expansion coefficients of the graphite crystal (a_c = 26 x 10^{-6} K^{-1} and a_a = -1.1 x 10^{-6} K^{-1}) and data for two directions x which give significantly different changes and expansion coefficients, then equations (3.9) and (3.10) become four simultaneous equations which can be solved for the two rates of crystal dimensional change. Good agreement was found between the X ray lattice parameter changes and the changes calculated from equations (3.9) and (3.10). Bridge, Kelly and Gray (1962) carried out a similar study on samples of polycrystalline graphite irradiated at Hanford over a range of irradiation temperatures from 30–306°C. The application of equations (3.9) and (3.10) to the two directions of Pile Grade A graphite again led to values of $\Delta d/d$ and $\Delta a/a$ in good agreement with $\Delta X_c/X_c$ and $\Delta X_a/X_a$ respectively.

In this review it is assumed, following Kelly, Martin and Nettley (1966a), Yoshikawa (1964) and Price (1974), that the dimensional changes of graphite crystallites can be observed directly on highly oriented pyrolytic graphite or on crystal flakes. Measurements of the thermal expansion coefficients of pyrolytic graphite parallel and perpendicular to the deposition plane correspond closely with those of single crystals and thus reflect strains parallel and perpendicular to the basal planes of the component crystallites. The perfection of the crystallite size can be varied by changing the final heat treatment temperature from ~2200°C, the deposition temperature, to 3600°C. Materials of this type were included in irradiation experiments at 150, 170, 200, 250, 300, 350, 450 and 650°C by Kelly, Martin and Nettley (1966a) who measured the dimensional changes parallel and perpendicular to the deposition plane, together with the principal thermal expansion coefficients. The results are summarised in Figs. 3.5 and 3.6.

The crystal dimensional changes $\Delta X_a/X_a$ parallel to the deposition plane (negative) and $\Delta X_c/X_c$ perpendicular to the deposition plane (positive) show a sigmoidal dependence on dose for the irradiations at temperatures below 300°C, but at the higher temperatures the changes are essentially parabolic. The lower temperature data show large volume changes at low doses, but the results at the higher temperatures show dimensional changes at constant volume. It is appropriate to define a parameter which can vary with dose and temperature.

$$\delta = \frac{\frac{1}{X_a}\frac{dX_a}{d\gamma}}{\frac{1}{X_c}\frac{dX_c}{d\gamma}} \tag{3.11}$$

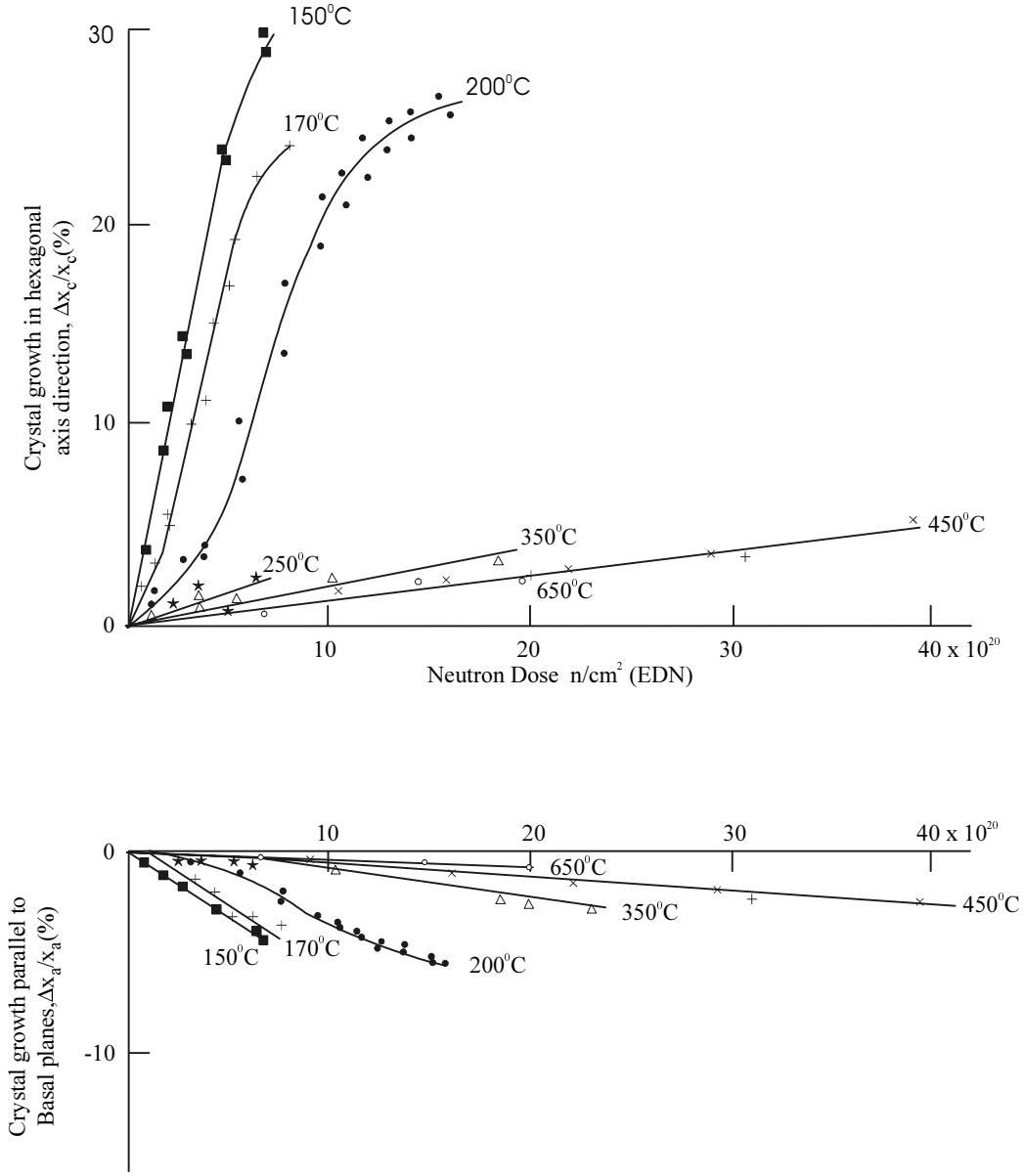

FIG. 3.5. Dimensional changes of pyrolytic graphite: Low temperature.

In the low temperature irradiations d is low at low doses and increases with dose to a value of -0.5, corresponding to changes at constant volume. The irradiations at higher temperatures take place at essentially constant volume, except for a very low dose period.

The irradiations of highly oriented pyrolytic graphite were extended to very high doses by Kelly and Brocklehurst (1971) and more detailed results at temperatures of 430 and 600°C on samples heat treated to different final temperatures, and hence crystal sizes, presented by Brocklehurst and Kelly (1993a). The results showed that the dimensional changes were insensitive to the crystal size for irradiation below 600°C, but increased with decreasing crystal size at higher temperatures. The earlier observation that the change at ~400°C took place at constant volume was confirmed, but at 600°C a small continuous volume increase was observed. Figures 3.7 and 3.8 illustrate these results.

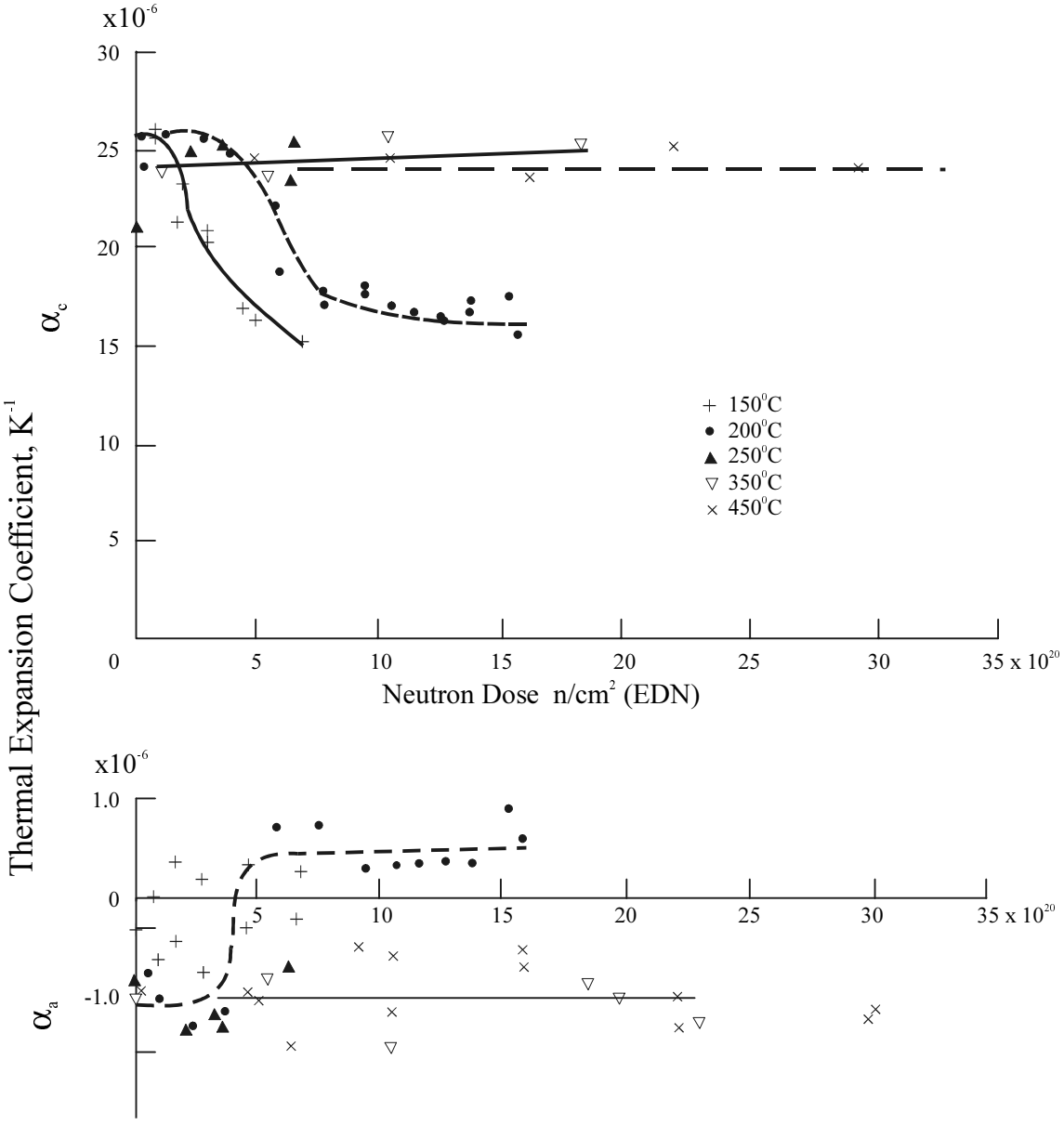

FIG. 3.6. Principal thermal expansion coefficients of highly irradiated oriented pyrolytic graphite.

Price (1974) exposed highly oriented pyrolytic graphite of varying perfection at 1300–1500°C and again found that the changes were larger in the less perfect materials. Table 3.1 shows values of the parameter d obtained in the higher temperature irradiations where it remains constant as a function of dose.

The irradiations below 300°C, where d varies with dose beginning at a low value characteristic of point defects and then increasing to the constant volume condition similar to the high temperature experiments, also show large changes in the principal thermal expansion coefficients which correspond closely with a_c and a_a. The expansion coefficient perpendicular to the deposition plane shows a decrease from ~26×10^{-6} K^{-1} to ~14×10^{-6} K^{-1} while the coefficient parallel to the deposition plane increases from a small negative value to a small positive value.

TABLE 3.1. VALUES OF d OBSERVED IN HIGH TEMPERATURE IRRADIATIONS

Irradiation temperature (°C)	Heat treatment temperature (°C)	d
430	2800	-0.50
600	2800	0.47
	2000 (as deposited)	-0.49
	2000 (HTT)	-0.49
600	3000–3300	-0.4
800		-0.2
900		-0.3
1000		-0.4
1100		-0.4
1200		-0.4
1350		-0.35

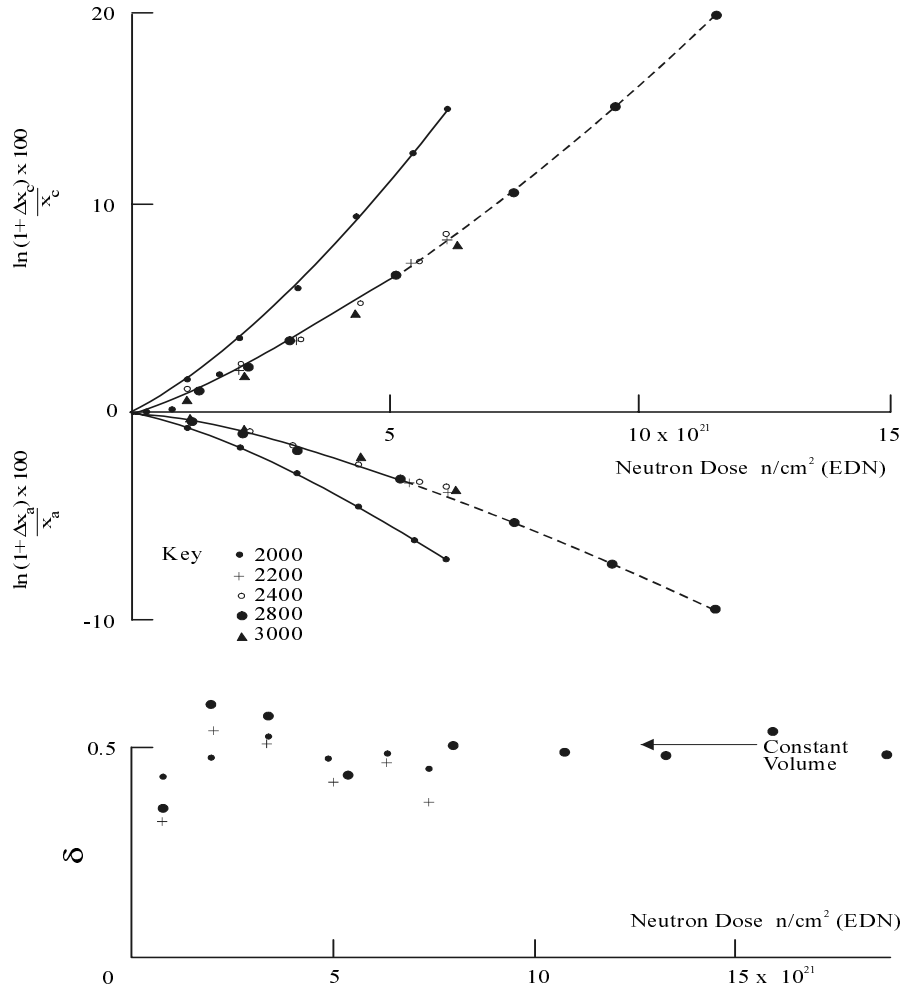

FIG. 3.7. Dimensional changes of highly oriented pyrolytic graphite irradiated at 430°C for different heat treatment temperatures.

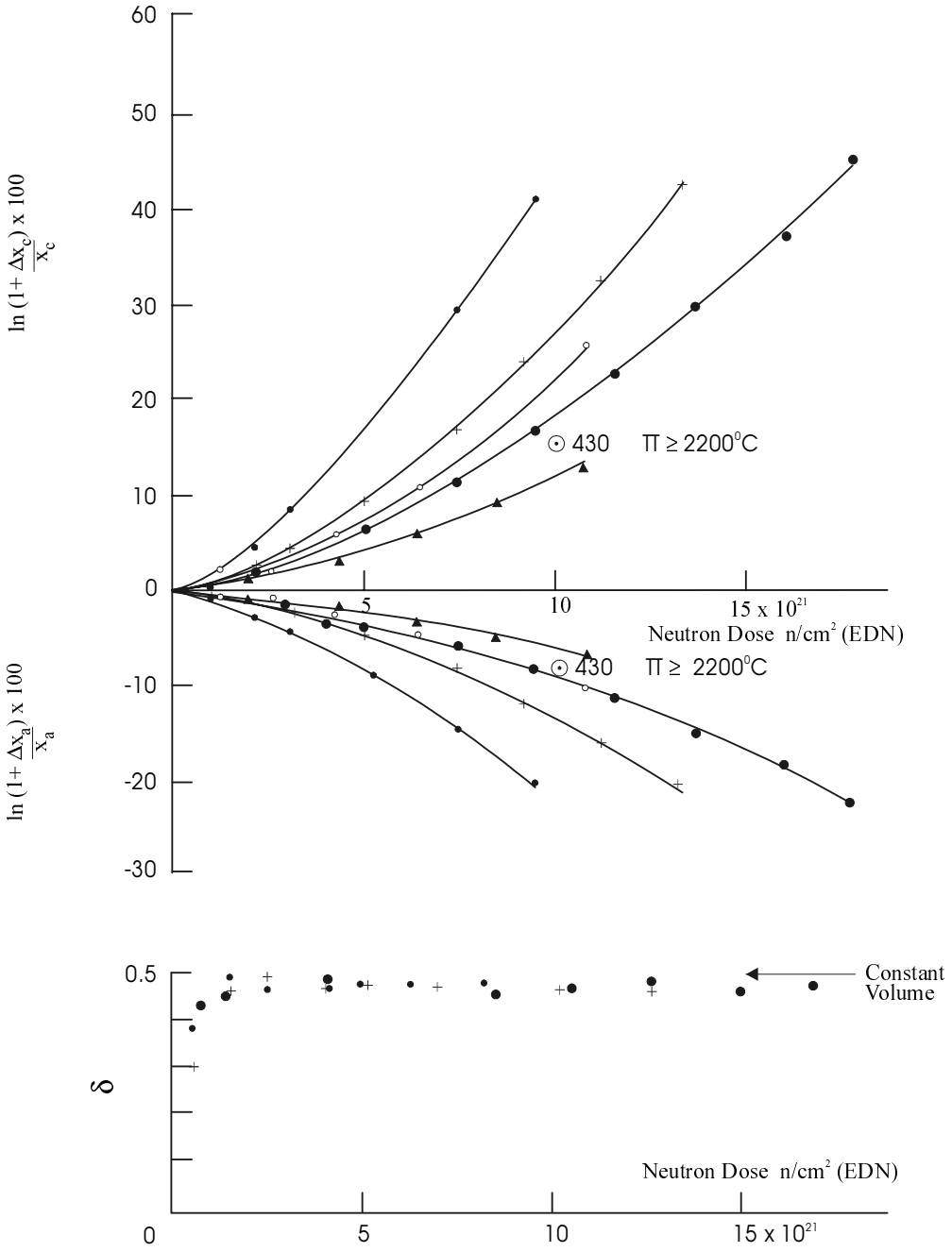

FIG. 3.8. Dimensional changes of highly oriented pyrolytic graphite irradiated at 600°C for different heat treatment temperatures.

A comparison of the X ray crystal lattice parameters with the direct measurements of crystal dimensional changes shows that they agree well at low doses, but the latter are larger as the dose increases. For irradiations at temperatures greater than 300°C the lattice parameter changes saturate while the crystal dimensional changes continue at least linearly with dose.

The changes in the crystal thermal expansion coefficients are apparently correlated with the changes in crystal lattice parameters, a_c decreasing when $\Delta d/d$ exceeds about 5% and ceasing when the changes stop (observed in irradiations at 200°C). In irradiations at temperatures greater than 300°C the lattice parameter changes are small and thus a_c and a_a do not change. The expansion $\Delta d/d$ may be assumed to absorb the "out-of-plane" lattice vibration amplitudes which

are responsible for a_c (see Kelly, 1981). The expansion coefficient a_a consists of two parts, one positive and one negative. The latter is due to the Poisson's ratio effect of the large expansion perpendicular to the layers and may also contain another negative contribution due to anharmonicity (Kelly and Walker, 1970; Harrison, 1977). The increase in the interlayer spacing eventually decouples the layer planes and permits the positive terms which are insensitive to the d-spacing to dominate.

The dimensional changes of polycrystalline graphite, which is an aggregate of crystallites with varying degrees of orientation, are a complicated mixture of the crystallite changes and porosity changes. In irradiations at constant temperature a number of authors have observed a linear correlation between the initial rates of dimensional change and the unirradiated thermal expansion coefficient (see Simmons, 1965). This relationship extends, for irradiations below ~600°C, from the extreme growth of highly oriented pyrolytic graphite perpendicular to the deposition plane to contraction parallel to the deposition plane. Other graphites have intermediate thermal expansion coefficients and intermediate dimensional changes, either positive or negative. The correlation is different at each irradiation temperature (see Simmons, 1965, for the correlations obtained at 30, 80 and 180°C). Experimentally, at each temperature the rate of dimensional change with respect to dose is given by

$$\frac{dG_x}{d\gamma} = A\alpha_x + B \tag{3.12}$$

At each temperature there is a value of a_x for which the graphite is dimensionally stable and this observation was used to specify graphites with improved dimensional behaviour for use in the United Kingdom Advanced Gas Cooled Reactors (UKAEA, 1965; Hutcheon, 1966). Equations (3.9) and (3.10) may be combined by eliminating the parameter A_x to yield

$$\frac{dG_x}{d\gamma} = \frac{(\alpha_x - \alpha_a)}{(\alpha_c - \alpha_a)}\left(\frac{1}{X_c}\frac{dX_c}{d\gamma} - \frac{1}{X_a}\frac{dX_a}{d\gamma}\right) + \frac{1}{X_a}\frac{dX_a}{d\gamma} \tag{3.13}$$

$= A\alpha_x + B$ as required

Equation (3.12) requires that all graphite crystallites behave the same way under the same irradiation conditions. The pyrolytic graphite data show that this is true for irradiations below 600°C but not at higher temperatures. In higher temperature irradiations the crystallite dimensional changes increase with decreasing crystallite size and so equation (3.12) is not satisfied.

The relationship between the rate of dimensional change and the thermal expansion coefficients was examined for several graphites at 170 and 200°C, by Kelly, Martin and Nettley (1966b). Given that the pyrolytic data give the rates of crystal dimensional change and thermal expansion coefficients it was shown that the values of A_x were the same for both up to a critical dose g* after which the value of A_x for dimensional changes becomes larger than for thermal expansion. Detailed analysis of the data on one graphite, Pile Grade A, together with measurements of the density of ground up samples showed that the difference was due to the generation of new pore space which was interpreted as an apparent increase in A_x in equation (3.9). Because of this an additional positive term was added to the macroscopic dimensional changes. Pile Grade A graphite shows (Table 2.1) an anisotropy of around 2 to 1 in properties

and the pore generation term in the graphite proves to have the same anisotropy, the effect being larger perpendicular to extrusion.

A large volume of data has been accumulated on a few nuclear graphites over a very wide range of irradiation temperatures. In the United Kingdom, Pile Grade A graphite used in the Magnox Reactor power stations and two near identical grades of Gilsonite coke-based graphites used in the later Advanced Gas Cooled Reactors. In the United States the CSF grade, closely similar to Pile Grade A, has also been irradiated over a wide range of temperatures. Henson et al. (1968) reported data on Pile Grade A graphite at temperatures from 300–1350°C, obtained in the PLUTO and DIDO reactors at Harwell, and using the very high fluxes in the Dounreay Fast Reactor. These results are shown in Figs 3.9–3.13. Gray and Pitner (1971) reported data on CSF graphite irradiated in the GETR, shown in Fig. 3.14. The high temperature irradiations were extended to higher doses and tabulated by Morgan and Gray (1972).

The dimensional changes of Pile Grade A graphite and CSF graphite are very similar. At low temperatures (< 300°C) the direction perpendicular to extrusion shows growth with the growth rate increasing with decreasing temperature, whilst the direction parallel to extrusion shows high shrinkage. The data at high temperatures show a smaller shrinkage parallel to extrusion, but perpendicular to extrusion there is an initial shrinkage which changes to growth, the change occurring at lower doses the higher the irradiation temperature.

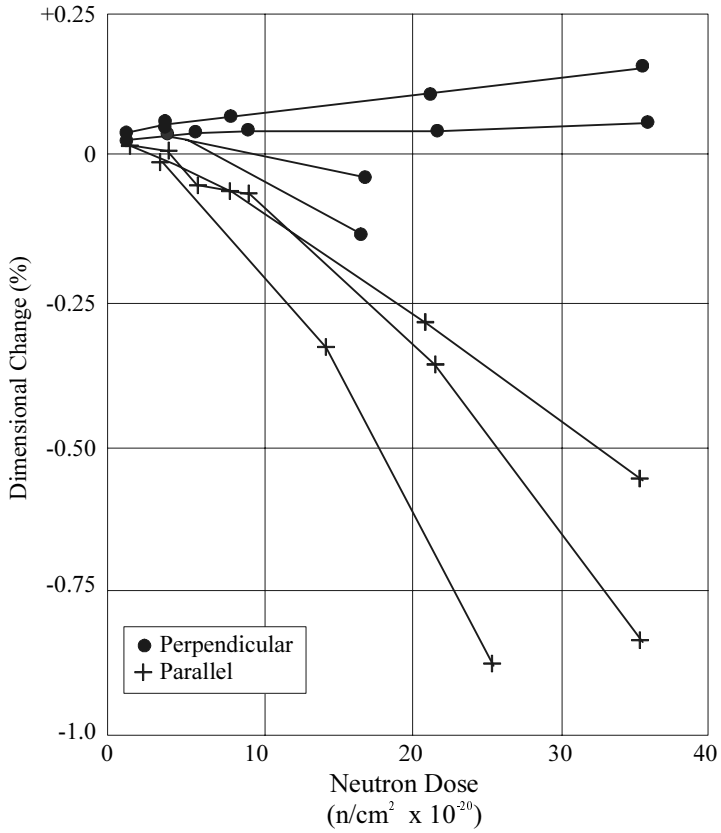

FIG. 3.9. Dimensional changes of PGA graphite irradiated at 900℃ in PLUTO.

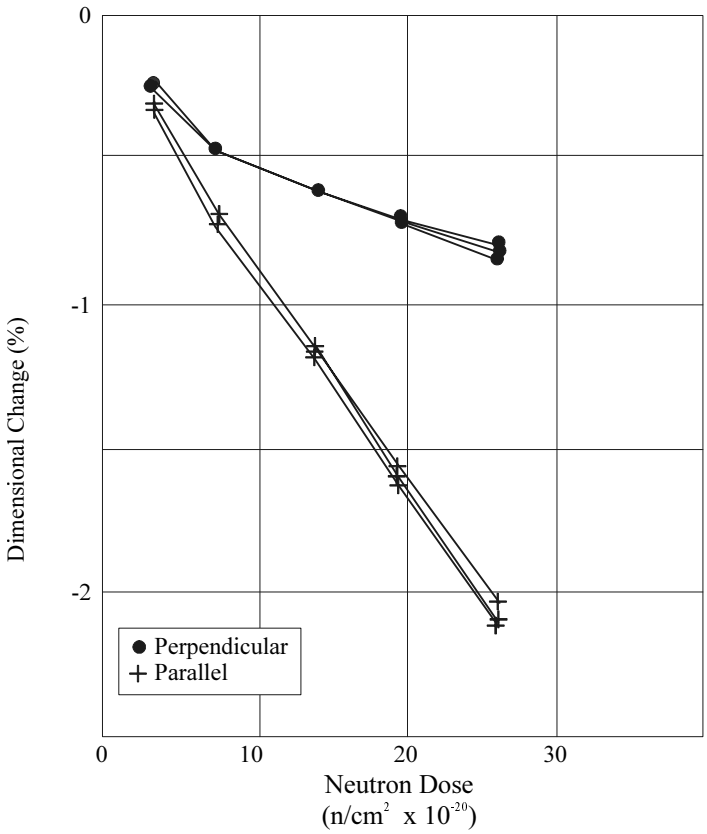

FIG. 3.10. Dimensional changes of PGA graphite irradiated at 1250–1350℃ in DIDO.

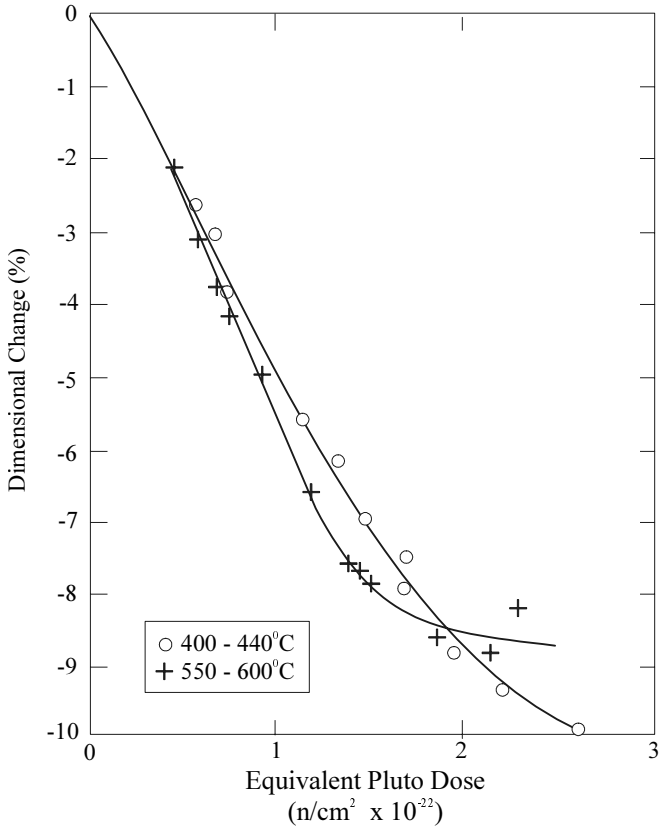

FIG. 3.11. Dimensional changes of PGA graphite parallel to extrusion in DFR.

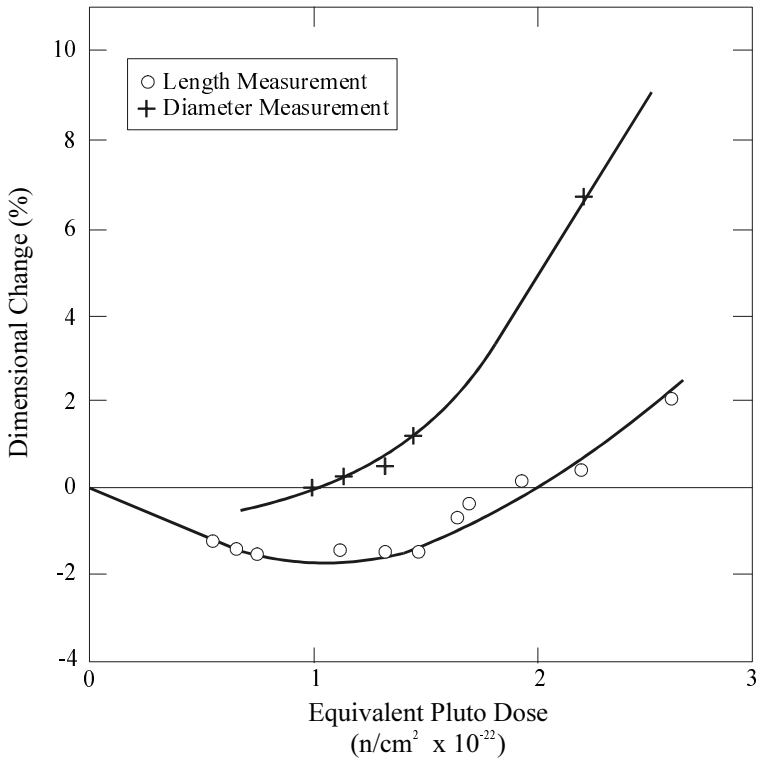

FIG. 3.12. Dimensional changes of PGA graphite perpendicular to extrusion at 400℃–440℃ in DFR..

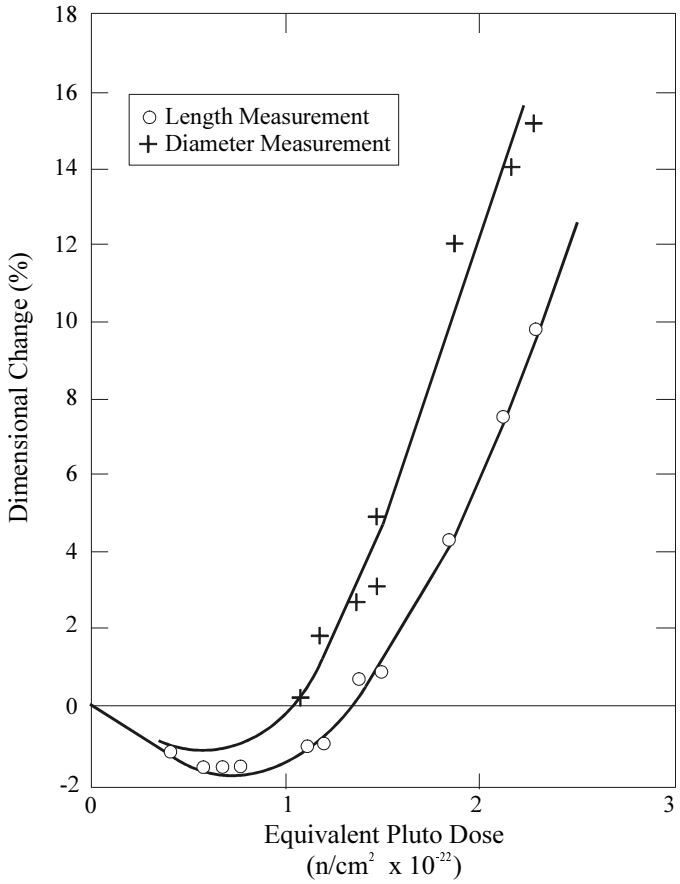

FIG. 3.13. Dimensional changes of PGA graphite perpendicular to extrusion at 550℃–650℃ in DFR..

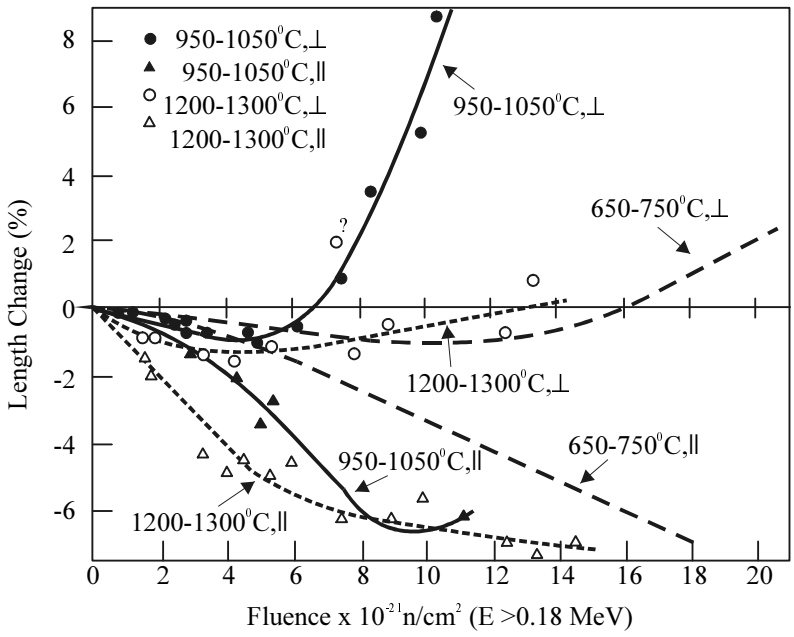

FIG. 3.14. Parallel and perpendicular length changes of CSF graphite.

The thermal expansion behaviour of Pile Grade A graphite is complicated. Irradiation at the lower temperatures shows, for both directions relative to extrusion, an increase followed by a decrease. At the higher irradiation temperatures the thermal expansion coefficient shows an increase in the perpendicular to extrusion direction in two stages, the first when the crystallite parameter $\Delta X_c/X_c$ reaches a value of about 5% (Simmons and Reynolds, 1962). This is interpreted as the closure, by the crystallite dimensional changes, of the cracks parallel to the basal planes created on cooling from the final heat treatment temperature and which can be directly observed (Thrower and Reynolds, 1963). These cracks, which have been postulated to be responsible for the difference between the volume thermal expansion coefficient of polycrystalline graphite and single crystal graphite, are known as Mrozowski cracks (Mrozowski, 1956). The large increase at high doses brings the volume expansion coefficient of the graphite close to that of a single crystal in spite of being accompanied by a large volume expansion due to pore generation. This has not been explained.

Brocklehurst and Kelly (1993a, 1993b) have presented data from irradiations at 600°C on Pile Grade A graphite heat treated to different final temperatures and also doped with boron to accelerate the damage rate and hence the dimensional changes. The irradiations included highly oriented pyrolytic graphite heat treated to different final temperatures to provide crystal dimensional changes. Detailed thermal expansion measurements were made on the Pile Grade A graphite in both directions relative to extrusion. The heat treatment series showed that the maximum volume shrinkage was independent of the heat treatment (ie degree of perfection). The maximum volume change of the boron-doped samples decreased with increasing boron content indicating an increasing crystal volume change; the expected acceleration of the damage was obtained.

The dimensional changes of an isotropic Gilsocarbon graphite irradiated at temperatures between 430 and 600°C are shown in Fig. 3.15. Very similar results were obtained (see Brocklehurst, 1984) on a pitch coke graphite known as VQMB. Brocklehurst and Kelly (1993b)

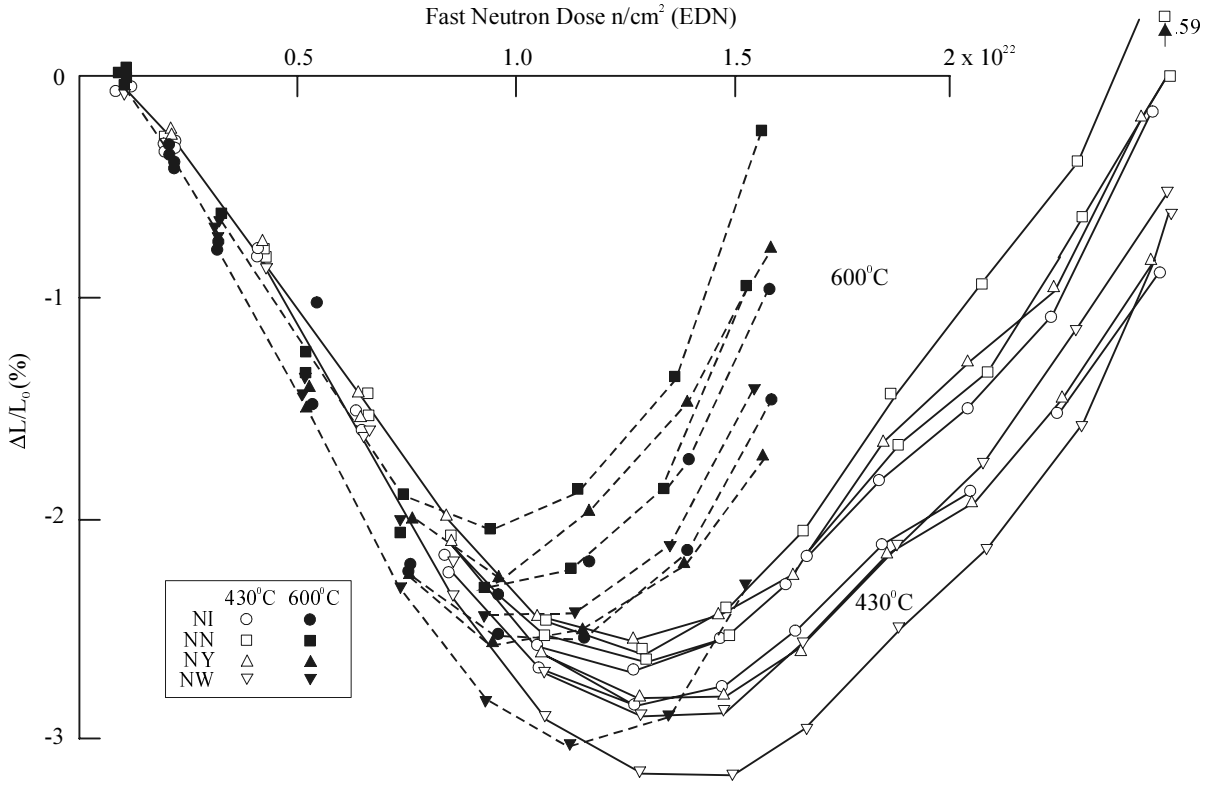

FIG. 3.15. Dimensional changes of CAGR moderator graphite in PLUTO at 430℃ and 600℃.

presented data on Gilsocarbon graphite doped with two levels of boron-11. The maximum volume changes were less the higher the boron content, as observed in Pile Grade A graphite, but the volume changes at 430°C were greater than those at 600°C. The initially relatively high thermal expansion coefficient was found to decrease to a considerably lower value.

Data on the fine grained isotropic POCO graphite grades have been summarised by Kelly (1989). The behaviour of grades AXZ-5Q1 and AXF-8Q1 is summarised in Figs 3.16–3.19. These graphites are unusual in showing volume growth or a high degree of stability at most irradiation temperatures. The initially high thermal expansion coefficients fall to very low values at each irradiation temperature. There does not appear to be any low temperature data but large growths would be expected on the basis of the thermal expansion coefficients.

GRAPHNOL N3M is, as already noted, a fine grain graphite developed for aerospace and fusion reactor applications. It has a high strength and strain to failure but a lower thermal expansion coefficient than the POCO grades to give an improved thermal shock resistance. It is finally heat treated at temperatures greater than 3000°C and is well graphitised and pure. The dimensional changes under irradiation have been examined at temperatures of 600°C and 875°C by Burchell and Eatherly (1991). The behaviour is similar to other isotropic graphites, showing a linear contraction of 2–3%, followed by expansion and a large decrease in thermal expansion coefficient at high dose.

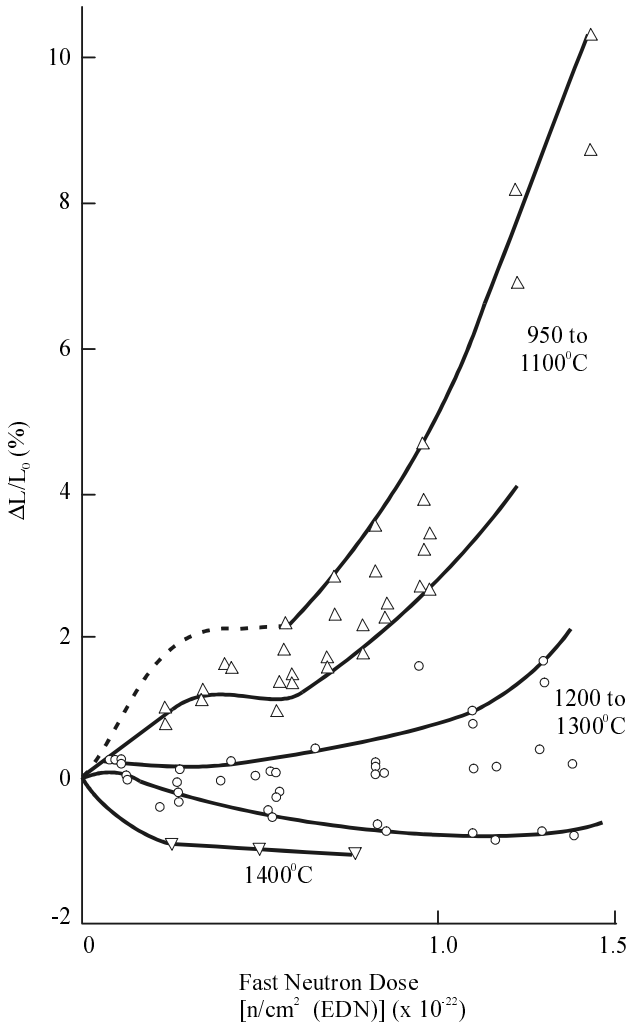

FIG. 3.16. Dimensional changes of POCO graphite grade AXF-8Q1.

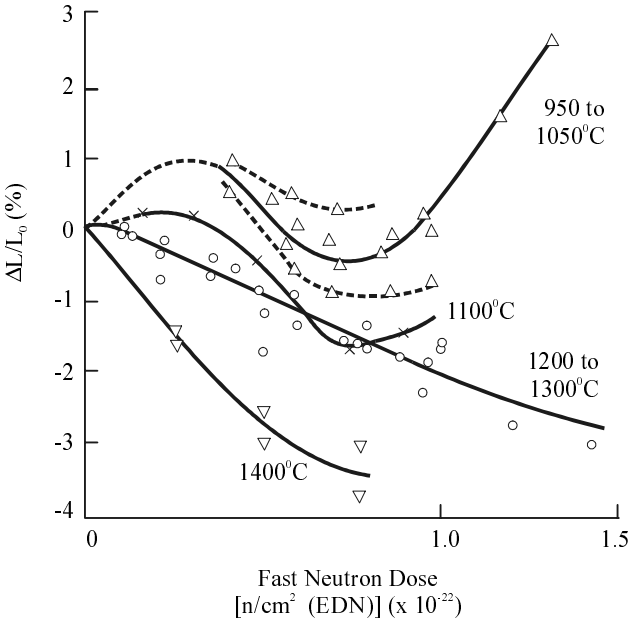

FIG. 3.17. Dimensional changes of POCO graphite grade AXZ-5Q1.

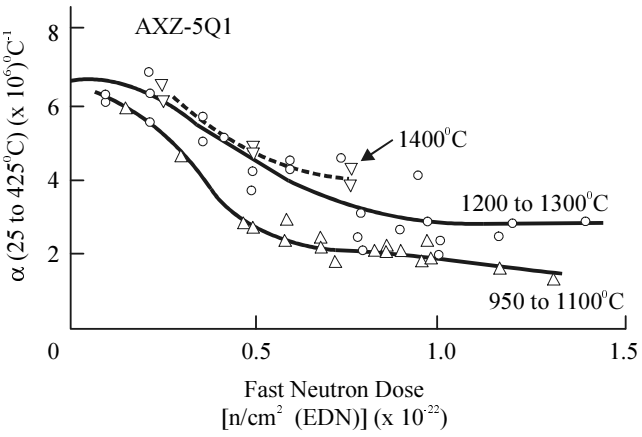

FIG. 3.18. Thermal expansion coefficient for POCO graphite grade AXZ-5Q1.

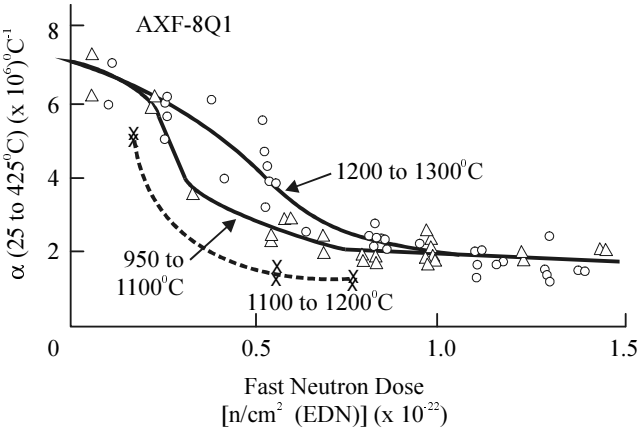

FIG. 3.19. Thermal expansion coefficient for POCO graphite grade AXF-8Q1.

Theory of dimensional changes in irradiated graphite

The theory of dimensional changes in irradiated graphite was originally developed to understand the relationship between crystal dimensional changes and macroscopic dimensional changes and thus to permit the specification of graphites with improved behaviour. A number of authors suggested that a relationship

$$\alpha_x = A\,\alpha_c + B\alpha_a \tag{3.14}$$

where A and B are constants (see Kelly, 1981, for a detailed review) existed between the thermal expansion in direction x of a polycrystal and the principal expansion coefficients of a graphite crystal. Simple models, such as a mechanical stack of crystallites, give A + B = 1. This relationship also holds for a non-porous body. Simmons (1965) showed that it could be shown thermodynamically that

$$\alpha_x = A_x\alpha_c + \left(1 - A_x\right)\alpha_a \tag{3.15}$$

and that the same relationship could be extended to dimensional changes using the relationship

$$\frac{dG_x}{d\gamma} = \frac{\partial^2 F}{\partial\gamma . \partial T_{xx}} = A_x \frac{1}{X_c}\frac{dX_c}{d\gamma} + (1 - A_x)\frac{1}{X_a}\frac{dX_a}{d\gamma} \tag{3.16}$$

where F is the free energy per unit volume and T_{xx} is a component of the macroscopic stress tensor.

In spite of the proof given by Simmons, this relationship is still not completely accepted. Kelly, Martin and Nettley (1966b) showed that this relationship broke down above a critical dose g* which depended on the graphite and the irradiation temperature. The generation of new pore space can be included in equation (3.16) by adding a term f_x. Equation (3.15) for thermal expansion is unchanged. Removal of the A_x term leads to

$$\frac{dG_x}{d\gamma} = \left(\frac{\alpha_x - \alpha_a}{\alpha_c - \alpha_a}\right)\left(\frac{1}{X_c}\frac{dX_c}{d\gamma} - \frac{1}{X_a}\frac{dX_a}{d\gamma}\right) + \frac{1}{X_a}\frac{dX_a}{d\gamma} + f_x \tag{3.17}$$

or

$$\frac{dG_x}{d\gamma} = \left(\frac{\alpha_x - \alpha_a}{\alpha_c - \alpha_a}\right)\frac{dX_T}{d\gamma} + \frac{1}{X_a}\frac{dX_a}{d\gamma} + f_x \tag{3.18}$$

where

$$X_T = \frac{\Delta X_c}{X_c} - \frac{\Delta X_a}{X_a} \tag{3.19}$$

Modelling of the internal processes in polycrystalline graphites suggested (Perks and Simmons, 1966) that the dimensional changes should depend on dX_T/dg as well as X_T. However Kelly, Martin and Nettley (1966b) proposed that the structure dependent factors in equation (3.18), α_x and f_x, depend only on X_T.

Equation (3.18) may be written in the form

$$G_x = \int A_x(X_T)\frac{dX_T}{d\gamma}d\gamma + \frac{\Delta X_a}{X_a} + F_x(X_T) \tag{3.20}$$

where

$$F_x = \int f_x d\gamma$$

This equation can be applied to the two directions relative to the extrusion direction and then used to show that it should be possible to obtain two unique functions of X_T from the experimental data:

$$f_1(X_T) = G_\perp - G_{II} = \int (A_\perp - A_{II}) \frac{dX_T}{d\gamma} d\gamma + (F_\perp - F_{II})$$

$$f_2(X_T) = 2G_\perp + G_{II} - 3\frac{\Delta X_a}{X_a} = \int (2A_\perp + A_{II}) \frac{dX_T}{d\gamma} d\gamma + (2F_\perp + F_{II}) \quad (3.21)$$

The parameter X_T can be obtained, together with $\Delta X_a/X_a$, from simultaneous irradiations of pyrolytic graphite. Brocklehurst and Kelly (1993b) have shown that for Pile Grade A graphite the two functions $f_1(X_T)$ and $f_2(X_T)$ are the same for irradiations at 200°C and 600°C, although the macroscopic dimensional change behaviour is quite different, that is a volume expansion at the lower temperature and a volume contraction followed by expansion at the higher temperature. The analysis of the higher temperature data extends well into the pore generation regime and thus accords with the idea of dependence on X_T only. A change in the final heat treatment temperature of the Pile Grade A graphite modifies the dimensional changes as a function of dose at 600°C substantially, but the two functions of X_T are unchanged, essentially demonstrating that the terms F_x depend principally upon X_T and weakly, if at all, on dX_T/dg.

For an isotropic graphite $f_1(X_T)$ is zero. The equation for $f_2(X_T)$ may be written as

$$f_2(X_T) = \frac{\Delta V}{V} - 3\frac{\Delta X_a}{X_a} = 3\int A_x \frac{dX_T}{d\gamma} d\gamma + F_v \quad (3.22)$$

where $\Delta V/V$ is the bulk volume change of the graphite and F_v is the pore volume generated. Equation (3.22) can be re-written in the form

$$f_2(X_T) = \frac{\Delta V}{V} - \left(\frac{\Delta X_c}{X_c} + 2\frac{\Delta X_a}{X_a}\right) + \left(\frac{\Delta X_c}{X_c} - \frac{\Delta X_a}{X_a}\right)$$

$$= \frac{\Delta V}{V} - \frac{\Delta V_c}{V_c} + X_T \quad (3.23)$$

where $\Delta V_c/V_c$ is the volume change of the crystallites. Re-arranging equation (3.23) leads to

$$\frac{\Delta V}{V} = \Phi(X_T) + \frac{\Delta V_c}{V_c} \quad (3.24)$$

This equation is useful because if dimensional change data are available at an irradiated temperature of 400–450°C then $\Delta V_c/V_c$ is approximately zero and $\Delta V/V$ is a unique function of X_T identical to $F(X_T)$. Given $\Delta V_c/V_c$ for other conditions it is then possible to predict $\Delta V/V$. Calculations of this kind have been made by Kelly and Burchell (1994) assuming that the ratio d (equation (3.11)) is constant with dose at a given irradiation temperature.

It is possible to analyse data taken at irradiation temperatures greater than 600°C where the crystallite dimensional changes depend upon their perfection (provided that all crystallites in the material behave the same). It has not been established that a single parameter which can be

measured pre-irradiation, such as L_a, determines the dimensional changes under irradiation, and it is uncertain whether d is independent of dose. The crystal volume change, if d is constant, can be written

$$\frac{\Delta V_c}{V_c} = \frac{\Delta X_c}{X_c} + 2\frac{\Delta X_a}{X_a} = X_T\left(\frac{1+2\delta}{1-\delta}\right) \tag{3.25}$$

and then, given $F(X_T)$, curves of $\Delta V/V$ as a function of X_T can be constructed. Each curve of this type has two well defined points: the first the value of X_T for which

$$\frac{1}{V}\frac{dV}{dX_T} = 0$$

and the second the value of X_T at which $\Delta V/V = 0$, determined from the calculated curves.

The assumption of constant d is not valid for irradiations below 300°C, but it does appear to be reasonable for higher temperature irradiations (Brocklehurst and Kelly, 1993a).

Simmons (private communication, 1991) has made two more recent analyses of the relationship between crystal dimensional changes and macroscopic dimensional changes in order to extend his earlier theory to higher doses (and hence pore generation). The first method is based on a stress analysis of a polycrystal including the presence of irradiation creep in basal slip. This analysis leads to the standard relationship for the thermal expansion coefficient, but shows that a further term must be added to equation (3.10) as postulated, but related to the irradiation creep in basal shear. The second model, based on a Fourier transform of stress, leads to similar conclusions.

The inherent simplicity of the atomic displacement process in graphite, which may be treated approximately as if individual atoms are displaced at random, has stimulated attempts to calculate the concentrations of individual lattice defects and hence property and dimensional changes. The calculations, in parallel with the data, are rather different for irradiation temperatures below 300°C, where large crystal volume changes occur, than those at higher temperatures where they do not.

The most comprehensive attempt to model the data at low temperatures was made by Woolley (1963), subsequently modified by Horner and Williamson (1966), while modelling of the higher temperature behaviour was undertaken by Kelly, Martin and Nettley (1966a) following analysis of the growth of interstitial dislocation loops in graphite by Lidiard and Perrin (1966). The Woolley model assumed that the damage can be described as single immobile vacancies, small mobile interstitial groups and larger sessile interstitial clusters assumed to occur at random in space and time, which correspond to the processes of recombination, nucleation and cluster growth respectively. (The phenomenon of irradiation annealing is omitted — this is the process of distribution of suitably sized interstitial groups by displacement collisions.) In order to explain the very large contractions parallel to the basal planes exceeding the changes in the nearest neighbour spacing $\Delta a/a$, Kelly, Martin and Nettley (1966a) introduced the concept of the collapsed vacancy lines created by random displacement sequences which prevented interstitial-vacancy recombination. This effect was incorporated into the Woolley model by Horner and Williamson and similar modifications were made by and Lidiard and Perrin. The

effect of the vacancy collapse was to accelerate the accumulation of interstitials, which since they lead to the growth e_{zz} parallel to the hexagonal axis and the accompanying lattice parameter changes $\Delta d/d$ improve agreement with experiment. The basal plane contraction also accelerates. Comparison with the crystal dimensional changes showed good agreement, given appropriate proportionality between concentrations and dimensional changes. However, as we shall see, the Woolley model gives much larger concentrations of sessile interstitial clusters (x 10) than observed in the electron microscope.

The other models assume two types of interstitial group can be formed from the initially displaced atoms. The first, later identified as consisting of 4 ± 2 atoms, ceases to grow once a particular configuration is achieved; and the second, interstitial dislocation loops, are homogeneously nucleated for irradiations below 450°C and then grow by two-dimensional diffusion of interstitials through a surrounding field of uncollapsed vacancies in which they may be absorbed. Lidiard and Perrin (1966) solved the equation and showed that in order to conform to the experimental data on the dimensional changes and lattice parameter changes at 200°C it was necessary to assume that the recombination rate of interstitials and vacancies quickly reached a constant level, in spite of the increasing total of interstitials. This was readily explained by the model of vacancy collapse, provided it is significant for tri-vacancies. The contributions of the two types of interstitial groups were separated, it being assumed that the concentrations of interstitials in growing loops was given by

$$C_i = e_{zz} - \frac{\Delta d}{d} \tag{3.26}$$

and the concentration of interstitials in small (4 ± 2) groups by

$$x_i = \frac{1}{K_i}\frac{\Delta d}{d} \tag{3.27}$$

as approximations.

For irradiations at temperatures greater than 300°C the lattice parameter changes are small and it is readily shown that the growth of a constant number of interstitial loops by diffusion for a constant vacancy concentration leads to a parabolic dependence of e_{zz} on the dose. This relationship is well obeyed by the results presented by Brocklehurst and Kelly (1993a). Measurement of the other properties shows that point defect concentrations are saturated, and the rate of vacancy collapse equals the rate of accumulation of interstitial atoms in loops. In irradiations below ~450°C the nucleation of the loops is homogeneous and hence all crystal dimensional changes are the same, independent of perfection, for a wide range of perfections. In irradiations at higher temperatures the nucleation of the loops is heterogeneous (except for very large crystals) and the number of loops and the consequent dimensional changes depend upon the perfection. The nature of the heterogeneous nuclei is not known. They may be small interstitial carbon groups which are removed by the process of graphitisation, the temperature of removal depending upon the size of the cluster.

The experimental data show that the changes continue to very large magnitudes, suggesting that fresh nucleation may occur, although no model has ever been proposed. Attempts to observe the defect structure at high doses have not been successful.

In summary, the dimensional changes of graphite crystals are due to the accumulation of point defects and extended defects created by the interstitial atoms, and vacancies created by the irradiation. The growth in the c-axis direction is due to interstitial atom clusters which are of two kinds, the interstitial dislocation loop and a small cluster. The concentration of the basal planes is due to point vacancies at low doses and collapsed vacancy lines at higher doses. When the latter are dominant, the dimensions change at constant crystal volume. In irradiations at high temperatures where vacancies are mobile, a proportion which increases with temperature reach crystallite boundaries perpendicular to the basal planes defining L_a, where they can collapse parallel to the basal plane producing a shrinkage equivalent to the collapsed lines. For small crystallite sizes in imperfect materials the majority of the newly created interstitials can reach such boundaries and the resulting dimensional changes approach the maximum possible.

REFERENCES TO CHAPTER 3

AUSTERMAN, S.B. (1958), USAEC Report NAA-SR-2457, Atomics International.
AUSTIN, A.E. and HARRISON, R.J. (1959), Proc. Third Biennial Carbon Conference, Pergamon Press, New York, p585.
AYASSE, J.B. and BONJOUR, E. (1976), Proc. Fourth SCI Conference on Industrial Carbons and Graphites, SCI, London, p620.
BACON, G.E. (1959), Proc. Third Conference on Carbon, Pergamon Press, p475.
BACON, G.E. (1960), J. Chim. Phys., 57, 829.
BACON, G.E. and WARREN, B.E. (1956), Acta Cryst., 9, 1029.
BRIDGE, H., KELLY, B.T. and GRAY, B.S. (1962), Proc. Fifth Conference on Carbon, Pergamon Press, 1, 289.
BROCKLEHURST, J.E. (1984), Irradiation Damage in CAGR Moderator Graphite, UKAEA Report ND-R-1117(S).
BROCKLEHURST, J.E. and KELLY, B.T. (1993a), Carbon, 31, 179.
BROCKLEHURST, J.E. and KELLY, B.T. (1993b), Carbon, 31, 155.
BURCHELL, T.D. and EATHERLY, W.P. (1991), J. Nuc. Mater., 179–181, 205.
CHINAGLIA, B., DOMENICI, M., PIERAGOSTINI, F. and WALTHER, H. (1965), Proc. Third Int. Conf. On the Peaceful Uses of Atomic Energy, United Nations, p399.
CHIPMAN, D.R. and WARREN, B.E. (1952), US Report KAPL-677.
GRAY, W.J. and PITNER, A.L. (1971), Carbon, 9, 699.
HARRISON, J.W. (1977), High Temperatures — High Pressures, 9, 211.
HENSON, R.W., PERKS, A.J. and SIMMONS, J.H.W. (1968), Carbon, 6, 789.
HENSON, R.W. and REYNOLDS, W.N. (1965), Carbon, 3, 277.
HORNER, P. and WILLIAMSON, G.K. (1966), Carbon, 4, 353.
HUTCHEON, J.M. (1966), Graphite for AGR Power Stations, Paper 4, AGR Symposium, Frankfurt.
IWATA, T. and NIHIRA, T. J. (1971), Phys. Soc. Japan, Vol. 31, p1761.
KEATING, D.T. (1955), Phys. Rev., 98, 1859.
KELLY, B.T. (1972), Proc. Third SCI Conference Industrial Carbons and Graphites, SCI, London, p483.
KELLY, B.T. (1981), Physics of Graphite, Applied Science Publishers, London.
KELLY, B.T. (1989), Fusion Technology, 16, 96.
KELLY, B.T. and BROCKLEHURST, J.E. (1971), Carbon, 9, 783.
KELLY, B.T. and BURCHELL, T.D. (1994), Carbon, 32, 499.
KELLY, B.T., MARTIN, W.H. and NETTLEY, P.T. (1966a), Phil. Trans. Roy. Soc. A, 260, 37.
KELLY, B.T., MARTIN, W.H. and NETTLEY, P.T. (1966b), Phil. Trans. Roy. Soc. A, 260, 51.
KELLY, B.T. and WALKER, P.L. (1970), Carbon, 8, 211.
LIDIARD, A.B. and PERRIN, R. (1966), PHIL. MAG., 14, 433.
MAETA, H., IWATA, T. and OKUDA, S. J. (1975), Phys. Soc. Japan, 39, 1558.
MARTIN, D.G. and HENSON, R.W. (1964), Phil. Mag., 9, 659.
MARTIN, D.G. and HENSON, R.W. (1967), Carbon, 5, 313 [3.34].
MORGAN, W.C. (1972), Carbon, 10, 73.
MORGAN, W.C. and GRAY, W.J. (1972), High Temperature Graphite Irradiations: 550 to 1450°C, BNWL-1672.
MROZOWSKI, S. (1956), Proceedings of the First and Second Conference on Carbon, University of Buffalo, p35.

NIGHTINGALE, R.E. (1958), Davidson J.M. and Snyder W.A. Proceedings of the Second United Nations Conference on the Peaceful Uses of Atomic Energy, United Nations, p295.
PERKS, A.J. and SIMMONS, J.H.W. (1966), Carbon, 4, 85.
PLUCHERY, M. (1963), Proc. Int. Conf. Irradiation Damage in Reactor Materials, IAEA, Vienna, p523.
PRICE, R.J. (1974), Carbon, 12, 159.
SIMMONS, J.H.W. (1959), Proc. Third Biennial Conference on Carbon, Pergamon Press, New York, p559.
SIMMONS, J.H.W. (1965), Radiation Damage in Graphite, Pergamon Press.
SIMMONS, J.H.W. and REYNOLDS W.N. (1962), Uranium and Graphite, Institute of Metals Monograph No. 27, p75.
SPENCE, G.B. (1963), Proc. Fifth Biennial Conference on Carbon, 2, Pergamon Press, New York, p531.
STONEHAM, A.M. (1973), J. Phys. C: Solid State Phys., 6, 223.
TEMKIN, D.E. (1970), Sov. Phys. Solid State, 11, 1614.
THROWER, P.A. and REYNOLDS, W.N. (1963), J. Nucl. Mater., 8, 221.
UKAEA. Report on the Life of the Graphite Core of the Advanced Gas Cooled Reactor, Emeléus Graphite Committee, UKAEA Report (1965).
WARREN, B.E. and CHIPMAN, D.R. (1953), US Report KAPL-938.
WOOLLEY, R.L. BRIT, J. (1963), Applied. Phys., 14, 778.
YOSHIKAWA, H.H. (1964), Nuclear Sci. Eng., 19, 461.

CHAPTER 4

STORED ENERGY AND THE THERMO-PHYSICAL PROPERTIES OF GRAPHITE

The lowest energy configuration of an assembly of carbon atoms is the perfect graphite crystal. The introduction of crystal lattice defects increases the energy of the crystal above that of the parent crystal. If the thermal vibrations introduced by heating the crystal permit rearrangement of these defects to states of lower energy then the change in energy is released as heat. This energy is known as Wigner energy, after the well-known physicist who first suggested that it might occur in neutron irradiated material. The phenomenon was already known to occur in self-bombarded (n,α) minerals and to metallurgists because of its occurrence in cold-worked metals. The first recorded, although not recognised, observation was made by Berzelius in gadinolite in 1815. In graphite, diamond and silicon carbide irradiated with fast neutrons at ambient temperature very large amounts of energy can be stored as lattice defects. Values of up to 2700 $J.g^{-1}$ have been observed in graphite which if released as heat under adiabatic conditions would raise its temperature by ~ 1500°C, an obviously undesirable occurrence!

Stored energy in graphite has two important practical effects. Firstly, following irradiations at temperatures below ~150°C, it is possible to reach a state in which a small temperature rise can be followed by a much larger rise due to the stored energy. Graphite irradiated at ~30°C for instance and then heated to 70°C can rise rapidly in temperature to ~400°C, which is approximately that required for thermal oxidation. Secondly, in the case of graphite irradiated at higher temperatures, the presence of stored energy reduces the heat capacity and hence affects the progress of any transient temperature condition. In other words the presence of stored energy can be responsible for, or seriously modify, reactor accidents.

Measurements of the stored energy content of graphite are generally made by one of two methods, although others are possible:

(i) The total stored energy can be determined as the difference in the heat of combustion of irradiated and unirradiated graphite. The standard method of measurement of the heat of combustion uses high accuracy bomb calorimetry. The heat of combustion of pure unirradiated graphite is 3.26×10^4 $J.g^{-1}$ while measurement accuracy is ± 4 $J.g^{-1}$. Figure 4.1 shows values of total stored energy determined this way as a function of dose for various irradiation temperatures. The energy content cannot increase indefinitely with dose and there is a large effect of irradiation temperature, the rate of energy storage decreasing with increasing temperature.

(ii) In the second method the temperature of the sample is raised in a controlled way and the energy release rate measured. This method generally requires two experiments on the same sample to determine the proportion of energy supplied by stored energy. Two well-known variants are:

   (a) To place the sample in isothermal, high heat capacity surroundings and observe the sample temperature-time relation in two successive runs. This is particularly useful when the sample has a very high release rate at low temperatures.

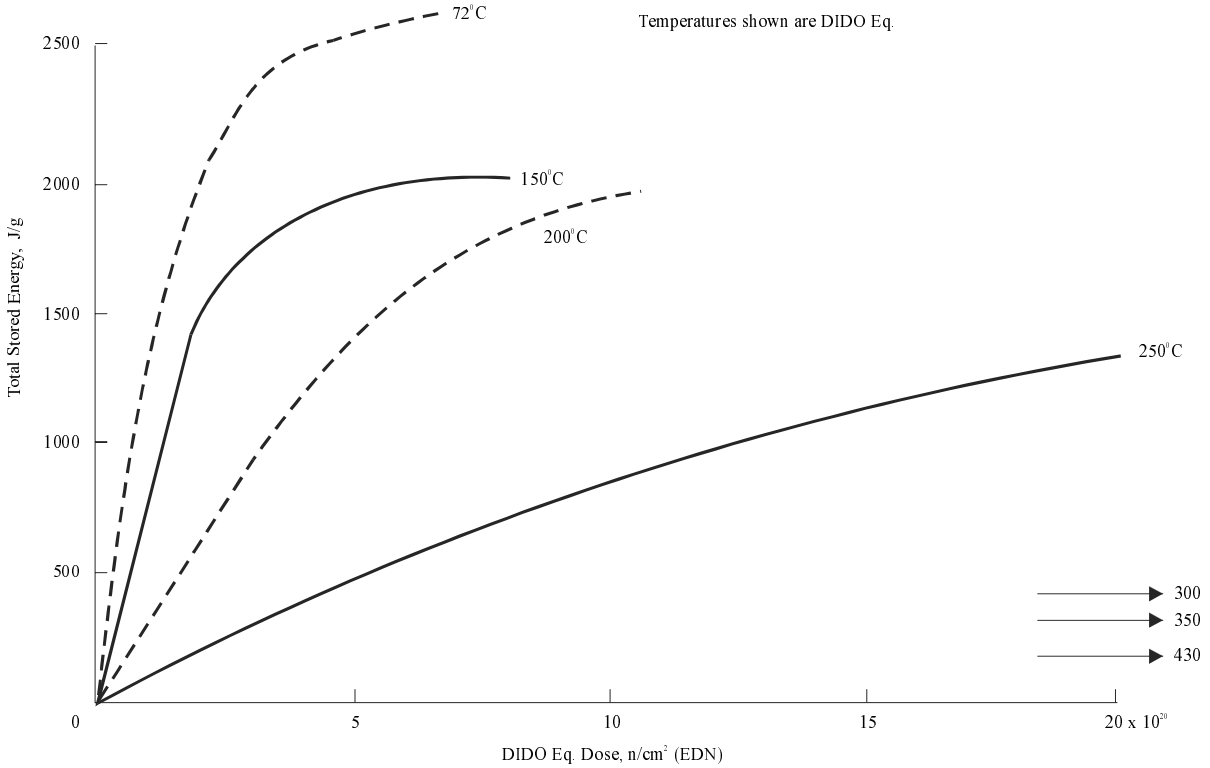

FIG. 4.1. Accumulation of total stored energy in graphite at various irradiation temperatures.

(b) To supply heat to the sample at the rate required to raise its temperature at a constant rate (linear rise method). The difference in energy supply between two experiments gives the energy release rate.

The energy release rate is usually expressed in terms of unit temperature rise

$$\frac{dS}{dT} = \frac{1}{a}\frac{dS}{dt} \tag{4.1}$$

where S is the stored energy per unit mass, a is the rate of temperature rise, t is the time and T the temperature. Details of the measurement methods are given by Simmons (1965).

The methods described in (ii) have most practical use in that the objective of the measurements is generally the prediction of the temperature progression of a sample subjected to an arbitrary heat source. The measurements of energy release in the case of constant temperature or constant rate of rise of temperature may be used to study the kinetics of energy release. Figure. 4.2 shows measurements reported by Bridge, Kelly and Gray (1962) on the rate of energy release per unit temperature rise on samples irradiated to various doses at an irradiation temperature of 30°C in a water cooled test hole in one of the US Production reactors, but measured in the United Kingdom. These measurements show a well-defined peak at about 200 °C which increases with dose to a maximum value and then diminishes. The energy release rate at higher temperatures increases continuously, but at a decreasing rate until the energy release rate becomes fairly constant. The release rate becomes measurable at a temperature about 80°C above the irradiation temperature for measurements made at ~2°C.min^{-1}. As the irradiation temperature is increased the stored energy peak at ~200°C disappears and the relatively constant

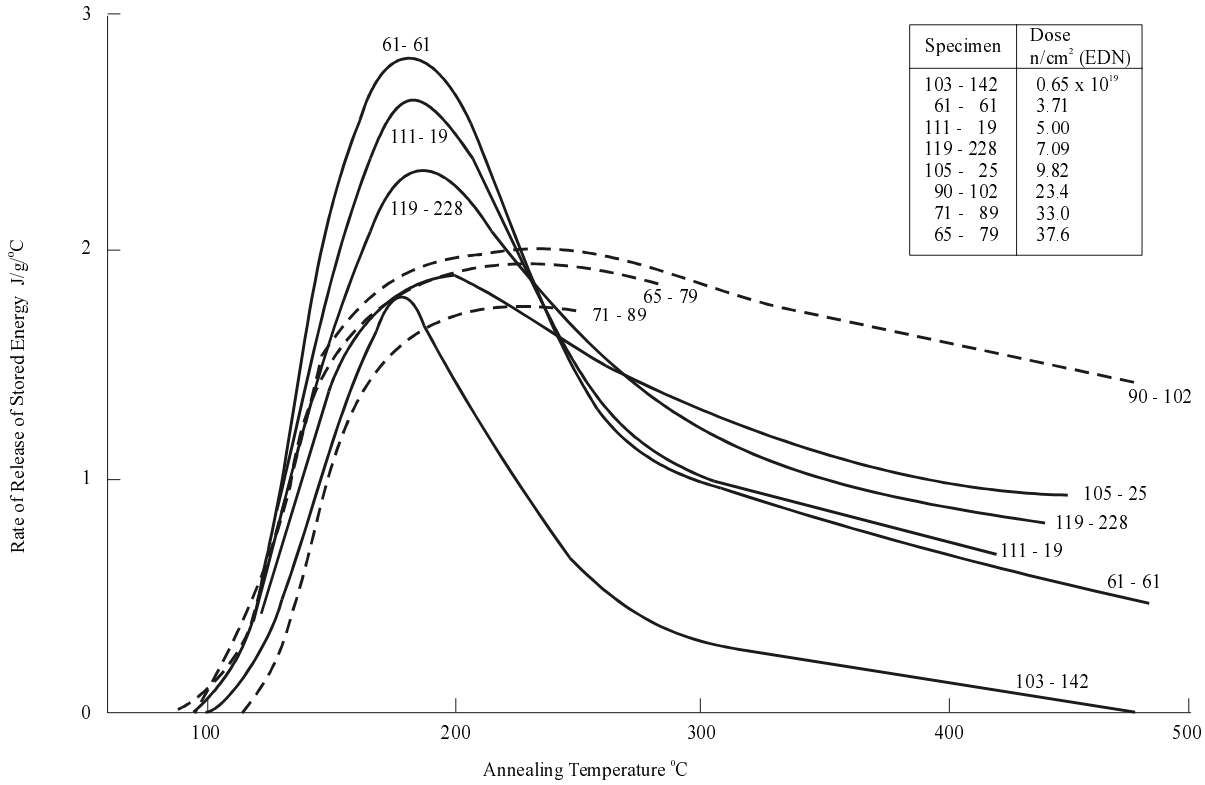

FIG. 4.2. Rate of release of stored energy for Hanford cooled test hole graphite irradiated at 30°C.

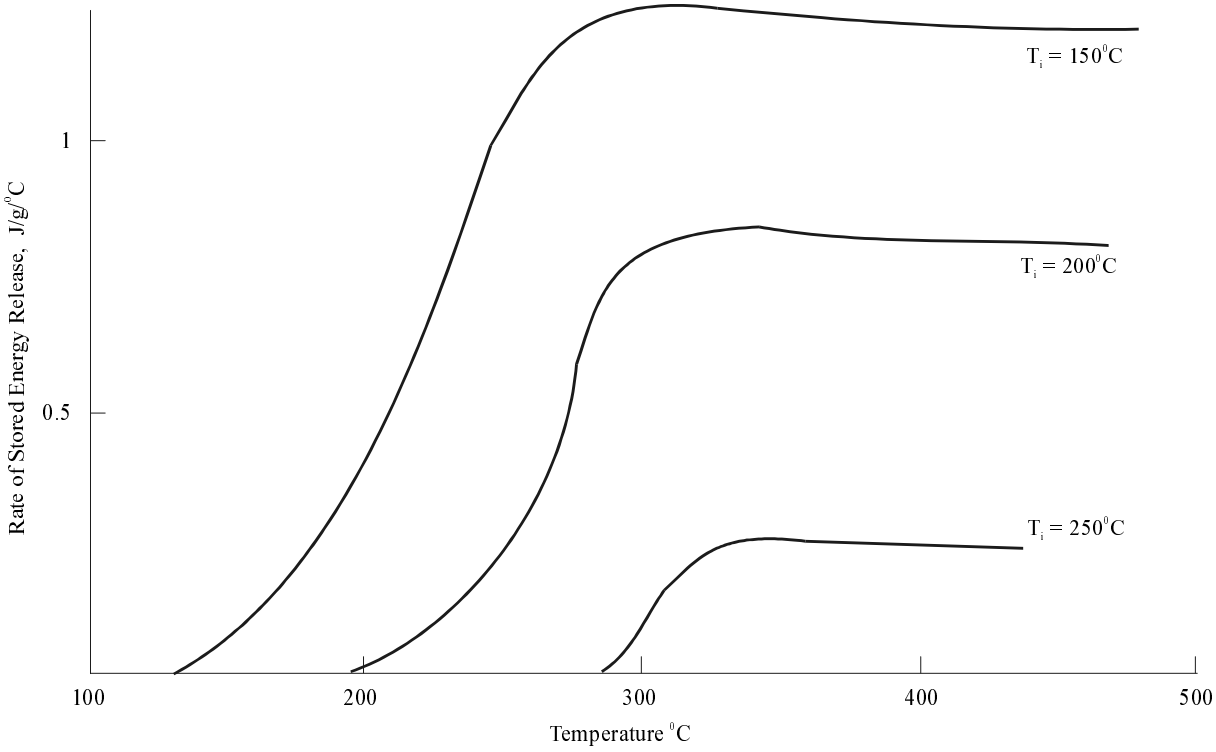

FIG. 4.3. Stored energy release curves at dose of 5×10^{20} n/cm^2 (EDN) for irradiation temperatures of 150 °C–250°C.

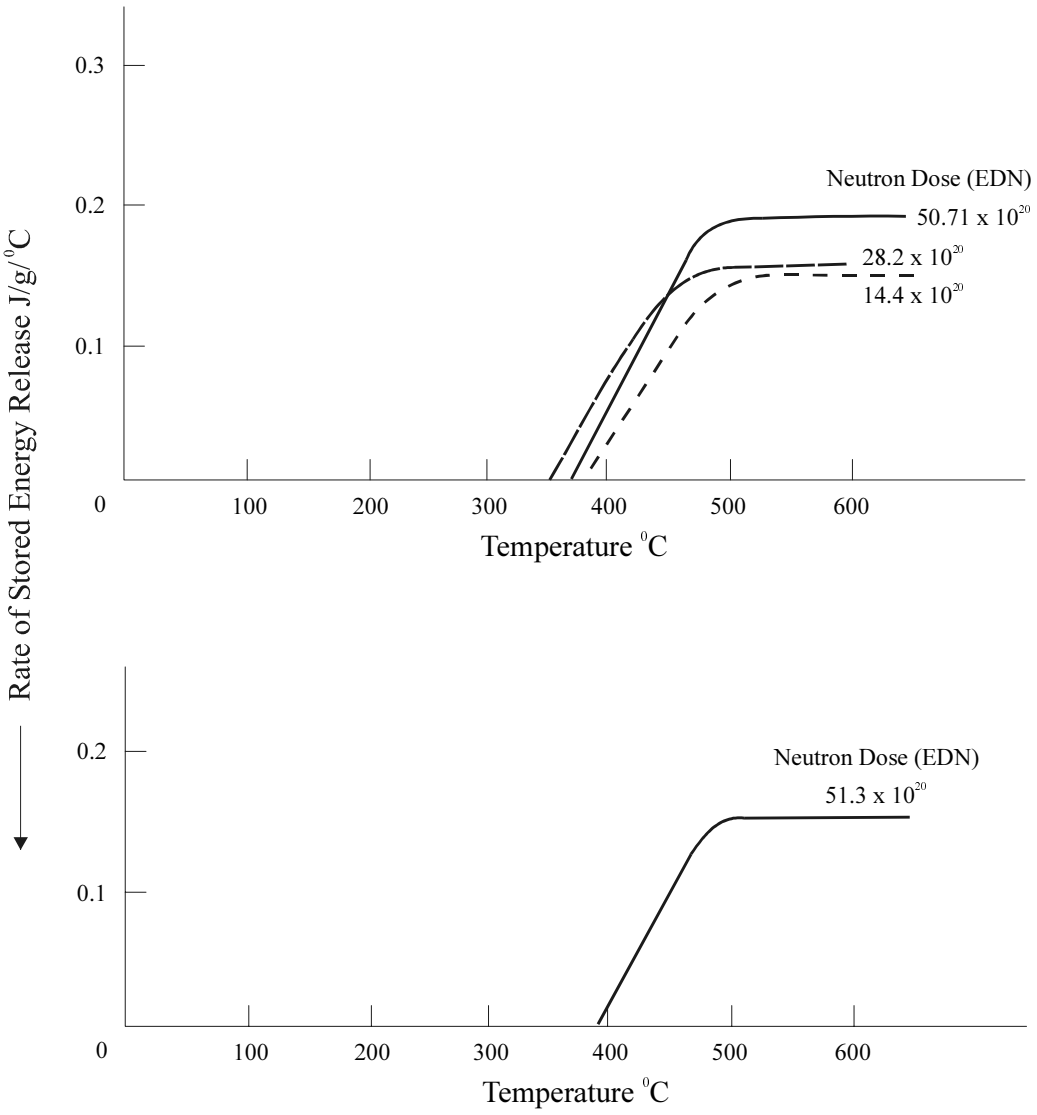

FIG. 4.4. Stored energy release curves for irradiation temperatures of 350 and 390°C.

level of stored energy release builds up more slowly. Figure 4.3 compares the energy release rates for a dose of 5×10^{20} n.cm^{-2} (EDN) following irradiation at 150, 200 and 250°C. Figure 4.4 shows measurements of energy release rate following irradiations at 350 and 390°C. The temperature at which the release becomes detectable increases with the irradiation temperature, the gap between the irradiation temperature and temperature of detection decreasing with increasing displacement rate and increasing with rate of temperature rise (Bridge and Mottershead, 1966).

Kelly *et al.*. (1979) have analysed the published data on the rate of release of stored energy up to 600°C for irradiation temperatures greater than 140°C and concluded that there is an irradiation temperature dependent saturation of the rate of release of stored energy. The predicted saturation levels agree well with later data obtained from operating reactors when the appropriate dose and temperature corrections are made, thus verifying the equivalent dose and

temperature corrections (see Chapter 1). Bell *et al.* (1962) showed that for the same range of irradiation conditions the constant energy release rates were related empirically to the total stored energy in Pile Grade A graphite by

$$\frac{dS}{dT} = \frac{S}{T^*} \tag{4.2}$$

where T^* = 1670 K, independent of irradiation temperature. Analysis of the power reactor data gives T^* = 1910 K which, within errors, is the same.

At first sight equation (4.2) implies a constant rate of energy release over a wide temperature range, however it is possible to measure *dS/dT* using incremental thermal annealing followed by bomb calorimetry (Bell and Greenough, 1959; Davidson, 1959). Measurements of this type indicated a stored energy release peak at high temperatures, 1000–1500°C. Rappeneau, Taupin and Grehier (1966) verified the existence of this peak using direct measurements in an all-graphite calorimeter.

Monitoring of the stored energy in power reactor graphite moderators is routine practice where the operating temperature is low, because of the effects it has on the thermal capacity of the moderator in accident situations. The saturation levels of stored energy for irradiations above ~300°C is too small to be of practical importance.

Stored energy measurements have been made following irradiation with neutrons at temperatures below ambient. Bochirol and Bonjour (1968) made measurements on neutron irradiated graphite exposed at 77 K and 27 K. Three graphites were examined: a stress-annealed very perfect pyrolytic graphite, an annealed pyrolytic graphite and a conventional reactor graphite. The stored energy varied between the materials, the least perfect showing a release extending over a wider temperature range, with less detailed structure.

The stored energy release rates per unit temperature rise show peaks at 75, 110 and 135 K (corresponding to activation energies of 0.09, 0.13 and 0.17 eV). Assuming that the defects are in the form of interstitial-vacancy pairs (Frenkel defects) produced at a rate predicted by the Thompson-Wright model gave a value of 7.1 eV for the Frenkel defect pair. Comparison of stored energies at 77 K in two different neutron spectra showed that the relative damage rates were accurately predicted by the displacement models. The accumulation of stored energy release up to a temperature of 570 K is given by

$$S_{77}^{570} = 1259\left[1 - e^{-0.0889\gamma}\right] \ \text{J.g}^{-1} \tag{4.3}$$

where γ is the neutron dose with energy > 1 MeV. No difference was observed between reactor and pyrolytic graphite. The non-linear accumulation of stored energy is explained by the overlap of the displacement groups described by Simmons (1965) which thus must have a mean diameter of 17×10^{-8} cm.

Austerman (1956) has reported stored energy release spectra in neutron irradiated samples exposed at 120 K.

Stored energy exhibits the phenomenon known as irradiation annealing. If an irradiated sample is exposed to a temperature significantly higher than the original irradiation temperature then the stored energy will decrease as a result of thermal rearrangement of the lattice defects (annealing). However, if the same sample is exposed to the same higher temperature in a neutron flux, the stored energy decreases to a greater extent and for a longer period than in the purely thermal case. This phenomenon was first described by Nightingale (1959), who measured, among other properties, the total stored energy changes of graphite irradiated at ambient and annealed at 375°C. The effect of irradiation annealing on the stored energy release rate in samples irradiated at a temperature of 130°C was examined by Bridge, Kelly and Gray (1962) and in more detail, including other properties at 150°C, by Gray *et al.* (1969). This work showed that while thermal annealing raised the temperature at which energy release began, the irradiation annealing lowered the level of the energy release rate over the whole range of temperatures.

It was expected that irradiation annealing might be of practical use in the first generation of graphite moderated power reactors but has not, to the author's knowledge, ever been used. Special cooling circuits were installed in the early UK Magnox reactors to permit raising the moderator temperature uniformly and hence induce irradiation annealing.

Theory of the release of stored energy in graphite

There has not been any detailed attempt to give a theory of the release of stored energy in terms of the defect concentrations, although correlation of total stored energy with simple models has been achieved. The importance of stored energy release in a variety of reactor accidents has led to detailed empirical methods of treatment of the release applicable to arbitrary temperature-time relationships.

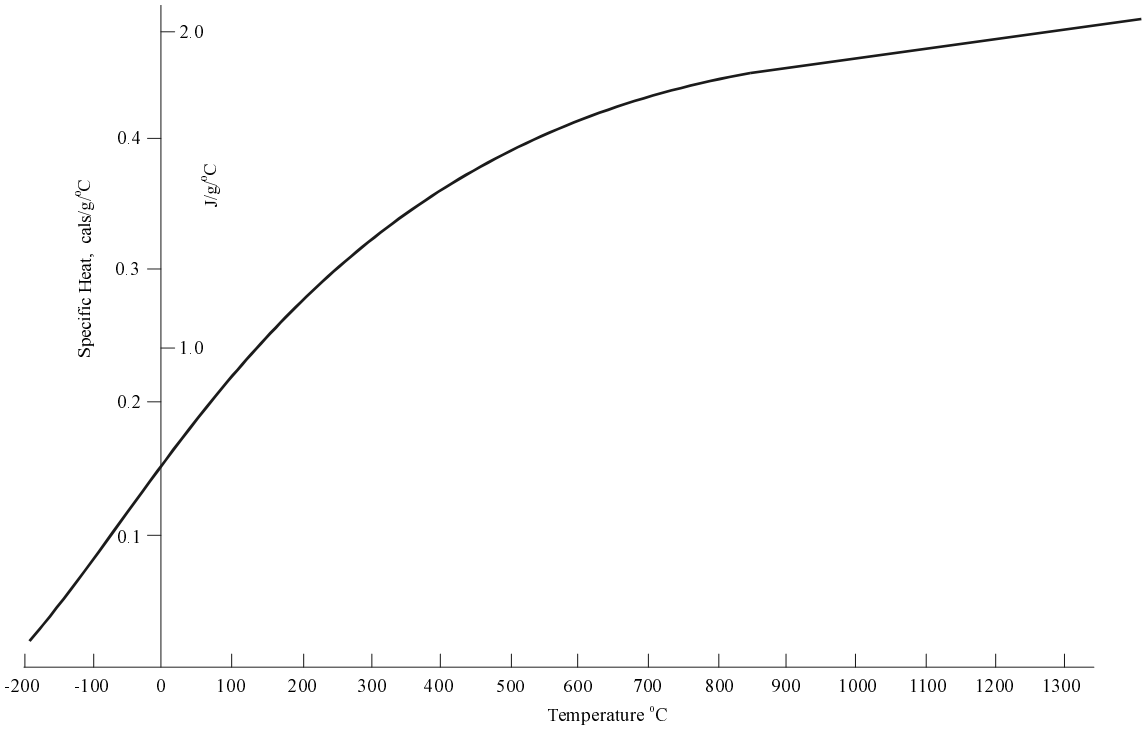

FIG. 4.5. Specific heat of graphite.

The simplest way of considering the effects of an energy release per unit temperature rise *dS/dT* as a function of temperature is to note first that this quantity is very insensitive to the conditions of measurement, that is the rate of temperature rise. This permits the definition of an effective specific heat for an irradiated graphite sample:

$$C'_p = C_p - \frac{dS}{dT} \tag{4.4}$$

Figure 4.5 shows the normal specific heat of graphite, C_p.

The conditions necessary for equation (4.4) to be valid were derived by Simmons (1965). If equation (4.4) is negative over a temperature range the effective specific heat is negative and the sample is self-heating, and the possibility of large, virtually adiabatic, temperature rises exists. This condition has only been observed for graphite irradiated at temperatures below 150 °C, where the sharp peak in the energy release rate at 200°C is observed.

Theoretically it is necessary to specify the state of the graphite and then express the rate of energy release in terms of the state of the graphite. It is usual, because the processes are controlled by thermal activation, to introduce the effect of temperature through a Boltzmann factor *exp*[*-E/kT*] where *E* is an activation energy and *k* is the Boltzmann constant.

Simmons (1965) has proposed a very general expression for the energy release rate with respect to time:

$$\frac{dS}{dt} = f(S)e^{-\frac{E}{kT}} \tag{4.5}$$

where *S* is the energy released or remaining. Equation (4.5) may be used in a variety of forms. A considerable number of calculations have been made assuming a constant activation energy E_0 (Cottrell *et al.*, 1958) to illustrate the effects of the parameters on the stored energy release. In this case equation (4.5) can be written

$$\int_{S_0}^{S} \frac{dS}{f(S)} = \int_0^t e^{-\frac{E_0}{kT}} dt \tag{4.6}$$

or

$$F(S) = \tau$$

where τ is a temperature reduced time.

The value of E_0 can be obtained experimentally from annealing experiments in which the rate of change *dP/dt* of a property *P* is measured for the same value of *P* at two different constant temperatures. Then

$$E_0 = \frac{kT_1T_2}{(T_1 - T_2)} \ln \left\{ \frac{\left(\frac{dP}{dt}\right)_1}{\left(\frac{dP}{dt}\right)_2} \right\} \tag{4.7}$$

The constancy or otherwise of E_0 is readily checked by determining it for different values of P. If E_0 is known to be constant, the value can be obtained by measuring a property $P(t)$ as a function of time at two different temperatures. If the value of P at a time t_1, temperature T_1 is the same as at a time t_n at temperature T_n, the value of τ must be the same, i.e.:

$$\tau = t_1 e^{-\frac{E_0}{kT_1}} = t_n e^{-\frac{E_0}{kT_n}} \tag{4.8}$$

and thence

$$E_0 = \frac{kT_1T_n}{(T_1 - T_n)} \ln \left(\frac{t_n}{t_1} \right) \tag{4.9}$$

Alternatively, the property P can be measured as a function of time at a constant rate of temperature rise a, but using different rates a and a'. In this case the integral in equation (4.6) is

$$\int_0^t e^{-\frac{E_0}{kat'}} dt' = \frac{E_0}{ka} \int_0^{x'} e^{-\frac{1}{x}} dx \tag{4.10}$$

with

$$x = \frac{kat'}{E_0}$$

The integral is given by

$$\int_o^x e^{-\frac{1}{y}} dy = x^2 e^{-\frac{1}{x}} \left[1 - 2!\, x + 3!\, x^2 - 4!\, x^3 ..... \right] \tag{4.11}$$

For most purposes

$$\tau = \frac{kT^2}{E_0 a} e^{-\frac{E_0}{kT}} \tag{4.12}$$

is an adequate approximation.

A significant amount of work was carried out in the USA using the relationship

$$\frac{dS}{dt} = -AS^{\gamma} e^{-\frac{E_0}{kT}} \tag{4.13}$$

with γ, the "order of reaction", in the range 6–8, which produces a sharply peaked curve of *dS/dT* as a function of temperature. Numerous relationships can be obtained between defined parameters such as S_m, the stored energy remaining, and the maximum release rate (which occurs at temperature T_m):

$$\left[\frac{dS}{dT}\right]_{\max} = \frac{S_m E_0}{kT_m^2 \gamma} \tag{4.14}$$

A single activation energy model is unlikely to be correct, given the very wide range of measurement temperatures at which energy release is observed when the temperature is raised at a constant rate. A simple model in which the activation energy varies was devised by Vand (1943) and further developed by Primak (1955, 1956, 1960). In the simplest form, due to Vand, it is assumed that the energy release process for each group of defects obeys first order kinetics. Thus for a group with activation energy *E* at constant temperature *T*

$$\frac{dS}{dt}(E,t) = -\nu S(E,t) e^{-\frac{E}{kT}} \tag{4.15}$$

where ν is a constant frequency factor. In an isothermal anneal equation (4.15) integrates to

$$S(E,t) = S_0(E) e^{-\nu t \exp\left(-\frac{E}{kT}\right)} \tag{4.16}$$

The function *exp[-νt exp(-E/kT)]* varies very rapidly with *E* for fixed time *t*, from 0 at $E = -\infty$ to 1 at $E = +\infty$, with an inflection point located at

$$E_0 = kT \ln(\nu t) \tag{4.17}$$

with a value 0.368. The variation with *E* is so rapid that to a good approximation the function can be replaced by a step function of unit height located at E_0. Equation (4.16) can be integrated over activation energy to give the total energy remaining from an initial spectrum $S_0(E)$.

$$S(t) = \int_0^\infty S_0(E) e^{-\nu t \exp\left(-\frac{E}{kT}\right)} dE \tag{4.18}$$

which, using the step function, can be approximated by

$$S(t) = \int_{E_0}^\infty S_0(E) dE \tag{4.19}$$

which gives on differentiation with respect to time

$$\frac{dS}{dt} = -S_0(E_0)\frac{dE_0}{dt} = -\frac{S_0(E_0)kT}{t} \tag{4.20}$$

E_0 can be regarded as the principal activation energy operating after time t at temperature T K. If the process were a true single activation energy process, then the activation energy would be blurred by this treatment from a sharp line to a spectrum covering a range ~ $2kT$ on either side of E_0.

If the temperature of the sample is raised at a constant rate a it is possible to make a similar approximation, but now the principal activation energy is given by

$$\left(\frac{E_0}{kT}\right) + \ln\left(\frac{E_0}{kT}\right) = \ln(\nu t) \tag{4.21}$$

where $T = at$. Equation (4.21) may be solved to give E_0 as a function of temperature for a given a, provided that ν is known. Nightingale (1959) analysed the thermal annealing of lattice parameter changes and showed that a value of $\nu = 7.5 \times 10^{13}$ s^{-1} was suitable to produce "matching" of changes in isothermal annealing at different temperatures and this value has been used by subsequent authors (Bridge, Kelly and Gray, 1962).

Using this value of ν, Bridge and Mottershead (1966) found, to a good approximation

$$E_0 = \left(33.7 - 1.83 \log_{10} a\right) T \times 10^{-4} - 0.037 \text{ eV} \tag{4.22}$$

with a in °C.min^{-1}, valid in the range $0.1 < a < 2 \times 10^3$°C.min^{-1}. As before, the measured rate of energy release per unit time

$$\frac{dS}{dt} = -S_0(E_0)\frac{dE_0}{dt} \tag{4.23}$$

$$\frac{dE_0}{dt} = ka\left(\frac{E_0}{kT}\right)\frac{\left[\frac{E_0}{kT} + 2\right]}{\left[\frac{E_0}{kT} + 1\right]} \tag{4.24}$$

$$= kaU \qquad \text{say}$$

where U is practically constant for a given value of a, that is $E_0 \propto T$. The activation energy spectrum for a sample can be obtained from the rate of energy release per unit temperature rise as

$$S_0(E_0) = -\frac{\left(\frac{dS}{dT}\right)_a}{kU} \tag{4.25}$$

For an arbitrary temperature history using the same methods, E_0 is obtained from

$$\nu \int_{O}^{t} e^{-\frac{E}{kT(t')}} dt' = 1 \tag{4.26}$$

Use of this method is not difficult with modern computers. It should be noted that given S versus T and E_0 versus T the function $E_0(S)$ is readily obtained which may be used in equation (4.5). Preston (1991) has made measurements on a number of samples obtained from the moderator of the BEPO reactor at Harwell and has demonstrated reasonable agreement between equation (4.22) and measured activation energies as a function of temperature. Given $E_0(S)$ of course $F(S)$ can be obtained. The Vand model has been applied to isothermal annealing by Bridge, Kelly and Gray (1962) and shown to give quite good agreement with the amount of energy released. The predicted shape of the energy release curve is not as well reproduced, but is probably adequate for calculations. Figure 4.6 illustrates the predictions and compares them against measurements.

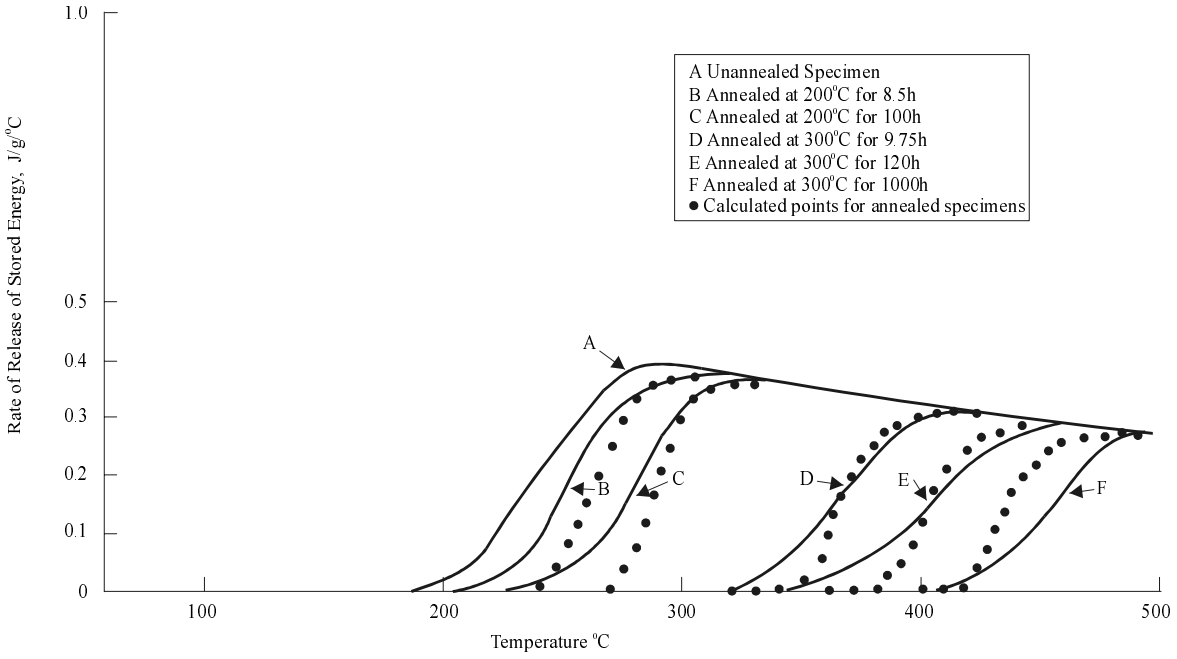

FIG. 4.6. The effect of annealing at 200 and 300 for various times on the linear rise curve of graphite irradiated at 155 to a dose of 2.35 × 10^{20} n/cm^2.

It is possible to devise an alternative treatment of stored energy based on a distribution of frequency factors ν (Lomer, 1959). In this treatment each group of processes is described by

$$\frac{dS(\nu,t)}{dt} = -\nu S(\nu,t) e^{-\frac{E_0}{kT}} \tag{4.27}$$

the activation energy being a fixed value E_0. If $S(\nu,t)d\nu$ is the stored energy released with frequency factor in the range ν to ν + $d\nu$ then the stored energy at time t is

$$S(t) = \int_{o}^{\infty} S(\nu,t)d\nu \tag{4.28}$$

which may be written

$$S(t) = \int_{0}^{\infty} S(\nu,0)e^{-\nu\tau}d\nu \tag{4.29}$$

where the reduced time τ is

$$\int e^{-\frac{E_0}{kT}}dt$$

and $S(\nu,0)$ is the initial stored energy release spectrum. Since the reduced time τ is known then the variation of stored energy with time is predictable. The exponential in equation (4.29) can, to a first approximation, be replaced by a step function

$$e^{-\nu\tau} = 1, \text{ for } \nu << \tau^{-1}$$

$$e^{-\nu\tau} = 0, \text{ for } \nu >> \tau^{-1}$$

giving

$$S(t) = \int_{0}^{\tau^{-1}} S(\nu,0)d\nu \tag{4.30}$$

This is equivalent (Simmons, 1965) to writing

$$\frac{dS}{dt} = f(S)e^{-\frac{E}{kT}} \tag{4.31}$$

The activation energies or frequency factors must be obtained experimentally and only a few measurements have been published of such determinations.

Åström (1961) measured stored energy release rates during isothermal annealing on samples irradiated to low doses (10^{17}–10^{18} n.cm^{-2}) at 35°C. Activation energies were determined in two temperature ranges, 70–100°C and 130–270°C. In the lower range he found that the activation energy increased with the radiation dose, increasing from ~0.4 to 1.0 eV. In the higher temperature range he found values of 1.2–2.0 eV, but with no clear dependence on dose or measurement temperature. Rimmer (1959) made measurements on higher dose samples irradiated at 40°C in the annealing temperature range 25–400°C and obtained values of 1.15–1.6 eV.

All of the theoretical studies have considered the situation for graphite containing a sharp peak in the energy release rate at 200°C and thus it is generally assumed that a reasonable approximation is to assume a constant activation energy. Solutions of equation (4.31) have been given by Cottrell *et al.*. (1958) using two sets of data corresponding to low doses and high doses

at an irradiation temperature of 30°C. In some cases it was found that the graphite temperature T stayed close to the coolant temperature T_c, but in other cases T exceeded T_c. The difference in behaviour depends upon the strength of coupling between the graphite temperature and the coolant temperature. Detailed analysis of the results showed that the strong coupling condition corresponds to

$$a_c q < 1\,°\mathrm{C}$$

while for loose coupling

$$a_c q > 10\,°\mathrm{C}$$

where a_c is the rate of rise of coolant temperature and q is a time constant (see equation (4.33)).

Cottrell *et al.* (1958) also studied the effect of a sudden increase in graphite and coolant temperatures on subsequent graphite temperatures. It was concluded that unless the graphite and coolant temperatures were raised by more than 70°C in full channel flow or 50°C in partial (8%) flow the graphite-coolant temperature difference remains small. Simmons (1965) presents simple approximate methods for analysing the effects of stored energy on moderator temperature. A separate but important problem is the propagation of stored energy release through the graphite moderator of a reactor. In the case of gas-cooled reactors, the only important practical situation, the release may spread by conduction or heat exchange with the reactor coolant gas. It is possible to make detailed calculations of the variations of coolant and moderator temperature with time in reactor fuel channels.

The effect of stored energy on the heat balance in the unit cell of a graphite moderated reactor is considered by Simmons (1965) and the details of the kinetics by Cottrell *et al.* (1958).

The heat balance is given by

$$C_p \rho A \frac{dT}{dt} = A\rho \frac{dS}{dt} + hP\left(T_c - T\right) \tag{4.32}$$

where A is the cross-sectional area of the graphite in a reactor unit cell
ρ is the graphite density
C_p is the specific heat of graphite
h is the heat transfer coefficient per unit length of channel
P is the perimeter of the fuel channel
T_c is the coolant temperature and T is the graphite (surface) temperature

Introducing a time constant $q = A\rho C_p/hP$, equation (4.32) becomes

$$\frac{dT}{dt} = \frac{1}{C_p}\frac{dS}{dt} + \frac{T_c - T}{q} \tag{4.33}$$

Simmons notes that it is useful to consider two special cases, rather than attempt a completely general discussion. The first case neglects the effect of thermal conduction. The stored energy release is then propagated by heat exchange with the coolant gas. Suppose the coolant gas entering a fuel channel is rapidly raised in temperature, then the graphite temperature near the coolant inlet will increase more rapidly than that further along the channel. If the stored energy is fairly constant along the channel (actually not a very realistic case because of the cosine dependence of the axial flux and the steadily rising temperature which tends to produce a peak in the stored energy in the cooler half of the reactor), the energy release will start at the lower temperature end. In the condition of loose coupling to the gas temperature the graphite temperature will then rise above the gas temperature and transfer heat to the coolant gas. The resulting rise in coolant temperature will then reduce the time required for the energy release to occur further along the channel; that is the spread of energy release is governed by the heat exchange between the graphite and coolant.

In the second case the heat transfer between the graphite and coolant is completely neglected and the release spreads by conduction only. Assuming that the stored energy is uniform, the thermal conductivity is constant, the initial temperature is uniform at a value T_1 and that heat losses from the channel ends can be neglected, then the heat balance equation is

$$C_p \frac{\partial T(z,t)}{\partial t} = \frac{dS}{dt} + \frac{\partial T(z,t)}{\partial z} \tag{4.34}$$

where z is the axial position.

In this case the graphite temperature would rise slowly due to the energy release and an adiabatic release would take place simultaneously throughout the graphite. If some heat is applied, say at $z = 0$, the release will start at the point and spread axially by conduction. Foreman (1959) has shown that if the stored energy is large enough the release will propagate as a temperature wave with a well-defined front at a velocity of a few cm.min^{-1}. It can be shown that the temperature in the wave front is a function of $y = z - vt$ where v is the velocity of the wave front. A point at temperature T_m is located on the wave front where $d^2T/dz^2 = 0$. For $T < T_m$ heat is supplied to the graphite, while for $T > T_m$ there is a net forward propagation of heat. The effect of spatial variation in stored energy or non-uniform temperature is to cause the wave to build up or decay. Foreman and Curtis (1960) have examined the effect of uniform cooling for this case. It was shown that propagation does take place provided the constant is above a critical value, but for lower values the wave is heavily damped. In practical cases the critical time constant was 2–4 hours.

The early air-cooled graphite moderated reactors accumulated large amounts of stored energy. A number of reactors employed the method of controlling stored energy by regular anneals. The first reactors to be annealed were those at Windscale and BEPO in the United Kingdom. The method used was to shut off the coolant flow and then operate at low power in order to raise the graphite temperatures to ~ 100°C following which the power was cut off and the temperature allowed to rise due to the stored energy release which then spread through the reactor. The reactor graphite temperatures rose rapidly to levels between 300°C and 400°C. In order for this technique to work it was necessary to choose the time of the anneal carefully so that there was enough energy to produce successful propagation but not so much that excessive

temperatures would arise. The amount of nuclear heating applied needed to be carefully controlled.

Eventually annealing became regarded as a potentially dangerous operation in air-cooled reactors because of the graphite-air reaction, which was enhanced by irradiation damage. In 1957 one of the two Windscale Production Piles caught fire during an annealing operation and the annealing process was reviewed as a result and improved methods devised. Dickson *et al.*. (1958) describe an improved technique used on the BEPO reactor in which a flow of pre-heated air at 140°C was maintained to the reactor throughout the anneal, permitting quasi-adiabatic anneals. Similar techniques were applied in France and the USA (see Simmons, 1965). The effect of repeated anneals on the long term changes in dimensions and properties has been reported by Woodruff (1959).

The thermal conductivity of graphite

The thermal conductivity of a graphite crystal has two principal tensor components, measured parallel and perpendicular to the basal plane. The conductivities are both dominated by lattice vibrations (phonons) except at very low temperatures (~1 K) and possibly at very high temperatures where the electronic component is significant (see Kelly (1969) for a review). The conductivities are controlled at low temperatures by the scattering of the phonons at crystal boundaries, whereas at high temperatures they are scattered by other phonons. In the former case the conductivity increases with temperature and in the latter decreases with increasing temperature, so that there is a peak at intermediate temperatures for not too imperfect materials where the first process dominates. The conductivity is much higher parallel to the basal planes than perpendicular to them. In all except very well oriented materials it is found that the conductivity is dominated by the basal conductivity of the component crystallites (Taylor, Gilchrist and Poston, 1968; Kelly, 1981). It is generally possible to write, for a direction x:

$$K_x = \frac{K_a}{\beta_x} \tag{4.35}$$

where β_x is a constant and K_a is the basal conductivity of the component crystallites. For low density poorly crystalline carbons the matrix conductivity is low because of the small crystallite size and the conductivity is dominated by heat transfer across the pores, either by radiation or gaseous conductivity, so that, strictly speaking, equation (4.35) must be verified for each new material. It is known to be well obeyed for well-graphitised materials with up to 50% total porosity. The basal conductivity K_a of a graphite crystal for temperatures greater than 1 K is given by (Kelly, 1969):

$$\frac{1}{K_a} = \frac{1}{K_B} + \frac{1}{K_U} + \frac{1}{K_D} \tag{4.36}$$

where

$1/K_B$ is the thermal resistance due to crystallite boundary scattering,
$1/K_U$ is the thermal resistance due to phonon scattering,
$1/K_D$ is the thermal resistance due to lattice defects.

The thermal resistance due to crystallite boundary scattering may be written

$$\frac{1}{K_B} = \frac{1}{F(T)} L_a \tag{4.37}$$

where L_a is the crystallite size measured parallel to the basal planes and $F(T)$ is a function of measurement temperature and the crystal elastic constants. $1/K_U$ has been derived from measurements of conductivity over a wide temperature range and is roughly of the form $AT^n \exp[\theta/T]$ where n and θ are constants. $1/K_D$ is not usually significant in unirradiated graphite.

The effect of irradiation is to increase the thermal resistance term. It would be expected that different lattice defects would scatter phonons, with different dependencies on the phonon frequencies leading to different temperature dependencies for the thermal resistances. It is difficult to develop appropriate theories of the scattering because of the anisotropic nature of the crystal lattice, although some attempts have been made (Dreyfus and Maynard, 1967; Kelly, 1969; Klemens, 1953). The assumption is always made that the lattice vibration spectrum is not changed by the presence of the crystal lattice defects, which is probably not correct at high damage levels.

In order to make progress with understanding the changes in thermal resistance under irradiation it has become customary to plot the fractional change in thermal resistance against dose for fixed irradiation temperatures at a particular measurement temperature. This is if β_x

$$\frac{\dfrac{1}{K_x(\gamma,T_m)} - \dfrac{1}{K_x(0,T_m)}}{\dfrac{1}{K_x(0,T_m)}} = \frac{K_x(0,T_m)}{K_x(\gamma,T_m)} - 1$$

$$= \frac{K_a(0,T_m)}{K_a(\gamma,T_m)} - 1 \tag{4.38}$$

does not change and where $K_a(0,T_m)$ is the basal conductivity at measurement temperature T_m for zero dose.

$1/K_a(\gamma,T_m)$ is the thermal resistance at dose γ, measurement temperature T_m. Figure 4.7 shows the fractional changes in thermal resistance at ambient temperature of Pile Grade A graphite irradiated with reactor neutrons over a wide range of irradiation temperatures. The changes are independent of direction of cut of the samples, as expected from equation (4.38), and strongly dependent on the irradiation temperature, decreasing with increasing temperature. The changes bear a strong resemblance to the variation of total stored energy with dose and irradiation temperature.

Bell *et al.*. (1962) compared their measurements of thermal resistivity change in Pile Grade A at ambient temperature with total stored energy, S, measured on the same samples and obtained a good correlation

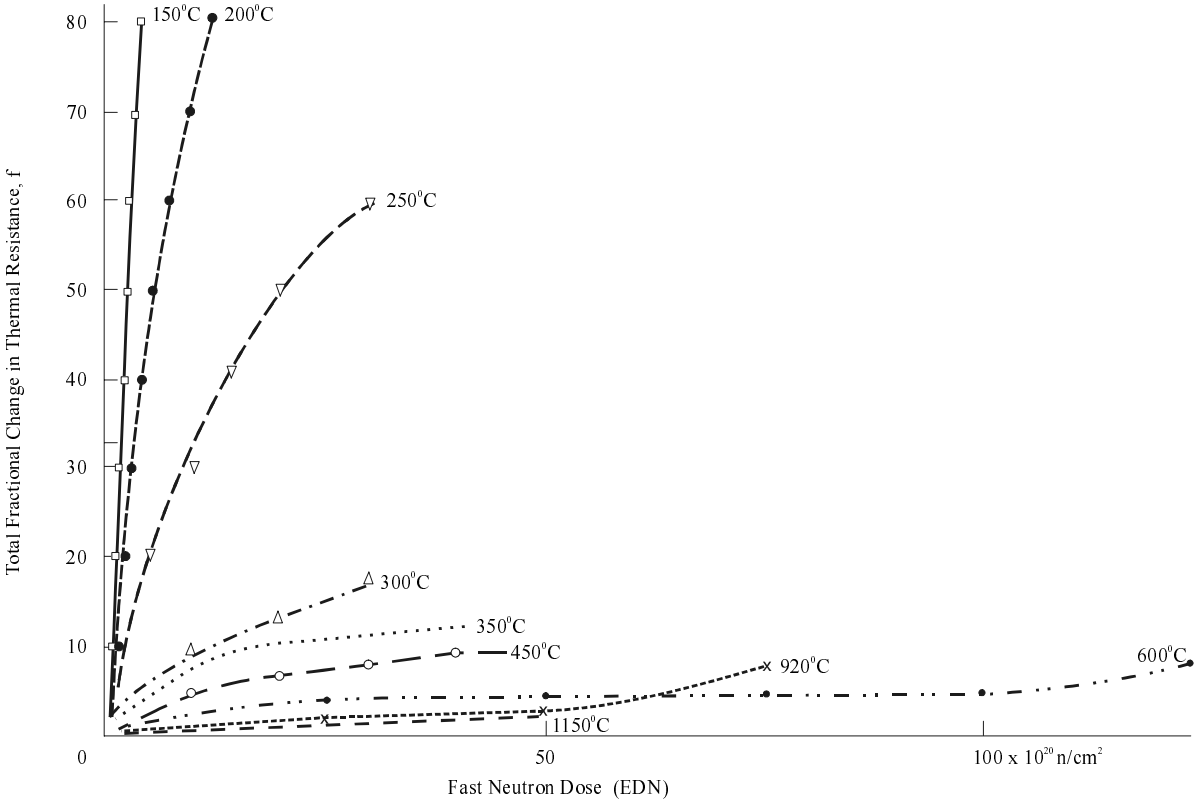

FIG. 4.7. Fractional changes in thermal resistance of PGA graphite at various irradiation temperatures.

$$S = 26.1\left[\frac{K_0}{K} - 1\right] \quad \text{J.g}^{-1} \tag{4.39}$$

for irradiation temperatures between 150 and 350°C. The total stored energy and thermal resistivity changes are available for CSF graphite irradiated at 30°C and a similar correlation is obtained (see Bell *et al.*., 1962). Smith and Rasor (1956) report data on a number of graphites irradiated at 30°C.

Measurements of the temperature dependence of thermal conductivity post-irradiation have been surprisingly rare. Mottershead and James (1967) reported data on Pile Grade A graphite and data on CSF graphite are reported by Carter (1959). The temperature dependence post-irradiation is much reduced, tending in the extreme to lead to proportionality to the specific heat. Taylor, Kelly and Gilchrist (1969) have made measurements on highly oriented pyrolytic graphite parallel and perpendicular to the deposition plane (or basal planes) from which the additional thermal resistance may be derived for both crystallographic directions.

A detailed analysis of the effect of irradiation on the temperature dependence of thermal conductivity was given by Carter (1959) who assumed that the scattering of phonons is independent of temperature, an assumption which at the time was apparently supported by the evidence. A similar method was described by Simmons (1965). Simmons noted that because of the near two-dimensional nature of the crystal lattice it is a good approximation to write

$$K_a = \frac{1}{2}\rho C_p V l \tag{4.40}$$

where l is the phonon mean free path and V is the mean phonon group velocity parallel to the basal planes. In considering the effect of irradiation on thermal conductivity it is convenient to write

$$\frac{1}{l} = f\left(T_m\right) + G \tag{4.41}$$

where $f(T_m)$ is proportional to the scattering power in the unirradiated state and G represents the additional scattering due to the radiation induced lattice defects. The term $f(T_m)$ includes phonon-phonon scattering and pre-irradiation lattice defects (crystal boundaries, etc). Assuming that to a good approximation the specific heat is unchanged by irradiation (true for temperatures above ambient, but not for low temperatures) then

$$\frac{K\left(0,T_m\right)}{K\left(\gamma,T_m\right)} - 1 = \frac{G}{f\left(T_m\right)} \tag{4.42}$$

If G is independent of temperature then it is possible to relate values of fractional change measured at two different temperatures, that is

$$\left[\frac{K\left(0,T_m'\right)}{K\left(\gamma,T_m'\right)} - 1\right] = \left[\frac{f\left(T_m\right)}{f\left(T_m'\right)}\right]\left[\frac{K\left(0,T_m\right)}{K\left(\gamma,T_m\right)} - 1\right] \tag{4.43}$$

It may be deduced that because $f(T_m)$ contains the effect of defects present pre-irradiation then the fractional changes in thermal resistance will be less in an imperfect graphite, for the same defect content, than in a perfect graphite.

Taylor, Kelly and Gilchrist (1969) reported measurements of the thermal resistance produced by irradiation in highly oriented pyrolytic graphite parallel and perpendicular to the deposition planes (ie basal planes). This amounts to examining the same defects with phonons propagating in different directions. The results show that the thermal resistance added by irradiation at temperatures in the range 30–450°C is not independent of temperature. In the direction parallel to the basal planes the additional resistance is fairly constant for measurement temperatures greater than 300 K, (there is a shallow minimum at about 550 K), but increases with decreasing temperature at low temperatures. The shape of this curve is apparently independent of temperature and also of the annealing condition. In the direction perpendicular to the deposition plane the temperature dependence was similar. The apparent insensitivity of the temperature dependence of the irradiation induced thermal resistance parallel to the basal planes means that given the fractional changes in thermal resistance at ambient (here denoted by f) the thermal conductivity in direction x of the polycrystal at temperature T_m K is given by

$$K_x\left(T_m\right) = K_x\left(0,T_m\right)\left[1 + f\ \delta\left(T_m\right)\left\{\frac{K_x\left(0,T_m\right)}{K_x\left(0,300\right)}\right\}\right] \tag{4.44}$$

where $\delta(T_m)$ is the temperature dependence of the thermal resistance due to irradiation normalised to unity at 300 K (see Fig. 28 of Kelly, 1969). Later work due to Binkele (1972, 1978) and to Brown *et al.*. (1990) has shown that $\delta(T_m)$ is not independent of irradiation temperature, showing less temperature dependence for irradiation temperatures greater than 450°C. It should be noted that some care is necessary in interpreting plots of thermal resistance with dose because of changes in the parameter β_x due to structural changes.

Taylor, Kelly and Gilchrist (1969) have tried to relate the changes in thermal resistance parallel to the basal planes to concentrations of defects estimated from the crystal dimensional changes and lattice parameter changes. The concentrations of various defects were estimated by Henson *et al.*. (1968). It was assumed that for irradiations at temperatures below ~ 450°C only the sub-microscopic(4 ±2 atoms) interstitial groups and point vacancies contributed significantly to the irradiation induced thermal resistance, the interstitial dislocation loops and collapsed vacancy lines being relatively insignificant. Given these assumptions, for a polycrystalline graphite in direction x

$$\Delta\left(\frac{1}{K_x}\right) = \alpha_x\left[\delta\, x_i\, S_i^2 + \beta\, C_v\, S_v^2\right] \tag{4.45}$$

where δ and β are numerical constants appropriate to ambient temperature, α_x is a factor allowing for porosity and tortuosity, x_i and C_v are the concentrations as before and S_i and S_v are the scattering parameters, of order unity. Using the estimated defect concentrations it is possible to plot $\Delta(1/K_x)/C_v$ against x_i/C_v and then, given theoretical estimates of δ and β, to obtain S_i^2 and S_v^2. Kelly (1969) obtained S_i^2 and S_v^2 and found 3.2 and 0.72 respectively, in fair agreement with expectation. Thermal resistance changes in Pile Grade A graphite following irradiation at 650, 900 and 1350°C requires an additional contribution which has been attributed to the presence of small uncollapsed vacancy loops which lead to a thermal resistance

$$\Delta\left(\frac{1}{K_x}\right) = \alpha_x\left[C_v\,\beta S_v^2 + \eta\frac{C_{v,Loop}}{r_0}\right] \tag{4.46}$$

where r_o is the loop radius, $C_{v,Loop}$ the concentration of vacancies in such loops and η a constant appropriate to room temperature.

It is possible to compare measurements of the changes in thermal resistance parallel to the basal planes with predictions from lattice parameter changes which are used to estimate the point defect concentrations x_i and C_v. The results are presented by Taylor, Kelly and Gilchrist (1969). The agreement is good.

The situation for this range of irradiation temperature is apparently quite satisfactory, however comparison with inferences from the stored energy and dimensional changes shows that there are difficulties. If the total stored energy is written in the form

$$S = 19.4\times10^2\left[x_i E_{fi} + C_v E_{fv}\right] \quad \text{cal.g}^{-1} \tag{4.47}$$

where E_{fi} and E_{fv} are the energies of formation of the interstitial atoms in the groups and point vacancies in eV, the energy of defects which constitute interstitial and vacancy loops is neglected. The experimental data are such that for all except small doses x_i/C_v is small and equation (4.47) becomes, on combination with equation (4.45)

$$S = 5f\,E_{fv} \quad \text{cal.g}^{-1} \tag{4.48}$$

for Pile Grade A graphite. The experimental value is $6.5f$ leading to E_{fv} ~1.3 eV, which is much less than the expected value of about 7 eV for a single vacancy. An analysis by Henson and Reynolds (1965) showed that the apparent formation energy of the vacancies decreased substantially for apparent concentrations greater than 1%. It was suggested that this was due to long range attractive interactions between vacancies and the formation of small uncollapsed vacancy loops, but the rate of formation of collapsed vacancy lines would be much greater than is observed if the point vacancy concentrations that are estimated are real. The alternative view is that phonon scattering and in-plane ($\Delta a/a$) lattice parameter changes are in part due to the ends of the collapsed vacancy lines (which strictly are two-dimensional dislocation dipoles one layer thick). The scattering by such dipoles has been considered by Kelly (1969) but has not been applied to the data in detail. There are two obvious simplifications, where the phonon wavelength is much greater or less than the dipole separation, but there is difficulty in making the calculations (Kelly, 1969).

The phonon scattering due to point defects can be considered as the result of three factors, assuming that the phonon wavelength is much larger than the defect size:

(i) The mass defect associated with the presence of the defect.

(ii) The change in strength of the local interatomic bonds.

(iii) The strain field of the defect.

The major difficulty in assessing the scattering of phonons by defects in graphite is the fundamental separation of the phonons into two groups, one in which the atomic motion is perpendicular to the layer planes and the other in which it is parallel to the layer planes. This latter group can be further sub-divided into longitudinal and transverse components. The scattering of phonons into the same polarisation is relatively easy but the scattering of in-plane states to out-of-plane states and vice versa is dependent on the details of the defect structure, a subject not yet satisfactorily resolved for point defects or small defect groups. It would, for instance, be expected that the scattering would decrease as the temperature falls and the mean phonon wavelength increases. The data apparently show that the opposite is true. Recent studies on irradiated graphite at low measurement temperatures show that this increase in scattering is resonant in form, although the mechanism is unclear. It remains difficult to understand why varying proportions of interstitial and vacancy defects produce the same or closely similar scattering curves, although this may be due to the relative paucity of data at low temperature on graphite irradiated at ambient or higher temperatures. This general area of defect scattering in an anisotropic lattice requires a great deal of work.

There are many calculations of the lattice vibration spectrum of graphite (see Kelly, 1981) but for most purposes the semi-continuum model due to Komatsu (1955, 1958, 1964), Komatsu and Nagamiya (1951) and Nagamiya and Komatsu (1954) is adequate. In this model the basal

planes are replaced by elastic sheets, the sheets interacting through forces which resist shear and compression-tension forces. The equations of motion of the layers are readily soluble and lead to the following frequency-wave number relations for the three acoustic modes:

$$\nu_1^2 = V_L^2\left[\sigma_x^2 + \sigma_y^2\right] + \left(\frac{\zeta}{\pi^2 d^2}\right)\sin^2\left(\pi d\sigma_z\right)$$

$$\nu_2^2 = V_T^2\left[\sigma_x^2 + \sigma_y^2\right] + \left(\frac{\zeta}{\pi^2 d^2}\right)\sin^2\left(\pi d\sigma_z\right) \qquad (4.49)$$

$$\nu_3^2 = 4\pi^2\delta^2\left[\sigma_x^2 + \sigma_y^2\right]^2 + \left(\frac{\mu^2}{\pi^2 d^2}\right)\sin^2\left(\pi d\sigma_z\right) + \zeta\left[\sigma_x^2 + \sigma_y^2\right]$$

where ν_1 and ν_2 are the in-plane longitudinal and transverse mode frequencies and ν_3 is the frequency of the out-of-plane mode; σ_x, σ_y and σ_z are the wave number components parallel to the principal co-ordinate axes with the z-axis parallel to the hexagonal axis; and d is the interlayer spacing. The parameters V_L, V_T, μ and ζ are related to the crystal elastic constants as follows:

$$V_L^2 = \frac{C_{11}}{\rho}$$

$$V_T^2 = \frac{1}{2\rho}\left(C_{11} - C_{12}\right)$$

$$\mu^2 = \frac{C_{33}}{\rho} \qquad (4.50)$$

$$\zeta = \frac{C_{44}}{\rho}$$

where the C_{ij} are the usual elastic constants (see Chapter 5). The parameter δ (value 6.11×10^{-3} $cm^2.s^{-2}$) is a bond bending resistance in a single layer plane which is characteristic of layer lattices. The unusual dependence of the term containing δ on a wave number is very important for explanation of the properties of graphite. The wave numbers may be written in terms of $\sigma^2_a = \sigma^2_x + \sigma^2_y$ and σ^2_z.

The near two-dimensional nature of the graphite lattice reduces the frequency dependence of the scattering processes compared to the well-understood three dimensional case. For point defects the scattering is dependent on the third power of the frequency rather than the fourth power and for sessile dislocations is frequency independent rather than a first power dependence. Scattering by grain boundaries and extended defects remains describable by a constant mean free path.

Dreyfus and Maynard (1967) considered the effect of an interstitial atom which couples adjacent layer planes, a model which has been proposed by various authors (see Heggie, 1992, for a summary of models). There is a need for further studies of phonon scattering in a highly anisotropic lattice.

Hove (1959) and Deegan (1956) described the effect of annealing on thermal conductivity post-irradiation at low temperatures (~100 K). Their results showed that as annealing proceeds the thermal resistivity decreases and then increases again. This phenomenon also appears in low temperature electron irradiations, showing an inverse annealing peak between 220 and 270 K (Goggin and Reynolds, 1963).

The effect of annealing on thermal resistivity following irradiation at ~30°C and measured at room temperature has been described (Kinchin, 1956; Woods, Bupp and Fletcher, 1956). Pulse annealing experiments have been described by Hook (1952), and Austerman (1955) has measured the activation energies for annealing using thermal conductivity. In graphite irradiated at ambient temperature to moderate doses the annealing is very similar to the recovery of stored energy, showing a peak in the annealing rate at 200°C. High dose samples irradiated at 150, 200, 250 and 350°C show steady annealing with increasing temperature, with an increased rate at high temperatures and complete recovery (in the absence of structural damage) at 1850°C, the peak temperature tending to be higher for higher total damage.

The effect of annealing on the principal thermal conductivities of highly oriented pyrolytic graphite irradiated at various temperatures between 150°C and 450°C was described by Kelly (1969). The annealing is gradual up to 900°C and then increases, being complete by 1700°C. The temperature dependence of the principal conductivities was also examined after annealing at various temperatures and the additional thermal resistance determined as a function of temperature. The same unusual temperature dependence was found, simply reduced in magnitude with increasing annealing temperature. It was shown that the changes on annealing were predictable, using the same relationships as those for continuous irradiation with estimated interstitial and vacancy concentrations.

The analysis of irradiation annealing of graphite following irradiations at 150°C and 225°C by Gray *et al.*. (1969) led to the following relationship for Pile Grade A graphite:

$$\frac{K_o}{K} - 1 = 25x_i + 6C_v + 11C_{2v} \tag{4.51}$$

where C_{2v} is the di-vacancy concentration (x_i, C_v and C_{2v} are in units of %), the numerical values being based on the work of Kelly (1967) and Taylor, Kelly and Gilchrist (1969).

REFERENCES TO CHAPTER 4

ÅSTRÖM, H.U. (1961), Arkiv för Fysik, 20, 161.

AUSTERMAN, S.B., (1955), Activation Temperatures for Annealing of Neutron-Damaged Graphite as Determined by Isothermal Pulse Annealing, Report NAA-SR-1198.

AUSTERMAN, S.B. (1956), Stored Energy Release in Graphite Irradiated at Low Temperatures, Report NAA-SR-1564.

BELL, J.C., BRIDGE, H., COTTRELL, A.H., GREENOUGH, G.B., REYNOLDS, W.N. and SIMMONS, J.H.W. (1962), Phil. Trans. Roy. Soc. A, 254, 361.

BELL, J.C. and GREENOUGH, G.B. (1959), Report of US/UK Graphite Conference, 1957, TID-7565, Part 1, p102.

BINKELE, L. (1972), High Temperatures — High Pressures, 4, 401.

BINKELE, L. (1978), J. Non-Equilib. Thermodynamics, 3, 257.

BOCHIROL, L. and BONJOUR, E. (1968), Carbon, 6, 661.

BRIDGE, H., KELLY, B.T. and GRAY, B.S. (1962), Proc. Fifth Conference on Carbon, Pergamon Press, 1,289.

BRIDGE, H. and MOTTERSHEAD, D. (1966), J. Nucl. Mater., 20, 281.

BROWN, R.G., BROCKLEHURST, J.E. and HODGETTS, N.S.P. (1990), Thermal Conductivity of CAGR Graphites — An Examination of the Temperature Dependence, UKAEA Report ND-M-1579(S) Addendum 2.

CARTER, R.L. (1959), Report of US/UK Graphite Conference, 1957, TID-7565, Part 1, p33.

COTTRELL, A.H., BELL, J.C., GREENOUGH, G.B., LOMER, W.M. and
SIMMONS, J.H.W. (1958), Proceedings of the Second United Nations Conference on the Peaceful Uses of Atomic Energy, United Nations, p315.

DAVIDSON, J.M. (1959), Report of US/UK Graphite Conference, 1957, TID-7565,
Part 1, p11.

DEEGAN, G.E. (1956), Thermal and Electrical Properties of Graphite Irradiated at Temperatures from 100 to 425 K, Report NAA-SR-1716.

DICKSON, J.L., KINCHIN, G.H., JACKSON, R.F., LOMER, W.M. and
SIMMONS, J.H.W. (1958), Proceedings of the Second United Nations Conference on the Peaceful Uses of Atomic Energy, United Nations, p250.

DREYFUS, B. and MAYNARD, R. J. (1967), Physique, 28, 955.

FOREMAN, A.J.E. (1959), Report of US/UK Graphite Conference, 1957, TID-7565,
Part 1, p115.

FOREMAN, A.J.E. and CURTIS, A.R. (1960), Propagation of Thermal Waves through Graphite with Uniform Cooling, Report AERE-R3500.

GOGGIN, P.R. and REYNOLDS, W.N. (1963), Phil. Mag., 8, 265.

GRAY, B.S., BROCKLEHURST, J.E., KELLY, B.T., SØRENSEN, H. and
DIETRICH, O.W. (1969), UKAEA Report TRG 1858(C).

HEGGIE, M.L. (1992), Carbon, 30, 71.

HENSON, R.W., PERKS, A.J. and SIMMONS, J.H.W. (1968),Carbon, 6, 789.

HENSON, R.W. and REYNOLDS, W.N. (1965), Carbon, 3, 277.

HOOK, A.S. (1952), Changes in the Thermal and Electrical Properties of Irradiated Graphite during Pulse-Annealing, NAA-SR-119.

HOVE, J.E. (1959), Prog. Nuclear Energy Series V, 2, 551.

KELLY, B.T. (1967), Carbon, 5, 247.

KELLY, B.T. (1969), Chemistry and Physics of Carbon, 5 (Ed. P.L. WALKER, JR), MARCEL DEKKER, New York, 119.

KELLY, B.T. (1981), Physics of Graphite, Applied Science Publishers, London.

KELLY, B.T., BROCKLEHURST, J.E. and GILCHRIST, K.E. (1979), Extended Abstracts 14thBiennial Carbon Conference, Pennsylvania, p473.
KINCHIN, G.H. (1956), Proceedings of the United Nations Conference on the Peaceful Uses of Atomic Energy, United Nations, 7, p472.
KLEMENS, P.G. (1953), Aust. J. Phys., 6, 405.
KOMATSU, K. (1955), J. Phys. Soc. Japan, 10, 346.
KOMATSU, K. (1958), J. Phys. Chem. Solids, 6, 380.
KOMATSU, K. (1964), J. Phys. Chem. Solids, 25, 707.
KOMATSU, K. and NAGAMIYA, T. (1951), J. Phys. Soc. Japan, 6, 438.
LOMER, W.M. (1959), Report of US/UK Graphite Conference, 1957, TID-7565, Part 1, 111.
MOTTERSHEAD, D. and JAMES, A. (1967), Conference on Industrial Carbon and Graphite, 1966, Society of Chemical Industry, London.
NAGAMIYA, T. and KOMATSU, K. (1954), J. Chem. Phys., 22, 1457.
NIGHTINGALE, R.E. (1959), Report of US/UK Graphite Conference, 1957, TID-7565, Part 1, p21.
PRESTON, S.D. (1991), BEPO Stored Energy Measurements, UKAEA Report AEA TRS 5099.
PRIMAK, W. (1955), PHYS. Rev., 100, 1677.
PRIMAK, W. (1956), Phys. Rev., 103, 1681.
PRIMAK, W. (1960), J. Applied Phys., 31, 1524.
RAPPENEAU, J., TAUPIN, J.L. and GREHIER, J. (1966), Carbon, 4, 115.
RIMMER, D.E. (1959), The Validity of the Constant Activation Energy Model for the Release of Stored Energy in Graphite, Report AERE-R3061.
SIMMONS, J.H.W. (1965), Radiation Damage in Graphite, Pergamon Press.
SMITH, A.W. and RASOR, N.S. (1956), Phys. Rev., 104, 885.
TAYLOR, R., GILCHRIST, K. and POSTON, J. (1968), Carbon, 6, 537.
TAYLOR, R., KELLY, B.T. and GILCHRIST, K.E. J. (1969), Phys. Chem. Solids, 30, 2251.
VAND, V. (1943), Proc. Phys. Soc. A, 55, 222.
WOODRUFF, E.M. (1959), Report of US/UK Graphite Conference, 1957, TID-7565, Part 1, p1.
WOODS, W.K., BUPP, L.P. and FLETCHER, J.F. (1956), Proceedings of the United Nations Conference on the Peaceful Uses of Atomic Energy, United Nations, 7, p455.

CHAPTER 5

MECHANICAL PROPERTIES AND IRRADIATION CREEP OF GRAPHITE

In the unirradiated state orthodox polycrystalline graphites are near brittle materials with low elastic moduli (~10^{11} dyn.cm^{-2}). The mechanical strengths and the elastic moduli decrease slowly with increasing heat treatment temperature and the stress-strain curves become increasingly non-linear. The strain to failure is roughly one order of magnitude greater in compression than tension.

Normal extruded or moulded polycrystalline graphite possesses an axis of symmetry parallel to the extrusion or pressing direction and thus has the same symmetry as a graphite crystal. The same symmetry applies to highly oriented pyrolytic graphite and thus in every case the elastic deformation can be described by five elastic compliances S_{ij} or moduli C_{ij} (the same symbols with a dash apply to crystal values). An isotropic graphite requires only three compliances or moduli. Table V.1 compares typical elastic compliances for an isotropic graphite (Gilsocarbon) and an anisotropic graphite (Pile Grade A) measured at small strains (Goggin and Reynolds, 1967).

TABLE V.1

TYPICAL ELASTIC COMPLIANCES FOR ANISOTROPIC AND ISOTROPIC GRAPHITE

Elastic Compliance	Pile Grade A (Anisotropic) cm^2/dyn	Gilsocarbon (Isotropic) cm^2/dyn
S_{11}	2.150×10^{-11}	1.370×10^{-11}
S_{12}	-0.127×10^{-11}	-0.148×10^{-11}
S_{13}	-0.123×10^{-11}	-
S_{33}	1.087×10^{-11}	-
S_{44}	3.333×10^{-11}	3.030×10^{-11}

The elastic constants reported in the literature are generally determined in one of two ways: dynamically, that is at very small strains (although not generally well defined); or quasi-statically where the strain is measured as a function of stress. The non-linearity of the stress-strain curves presents a difficulty since the compliances increase with strain, there is significant hysteresis on unloading and a permanent set occurs. Figure 5.1 shows the stress-strain relations of an unirradiated polycrystalline graphite.

The effect of irradiation with fast neutrons is to initially increase the elastic moduli by substantial factors, depending upon the material, at low doses, followed by subsequent increases and decreases. The effects of irradiation on the crystal elastic constants have been examined using the best available single crystals (Ticonderoga flake) or highly oriented pyrolytic graphite. Very thorough studies of this type were reported by Seldin and Nezbeda (1970). Highly oriented pyrolytic graphite and carefully chosen Ticonderoga flakes were irradiated at 50, 650 and 1000°C. It was found that in each case only the crystal elastic constants C_{33} and C_{44} changed. At

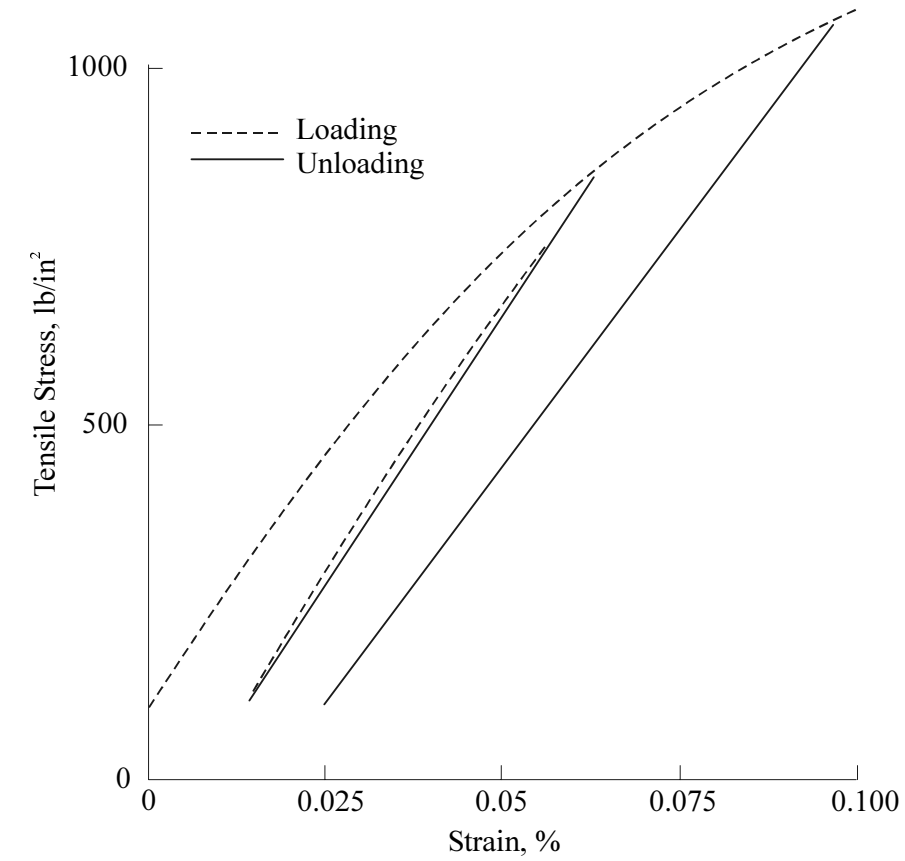

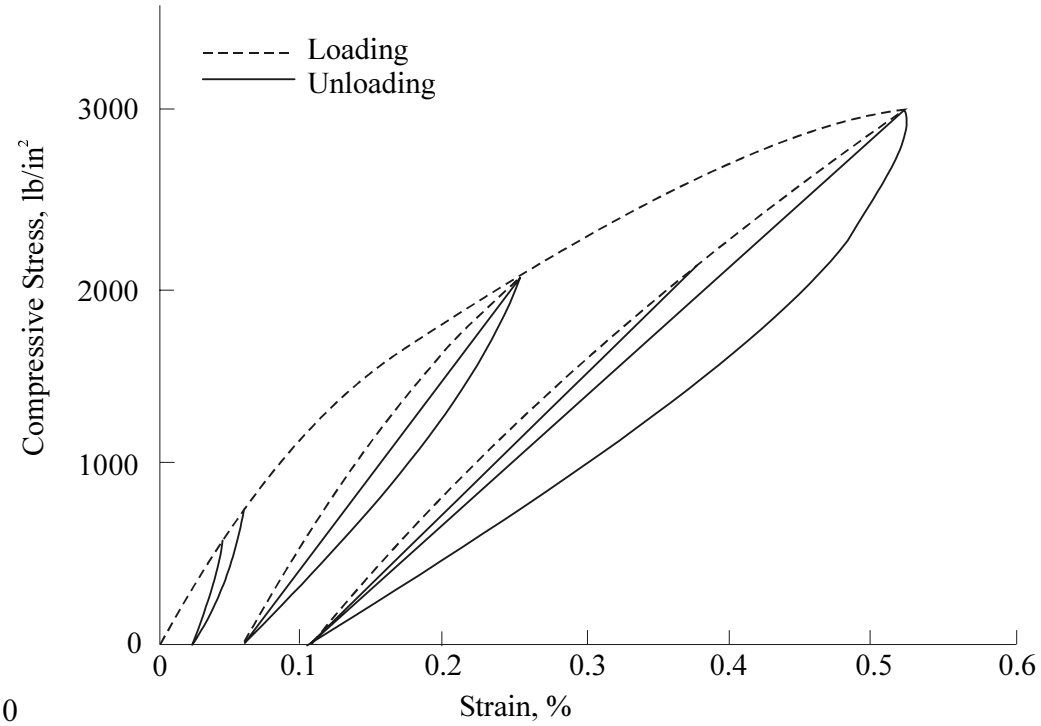

FIG. 5.1. Stress and strain diagrams for unirradiated graphite.

the elastic modulus C_{33} in highly oriented pyrolytic graphite decreased slightly from an initial value of 3.65×10^{11}dyn.cm^{-2}, the expected value for the crystal in that direction. The dose range examined was ~10^{19}n.cm^{-2}. The changes in C_{44} were much larger, from initial values of 0.021–0.030×10^{11}dyn.cm^{-2} to a near saturation value of 0.4×10^{11}dyn.cm^{-2}, close to the value expected for a perfect crystal. The single crystal samples irradiated at 650 and 1000°C showed large increases in C_{44} also, tending to values of ~0.3×10^{11} dyn.cm^{-2}, but only very small changes were observed in the C_{44} of the pyrolytic graphite.

Baker and Kelly (1964) reported increases in the C_{44} of single crystal graphite on neutron irradiation at ~100°C by an order of magnitude. Jenkins and Jouquet (1968) obtained large increases in C_{44} in hot worked pyrolytic graphite on irradiation at 30°C. Summers *et al.* (1966) reported decreases in C_{33} in highly oriented pyrolytic graphite following irradiation at 150°C.

Ayasse and Bonjour (1976) irradiated highly oriented pyrolytic graphite at 77 K and measured the changes in C_{33}. The initial value was found to be 3.4×10^{11} dyn.cm^{-2}. C_{33} was decreased with increasing dose, by about 7% at a dose of 4×10^{18}n.cm^{-2} (E > 1 MeV). The recovery of these changes with annealing was gradual, rather similar to dimensional changes perpendicular to the deposition plane (about 1.5% at peak dose).

The elastic moduli C_{33} and C_{44} are both associated with the interlayer forces, which might be expected to weaken as the interlayer spacing increased with the introduction of lattice defects. The reduction in C_{33} with dose is readily explained in this way, but the large and material dependent changes in C_{44} have been attributed to the pinning of glissile dislocations in the basal planes, which normally decrease the shear constants. It is known that in very pure metals such as copper the elastic moduli are reduced by 5–10% because of the presence of glissile dislocations which respond to shear stresses. The graphite crystal is unusual in having only two slip systems in the basal planes and the near two-dimensional nature of the crystal probably removes obstacles to dislocation movement in basal plane shear.

It is fortunate that very thorough transmission electron microscope studies on crystalline graphite (Amelinckx and Delavignette, 1960; Amelinckx *et al.*, 1966) have permitted detailed study of the basal dislocations. The effect of the basal dislocations is to reduce the crystal shear modulus C_{44}. The basal dislocations are split into partial dislocations with Burger's vector $1/3a(10\bar{1}0)$. The total Burger's vector of the two partials, which constitute the total dislocation, is

$$\frac{1}{3}a\left(2\bar{1}\bar{1}0\right) = \frac{1}{3}a\left(10\bar{1}0\right) + \frac{1}{3}a\left(1\bar{1}00\right) \qquad (5.1)$$

In isolated full dislocations the separation of the partial dislocations varies from ~500×10^{-8} cm to 1000×10^{-8}cm depending upon the orientation in the basal planes.

The basal dislocations are readily observed as isolated dislocations or as triangular networks which are 50% stacking faults with ABC stacking. The large separation of the dislocations compared to the crystallite size in the basal planes in polycrystalline graphites means that the dislocation distribution is more likely to consist of the triangular networks which may be responsible for the roughly one layer in six which is apparently mis-stacked in well crystallised polycrystalline graphite, although such a correspondence has not been directly established.

The theory of the effect of isolated dislocations on the elastic moduli has been considered by many workers, particularly Eshelby (1949), Friedel (1953) and Mott (1952). Assume that a crystal contains a uniform density Λ_0 of dislocations in the basal planes and further suppose that under an applied shear stress τ the dislocations glide an average distance x in the direction of the stress. This adds a strain

$$\varepsilon_p = \Lambda_0 \mathbf{b} x \tag{5.2}$$

to the elastic strain τ/C_{44} , where **b** is the Burger's vector. Two quite distinct models have been formulated to estimate the value of x for graphite.

Friedel (1953) described a model in which the isolated dislocations are in the form of N_0 independent arcs per unit volume, each of length L_0 . Equation (5.2) can then be written

$$\varepsilon_p = N_0 \mathbf{b} \alpha \tag{5.3}$$

where α is the area swept out by each arc due to the stress τ. If the line tension of the dislocation is T, Friedel showed that

$$\alpha = \frac{L_0^3 \mathbf{b} \tau}{12T} \tag{5.4}$$

which leads to an apparent decrease in the shear modulus G (=C_{44}) for the crystal of

$$\frac{\Delta G}{G} = \frac{G\mathbf{b}^2 N_0 L_0^3}{12T} \tag{5.5}$$

Chou and Eshelby (1962) presented calculations of the line tension T for both edge and screw dislocations.

Woolley (1965) formulated a model in which the dislocations react to form twist boundaries perpendicular to the crystal hexagonal axis. It is supposed that these twist boundaries are separated by a distance H and confined to slip planes of diameter L_a. The whole boundary now moves under the shear stress τ. Woolley considered the behaviour of a set of n parallel dislocations of which the outer pair, at $\pm L_a$, were firmly fixed and obtained for large n

$$x = \frac{\pi L_a^2 \tau}{K_s b n} \tag{5.6}$$

where K_s is a mean elastic modulus (Eshelby, 1949).

In each case the apparent crystal shear modulus is given by

$$C_{44}^1 = \frac{C_{44}}{1+B} \tag{5.7}$$

where B is the effect of the glissile basal dislocations. Equations (5.5) and (5.7) can give large reductions in C_{44} using reasonable values for the parameters.

It would be expected from this model that the apparent mechanical shear modulus of graphite crystallites would vary from material to material, but if the dislocations can be pinned by irradiation and their strain contribution removed then the shear moduli should all tend to the same value.

Kelly (1964) applied equation (5.5) to the changes in Young's modulus with dose in polycrystalline graphite, finding that if pinning points on dislocation lines changed the arc lengths L, and number of arcs N, in accordance with

$$\Lambda_0 = N_0 L_0 = N L \tag{5.8}$$

and assumed linear increase of pinning points with dose, then the data due to Simmons (1957) could be fitted with $B = 2$. This analysis is only valid if, for small doses, the elastic moduli of the polycrystalline graphite are proportional to the crystal shear constant C_{44}. Consideration of the elastic energy of a porous polycrystal shows that this is likely to be true, particularly if there is a tendency for the uniform stress approximation to be appropriate (Kelly, 1964).

Measurements of modulus changes at higher doses were made following irradiation at temperatures from 150–650°C (Kelly, 1964) on Pile Grade A graphite. These results show that the fractional changes in Young's modulus are independent of direction, as expected if the macroscopic deformation is controlled by a single microscopic deformation model (basal shear). The results show two clearly different regions of behaviour. In irradiations below ~300°C the Young's modulus increases by a factor of about 3, peaks and then decreases, followed by an increase and later still a catastrophic decrease followed by disintegration. In irradiations above 300°C an initial increase occurs to a level which decreases with increasing temperature, remains constant, then increases and finally falls. In both regions increasing the irradiation temperature increases the dose at which any characteristic feature of the changes occurs.

Data on other graphites are not so extensive. Results on Gilsocarbon graphite have been presented by Birch (1981), and Goggin and Reynolds (1967), for experiments carried out at ambient. Birch also studied the changes in the stress-strain curves, while both studies measured the changes in the shear modulus and Poisson's ratio. Taylor *et al.* (1967) measured the changes in elastic modulus and Poisson's ratio of three isotropic graphites following irradiation at 150°C. The pattern of the data is similar to that observed in Pile Grade A graphite, but there are significant differences in the data of Birch, and Goggin and Reynolds, in the shear modulus behaviour. The changes in the shear modulus at small strains measured by Goggin and Reynolds are the same as those of the Young's modulus, but in the study by Birch the changes are smaller. Goggin and Reynolds measured the changes in the elastic constants at finite strains and found that they differed quite significantly from those at small strains (in some cases quite significantly), this has not been explained. The relationship

$$G = \frac{E}{2(1+\nu)} \tag{5.9}$$

where G is the shear modulus, E is the Young's modulus and ν is the Poisson's ratio may be derived assuming only isotropy and the principle of superposition. Goggin and Reynolds (1967) measured E, G and ν on isotropic graphite before and after irradiation. They found

$$G = 3.3 \times 10^{10} \text{ dyn.cm}^{-2} \qquad \frac{E}{2(1+\nu)} = 3.28 \times 10^{10} \text{ dyn.cm}^{-2}$$

before irradiation and

$$G = 11 \times 10^{10} \text{ dyn.cm}^{-2} \qquad \frac{E}{2(1+\nu)} = 12.4 \times 10^{10} \text{ dyn.cm}^{-2}$$

following a brief irradiation at ambient temperature. The agreement with theory suggests that these data are correct with regard to the shear modulus changes.

Extensive data have recently become available on the Young's modulus, shear modulus and Poisson's ratio changes in the near isotropic H-451 nuclear graphite. Equation (5.9) is quite well obeyed (the deviation from isotropy may have some effect) in irradiations at temperatures from 600–1200°C, even when pore generation is present.

The following explanation of these results has been proposed. Simmons (1957) and Kelly (1964) proposed that all of the elastic compliances of porous polycrystalline graphite are dominated by the basal shear of the component crystallites. This assumption is expressed as

$$\begin{aligned} S_{ij} &= \alpha_{ij} S^{1}_{44} \\ C_{ij} &= \beta_{ij} C^{1}_{44} \end{aligned} \qquad (5.10)$$

where $C^{1}_{44} = 1/S^{1}_{44}$ and α_{ij} and β_{ij} are "structure factors". If this is correct it also explains the following:

(i) The similarity of all of the stress-strain relationships of a polycrystalline graphite, all of which exhibit non-linearity, permanent set and hysteresis.

(ii) In irradiations to small doses all of the elastic compliances and moduli change by the same factor. Only the shear constant S^{1}_{44} is significantly increased in single crystals and highly oriented pyrolytic graphite.

Equation (5.10) can be derived, either by assuming, as must be the case, that all of the elastic constants (compliances and moduli) must be linear functions of the five elastic compliances or moduli and noting the large difference in the shear constant term, or by equating the macroscopic strain energy of a graphite cube to the sum of the strain energies of the component crystallites. The likely dominance of shear strain energy leading to (5.10) is obvious. However equation (5.10) can only hold in a porous polycrystalline graphite, not in a fully dense material. This may be shown as follows.

In an isotropic body it is readily shown using the principle of superposition that

$$\text{Shear Modulus } G = \frac{E}{2(1+\nu)} \quad \text{Bulk Modulus } K = \frac{E}{3(1-2\nu)} \qquad (5.11)$$

Markham (1962) calculated the elastic constants of solid isotropic graphite and obtained, neglecting all terms except those which represent basal shear

$$S^1_{11} = \frac{1}{E} = \frac{2}{15}S_{44} \qquad S^1_{12} = -\frac{1}{15}S_{44} \qquad S^1_{44} = \frac{1}{G} = \frac{6}{15}S_{44} \qquad (5.12)$$

which leads in the conventional units to

$$\frac{E}{G} = 3 \qquad \nu = \frac{1}{2} \qquad (5.13)$$

which do not compare favourably with the observed values $E/G = 2.5$, $\nu = 0.2$, and also predicts $K = \infty$. The same conclusion may be obtained for the compressibility of anisotropic graphite without porosity, so that the presence of porosity is essential to equation (5.10).

In irradiations below ~300°C the initial rise in modulus is followed by a decrease of similar magnitude. Kelly (1964) postulated that this was a decrease in the shear constant C_{44} as the pinning fields of point defects overlapped and allowed the dislocation strain to be re-established, but Woolley (1965) suggested that it was due to the lattice distortion caused by point defects at these temperatures which reduced the lattice shear constant. The fall in C_{33} observed by Summers *et al.* (1966) in irradiations of highly oriented pyrolytic graphite at 150°C supports this explanation because the glissile dislocations have no effect on C_{33} (or only a small effect due to misorientation). The lattice changes are much smaller for irradiations above 300°C and the changes in the interlayer spacing are too small to reduce C_{44} and C_{33} and so the decrease does not occur. In both cases this stage of reflecting changes in the crystal elastic constants C_{44} rather than changes in the α_{ij} or β_{ij} is succeeded by a dose range where the opposite occurs and the crystallite dimensional changes modify the porosity and produce both increases and decreases in the α and β factors. The first change is an increase in β_{ij} (decrease in α_{ij}) due to a decrease in porosity, followed by a decrease in β_{ij} due to the generation of new pore space. These changes have been analysed by Kelly and Burchell (1994a) and shown to be a unique function of X_T for a given graphite (X_T is defined in equation (5.21)). The final fall in β_{ij} signals disintegration of the polycrystalline graphite into roughly coke particle sized pieces.

The situation regarding the dose dependence of Poisson's ratio is unsatisfactory. At small doses where equation (5.10) applies without changes in α_{ij} or β_{ij}, it would be expected that Poisson's ratio(s) would remain constant since the C^1_{44} cancels in Poisson's ratio which depends, in the shear-dominated model, only on ratios of α_{ij} 's. This is supported up to a point by experiment (Goggin and Reynolds, 1967).

There are no adequate data when the changes in α_{ij} or β_{ij} become significant — it is not obvious that these should change in the same ratio independent of α_{ij}, and thus changes in the Poisson's ratio may occur.

The effect of final heat treatment temperature on the initial modulus change at ambient temperature was first reported by Losty and Orchard (1963). It was found that the non-linearity of stress-strain curves, the permanent set and the increases in Young's modulus on irradiation increased with heat treatment temperature, becoming significant at about 1600°C. The crystal lattice is essentially turbostratic for lower heat treatment temperatures leading to problems with the definition of a basal dislocation. As the lattice becomes more three dimensional, glissile

dislocations can be defined and are created, thus giving rise to the reduction in the lattice shear constant. The presence of these dislocations leads to the proposed effects.

Brocklehurst and Kelly (1993) examined the effect of irradiation on a heat treated series of Pile Grade A graphite stock irradiated at 600°C. The initial increases were smaller the lower the final heat treatment temperature, but otherwise there are the expect behaviour (a period where the modulus change is constant, followed by the structure dependent rise and fall). There is some indication in this work of a change in anisotropy with dose.

It was observed by Kinchin (1956) that if a graphite sample was mechanically distorted before irradiation and then irradiated in the distorted state at ambient temperature that the sample remained distorted post-irradiation when the mechanical restraint was removed. Perks and Simmons (1964) showed that samples irradiated under stress showed different dimensional changes to those irradiated unstressed. The effects were very small (~100 ppm), but were interpreted as showing that graphite showed creep under irradiation at temperatures where no thermal creep was observed.

Detailed studies of dimensional changes under stress have since been described by many authors including Davidson and Losty (1958), Losty (1960, 1962) and Losty *et al.* (1962). These authors used springs under dead weight load which showed strain and which did not require any correction for dimensional changes. Exposure of samples of this type in the Calder Hall reactors in the United Kingdom showed that after a short transient period the rate of spring extension was proportional to the applied stress and atomic displacement rate. The strain was apparently independent of irradiation temperature between 140°C and 324°C.

Experiments were carried out in compression at low doses by Losty *et al.* (1962) using the Herald reactor with an irradiation temperature of 70°C. Similar creep behaviour was observed. Perks and Simmons (1964) carried out experiments with graphite in tension using the PLUTO reactor. Creep strains were observed which were several times the elastic strain. The creep ratios referred to unit stress and dose were larger in the direction perpendicular to extrusion in an anisotropic graphite than parallel to it.

Morgan (1963) carried out experiments at 625°C under compression. There were difficulties in separating the effects of stress level but the creep rates obtained were comparable with the other work.

Gray (1973) reported creep data on several graphites under compressive stress set at three different levels at temperatures of 550 and 800°C. The measurements included thermal expansion coefficient measured parallel to the stress direction. The results were the first to show creep strains, which were less than linear with dose and apparently in some cases negative. (The creep strains were defined, as usual, as the difference in dimensions between a stressed sample and an unstressed control sample.) It was also clear that the thermal expansion coefficients in the stress direction were increased by the creep strain, although the changes varied with the graphite. The dimensional changes perpendicular to the stress were measured and the lateral strain ratios determined. The results were interpreted as showing that creep strain modified the dimensional change term so that the definition of creep is no longer correct (leading to the apparent negative creep strains). The lateral strain ratios varied from 0.5 (constant volume) to 0.3. The implications of this work were neglected for some years.

Kelly and Brocklehurst (1977) summarised creep studies carried out in the United Kingdom since 1964, including data taken in tension, compression and shear on a wide variety of graphites (including radiolytically pre-oxidised, and pre-irradiated without stress to high doses) exposed at temperatures from 140–1040°C. The results of this work were summarised in the following equation, valid for 140–650°C:

$$e_c = 0.23 \times 10^{-20} \frac{T}{E_0} \gamma + \frac{T}{E_0} \left(1 - \exp\left[-4 \times 10^{-20} \gamma\right]\right) \qquad (5.14)$$

where e_c is the creep strain, T is the stress, γ is the dose (n.cm^{-2} EDN) and E_0 is the static Young's modulus prior to irradiation. The first term is the secondary creep strain, and the second the transient creep. It should be noted that both terms are inversely proportional to the unirradiated Young's modulus and the second term has the magnitude of one elastic strain. In the same work the lateral strain ratio was

$$e_c^1 = 0.3 e_c \qquad (5.15)$$

slightly larger than the unirradiated Poisson's ratio of most of the graphites studied. The creep rate increases slowly at higher temperatures and this is allowed for by introduction of a temperature factor $\beta(T)$, which is unity at 650°C and lower temperatures. This study included measurements of lateral strain due to creep (the creep Poisson's ratio), changes in thermal expansion coefficient, and recovery of creep strain both thermally and under irradiation without stress. Creep rate was also measured on graphite doped with ^{11}B to enhance the crystal dimensional change rate. The creep Poisson's ratio in this series of experiments was ~0.3.

Irradiation creep experiments carried out by Kennedy and co-workers (1977, 1979) at 600 and 900°C indicate that in addition to the change in the thermal expansion coefficient there is a small change in modulus. This is accompanied by a large change in Poisson's ratio, at 900°C falling from a value of ~0.14 to zero at ~2.5% creep strain in H-451 graphite. This is at odds with the finding in the UK.

It is clear that the transient stress was recoverable in the presence of thermal or irradiation annealing in the absence of stress which indicates that it is associated with stored elastic energy.

For temperatures greater than ~300°C the data from all sources agree that the creep rate is constant to ~650°C and then gradually increases up to ~1400°C and probably beyond. However at temperatures of 300°C and below, data obtained by Kennedy (1966a, 1966b) and Platonov (1966) show an increase in creep rate with decreasing temperature. This disagrees with the studies carried out in the UK, Kelly and Brocklehurst (1977), which show the same creep rate in the range 140–330°C as in the range 300–750°C. This discrepancy has never been fully resolved. See Figs 5.2 (a), (b).

Two theories of irradiation creep have been proposed. In the first (Kelly and Foreman, 1974) is an irradiation creep model due to Cottrell in which the internal stress generated by the

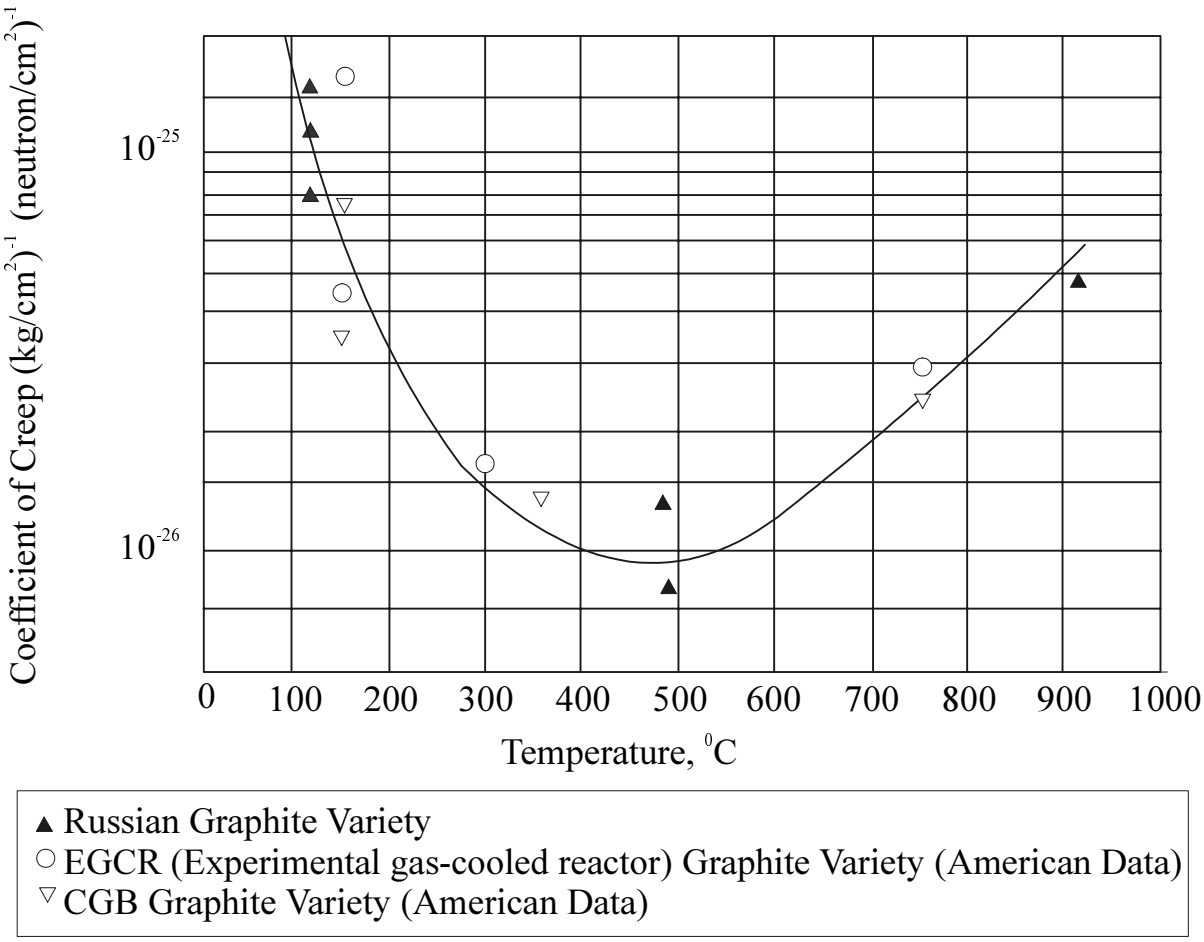

FIG. 5. 2(a). Variation of creep rate with temperature: Russian and American data.

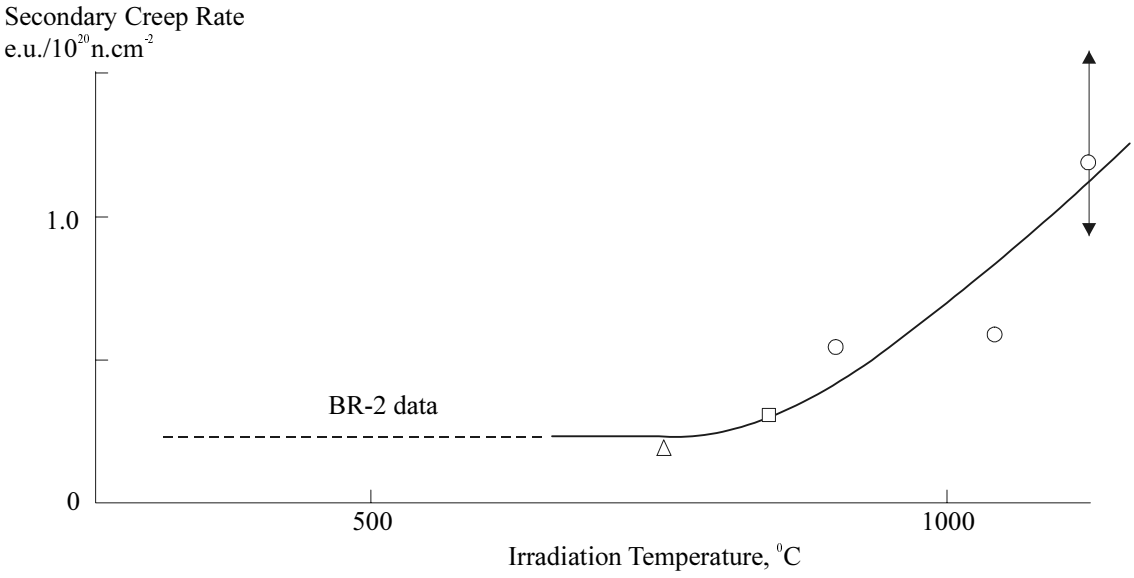

FIG. 5. 2(b). Variation of creep rate with temperature:UK data PLUTO.

incompatibility of the crystal dimensional changes eventually brings the crystallites to yield point and allows the polycrystalline graphite to flow under external stress. The second model is the dislocation pinning-unpinning model. In unirradiated graphite, it is assumed that a high density of dislocations within the basal planes constrains deformation of the crystallite by a small concentration of pinning points. When the graphite is irradiated these dislocations may be pinned, depending on the dose and temperature, which leads to the increase in modulus. As these small clusters of 4±2 atoms are short lived due to irradiation annealing there is only a temporary barrier to dislocation movement. Thus the pinning and unpinning of these dislocations due to irradiation will allow the crystal to flow in basal slip at a rate determined by the displacement of atoms.

To explain the pinning-unpinning theory of irradiation creep in graphite, Kelly and Brocklehurst (1972) considered the work done due to a stress T_{xx} at the macroscopic level on a volume of graphite divided into small volumes of graphite a at the microscopic level in unstressed and stressed graphite. They showed that the theoretical creep rate can be given by the difference between the strain rate in the unstressed graphite compared with that in the stressed graphite which leads to:

$$\dot{e}_c = \sum_r a_r \left[\frac{\partial [\sigma_{xz}]_r}{\partial T_{xx}} \Delta \dot{e}_{xzr} + \frac{\partial [\sigma_{yz}]_r}{\partial T_{xx}} \Delta \dot{e}_{yzr} + \frac{\partial [\sigma_{xy}]_r}{\partial T_{xx}} \Delta \dot{e}_{xyr} \right] \tag{5.16}$$

where $[\sigma_{ij}]_r$ denotes the stress on the r'th volume of graphite in the crystal local co-ordinate system and

$$\Delta \dot{e}_{ijr} = \left[\dot{e}_{ij} \right]_r - \left[\dot{e}_{ij}^{'} \right]_r \tag{5.17}$$

that is the difference in strain rate between the stressed and unstressed graphite, which by definition represents the creep strain rate.

Thus it is demonstrated that the dilation modes do not play a part, and the creep rate is determined by the crystal shear modes.

Making the assumptions that:

(i) The only mode of crystal deformation is basal slip,

(ii) The crystal strain rate for the graphite crystal in shear may be written as:

$$\Delta \dot{e}_{xzr} = K \left[\frac{\partial [\sigma_{xz}]_r}{\partial T_{xx}} \right] . T_{xx}$$

$$\Delta \dot{e}_{yzr} = K \left[\frac{\partial [\sigma_{yz}]_r}{\partial T_{xx}} \right] . T_{xx} \tag{5.18}$$

(iii) and the S_{44}, ($C_{44} = S_{44}^{-1}$), compliance of the graphite crystal is much larger than the other crystal compliances,

leads to

$$\text{Creep rate} = KT_{xx}\frac{C_{44}}{E_{xx}} \tag{5.19}$$

Thus the creep rate is proportional to the reciprocal of the unirradiated graphite modulus measured in the direction of creep. This theory assumes that Poisson's ratio in creep is the same as the elastic Poisson's ratio, and as previously discussed, there are conflicting views on this. Figure 5.3 shows the mean ratio of total creep strains parallel and perpendicular to the loading direction measured on three different graphites as a function of differential change in length. This gives a Poisson's ratio in creep of ~0.3 compared with ~0.2 for the elastic case, although there is a substantial amount of scatter (due to the difficulty in measuring lateral strains on the specimens used) and the ratio is the same order as that of the elastic ratio.

More evidence for the pinning-unpinning model was given by experiments carried out on graphite doped with boron (^{11}B), Kelly and Brocklehurst (1977), to accelerate the irradiation damage to the crystallite. These experiments showed that the creep rate was not affected by the doping, indicating that the process of irradiation creep is displacement driven not damage driven, which collaborates in with the basal slip theory.

Early irradiation creep experiments had shown that changes to the thermal expansion coefficient in irradiated specimens appeared to be dependent on the level of creep strain. Those specimens with a significant amount of compressive creep strain had a higher coefficient measured in the direction of stress compared with the unstressed specimens, whereas specimens with significant tensile creep strain had a lower thermal expansion coefficient compared to the unstressed specimens, see Fig. 5.4. This implies that creep strain modifies the dimensional change rate in the specimens, although annealing was shown to restore the thermal expansion coefficient to its original value but did not completely restore the creep deformation (Kelly and Brocklehurst, 1977). This finding also has implications related to dimensional change through the equation developed by Simmons (1965) discussed in Chapter 3.

To assess the interaction between creep strain, the thermal expansion coefficient and dimensional change rate, Kelly and Burchell (1994b) reanalysed the creep strain data for H-451 graphite using the Simmons (1965) theory for the relationship between the thermal expansion coefficient and dimensional change rate, giving

$$g_x = \left(\frac{\alpha_x - \alpha_a}{\alpha_c - \alpha_a}\right)\left(\frac{dX_T}{d\gamma}\right) + \frac{1}{X_a}\frac{dX_a}{d\gamma} \tag{5.20}$$

where α_x, α_a and α_c are the thermal expansion coefficients in the polycrystalline x direction and in the a and c crystallite axes. $(1/X_c)(dX_c/d\gamma)$ and $(1/X_a)(dX_a/d\gamma)$ are the crystal dimensional change rates and the shape factor is defined as:

$$\frac{dX_T}{d\gamma} = \frac{1}{X_c}\frac{dX_c}{d\gamma} - \frac{1}{X_a}\frac{dX_a}{d\gamma} \tag{5.21}$$

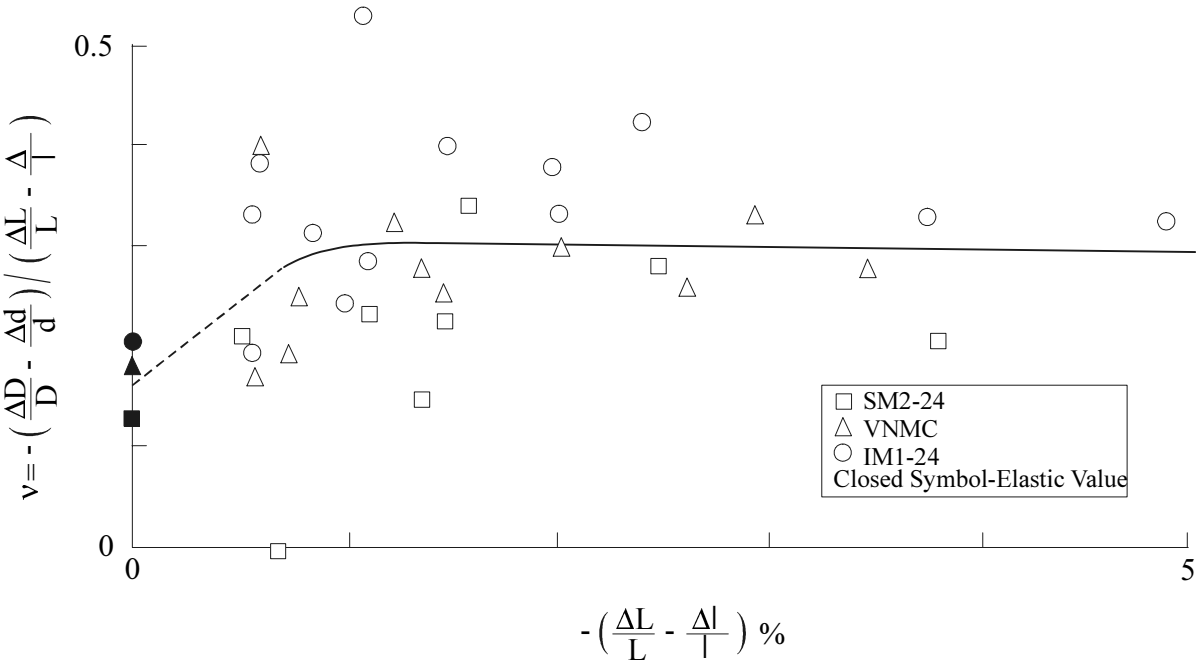

FIG. 5.3. Creep poisson's ratio as a function of longitudinal creep strain.

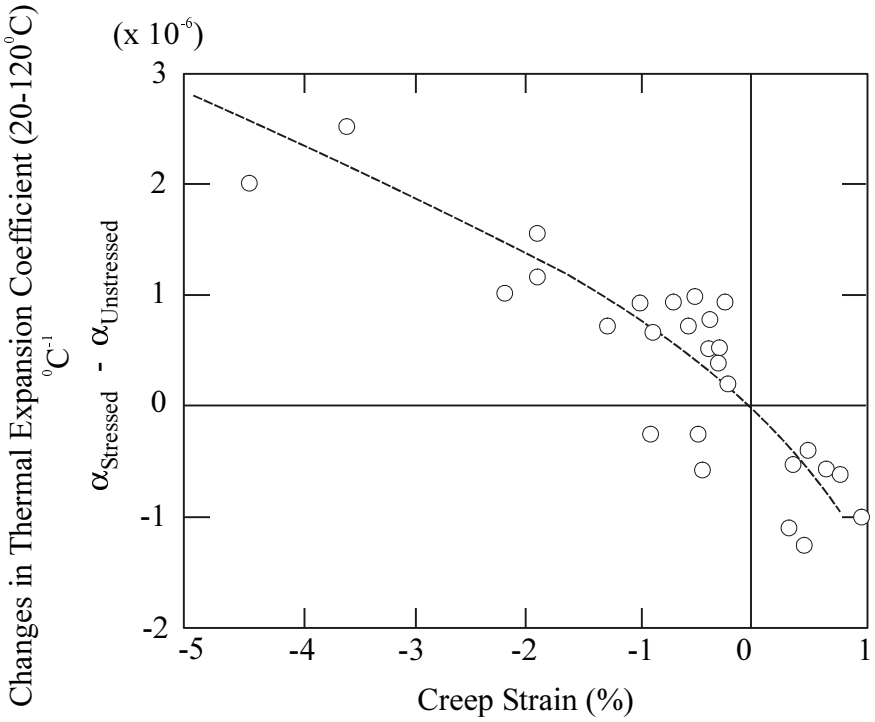

FIG. 5.4. Effect of creep strains on thermal expansion coefficient measured parallel to stress axis for Gilsocarbon graphite.

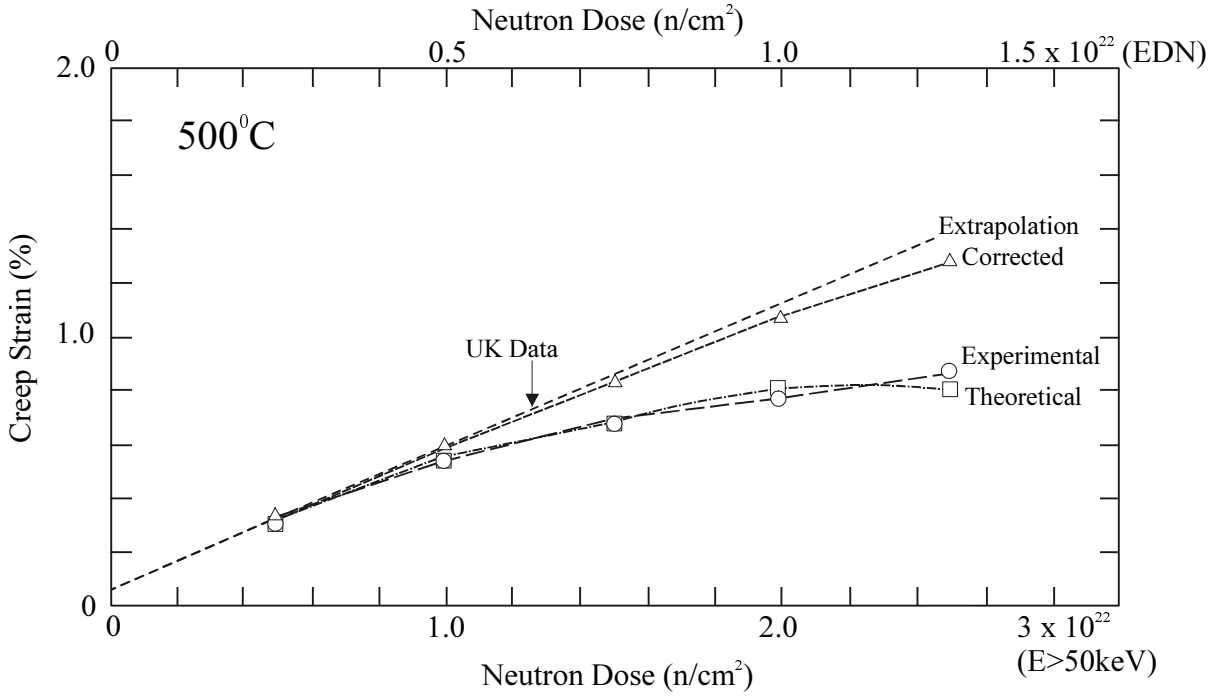

FIG. 5.5. Comparison of experimental apparent creep strains at 500°C (HFR, PETTEN) against predicted apparent creep strains for 5Mpa stress, and UK data.

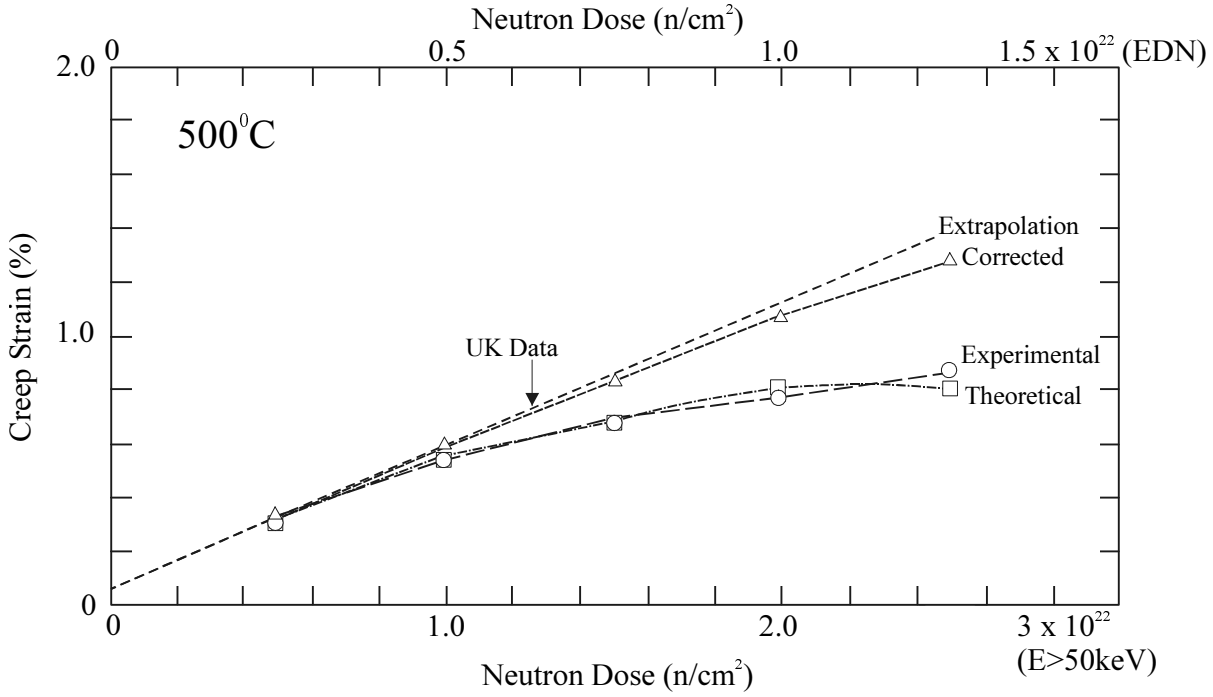

FIG. 5.6. Change in thermal expansion coefficient versus strain for Gilsocarbon graphite.

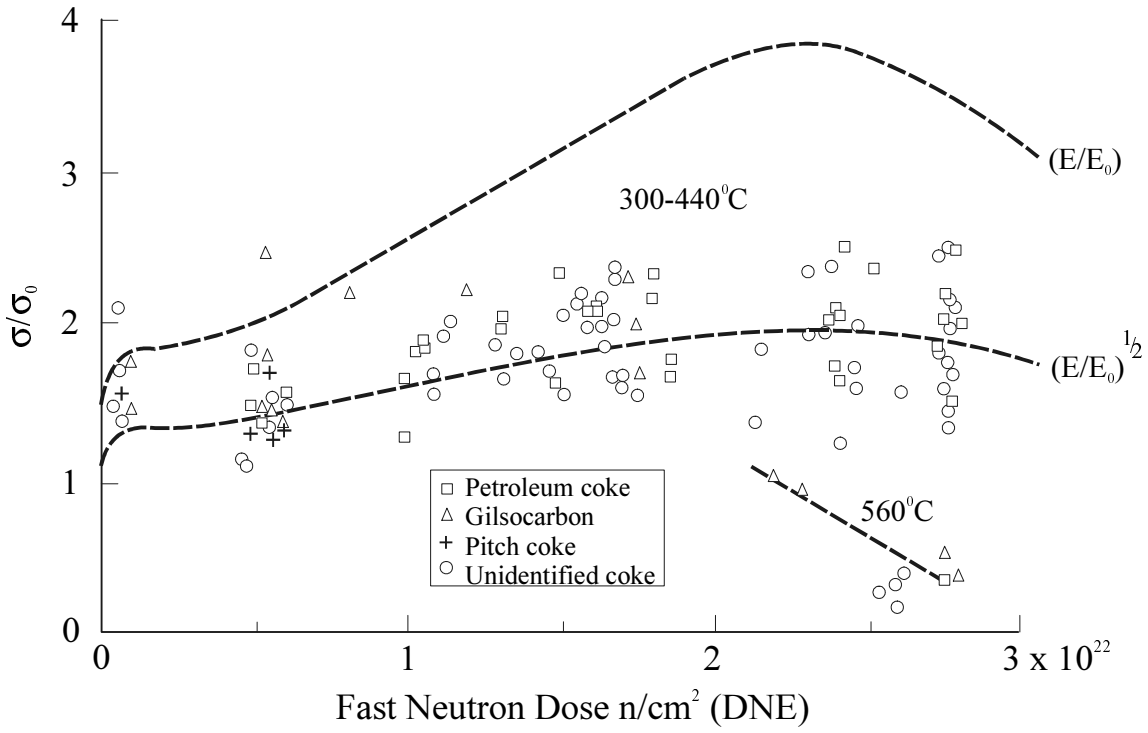

FIG. 5.7. Tensile strength changes with fast neutron dose for near-isotropic graphites irradiated in DFR..

When graphite creeps under stress the thermal expansion coefficient increases with compressive creep strain and decreases with tensile creep strain, thus changing the dimensional change rate as given below:

$$g'_x = \left(\frac{\alpha'_x - \alpha_a}{\alpha_c - \alpha_a}\right)\left(\frac{dX_T}{d\gamma}\right) + \frac{1}{X_a}\frac{dX_a}{d\gamma} \qquad (5.22)$$

The dash represents the change in the crept specimen. This leads to an apparent creep rate of

$$\frac{de'_c}{d\gamma} = \frac{de_c}{d\gamma} - \left(\frac{\alpha'_x - \alpha_x}{\alpha_c - \alpha_a}\right)\left(\frac{dX_T}{d\gamma}\right) \qquad (5.23)$$

Using this approach Kelly and Burchell (1994b) reconciled the apparent non-linear behaviour in the creep behaviour of H-451 graphite, confirming a linear relationship for creep strain against dose. See Fig. 5.5.

The implications of this to the reactor designer are most relevant in the multi-axial case where significant multi-axial strains can be generated. To enable these three-dimensional effects to be accounted for, information on the lateral changes in the thermal expansion coefficient as a function of creep strain were required. Unfortunately there is little reliable information on the transverse changes to the thermal expansion coefficient due to irradiation creep. However, there is now information on the change in thermal expansion coefficient which has been measured on stressed unirradiated Gilsocarbon graphite (Marsden *et al.*, 1995, 1996).

This work revealed an unexpected result, changes to the thermal expansion coefficient due to compressive and tensile loading at relatively small elastic strains were of the same order as in the case of significant creep strains, see Fig. 5.6.

The lateral coefficient gave a value of ~0.16, the same order as the elastic Poisson's ratio, although subject to significant scatter.

The strength of graphite is well known to increase with irradiation, Brocklehurst (1977), to a point where the properties decline due to large structural effects. Up to this point the strength in tension and shear increases according to

$$\sigma_f(\gamma, T) \geq \sigma_0 \left(\frac{E}{E_0} \right)^{\frac{1}{2}} \tag{5.24}$$

where σ_0 is the unirradiated strength in the same direction and mode, and E and E_0 are the irradiated and unirradiated values of Young's modulus.

The relationship above can be arrived at from the Griffith-Orowan theory of fracture of materials containing cracks. This gives the condition for propagation of a crack:

$$\sigma_f \sim \left(\frac{E\gamma}{C} \right)^{\frac{1}{2}} \tag{5.25}$$

neglecting numerical constants, where γ is the effective surface energy per unit area, E is the elastic modulus and C is the crack length. If both C and γ can be considered to be independent of dose, the inequality in equation (5.24) could be replaced by the equality sign.

Early work by Losty and Orchard (1963) at low dose and low temperature where changes to the macrostructure due to micro-structural changes in the crystallite could be expected to be small showed that the elastic strain energy to failure σ^2/E remained essentially constant. This is consistent with the Griffith - Orowan theory for no change in C or γ.

Irradiation experiments at 150°C by Taylor *et al.* (1967) showed that after fast neutron irradiation the strain energy to failure increased at first with increasing dose and then decreased. He postulated that the increase was due to an increase in γ and the decrease was due to an increase in C. He explained the increase in γ as being due to the initial reduction in plasticity with dose and the increase in C as being due to crack generation at higher doses.

Gilsocarbon graphite irradiated at higher temperatures, 900–1200°C, by Everett and Ridealgh (1972) showed an almost linear relationship between modulus and strength. This was similar to the findings of Engle (1977) who irradiated H-451 graphite in the range 600–1350°C.

Figure 5.7 summarises the relationship between modulus and strength. At high temperatures, ~1000°C, the strength-modulus relationship is at constant strain, whereas at lower temperatures the relationship is constant strain energy. At high irradiation doses and temperatures where structural effects are important the constant strain model appears to be more relevant.

Numerous attempts, Mason (1963), Amesz *et al.* (1973) and Lungagnani and Krefeld (1972), have been made to fit statistical expressions to small sample data — particularly Weibull's. However, for practical reasons, the graphite samples tested are usually smaller than ~10 times the grain size. This leads to a problem when testing graphite. In the case of tensile loading, the strength increases with increasing specimen volume until it eventually becomes constant. However the strength of bend samples increase with specimen volume at first and pass through a maximum before decreasing and to obtain good Weibull parameters large samples are required.

In recent years attempts have been made to produce graphite failure models based on the graphite microstructure, the most developed of these being that by Tucker and co-workers (1986, 1993).

They looked at six commonly used graphite failure models, three simple models based on critical strain, critical stress and critical strain energy density, a statistical model due to Weibull, the so-called Rose/Tucker model, and a fracture mechanics approach; and reviewed the performance of these models against experimental data for a variety of tests in bend and tension.

Both critical stress and critical strain failure criteria do not take account of changes to the microstructure during loading and thus give poor correlations. Critical strain energy density depends on the volume of material being considered; this is ambiguous in its application.

Weibull statistical theory, previously discussed in relation to specimen size, is based on the failure strength of an *i* th elementary volume being described by the function

$$g(\sigma_i) = A_i m \sigma_i^{m-1} \exp\left(- A_i \sigma_i^m\right) \qquad (5.26)$$

where σ_i is the stress on the *i* th volume dV_i, assumed to contain defects, m is the Weibull modulus and A_i is given by $A' dV_i$, where A' is a constant for a given material and type of loading. It is assumed that the probability of failure of an elemental volume under tensile stress will lead to catastrophic failure of the component.

The Rose/Tucker model is based on work by Buch (1976) and tries to take account of the microstructure of the graphite. The material is divided into small volumes typical of a particle size containing crystals of random orientation. The crystals are assumed to cleave only along the basal plane when the stress reaches a critical value. Under increasing load the probability of failure of each plane is calculated until a critical size is reached which satisfies the Griffith brittle failure criteria. Pores are treated as elemental volumes with no cleavage strength and the distribution of these is related to the microstructure porosity of the graphite under study.

In the fracture mechanics approach it is assumed that the graphite contains defects in the most damaging position in the model. The size of the defect is related to the structure of the graphite, but is otherwise insensitive to the microstructural changes, which give rise to failure.

The simple criteria based on critical strain, critical stress and strain energy density gave poor predictions for failure in most of the tests. The Weibull approach gave good correlation for geometry-related effects, but poor results for changes to microstructure. The Rose/Tucker

and fracture mechanics approach gave the best results, which led to a further model, Tucker and McLachlan (1993), based on the last two approaches. More recent work by Burchell (1994) simplified and improved the Tucker and McLachlan model.

These graphite failure models have only been partially successful in describing failure in irradiated graphites and there is scope for further development in this area for practical application to reactor systems.

REFERENCES TO CHAPTER 5

AMELINCKX, S. AND DELAVIGNETTE, P. (1960), *J. Applied Physics*, **31**, 2126.

AMELINCKX, S., DELAVIGNETTE, P. AND HEERSCHAP M. (1966), *Chemistry and Physics of Carbon*, **1** (Ed. P.L. Walker, Jr), Marcel Dekker, New York, 1.

AMESZ, J., DONEA, J. AND LANZA, F. (1973), *Extended Abstracts Eleventh Biennial Carbon Conf.* (USAEC Rep. Conf. 730601), 221.

AYASSE, J.B. AND BONJOUR, E. (1976), *Proc. Fourth SCI Conference on Industrial Carbons andGraphites*, SCI, London, 620 .

BAKER, C. AND KELLY, A. (1964), *Phil. Mag*., **9**, 927.

BIRCH, M. (1981), PhD Thesis, University of Liverpool (UKAEA Report ND-R-590 (S/X)).

BROCKLEHURST, J.E. (1977), *Chemistry and Physics of Carbon*, **13** (Eds. P.L. Walker, Jr and P.A. Thrower), Marcel Decker, New York, 145 (UKAEA Report TRG 2731(S)).

BROCKLEHURST, J.E. AND KELLY, B.T. (1993), *Carbon*, **31**, 155.

BUCH, J.D. (1976), *Properties Related to Fracture Toughness*, ASTM STP 605, 124.

BURCHELL, T D, (1994), Carbon.

CHOU, Y.T. AND ESHELBY, J.D. (1962), *J. Mech. Phys. Solids*, **10**, 27.

DAVIDSON, H.W. AND LOSTY, H.H.W. (1958), *Proc. Second International Conference on the Peaceful Uses of Atomic Energy*, United Nations, **7**, 307.

ESHELB,Y J.D. (1949), *Phil. Mag*., **40**, 903.

ENGLE, G.B. (1977), *Assessment of Grade H-451 Graphite for Replaceable Fuel and Reflector Elements in HTGR*, US Report GA-A14690.

EVERETT, M.R. AND RIDEALGH, F. (1972), *Int. Conf. Carbon*, Baden-Baden.

FRIEDEL, J. (1953), *Phil. Mag*., **44**, 444.

GOGGIN, P.R. AND REYNOLDS, W.N. (1967), *Phil. Mag*., **16**, 317.

GRAY, W.J. (1973), *Carbon*, **11**, 383.

JENKINS, G.M. AND JOUQUET, G. (1968), *Carbon*, **6**, 85.

KELLY, B.T. (1964), *Phil. Mag*., **9**, 721.

KELLY, B.T. AND FOREMAN, A.J.E. (1974), *Carbon*, **12**, 151.

KELLY, B.T. AND BROCKLEHURST, J.E. (1972), *3rd Conf. Ind. Carbon and Graphite*, 63.

KELLY, B.T. AND BROCKLEHURST, J.E. (1977), *J. Nuc. Mat*., **65**, 79.

KELLY, B.T. AND BURCHELL, T.D. (1994a), *Carbon*, **32**, 499.

KELLY, B.T. AND BURCHELL, T.D. (1994b), *Carbon*, **32**, 119.

KENNEDY, C.R. (1966a), USAEC Report ORNL-3951.

KENNEDY, C.R. (1966b), USAEC Report ORNL-4036.

KENNEDY, C.R., COOK, W.H. AND EATHERLY, W.P. (1977), *Extended Abstracts from 13th Biennial Carbon Conference*, Irvine, 342.

KENNEDY, C.R. AND EATHERLY, W.P. (1979), *Extended Abstracts from 14th Biennial Carbon Conference, Pennsylvania*, 453

KINCHIN, G.H. (1956), *Proceedings of the United Nations Conference on the Peaceful Uses of Atomic Energy*, **7**, 472

LOSTY, H.H.W. (1960), *Proc. Fourth Biennial Carbon Conference*, Pergamon Press, New York, 593.

LOSTY, H.H.W. (1962), *Uranium and Graphite*, Institute of Metals, Monograph No. 27, 81.

LOSTY, H.H.W., FIELDER, N.C., BELL, I.P. AND JENKINS, G.M. (1962), *Proc. Fifth Conference on Carbon*, Pergamon Press, **1**, 266.

LOSTY, H.H.W. AND ORCHARD, J.S. (1963), *Proc. Fifth Biennial Carbon Conference*, **1**, Pergamon Press, New York, 519.

LUNGAGNANI, V. AND KREFELD, R. (1972), *Proc. Conf. On Continuum Aspects of Graphite Design,* Gatlinburg, 1970, USAEC Rep. Conf. 701105.
MARKHAM, M.F. (1962), *Materials Research*, 107, July.
MARSDEN, B.J., PRESTON, S.D., DAVIES, M.A. AND MCLACHLAN, N. (1996), *Proc. Conf. Carbon 96*, Newcastle.
MARSDEN, B.J., PRESTON, S.D., MCLACHLAN, N. AND DAVIES, M.A. (1995), *IAEA Conf. Graphite Moderator Lifecycle Technologies*, Bath, 24th–27th September.
MASON, I.B. (1963), *Proc. Fifth Biennial Carbon Conf.*, **2**, Pergamon Press, New York, 597.
MORGAN, W.C. (1963). *The Effect of Low Compressive Stresses on Radiation-Induced Dimensional Changes in Graphite*, GE Report HW-SA-2925.
MOTT, N.F. (1952), *Phil. Mag*, **43**, 1151.
PERKS, A.J. AND SIMMONS, J.H.W. (1964), *Carbon*, **1**, 441.
PLATONOV, P.A. (1969), *Proc. Int. Conf. Irradiation Damage in Reactor Materials*, **1**, IAEA, VIENNA, 417.
SELDIN, E.J. AND NEZBEDA, C.W. (1970), *J. Applied Physics*, **41**, 3389.
SIMMONS, J.H.W. (1957), *Proc. Third Biennial Conference on Carbon*, Pergamon Press, New York, 559
SIMMONS, J.H.W. (1965), *Radiation Damage in Graphite*, Pergamon Press.
SUMMERS, L., WALKER, D.C.B. AND KELLY, B.T. (1966), *Phil. Mag*., **14**, 317.
TAYLOR, R., BROWN, R.G., GILCHRIST, K., HALL, E., HODDS, A.T., KELLY, B.T. AND MORRIS, F. (1967), *Carbon*, **5**, 519.
TUCKER, M.O., ROSE, A.P.G. AND BURCHELL, T.D. (1986), *Carbon*, **24**, 581.
TUCKER, M.O. AND MCLACHLAN, N. (1993), *J. Physics D: Appl. Phys*., **26**, 893.
WOOLLEY, R.L. (1965), *Phil. Mag*., **11**, 179.

CHAPTER 6

THE ELECTRONIC PROPERTIES OF IRRADIATED GRAPHITE

The electronic properties of graphite are very sensitive to irradiation and can be described in terms of energy band structure. A number of band models have been employed, of which the best known is the simple two-band model. This model will first be described, followed by a discussion of the unirradiated electronic properties, and finally an examination of the effects of irradiation on those properties.

6.1. Two-band model

Electrical conduction in graphite can be described in terms of two slightly overlapping energy bands, with an energy level distribution as shown in Fig. 6.1. For a perfect crystal the

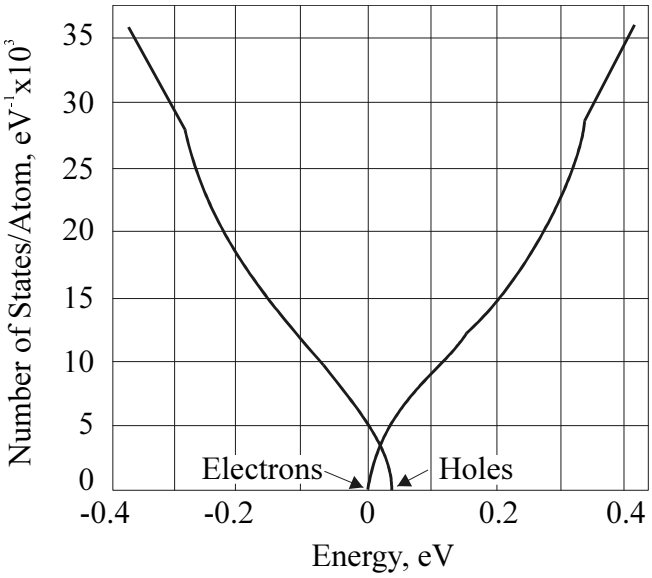

FIG. 6.1. Density of electron energy states.

Fermi surface is near the overlap level. (The Fermi surface may be thought of as the level at which the states are exactly half occupied under the prevailing conditions.) Graphite is thus essentially a semiconductor with a zero energy gap, with equal numbers of electrons and holes contributing to conduction. The effect of irradiation is to introduce defects which reduce the mobility of the carriers by scattering the electrons and which trap some of the electrons, lowering the level of the Fermi surface. It is conventional to assume a parabolic energy-wave number relationship for each of the two bands near the overlap point:

$$E_e(k) = \frac{\hbar^2}{2m_e}\left(k_x^2 + k_y^2\right) = \frac{\hbar^2 K^2}{2m_e} \text{ for electrons}$$

$$E_h(k) = E_0 - \frac{\hbar^2}{2m_h}\left(k_x^2 + k_y^2\right) = E_0 - \frac{\hbar^2 K^2}{2m_h} \text{ for holes} \tag{6.1}$$

E_0 is the overlap ($E_0 > 0$) or separation ($E_0 < 0$) of the energy bands, m_e and m_h are the effective masses of electrons and holes, and K is the wave number measured from the edge of the

Brillouin zone, which is hexagonal with top and bottom faces at $k_z = \pm\pi/d$, where d is the separation of the planes. (For a more comprehensive review of calculations on the Brillouin zone and energy bands see Kelly, 1981.)

Using the model represented by equation (6.1), Johnston (see Reynolds and Goggin, 1960) derived expressions for the electrical resistivity, Hall coefficient and magneto-resistivity of graphite:

Electrical resistivity

$$\rho_0 = \frac{V_x}{J_x} = \frac{1}{e\left(\mu_h n_h + \mu_e n_e\right)} \tag{6.2}$$

Hall coefficient

$$R = \frac{V_y}{B_z J_x} = \frac{1}{e}\frac{\left(\mu_h^2 n_h - \mu_e^2 n_e\right)}{\left(\mu_h n_h + \mu_e n_e\right)^2}\frac{1}{\cos^2\alpha} \tag{6.3}$$

Magneto-resistivity

$$\frac{\Delta\rho}{\rho} = \frac{B_z^2\cos^2\alpha}{\mu_h n_h + \mu_e n_e}\left[\mu_h^3 n_h + \mu_e^3 n_e - \frac{\left(\mu_h^2 n_h - \mu_e^2 n_e\right)^2}{\mu_h n_h + \mu_e n_e}\right] \tag{6.4}$$

n_h and μ_h are the concentration (cm^{-3}) and basal plane mobility ($cm^2.s^{-1}.V^{-1}$) of the holes in the lower band, and n_e and μ_e are the same quantities for electrons in the upper band. The magnetic field B_z is in gauss divided by 10^{-8} and e is 1.6×10^{-19} C. The formulae are valid for the case in which the axis of the cylindrical energy surfaces is in the y-z plane at an angle α to the z (hexagonal) axis. Equations (6.3) and (6.4) are only valid for weak fields ($(\mu_h B_z)^2$ and $(\mu_e B_z)^2 << 1$). In high fields, especially at low temperatures, these properties oscillate with the field. B_x and B_y are both zero.

The carrier concentrations are given by

$$n_h = \frac{8\pi k T m_h}{\hbar^2 d}\ln\left[1+\exp\left(\frac{E_0 - E_f}{k T}\right)\right]$$
$$n_e = \frac{8\pi k T m_e}{\hbar^2 d}\ln\left[1+\exp\left(\frac{E_f}{k T}\right)\right] \tag{6.5}$$

where E_f is the Fermi energy measured from the bottom of the conduction band and k is Boltzmann's constant. It is also possible to write the carrier mobilities as

$$\mu_h = \frac{e\tau_h}{m_h} \qquad \mu_e = \frac{e\tau_e}{m_e} \tag{6.6}$$

where τ_h, τ_e are the relaxation times for scattering.

6.2. Unirradiated properties

Soule (1958), Shoenberg (1952) and Berlincourt and Steele (1955) performed experiments to determine how the above properties and the diamagnetic susceptibility vary with the magnetic field. This enabled McClure (1958) to calculate the band structure of graphite, giving values for the concentration and mobility of the carriers. Table 6.1 gives typical values at several temperatures, taken from McClure (with n in cm^{-3} and μ in $cm^2.s^{-1}.V^{-1}$).

TABLE 6.1. PROPERTIES OF CURRENT CARRIERS IN GRAPHITE

	4.2 K	77 K	298 K
n_h	2.8×10^{18}	2.1×10^{18}	7.0×10^{18}
n_e	2.9×10^{18}	2.2×10^{18}	7.0×10^{18}
μ_h	104.0×10^{4}	7.3×10^{4}	1.0×10^{4}
μ_e	83.9×10^{4}	6.3×10^{4}	1.1×10^{4}

It can be seen that the carrier concentrations generally increase with temperature, whilst the mobilities decrease. The mobility decrease is dominant, and hence the resistivity of good graphite crystals increases with temperature.

The first measurements of the electrical resistivity of very perfect or highly oriented polycrystalline graphites parallel to the basal planes, ρ_a, appear to have been by Washburn (1915) and Ryschkewitsch (1923) who used Ceylon graphite. It was observed by Washburn and Krishnan and Ganguli (1939) that the resistivity perpendicular to the basal planes, ρ_c, was 200 – 10 000 times greater than ρ_a. At an angle θ to the axis the resistivity is given by

$$\rho(\theta) = \rho_a \sin^2\theta + \rho_c \cos^2\theta \tag{6.7}$$

More modern studies on good graphite crystals began with Kinchin (1953) and Dutta (1953), followed by Primak (1956) and Soule (1958). Figures 6.2 and 6.3 show the results of Soule's measurements parallel to the basal planes and Primak's measurements perpendicular to the planes. It can be seen that the behaviour of ρ_c and ρ_a are different, the increase in ρ_c levelling off above ~100 K.

Klein (1966) has published numerous studies on highly oriented pyrolytic graphite of varying perfection. Figure 6.4 shows the variation of resistivity parallel (solid curves) and perpendicular (broken curves) to the deposition planes with heat treatment temperature. Extensive studies have also been published by Spain *et al.* (1967). It has been found that the most perfect samples exhibit very similar behaviour to the best natural crystals. There is, however, a problem with the measurements of ρ_c in the more perfect samples which remains unresolved. The problem is that pyrolytic graphites give $\rho_c/\rho_a \sim 10^5$, whereas natural single crystals give $\rho_c/\rho_a \sim 10^2$, although some samples of natural graphite also give a high ratio (Spain, 1971). The view can be taken that it is either the natural graphites or else the highly oriented pyrolytic graphites which have the intrinsic resistivity.

If the natural graphites have the intrinsic resistivity, then an explanation needs to be found for the high resistivity of the pyrolytic graphites in the *c* direction. One proposal is that there are thin sheets of disordered material in the basal planes with a high resistance, although this has been rejected by Young (1968). Another proposed explanation is that localisation of the charge carriers is produced by defects in the pyrolytic graphite. Ono (1976) showed that a ρ_c/ρ_a value

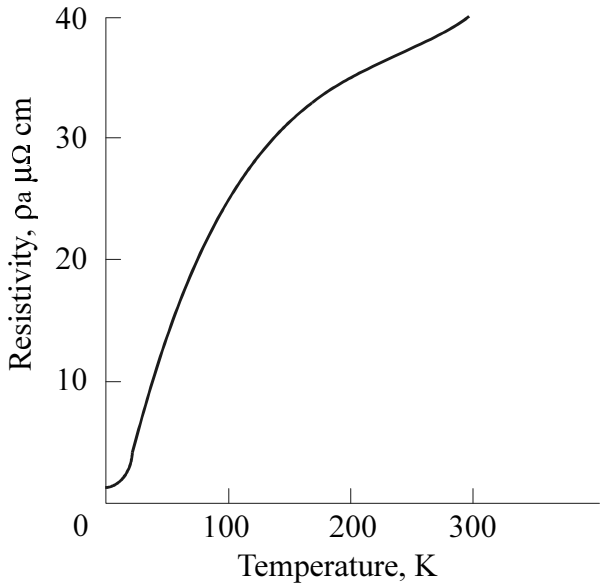

FIG. 6.2. Electrical resistance of graphite crystals parallel to Basal planes.

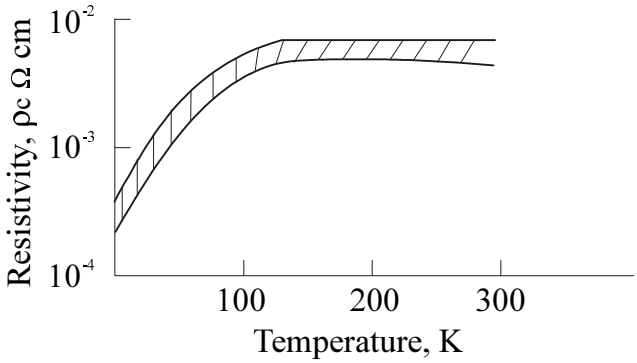

FIG. 6.3. Electrical resistance of graphite crystals parallel to hexagonal axis.

of ~10^4 at room temperature could be obtained with this explanation if the dislocation density was ~10^{11} cm^{-2}, but this is about a hundred times greater than the value commonly observed in highly oriented pyrolytic graphite. This explanation also fails to correctly predict the temperature dependence.

If the highly oriented pyrolytic graphites have the intrinsic resistivity, then the low resistivity of natural graphites needs explaining. A possible explanation is the presence of screw dislocations with Burgers vector parallel to the hexagonal axis, causing a short circuit. However, this explanation requires dislocation densities of ~10^{15} cm^{-2}, compared to observed densities of ~10^6 cm^{-2}.

Imperfect orientations would mix the *c* and *a* directions, but it can be shown that this cannot account for the observed values of ρ_c in either highly oriented pyrolytic graphite or natural graphite.

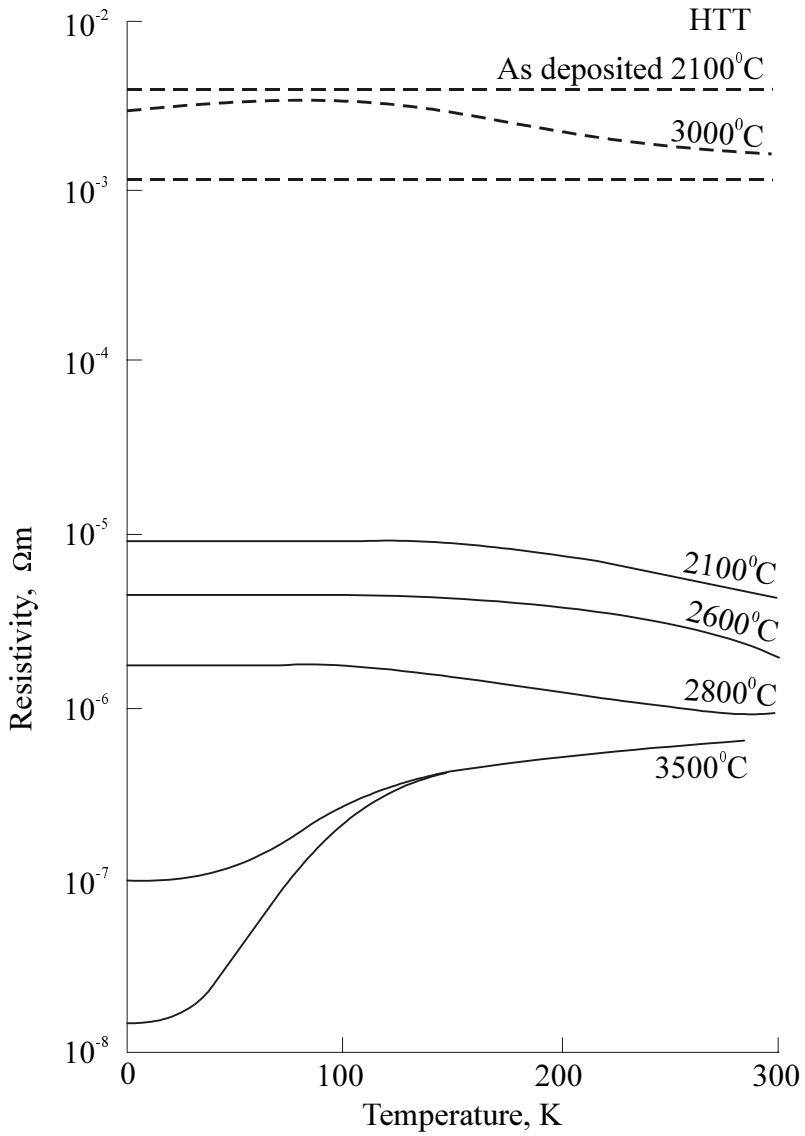

FIG. 6.4. Variation of electrical resistivity of highly oriented pyrolytic carbons with heat treatment temperature.

It can be seen from equations (6.3) and (6.4) that the Hall coefficient depends essentially on the difference between the contributions of the positive and negative carriers to the conduction, whilst the magneto-resistivity depends mainly on the mobility of the carriers. (Magneto-resistivity is the change in electrical resistivity which occurs when a magnetic field is applied.) Tables 6.2 and 6.3 show typical values of Hall coefficient and magneto-resistance for different graphites.

TABLE 6.2. HALL COEFFICIENTS OF GRAPHITES

Material	Heat treatment temperature (°C)	Hall coefficient (R) at 300 K (cm^3/C)
Petroleum-coke graphite (CSF)	2800	-0.06
Petroleum-coke graphite (AGX)	2600	-0.051
Petroleum-coke graphite (ECA)	3000	-0.049
Natural-graphite compact (pitch bonded)	3000	-0.038

TABLE 6.3. MAGNETO-RESISTANCE IN GRAPHITES AT 2140 GAUSS

Material	Heat treatment Temperature (°C)	Magneto-resistance ratio 300 K	195 K	77 K	4.2 K
Petroleum-coke graphite	2600	0.0016	0.0020	0.0039	
Petroleum-coke graphite (AGOT)	2800	0.0046			
Petroleum-coke graphite (C-15)	3000	0.013			
Single crystal		0.093		2.24	259

It can be seen that the magneto-resistance for polycrystalline graphites is much less than for single crystals. This is due to several factors:

(i) Scattering of charge carriers at imperfections reduces the mean free path, reducing $\Delta\rho$.

(ii) Imperfections also trap the charge carriers, reducing $\Delta\rho$.

(iii) The presence of crystalline imperfections and boundaries increases ρ.

The first reported measurements of the Hall coefficient and magneto-resistance on graphite crystals were by Kinchin (1953). The measurements were made in a magnetic field of up to 9000 G parallel to the hexagonal axis. The Hall coefficient was measured at temperatures from 4.2 K to 473 K and was found to vary significantly with both temperature and field for temperatures below 77 K (increasing for lower temperatures, and first increasing then decreasing for higher fields). The magneto-resistance was measured as a function of field at 4.2 K and 290 K. At the higher temperature the variation with field was found to be proportional to $B^{1.74}$, and less rapid at the lower temperature for both single crystals and polycrystalline specimens. This clearly contradicts the theoretical variation of B^2 in equation (6.4). In the single crystals, the actual magnitude was found to be remarkably large, values of $\Delta\rho/\rho$ of 526 were reached at a specimen temperature of 4.2 K in a field of less than 10 000 G, with a room temperature value as large as 0.43. A much more detailed study was performed by Soule (1958) on specially purified natural crystals cut to dumb-bell shapes at temperatures of 4.2, 77 and 298 K in fields ranging from 25 to 25 000 G. The results are shown in Figs 6.5 –6.7. The form of the temperature and field dependencies was different to that found by Kinchin, but was in good agreement with Berlincourt and Steele (1955). Both properties showed oscillations at 4.2 K: these are called Shubnikov-De Haas effects and are due to the quantisation of carrier orbitals in applied magnetic fields. Soule estimated carrier densities of $2–3 \times 10^{18}$ cm^{-3} for both holes and electrons, and found μ_e/μ_h varied monotonically from 1.1 at room temperature to 0.77 at 4.2 K. Soule then used the magneto-resistance measurements at low fields to derive mobilities ranging from ~10^4 $cm^2.s^{-1}.V^{-1}$ at room temperature to over 10^6 $cm^2.s^{-1}.V^{-1}$ at 4.2 K. These were the first reliable determinations of these quantities in the graphite crystal.

Measurements of the Hall coefficient of Kish graphite and highly oriented pyrolytic graphite have been published by Kawamura *et al.* (1976, 1977) and Dillon *et al.* (1978), respectively. At 298 K the Hall coefficient is similar in both single crystal and highly oriented pyrolytic graphite and shows very little dependence on the magnetic field. At 77 K the single crystal value is higher for fields below 3000 G but is similar to the pyrolytic graphite value for

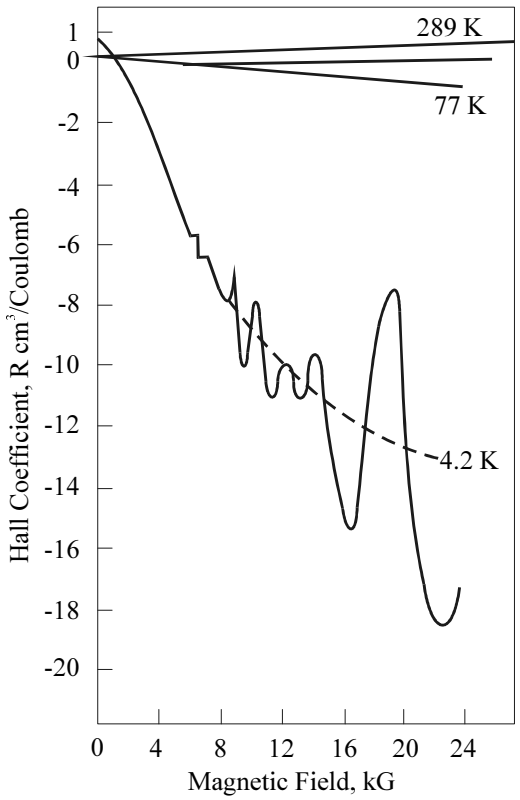

FIG. 6.5. Hall effect of graphite crystal EP-14 high field parallel to hexagonal axis.

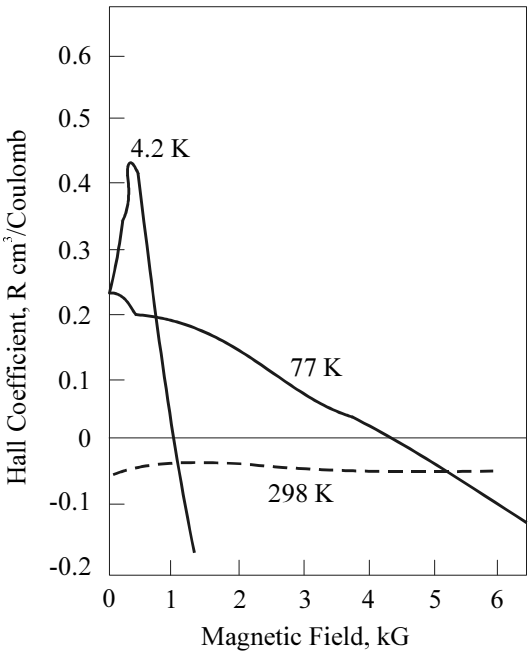

FIG. 6.6. Hall effect of graphite crystal EP-14 low field parallel to hexagonal axis.

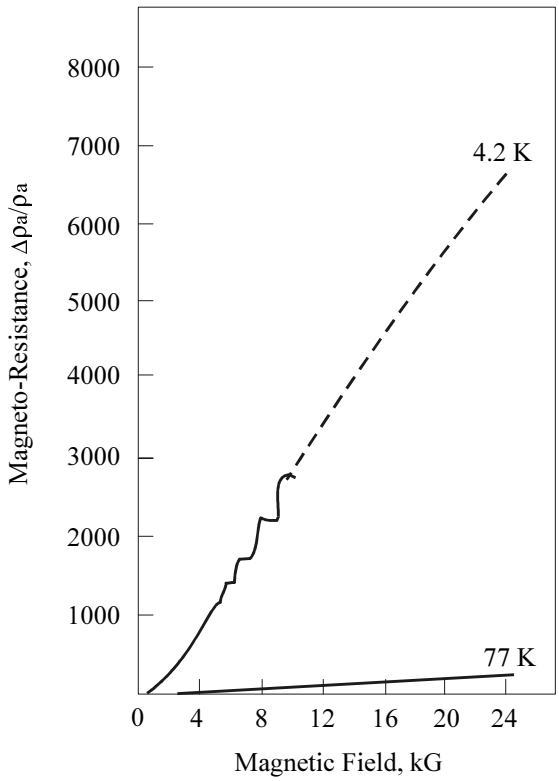

FIG. 6.7. Magneto-resistance of graphite crystal EP-14 field parallel to hexagonal axis.

higher fields. The field dependence of both types of graphite is similar at 4.2 K, but the pyrolytic value is much lower.

The effect on the Hall coefficient and magneto-resistance of varying the heat treatment temperature of highly oriented pyrocarbons is shown in Figs 6.8 and 6.9 for measurements at ambient temperature. It is notable that the magneto-resistance is negative in the less perfect materials, which indicates that the number of charge carriers is increased or that the scattering is reduced by the magnetic field.

There are numerous measurements of the Hall coefficient and magneto-resistance of polycrystalline graphite. An important point to note is the negative magneto-resistance at low heat treatment temperatures. For heat treatment temperatures below 2600°C the magneto-resistance increases with temperature, whereas above 2800°C it decreases as the temperature increases. A thorough review of magneto-resistance behaviour is given by Delhaes (1971).

The thermo-electric power of graphite is expected to give an indication of the effective sign and concentration of current carriers. There are a number of published measurements on natural crystals and Kish graphites, which are shown in Fig. 6.10. The measurements by Takezawa *et al.* (1972) were on Kish graphite parallel to the basal planes and showed complicated behaviour at low temperatures. There is a sharp negative dip at 35 K and a broad positive peak at 120 K. There is a change in sign from negative to positive at 65 K and from positive to negative at 235 K. Figure 6.10 also shows results obtained by Tamarin *et al.* (1969), which exhibit a similar behaviour.

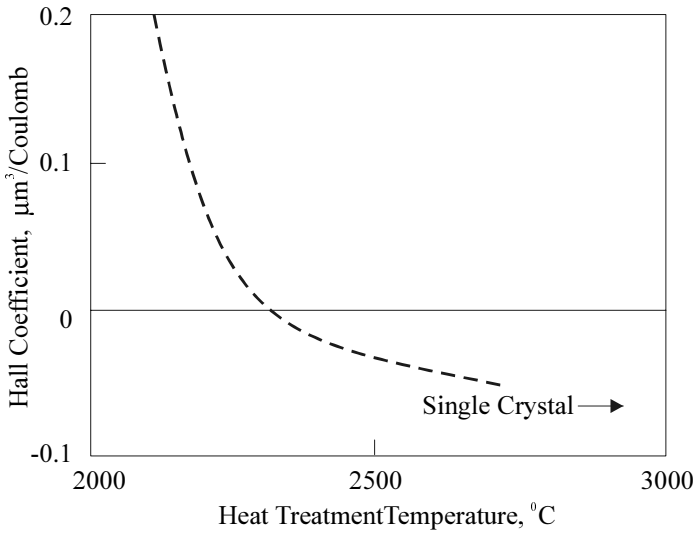

FIG. 6.8. Hall coefficient at room temperature in pyrolytic carbons after heat treatment to various temperatures.

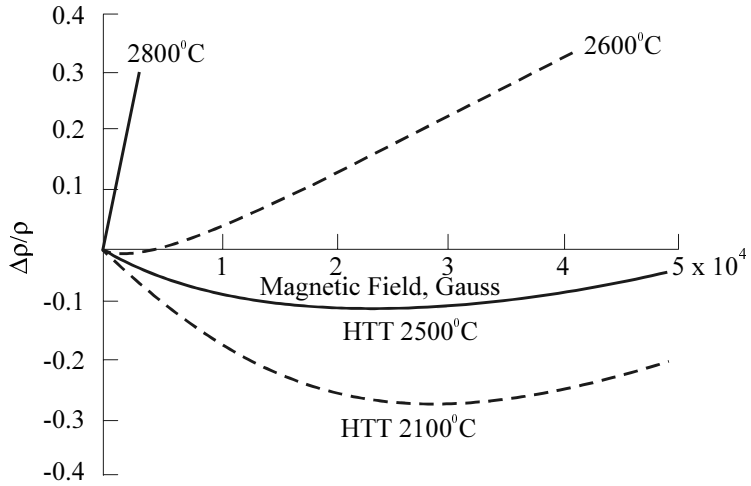

FIG. 6.9. Field dependence of magneto-resistance in pyrolytic carbon after heat treatment to various temperatures.

Measurements of thermo-electric power on highly oriented pyrolytic graphite have been reported by Spain *et al.* (1967), De Combarieu *et al.* (1973), Rasor (1955) and Klein (1964). The effects of heat treatment temperature, as measured by Klein (1962) parallel to the basal planes, are shown in Fig. 6.11. Figure 6.12 shows measurements by Klein perpendicular to the basal planes.

The effect of a magnetic field on the thermo-electric power was investigated by Sugihara *et al.* (1972) who measured the power in the basal planes in a magnetic field parallel to the hexagonal axis of Kish graphite: they found that the depth of the minimum at 35 K increased rapidly with the magnetic field, reaching -200 $\mu V.K^{-1}$ at a field of 6.8 kOe.

Graphite has a very high diamagnetic susceptibility in the hexagonal axis direction. Detailed measurements on a graphite crystal were reported by Ganguli and Krishnan (1941) and Poquet *et al.* (1960). Ganguli and Krishnan showed that the temperature dependence was characteristic of the susceptibility of a free electron gas. The difference in susceptibility

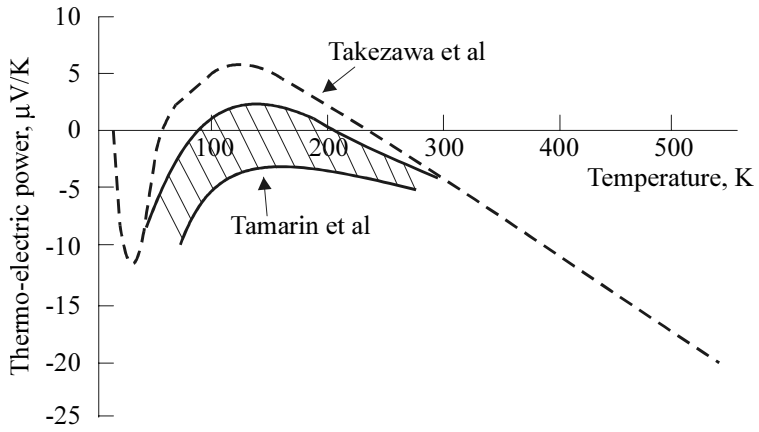

FIG. 6.10. Thermo-electric power measurements on very perfect graphites.

perpendicular and parallel to the basal planes is about 30×10^{-6} emu.g^{-1} at liquid helium temperatures, decreasing at higher temperatures. The susceptibility parallel to the basal planes is independent of temperature and is about -0.5×10^{-6} emu.g^{-1}. The difference between the susceptibilities measured parallel (χ_1) and perpendicular (χ_2) to the basal planes was given by Poquet *et al.* as

$$\chi_1 - \chi_2 = \left\{1.3 + 28.5\left(1 - \exp\left[-\frac{330}{T}\right]\right)\right\} \times 10^{-6} \qquad \text{emu.g}^{-1} \tag{6.8}$$

with average susceptibility

$$\bar{\chi} = \frac{\chi_1 + \chi_2}{3} = -7.2 \times 10^{-6} \qquad \text{emu.g}^{-1} \tag{6.9}$$

Several attempts were made to calculate the high magnitude of the susceptibility (Hove, 1955; McClure, 1956; and Haering and Wallace, 1957). Eventually McClure (1960) showed that it was possible to explain the high susceptibility using the band parameters obtained from his analysis of the oscillatory Hall constant and magnetic susceptibility. The high susceptibility arises from band to band transitions, brought about by the changes in the band energies near the zone boundaries. McClure calculated the dependence of the susceptibility on temperature and the Fermi surface level.

There have been numerous measurements of susceptibility on polycrystalline graphites and soft carbons heat treated to various temperatures, particularly by the French (Mazza *et al.*, 1962; Mazza, 1964; Pacault and Gasparoux, 1967) and by Fishbach (1971). The French found that the temperature dependence of the average susceptibility of soft carbons could be represented by

$$\bar{\chi} = \frac{1}{3} K_0 \left[1 - \exp\left(-\frac{T_0}{T}\right)\right] \tag{6.10}$$

K_0 and T_0 are functions of the heat treatment temperature. Table 6.4 shows values obtained by Pacault *et al.* (1960), who found that $T_0 = 3.8 \times 10^4 / L_a$, to within 10%. The susceptibility changes with the degree of graphitisation, reaching a maximum of around 22×10^{-6} emu.g^{-1} and

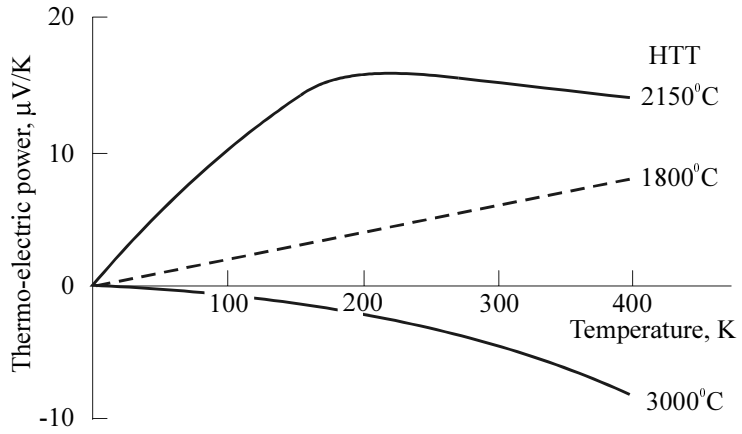

FIG. 6.11. Thermo-electric power measurements on highly oriented pyrolytic graphite, parallel to basal planes.

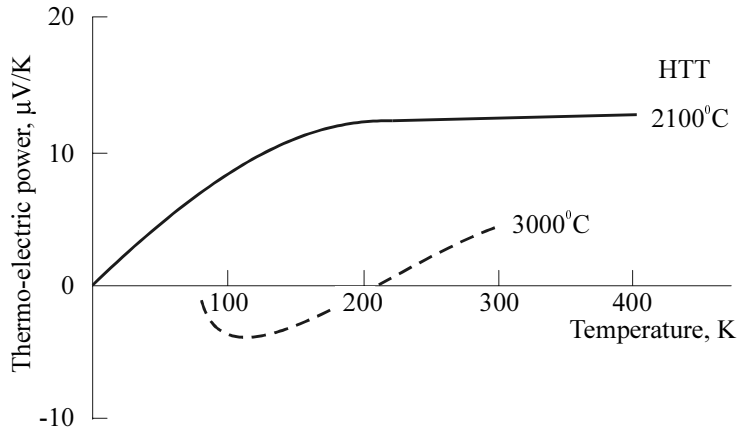

FIG. 6.12. Thermo-electric power measurements on highly oriented pyrolytic graphite, perpendicular to basal planes.

then decreasing to a constant value of around 20×10^{-6} emu.g^{-1} as the graphitisation temperature increases. Some room temperature measurements on pyrocarbon have shown total susceptibilities of up to 1.5 times the single crystal value, with a value of 35×10^{-6} emu.g^{-1} for turbostratic pyrocarbon with L_a ~250×10^{-8} cm (Fishbach, 1971) and rhombohedral graphite (Gasparoux, 1965). The results indicate that the susceptibility is dependent on both the crystallite size and the stacking order.

TABLE 6.4. EFFECT OF HEAT TREATMENT TEMPERATURE ON SUSCEPTIBILITY PARAMETERS DIAMAGNETIC

Heat treatment temperature (°C)	K_0 (x 10^{-6} g^{-1})	T_0 (K)
Single crystal	-28.5	338
2650	-24.9	330
2000	-23.3	365
1900	-17.3	450
1800	-13.6	510
1700	-9.6	570
1600	-6.2	750
1500	-2.2	1550

Graphite also has a paramagnetic susceptibility, which has been investigated by measurements of electron spin resonance. Castle (1953, 1954) observed a spin resonance line with a *g*-value of 2.008 and a line width of 200 Oe in highly purified Ceylon graphite powder. A spin concentration of 10^{-4} to 10^{-5} per atom was found, which was attributed to the charge carriers. Wagoner (1960) thoroughly studied the spin resonance of a graphite crystal using 3 cm microwaves and found *g*-values at room temperature of 2.0495 with the magnetic field parallel to the hexagonal axis and 2.0026 with the field perpendicular to the hexagonal axis. The dependence on orientation is given by

$$g = 2.0026 + 0.047\cos^2\theta \tag{6.11}$$

where θ is the angle between the field and the hexagonal axis. Line widths were only a few G. This anisotropy increases with decreasing temperature, with a value of 2.127 at 77 K for the field parallel to the hexagonal axis, with the perpendicular value unchanged. Wagoner showed that the temperature dependence and line shape were in agreement with the paramagnetic susceptibility being due to the charge carriers.

6.3. Irradiated properties

The effect of irradiation on the electronic properties of graphite is similar at all irradiation temperatures, although higher doses are required to produce the same effect at higher temperatures. It introduces:

(i) Scattering centres, reducing the charge carrier mobility.

(ii) Traps for electrons.

(iii) Additional electron spin resonance.

The earliest studies are summarised by Hove (1956). Polycrystalline nuclear graphites, such as KC and CSF, were irradiated with fast neutrons. The electrical resistivity increases by a factor of around three, then decreases slowly, later increasing slowly, with the fractional change being independent of the direction and the initial rate of increase of resistivity depending inversely on the irradiation temperature. The Hall coefficient rises from a small negative value to a positive peak which then decreases. The magneto-resistance falls rapidly to zero. The diamagnetic susceptibility falls and the spin resonance intensity increases. The thermo-electric power changes in a complex way. These measurements were compared with a theory containing two unknowns, the relaxation time τ and the degeneracy energy ΔE, based on the Wallace model of the energy band structure of graphite (Wallace, 1947a, 1947b). This theory gives:

Resistivity

$$\frac{\rho}{\rho_0} = \left(\frac{\tau_0}{\tau}\right)\frac{\left\{\ln 2\cosh\left(\Delta E_0 / 2kT\right)\right\}}{\left\{\ln 2\cosh\left(\Delta E / 2kT\right)\right\}} \tag{6.12}$$

Hall coefficient

$$R = \frac{9\pi}{16}\frac{a^2 d}{ek^2T^2}\frac{\tanh\left(\Delta E / 2kT\right)}{\left\{\ln 2\cosh\left(\Delta E / 2kT\right)\right\}^2} \tag{6.13}$$

Diamagnetism

$$\chi = C_2(T)\ \mathrm{sech}^2\left(\Delta E / 2kT\right) \tag{6.14}$$

Magneto-resistance

$$A = C_1(T)\ \frac{\tau^2\ \mathrm{sech}^2\left(\Delta E / 2kT\right)}{\left\{\ln 2\cosh\left(\Delta E / 2kT\right)\right\}} \tag{6.15}$$

Thermo-electric power

$$Q = \pm\frac{2k}{e}\left[\sum_i^{\infty}\frac{\dfrac{(-1)^n}{(n+1)^2}\ \phi\left(\dfrac{[n+1]|\Delta E|}{2kT}\right) - \left(\dfrac{\Delta E}{2kT}\right)^2\ \tanh\left(\dfrac{|\Delta E|}{2kT}\right) + \dfrac{|\Delta E|}{2kT}}{\left\{\ln 2\cosh\left(\Delta E / 2kT\right)\right\}}\right] \tag{6.16}$$

where

$$\phi(x) = 1 - \exp(-x)\left[1 + x + \frac{x^2}{2}\right]$$

C_1 and C_2 are temperature-dependent parameters. Use of these equations as a ratio of initial to final properties allows the unknowns to be evaluated. It was also assumed that the electrons are trapped at a constant rate, dN_e/dt.

The relationship for the Hall coefficient was fitted to the data using equation (6.13). The results then completely determined the variation of diamagnetism. The relaxation time could then be obtained from equation (6.12) and the magneto-resistance determined. The same analysis was also performed on the observed annealing curves. It was found that the thermo-electric power was not quite consistent with the others, requiring a value of dN_e/dt 40% larger.

Whilst this analysis is satisfactory in many ways, it says nothing about which defects contribute to τ and dN_e/dt. Simple theories of scattering suggest that for scattering by interstitials and vacancies, τ is proportional to the density of states, and for scattering by boundaries and dislocations, τ is constant.

Austerman and Hove (1955) irradiated polycrystalline reactor graphite at 4 K with 1.25 MeV electrons and measured the change in electrical resistivity produced by the irradiation and changes which occurred during subsequent annealing. The annealing results are shown in Fig. 6.13. No annealing takes place below 80 K, but there is a sudden increase in the resistivity, peaking at 140 K, followed by a decrease. The decrease can be explained by reintegration of the interstitial atoms with the vacant lattice sites, and the increase by either an increase in the number of scattering centres or the release of electrons from electron traps.

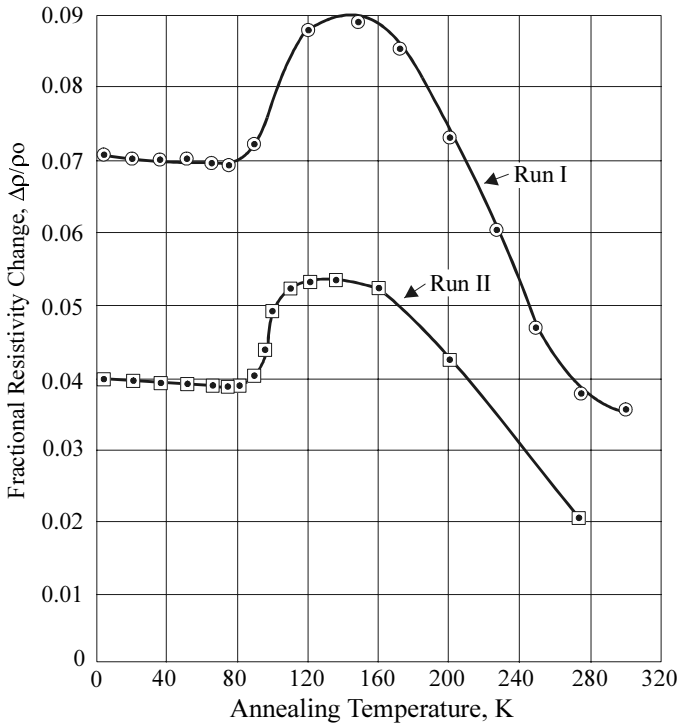

FIG. 6.13. Effect of annealing on electrical resistivity of graphite irradiated at 4 K.

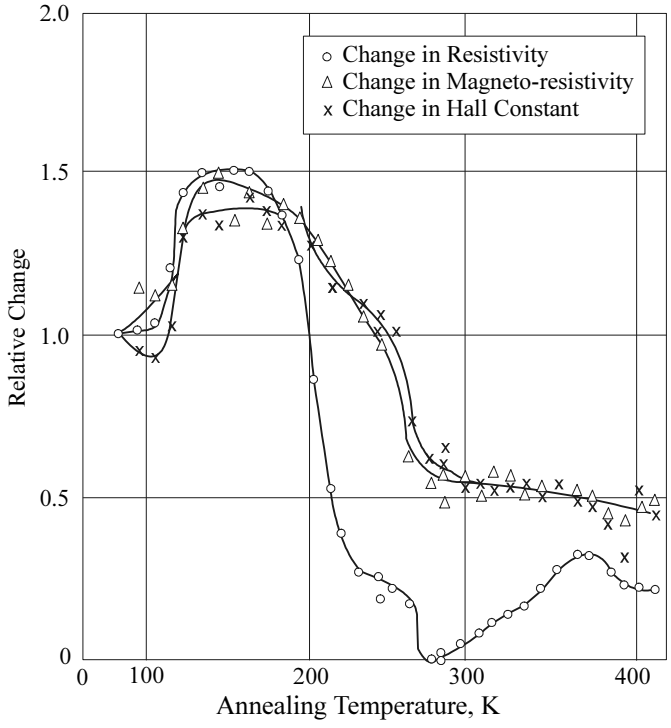

FIG. 6.14. Effect of annealing on electrical properties of graphite irradiated at 77 K.

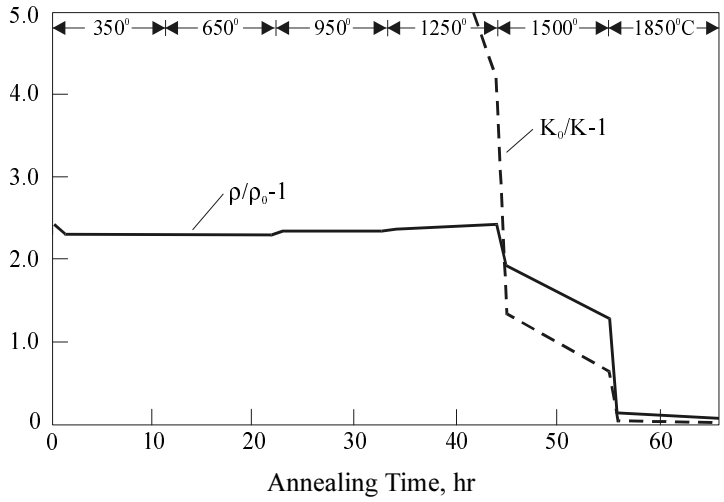

FIG. 6.15. Effect of annealing on the resistivity of irradiated graphite.

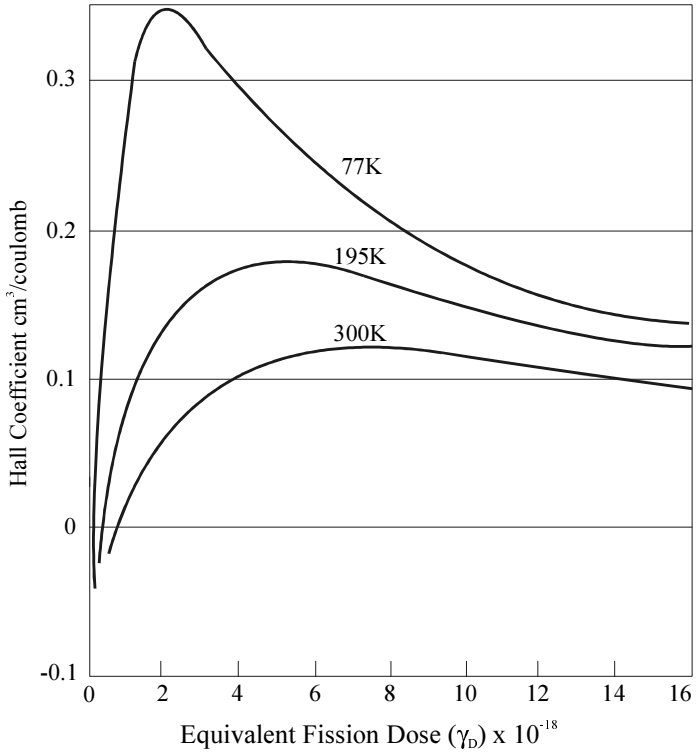

FIG. 6.16. Effect of radiation at 30°C on the Hall coefficient of polycrystalline graphite.

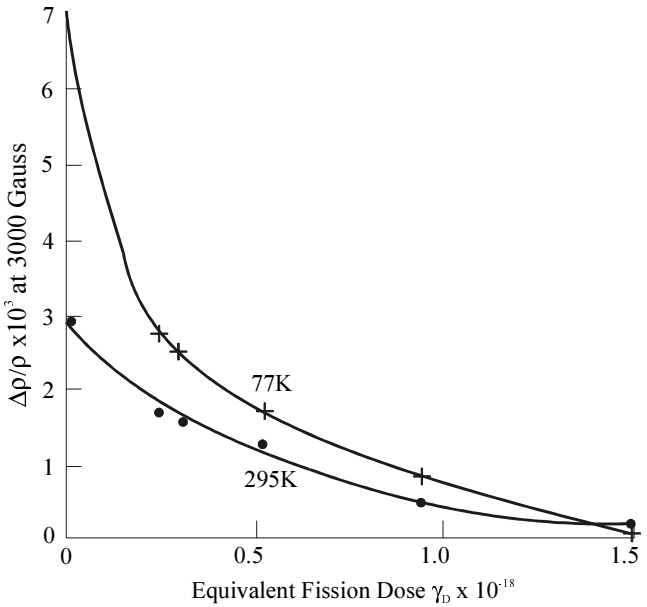

FIG. 6.17. Effect of radiation at 30°C on the magneto-resistivity of polycrystalline graphite.

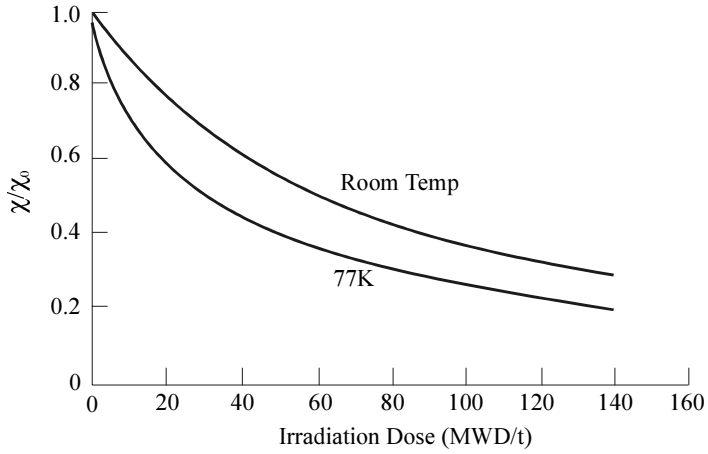

FIG. 6.18. Effect of radiation at 30°C on the diamagnetic susceptibility of AGOT-KC graphite.

Polycrystalline graphite was irradiated at liquid nitrogen temperatures by 4 MeV electrons by Reynolds and Goggin (1960), followed by pulse annealing. They measured the changes in the electrical resistivity, the Hall coefficient and the magneto-resistivity and found that all three properties had the inverse annealing peak reported by Austerman and Hove. The results are summarised in Fig. 6.14. The results were analysed using equations (6.2)–(6.4) to give the number of trapped electrons and the carrier mobilities. During irradiation the number of electron traps increases and the mobility of the carriers decreases. Similar changes are produced during the initial stages of annealing. It is believed (Simmons, 1965) that the effects are caused by a dispersal of close vacancy-interstitial pairs under the influence of a short-range force in the vicinity of the vacancies. When an interstitial atom is far enough from a vacancy it can capture an electron, becoming a scattering centre and reducing the mobility of the electrons.

Changes in electrical resistivity under irradiation by protons and neutrons have a similar annealing behaviour to that for electron irradiations (Austerman, 1958; Hove, 1959). A similar annealing peak to that found by Austerman and Hove (1955) was reported by Klabunde *et al.* (1961) on pyrolytic graphite irradiated with neutrons at liquid helium temperatures.

Studies on more perfect and highly oriented graphite were reported by Primak and Fuchs (1954, 1956). They irradiated flakes of natural graphite at 35–60°C. A considerable increase in the electrical resistivity was observed both parallel and perpendicular to the basal planes. Parallel to the planes the change was around a factor of 10, which was about five times larger than for a polycrystal irradiated under the same conditions. If the irradiation damage is assumed to be identical in both samples, then the greater change in the natural graphite is due to the smaller value of the initial resistivity. Highly oriented pyrolytic graphites were irradiated with neutrons by Blackman *et al.* (1961a), who showed that the resistance changes increased with the perfection. However, they also found that the resistivity parallel to the hexagonal axis decreased, contradicting the results of Primak and Fuchs (1954, 1956).

Primak and Fuchs also studied the effect of irradiation on the temperature coefficient of resistivity. In natural graphite the coefficient is positive, due to the variation of electron scattering with temperature. Radiation defects are a temperature-independent scattering, and hence reduce the temperature coefficient. Artificial graphites, however, have a negative coefficient, due to the variation of the number of electrons in the conduction band with temperature. Irradiation produces electron traps and increases the number of current carriers, and since this is independent of the temperature reduces the temperature coefficient. Comparing relative changes in electrical resistivity, ρ/ρ_0, with relative changes in thermal resistivity, κ_0/κ, shows that they are roughly equal for low doses, but as the dose is increased ρ/ρ_0 saturates at ~3, whereas κ_0/κ continues to increase, reaching values of 100. This shows that the saturation in resistivity is not due to a saturation of radiation defects. Figure 6.15 compares the effect of annealing on electrical and thermal resistivity changes on a sample which has received a very large dose. It can be seen that the annealing of the thermal resistivity is almost complete before the electrical resistivity begins to anneal.

Figure 6.16 shows the effect of irradiation on the Hall coefficient of polycrystalline graphite, determined by Kinchin (1954). The curves can be interpreted as being caused by the irradiation producing electron traps. The trapping of electrons results in an excess of positive charge carriers, causing the sign of the Hall coefficient to change from negative to positive, as indicated by equation (6.3). As the irradiation increases, the number of positive current carriers increases, and the Hall coefficient tends towards becoming inversely proportional to the number of current carriers. Blackman *et al.* (1961a) studied the effect of irradiation on the Hall coefficient of pyrolytic graphites and found that the effect was very similar to polycrystalline graphite, although the changes were larger.

Kinchin (1954) also examined the effect of irradiation on magneto-resistivity; the results are shown in Fig. 6.17. The reduction in magneto-resistance with increasing irradiation can be interpreted, using equation (6.4), as being due to a reduction in the carrier mobilities by scattering from radiation defects.

The effect of annealing on the Hall coefficient and magneto-resistivity was studied by Eatherly and by Hook (see Hove, 1956) using pulse annealing. Similar anomalies to those reported for the annealing effect on electrical resistivity were found.

The effect of irradiation on the thermo-electric power parallel to the basal planes for pyrolytic graphite was investigated by Blackman *et al.* (1961b) and is to change the sign from negative to positive, although the negative dip in Fig. 6.10 is still present. Blackman *et al.* (1961a) also studied the effect of irradiation perpendicular to the basal planes and found that the initially slightly positive power (~4.0 $\mu V.K^{-1}$) was considerably increased to 39 $\mu V.K^{-1}$ after a small irradiation with neutrons. Annealing had little effect below temperatures of 2000°C, above which recovery occurred.

As mentioned earlier, graphite has a high diamagnetic susceptibility. This is considerably reduced by irradiation. Measurements obtained by Hove and McClelland (1957) are shown in Fig. 6.18. Hove and McClelland interpreted the reduction in susceptibility as being due to a lowering of the energy of the Fermi surface due to electron trapping. McClelland (1952) described the effect of annealing on the diamagnetic susceptibility — the behaviour is generally the same as for electrical properties.

The effect of irradiation on electron spin resonance was investigated by Hennig and Smaller (1955) for polycrystalline graphite and by Müller (1961) and Wagoner (1961) for natural graphite crystals. Müller's work showed that the electron spin resonance in both unirradiated and irradiated graphite was due to the current carriers. Müller examined the effect of irradiation on the *g*-value and found that irradiation reduced the *g*-value, asymptotically approaching 2 at high doses. (Recall the values quoted earlier for unirradiated graphite of 2.0495 and 2.0026 for the magnetic field perpendicular and parallel to the basal planes, respectively.) This can be explained by irradiation induced electron traps lowering the Fermi level into the valence band.

It can be concluded that, whilst the understanding of the electronic properties of graphite is satisfactory with regard to the relationships between the different properties, there is difficulty identifying the defects responsible for particular effects.

REFERENCES TO CHAPTER 6

AUSTERMAN, S.B. (1958), Low Temperature Irradiation and Annealing Experiments in Graphite,Report NAA-SR-2457.

AUSTERMAN, S.B AND HOVE, J.E. (1955), Phys. Rev., **100**, 1214.

BERLINCOURT, T.G. AND STEELE, M.C. (1955), Phys. Rev., **98**, 956.

BLACKMAN, L.C.F., SAUNDERS, G. AND UBBELOHDE, A.R. (1961a), Proc. Phys. Soc., **78**, 1048.

BLACKMAN, L.C., SAUNDERS, G. AND UBBELOHDE, A.R. (1961b), Proc. Roy. Soc. A, **264**, 19.

CASTLE, J. (1953), Phys. Rev., **92**, 1063.

CASTLE, J. (1954), Phys. Rev., **95**, 846.

DE COMBARIEU, A., JAY-GERIN, J.P. AND MAYNARD, R. (1973), J. Phys. Chem. Solids, **34**,189.

DELHAES, P. (1971), Chemistry and Physics of Carbon, **7** (Ed. P.L. Walker, Jr), MARCEL DEKKER, New York, 193.

DILLON, R.O., SPAIN, I.L., WOOLLAM, J.A. AND LOWREY, W.H. (1978), J. Phys. Chem. Solids, **39**, 907.

DUTTA, A.K. (1953), Phys. Rev., **90**, 187.

FISHBACH, D.B. (1971), Chemistry and Physics of Carbon, **7**, (Ed. P.L. Walker, Jr), MARCEL DEKKER, New York, 1.

GANGULI, N. AND KRISHNAN, K.S. (1941), Proc. Roy. Soc., **177**, 168.

GASPAROUX, H. THESIS, (1965), University of Bordeaux.

HAERING, R.R. AND WALLACE, P.R. (1957), J. Phys. Chem. Solids, **3**, 253.

HENNIG, G.R. AND SMALLER, B. (1955), Paramagnetism of Irradiated Graphite, ANL-5385.

HOVE, J.E. (1955), Phys. Rev., **100**, 645.

HOVE, J.E. (1956), Proc. First and Second Carbon Conferences, Waverley Press, Baltimore, 125.

HOVE, J.E. Prog. in Nucl. Energy V, **2**, Pergamon Press, 551 (1959).

HOVE, J.E. AND MCCLELLAND, J.D. J. Chem. Phys., **26**, 1028 (1957).

KAWAMURA, K., SAITO, T. AND TSUZUKU, T. J. Phys. Soc. Japan, **42**, 574 (1977).

KAWAMURA, K., SATO, N., AOKI, T. AND TSUZUKU, T. J. Phys. Soc. Japan, **41**, 2027 (1976).

KELLY, B.T. (1981), Physics of Graphite, Applied Science Publishers, London.

KINCHIN, G.H. (1953), Proc. Roy. Soc. A, **217**, 9.

KINCHIN, G.H. (1954), J. Nuclear Energy, **1**, 124.

KLABUNDE, C.E., BLEWITT, T.H. AND COLTMAN, R.R. (1961), Bull. Am. Phys. Soc., **6**, 129

KLEIN, C.A. (1962), J. Applied Phys., **33**, 3338.

KLEIN, C.A. (1964), J. Applied Phys., **35**, 2947.

KLEIN, C.A. (1966), Chemistry and Physics of Carbon, **2** (Ed. P.L. Walker, Jr), Marcel Dekker, New York, 225.

KRISHNAN, K.S. AND GANGULI, N. (1939), Nature, **144**, 667.

MAZZA, M. (1964), J. Chim. Phys., **61**, 721.

MAZZA, M., MARCHAND, A. AND PACAULT, A. (1962), J. Chim. Phys., **59**, 657.

MCCLELLAND, J.D. (1952), Change in Magnetic Susceptibility of Irradiated Graphite during Pulse Annealing, Report NAA-SR-211.

MCCLURE, J.W. (1956), Phys. Rev., **104**, 666.

MCCLURE, J.W. (1958), Phys. Rev., **112**, 715.
MCCLURE, J.W. (1960), Proc. Fourth Biennial Carbon Conference, Pergamon Press, 177.
MÜLLER, K.A. (1961), Phys. Rev., **123**, 1550.
ONO, S. J. (1976), Phys. Soc. Japan, **40**, 498.
PACAULT, A. AND GASPAROUX, H. (1967), Comptes Rend. C, **264**, 1160.
PACAULT, A., MARCHAND, A., BOTHOREL, P., ZANCHETTA, J., BOY, F., CHERVILLE, J.V. AND OBERLIN, M. (1960), J. Chim. Phys., **57**, 892.
POQUET, E., LUMBROSO, N., HOARAU, J., MARCHAND, A., PACAULT, A. AND SOULE, D.E. (1960), J. Chim. Phys., **57**, 866.
PRIMAK, W. Phys. Rev., **103**, 544 (1956).
PRIMAK, W. AND FUCHS, L.H. Phys. Rev., **95**, 22 (1954).
PRIMAK, W. AND FUCHS, L.H. Phys. Rev., **103**, 541 (1956).
RASOR, N.S. (1955), Nuclear Engineering and Manufacturing, NAA, Downey, California.
REYNOLDS, W.N. AND GOGGIN, P.R. (1960), Phil. Mag., **5**, 1049.
RYSCHKEWITSCH, E. (1923), Zeits. für Elektrochem. und Ang. Physik. Chemie, **29**, 474.
SHOENBERG, D. (1952), Phil. Trans. Roy. Soc. A, **245**, 1.
SIMMONS, J.H.W. (1958), Radiation Damage in Graphite, Pergamon Press, London (1965).
SOULE, D.E. Phys. Rev., **112**, 698 & 708.
SPAIN, I.L. (1971), The Physics of Semimetals and Narrow-Gap Semiconductors (Eds. D.L. Carter and R.T. Bate), Pergamon Press, New York.
SPAIN, I.L., UBBELOHDE, A.R. AND YOUNG, D.A. (1967), Phil. Trans. Roy. Soc. A, **262**, 345.
SUGIHARA, K., TAKEZAWA, T., TSUZUKU, T., HISHIYAMA, Y. AND ONO, A. J. (1972), Phys. Chem. Solids, **33**, 1475.
TAKEZAWA, T., TSUZUKU, T., ONO, A. AND HISHIYAMA, Y. (1972), Phil. Mag., **19**, 623.
TAMARIN, P.V., SHALYT, S.S. AND VOLGA, V.I. (1969), Soviet Physics: Solid State, **11**, 1399.
WAGONER, G. (1960), Proc. Fourth Biennial Carbon Conference, Pergamon Press, New York, 197.
WAGONER, G. (1961), Bull. Am. Phys. Soc., **6**, 129.
WALLACE, P.R. (1947a), Phys. Rev., **71**, 622.
WALLACE, P.R. (1947b), Phys. Rev., **72**, 258.
WASHBURN, G.E. (1915), Ann. Physik, **48**, 236.
YOUNG, D.A. (1968), Carbon, **6**, 135.

CHAPTER 7

PYROCARBON IN HIGH TEMPERATURE NUCLEAR REACTORS

7.1. Introduction

A wide range of carbons, from sooty deposits to highly oriented pyrolytic graphite, has been deposited onto surfaces by the pyrolysis of various hydrocarbon gases. These have been employed in a variety of applications, ranging from rocket nozzles to various bio-engineering topics such as heart valves. In this chapter, we confine our attention to the employment of pyrocarbon (PyC) in the spherical coated fuel particles of the high temperature reactor system (Price and Shepherd, 1979).

A high temperature reactor (HTR) contains typically 10^{10} of such particles, each of diameter about 1 mm. An individual particle consists of a kernel of fissile or fertile fuel, surrounded by a number of layers which are designed to retain the fission products that are being created during the course of the irradiation. The fuel may be oxides or carbides of uranium, plutonium or thorium in the form of spheres typically 500–800μm in diameter that have been manufactured by one of a variety of processes that include gel precipitation (Huschka and Vygen, 1977) and the agglomeration of sub-micron powders (Allen *et al*, 1977).

Two distinct particle designs have been employed (Stansfield, 1991). The so called BISO coated particle possesses two layers, namely a highly porous PyC coating, referred to as the buffer layer (typically 30μm thick), which is surrounded by a denser PyC layer, say about 50μm thick. The buffer is designed to protect this denser PyC layer from damage by recoiling fission fragments emanating from the kernel, and is thus essentially a sacrificial coating. It also serves to provide voidage, additional to that contained in the fuel, for gases created by fission to occupy, thereby ameliorating the pressure they exert on the outer, denser PyC layer. The purpose of this PyC layer is to retain fission products. While its retentive ability has proved excellent for gases, it is not so good for some of the metallic fission products, in particular caesium. As a result, BISO particle designs tend only to be appropriate at comparatively low irradiation temperatures and for low burnups, when the retention of fission products in the kernel will be comparatively high. It is for these reasons that in general BISO particles have only been employed in fertile fuel particles; also, compared with the TRISO particle design discussed below, it is easier to re-process the particles, and so extract the bred fissile fuel for subsequent re-use in the reactor.

In all other cases the particle normally includes a silicon carbide (or zirconium carbide) layer, thereby improving the retention of fission products. Fig 7.1 represents a schematic illustration of this so called TRISO particle. It shows that the SiC layer is sandwiched between two PyC coatings, namely an inner pyrocarbon (IPyC) and an outer pyrocarbon (OPyC) layer. As in the BISO particle design, there is also a buffer layer, in this case protecting the IPyC from damage by recoiling fission fragments and, as before, providing additional voidage within the particle to accommodate the gases created by fission.

Each of these layers makes a number of contributions to the overall viability of this coated particle design. They are deposited sequentially in a fluidised bed at appropriate temperatures and with suitable gas compositions. Because the SiC layer is normally deposited from a gas that contains methyl trichlorosilane, one purpose of the IPyC is to protect the fuel kernel from the chlorine compounds that are produced during this process. Again, while not shown in Fig 7.1, an

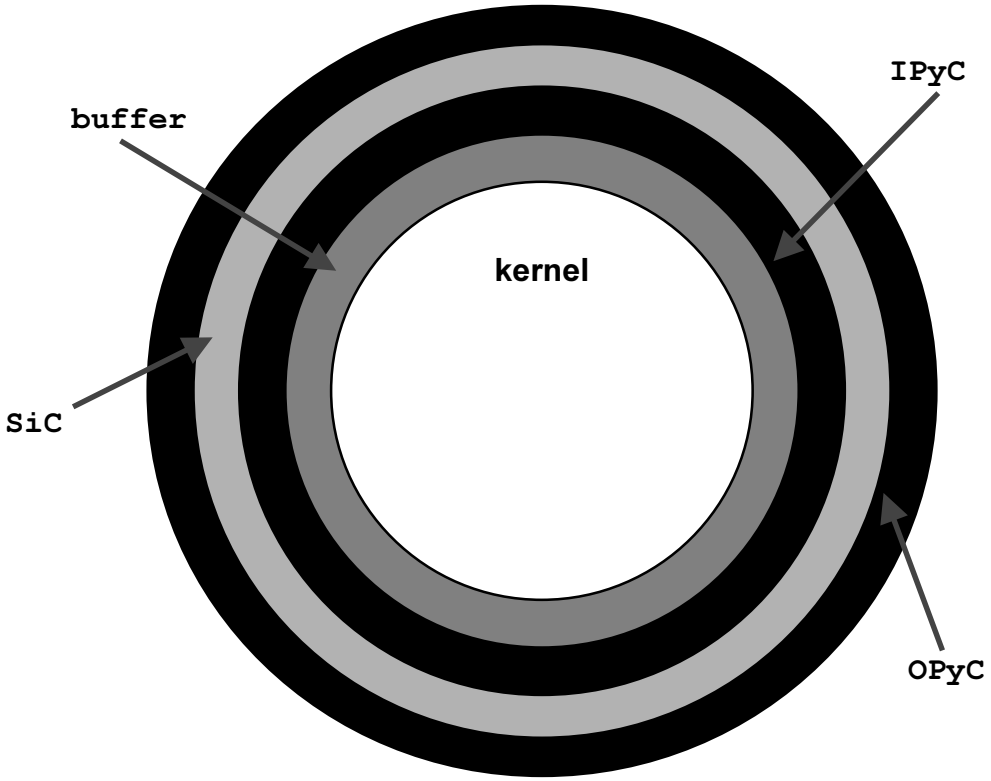

FIG. 7.1. Schematic illustration of a TRISO particle.

additional, thin PyC seal layer may be deposited between the buffer and IPyC coating in the case when the temperature required to deposit the latter with the required properties is high, as is the

case when methane is the carbon source. This seal layer is deposited at a comparatively lower temperature, and is designed to isolate the fuel from methane gas during the IPyC deposition process, thereby arresting kernel-buffer chemical reactions. Because the seal layer is purely a manufacturing requirement and its subsequent behaviour during irradiation is immaterial, it will not be discussed further. For further details of the manufacturing processes of coated particles, see Ford *et al* (1972/3).

During irradiation, the SiC layer is normally regarded as the principal barrier for fission products, both as an impermeable layer for the metallic fission products, and also as a pressure vessel that withstands the pressure of gases inside the particle that are created by fission. In addition, dimensionally it is comparatively stable under irradiation, and also exhibits a significant tensile strength, provided the surfaces are sufficiently smooth (Evans *et al*, 1973). (On the other hand, if the SiC coating were to fail during irradiation and at least one of the PyC coatings were to remain intact, at least partial retention of fission products would still be achieved, since the particle would then be essentially of BISO design.)

The PyC layers contribute additional features towards maintaining the integrity of a particle. For example, they provide additional diffusion barriers to fission products, while the OPyC layer protects the SiC coating from possible external mechanical interactions and chemical attack. The other major part the PyC layers play is to assist the SiC layer in its role as a pressure vessel. During irradiation both PyC layers will shrink, thereby compressing the SiC coating and counteracting the hoop stresses created in it by the internal gas pressure. However, these compressive stresses must not be so large that the attendant tangential stresses in the PyC layers exceed the fracture stress. (Also, if the IPyC layer is to make a contribution, the radial

stress between the IPyC and SiC layers must not be so great that debonding between the two occurs.) For this requirement to be met, these two layers must be approximately isotropic. This is because the rate of shrinkage of unrestrained anisotropic layers is so high that the stresses required to prevent such shrinkage by creep (since the PyC layers are almost completely restrained by the SiC) are unacceptably large. A detailed mathematical account of the stresses created in the various layers of TRISO particles during irradiation, together with a more extensive physical description of the various factors contributing to these stresses compared with that presented here, has been given by Martin (1973).

Because pyrocarbons with a very wide range of structures are obtainable, it is clearly important that the appropriate deposition conditions be employed if coated particles with an acceptable irradiation behaviour are to be manufactured. Accordingly, Section 7.2 discusses the various experimental conditions that have been used in the deposition of PyC layers during the manufacture of coated particles and the resulting structures. Section 7.3 refers to some of the other physical properties of these coatings immediately after manufacture, while Section 7.4 describes the effect of irradiation on these structures and properties, the emphasis being on isotropic pyrocarbons. Brief reference to PyC alloys is made in Section 7.5 before the discussion and conclusions relating to this chapter are presented in Section 7.6.

7.2. Structures and Deposition of PyC

7.2.1. *Structures of PyC*

The structure and properties of PyC coatings can vary considerably in accordance with the deposition conditions. In an optical microscope, four distinct structures have been identified (Bokros, 1969, p24) which may be described as columnar, granular, laminar and isotropic; these are illustrated in Fig 7.2. The first two of these possess a clear grain structure, with the columnar deposits possessing grains that are elongated normal to the plane of deposition and granular deposits comprising many grains which are approximately equiaxed. Although laminar deposits do not possess an identifiable grain structure, their name derives from the fact that a series of concentric rings of growth features are observed. By contrast, isotropic deposits appear to be almost featureless, with no identifiable structure. Comparatively little reference will be made to the columnar deposits since, being observed more frequently in material deposited onto static surfaces, they feature only occasionally in reports relating to the manufacture of coated particles. By contrast far more emphasis will be placed on the isotropic coatings and their properties, since these are of practical interest in the manufacture of coated particles.

Within regions that are not resolvable using an optical microscope are crystallites whose dimensions are typically 1–10 nm, each comprising a sequence of more or less hexagonal planes of carbon arranged in a stack, but with little correlation between adjacent layers. (Graphitisation of this material at high temperatures would then cause these layers to re-align with respect to each other.) The crystallite size is normally obtained from the broadening of the X ray diffraction $\{000l\}$ lines to give L_c , the height of the stack of planes. The comparable derivation of L_a is more difficult, but has been shown to be comparable to the L_c value. The amount of correlation between layers (or the degree of graphitisation) may be deduced from the X ray *c*-spacing, since this increases with their relative disorder.

Because ideally isotropic coatings are required on coated particles, it is important to measure their degree of anisotropy; in the case of deposits containing some degree of anisotropy, the carbon layers comprising the crystallites will tend to line up preferentially, parallel to the surface onto which they are being deposited.

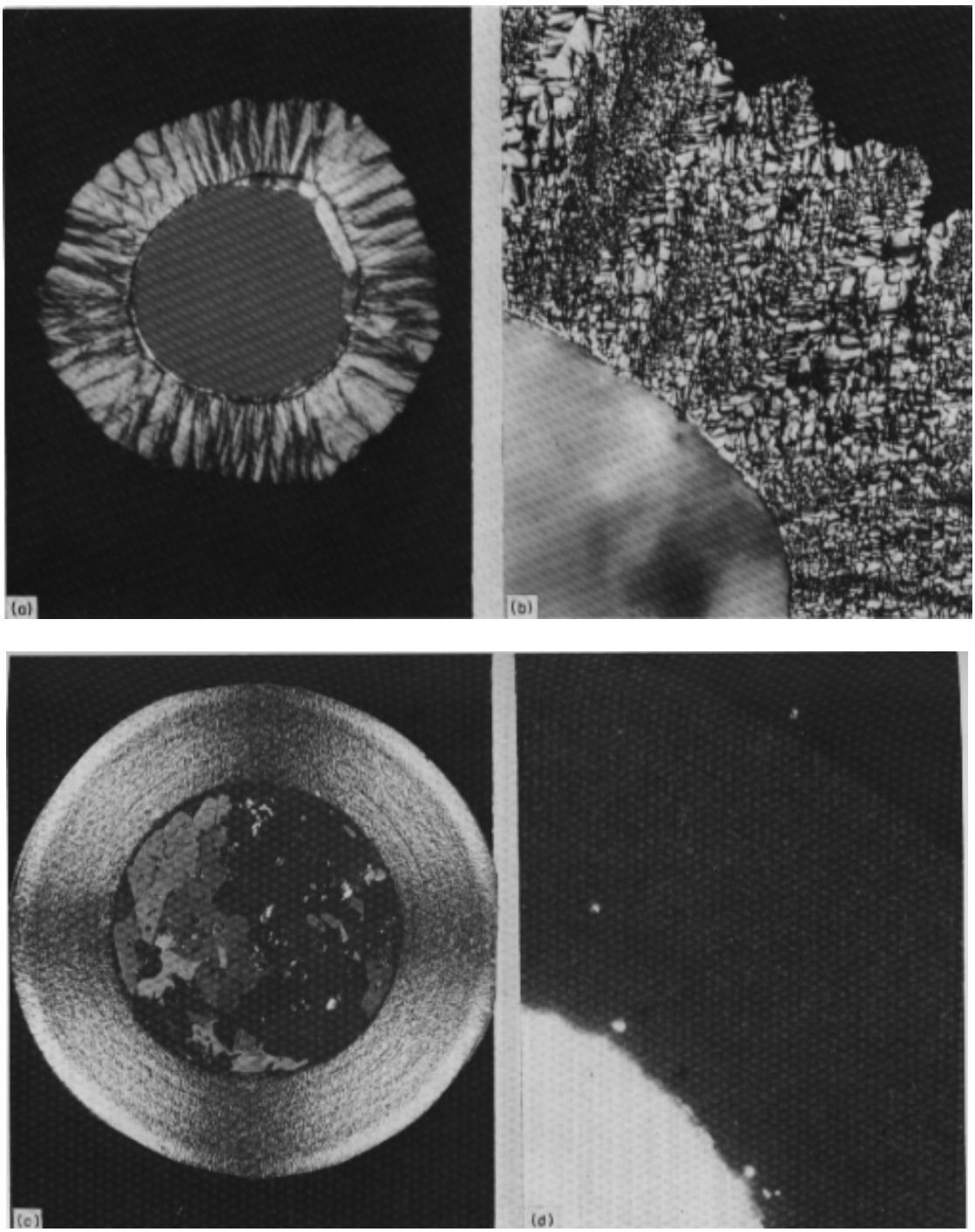

FIG. 7.2. Some microstructures of pyrocarbons deposited in fluidised beds, as observed in an optical microscope. (a) Columnar (due to Bard et al, 1968), (b) Granular, (c) Luminar and (d) (in polarised light) isotropic. After Bokros (1969, p24).

Undoubtedly the best way of defining the anisotropy is via the Bacon Anisotropy Factor (BAF) defined by

$$BAF = 2 \cdot \frac{\int_0^{\pi/2} I(\phi) \,.\cos^2\phi \,.\sin\phi \,.d\phi}{\int_0^{\pi/2} I(\phi) \,.\sin^3\phi \,.d\phi} \tag{7.1}$$

where $I(\phi)$ is the relative number of atoms in {0002} planes per unit solid angle that make an angle ϕ with the deposition plane normal. $I(\phi)$ may be obtained from variations in intensity of the {0002} X ray Debye-Scherrer diffraction ring. Values of the BAF range from unity (isotropic) to infinity (completely aligned planes). Generally these X ray measurements have been made on PyC that had been deposited on discs at the same time as the coatings on particles, and sometimes it has been assumed that the structures of the two are identical. However, on the basis of his X ray studies, Pluchery (1973) has stated that his results show there is no meaningful correlation between BAF values measured on coated particles and those determined from coated discs that are manufactured simultaneously. Because of this, it is worth noting that Tempest (1978) has described a method of measuring BAF values on the PyC layers of intact particles. Many BAF values reported in the literature were obtained from what, experimentally, are simpler studies of optical activity, from measurements of reflected light under a polarising microscope (Stevens, 1975). However, it should be noted that BAF values derived by optical and X ray methods on the same material will not necessarily be identical.

Density is another structural parameter that must be controlled if particles are to behave satisfactorily during irradiation. Its value should be greater than ~1.6 $Mg.m^{-3}$, because, if lower, the PyC would densify so rapidly during irradiation that stresses higher than those required to fracture the layer would be built up. Normally densities are measured by sink-float methods, by observing the depth to which PyC fragments sink in a column of liquid possessing a known density gradient. Because liquid can penetrate the open porosity of samples, density values so obtained provide a measure of the volume fraction occupied by closed porosity. While closed porosity is normally assumed to make a greater contribution to the overall porosity compared with the open fraction, Allen *et al* (1977) have pointed out that their relative contributions depend on the deposition conditions, details of which have been given by Ford and Bilsby (1976). For example, coatings with a sink-float density of 1.85 $Mg.m^{-3}$ could be manufactured with overall (bulk) densities ranging between 1.0 and 1.85 $Mg.m^{-3}$. Clearly low bulk density values are undesirable, if they cause too rapid a densification during irradiation, or if materials containing large open porosity fractions provide easy escape routes for fission products. However, appropriate manufacturing procedures would appear to obviate such undesirable possibilities. The above discussion refers to the IPyC and OPyC layers. By contrast, the requirements for the buffer layer are quite the opposite. Low density materials containing a large open porosity fraction to provide voidage for the gases created during fission are required. As a result, bulk densities of the buffer layer are typically 50% of the fully dense material value, with half the porosity at the time of manufacture being open. This fraction is believed to increase, both during manufacture when the other layers are being deposited and also during irradiation, when most of the original overall porosity is believed to be available to the internal gases (Ford *et al*, (1972/3)).

Details of pore structures may be derived from X ray small angle scattering measurements. For example, Krautwasser and Nickel (1975) have concluded from a study of various PyC deposits that generally the porosity consists predominantly of pores that are under 2.5 nm in diameter. This conclusion appears to be confirmed by scanning and transmission electron microscopy observations (Kaae, 1985), who demonstrated that the majority of the porosity did not lie in the 100 nm–1μm diametral size range, and is almost certainly contained within the microporosity that occurs between individual carbon crystallites. Such crystallites have been observed to be arranged in the form of long, bent, or twisted ribbons or fibres (Pollmann *et al* 1977).

7.2.2. *Deposition of PyC*

The coating of fuel spheres with the various PyC (and SiC) layers is performed consecutively in a fluidised bed. A standard fluidised bed consists essentially of an upright cylindrical vessel with a conical end at its bottom through which, at its apex. the appropriate gas mixture enters. The gas flow levitates the particles, which partly fill the vessel, and this is heated by an external furnace. This levitation results in a cyclic motion of individual particles which periodically enter the region of the vessel where most of the deposition takes place (the deposition zone). This arrangement, together with an alternative, and claimed to be improved, design involving a purely cylindrical reaction vessel, with gas entering uniformly at the bottom through a porous plate, has been described by Lackey *et al* (1977).

The specification of conditions that are required to produce coatings with certain required structures and properties is difficult because it depends on so many experimental variables, including the design of the fluidised bed itself. Amongst the readily identifiable variables are the following: temperature of the bed, nature of the hydrocarbon employed as the carbon source, the hydrocarbon partial fraction in the gas, the gas diluent species, the bed surface area, the volume of the deposition zone and the gas flow rate. The ratio of these last two variables may be regarded as the time a particular gas molecule can spend in the vicinity of particles that are contained in the deposition zone; this is sometimes defined as the contact time. Given these circumstances, any numerical values of these variables presented below which are correlated with a specific PyC structure or property must be regarded only as guidelines, since they do not represent a complete specification of the necessary coating conditions. However, and at the risk of over-simplifying what is a highly complex topic, it would appear that the bed temperature and the rate of deposition of a layer are two of the most important parameters. Clearly the deposition rate will depend on a number of the above mentioned variables, for example the hydrocarbon partial pressure and the bed surface area. In addition, this rate will be governed by the nature of the diluent gas as well as by its partial pressure. Commonly argon or helium has been used. However it has been shown (Kobayashi *et al*, 1972, 1974) that chlorine can enhance and hydrogen decrease the rate of deposition if these gases are included in the diluent. As discussed below, the reason why bed temperatures and deposition rates are so important is because these parameters significantly affect the extent that molecular aggregates can develop in the gas phase and then restructure once they have been deposited onto surfaces.

Appropriate temperatures required to obtain isotropic layers that are suitable for coated particles depend on the hydrocarbon that is chosen. If methane is used, temperatures in the range ~1900–2000 °C are required. However, because hydrocarbons possessing a higher molecular weight can produce acceptable deposits at lower temperatures, they have become more popular. For example, in the case of the two most used hydrocarbons, namely propylene and acetylene, temperatures around 1200–1400 °C may be employed. Manufacturing considerations of these and other higher molecular weight hydrocarbons are reported by Ford *et al* (1972/3). In order to emphasise this particular manufacturing difference, these two types of coating are often referred to as high temperature isotropic (HTI) and low temperature isotropic (LTI) respectively. Suitable deposition rates tend to be higher when bed temperatures and required coating densities are comparatively lower. For example, Huschka and Vygen (1977) have reported rates for HTI pyrocarbon coatings deposited at 2000 °C of 0.7μm/min, whereas for LTI layers deposited from an acetylene/propylene mixture at 1300 °C it was 4–6μm/min.

Bokros (1965) has investigated the various types of layers that can be obtained and their properties when methane is employed as the source gas; for more details than can be presented here the interested reader should consult this reference. Fig 7.3 shows schematically the structures which are obtained when temperatures and methane concentrations are varied

(Bokros, 1969, p28). This shows that the anisotropic laminar and granular structures are obtained at respectively low and high deposition temperatures. However, granular structures only occur at low methane concentrations, when deposition rates will be comparatively lower. Figs 7.4 and 7.5 are three dimensional plots of respectively coating density and BAF, each as functions of bed temperature and methane concentration (Bokros, 1965). At low temperatures, when laminar structures occur, coating densities are comparatively high, as also are densities of the granular deposits produced at high temperatures. In the region of Fig 7.4 where isotropic structures occur, the noteworthy feature is the minimum in density with increasing temperature, an observation which has been observed by many workers, using a variety of hydrocarbon gases. Figure 7.5 illustrates that laminar and granular layers are highly anisotropic. In addition, Figs 7.4 and 7.5 demonstrate that if isotropic layers with densities above ~ 1.6 $Mg.m^{-3}$ are required, deposition temperatures in the vicinity of 1900 °C are called for.

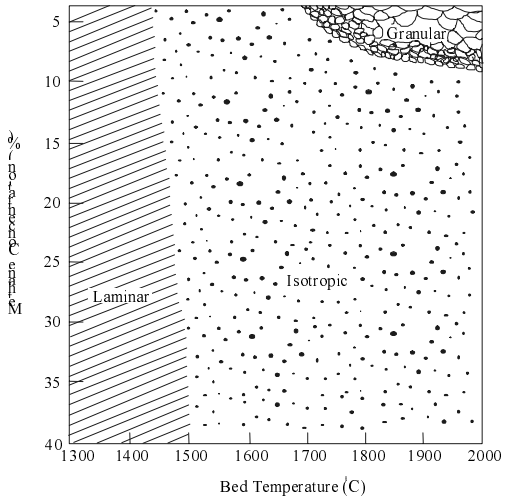

FIG. 7.3. Schematic illustration of structures produced over a range of deposition conditions for methane derived pyrocarbons.

Another feature of these structures, also reported by Bokros (1965), is that crystallite sizes increase with increasing deposition temperature and decreasing methane concentration, the only exception being in the dependence with temperature, in the region where densities decrease with increasing temperature. Crystallite sizes (L_c) in the range 3–10 nm were reported.

Turning next to depositions using higher molecular weight hydrocarbons, in particular acetylene, propylene, propane and butane, it appears that by appropriate adjustment of the deposition conditions, PyC structures that are similar to those using methane as the deposition gas can be obtained. As already noted, fluidised bed temperatures required to obtain satisfactory, isotropic coatings are lower compared with those derived from methane. However one feature of all isotropic coatings is that their hydrogen content decreases with increasing deposition temperature (Ford *et al*, 1972/3).

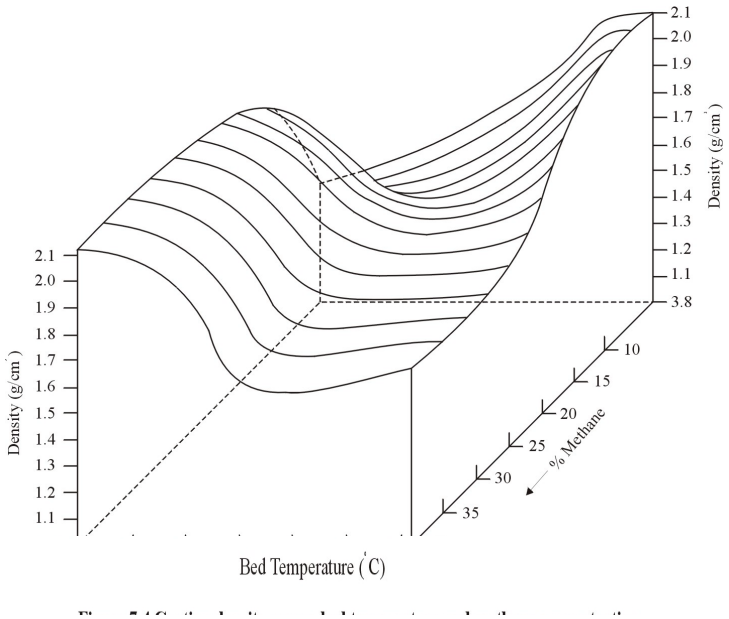

FIG. 7.4. Coating density versus bed temperature and methane concentration.

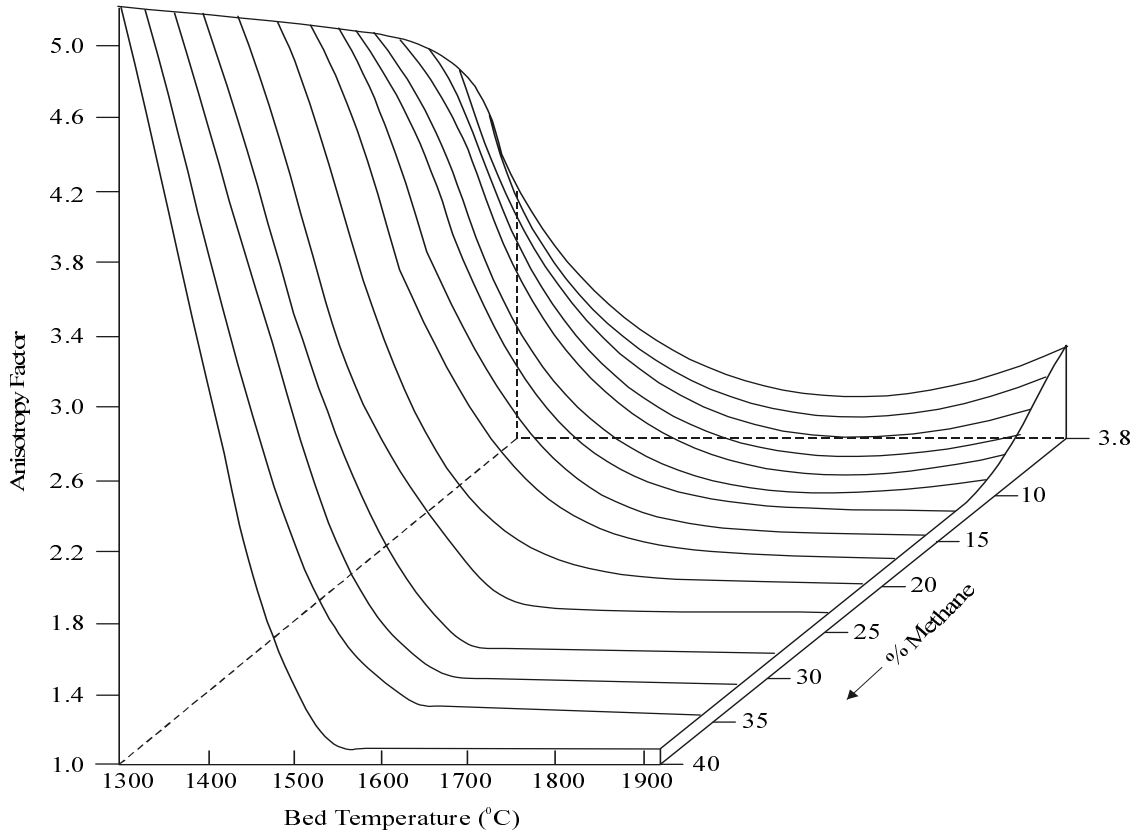

FIG. 7.5. Bacon Anisotropy Factor (BAF) versus bed temperature and methane concentration.

Figure 7.6 illustrates how, using propane as the deposition gas, the PyC density, deposition rate, crystallite size and anisotropy factor vary with bed temperature and hydrocarbon concentration (Bokros, 1969 p38, quoting Beatty, 1967). (Note that the anisotropy factor quoted in Fig. 7.6., $\sigma_{0Z} / \sigma_{0X}$, is in fact the BAF.)

From an examination of the contours in the graphs shown in Fig. 7.6., it is evident that qualitatively the trends are very similar to those already noted for methane derived coatings. For example, as the deposition temperature increases the density passes through a minimum value, whereas the crystallite size increases monotonically. Fig. 7.6. also shows that isotropic coatings are more likely to occur using relatively higher propane partial pressures, which in turn result in higher deposition rates. (These rates are in keeping with those quoted above due to Huschka and Vygen (1977) for LTI coatings.) However, if Fig. 7.6. is compared with Figs 7.4. and 7.5., it will be apparent that, unlike coatings derived from methane, relatively high density isotropic PyC layers can be prepared at comparatively lower temperatures, i.e. below the density minimum.

Contour line plots of the type shown in Fig. 7.6. do not appear to have been produced for the other hydrocarbon gases from which LTI coatings can be prepared. However, almost certainly they are likely to be very similar to those shown in Fig. 7.6. Bard *et al* (1968) have shown that over the temperature range 1200–1400 °C, structures resulting from different hydrocarbons are comparable, provided the deposition rate is the same. (However, it should be noted that most of their deposition rates were low, <1μm/min, with the result that many of the deposits they obtained possessed columnar or laminar structures.) Useful plots of density variations with deposition conditions for a number of hydrocarbon gases and the way these differ (but without quoting deposition rates) have been given by Ford *et al* (1972/3).

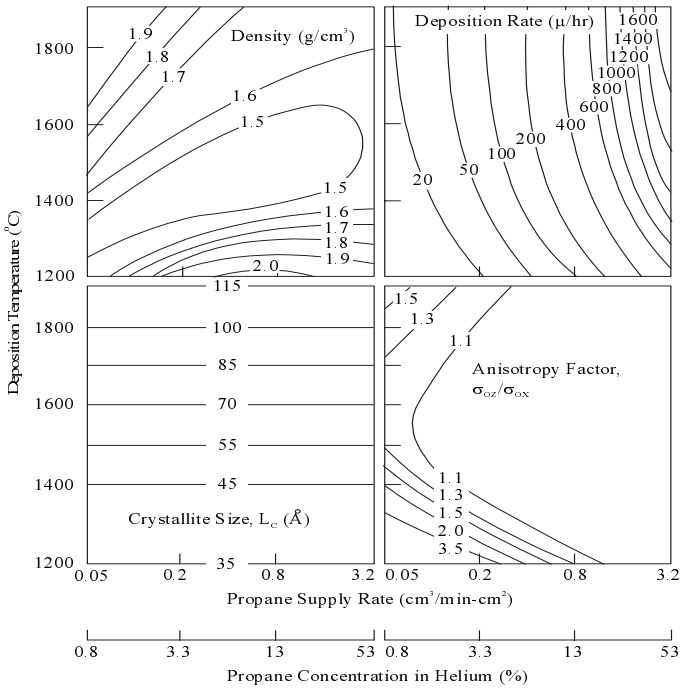

FIG. 7.6. Structural properties of PyC coatings deposited from propane as a function of bed temperature and propane concentration.

The above discussion has centred on the deposition of the IPyC and OPyC layers in the manufacture of TRISO coated particles and the outer PyC layer of BISO particles. In addition to the requirement that these layers should be isotropic and sufficiently dense, it is also necessary that they be impermeable to the gases that are created by fission. This implies the absence of inter-connected open porosity between the inner and outer surface. Most reported measurements of PyC densities only give an indication of the closed porosity. However, Ford and Bilsby (1976) have measured both open and closed porosities and shown that while isotropic coatings with relatively small amounts of open porosity may be produced, nevertheless if the hydrocarbon partial pressure is increased the open porosity component is enhanced. This suggests that while sufficiently high deposition rates are required in order to achieve isotropic layers, they should be no higher than are necessary. (This is also a desirable requirement in terms of producing particle batches with controlled coating thicknesses.) On the other hand, Ford and Bilsby (1976), in the particular conditions of their experiments, have shown that under similar coating conditions the open porosity fraction decreases with layer thickness, suggesting that pores accessible to gases and liquids only reside near to surfaces. Nevertheless, when deposition rates are sufficiently high, layers containing fully inter-connected porosity, and therefore permeable to gases, are to be expected. Indeed, the buffer layer is the one layer which is required to possess such properties. Acetylene is the hydrocarbon most commonly used to deposit the buffer layer. Compared with other hydrocarbons, appropriate deposition temperatures are lower and the density is more strongly dependent on the hydrocarbon partial pressure and bed temperature. Overall porosities of typically 50% can be achieved of which at least half is open (Ford *et al*, 1972/3). Corresponding buffer deposition rates of 6–10 μm/min at 1250 °C have been quoted (Huschka and Vygen, 1977).

7.2.3. *Models relating Deposition Conditions with Structures*

A number of models has been put forward to explain the structures and properties of PyC that are obtained following a variety of deposition conditions, some being more comprehensive than others. While these models may differ in detail (and may not necessarily be in conflict), it is worth noting that many of the underlying principles are similar. For example, it is universally agreed that molecules form aggregates in the gas phase and these are deposited subsequently onto surfaces. Therefore, the models have to consider the size and nature of these aggregates at the time when they are deposited and whether, once deposited, any rearrangement or restructuring takes place.

The model by Bokros (1969, p56) was proposed to account for the characteristics of coatings he had obtained from methane. In the 900–1400°C temperature region, it was envisaged that at very low partial pressures of methane the aggregates depositing onto particles are very small, but that with increasing pressure they will become larger and planar. Because such larger aggregates are likely to stack better onto surfaces compared with smaller ones it is expected that the resulting layers will be comparatively more dense and anisotropic.

Further increases in the partial pressure will enable these aggregates to act as nuclei for the formation of droplets which, on deposition, will possess no overall preferred orientation, thereby resulting in an isotropic layer. At more elevated temperatures these droplets will be in a more advanced state of pyrolysis and therefore be more akin to soot particles. Thus, in the region of 1600 °C they will result in a layer of reduced density that is isotropic. However, at even more elevated temperatures, the density will increase because these particles will be able to restructure.

The model put forward by Ford and Bilsby (1976) was designed to explain why the open porosity of coatings deposited from propylene increased with increasing hydrocarbon partial

pressure. It starts from the fact that spherical growth features were observed in their deposits. In the gas phase, liquid drops are formed which, at higher partial pressures, can join together to form larger aggregates. At low partial pressures, it was envisaged that droplets can arrive individually onto surfaces and coalesce before complete carburisation, thereby trapping some closed porosity. The lower the deposition temperature, the greater the coalescence and hence the higher the density, since the droplets will be more liquid. By contrast, at high partial pressures, much larger aggregates will occur and coalescence is less likely to isolate completely the spaces between them, thereby creating open pores. During the next and subsequent passes of particles through the deposition zone of the bed, this porosity is supposed to be partly infilled with liquid droplets. By this means, a porous outer layer is maintained as the coating proceeds, and the infilling droplets after carbonising will be indistinguishable from the previously formed spherical growth features, in keeping with the observations.

Kaae (1985) found that layers deposited from propylene at 1300 °C exhibited a high anisotropy if the coating rate was < 0.3μm/min, but that if deposited at rates > 2μm/min they were isotropic. Electron microscope studies indicated that at low deposition rates the structure of layers consisted of small spheres to which were attached larger cones. By contrast, coatings produced at higher deposition rates exhibited larger spheres and comparatively smaller cones. The spheres were assumed to be formed in the gas phase, prior to deposition, with larger ones occurring at higher propylene partial pressures, when the deposition rate is higher. It was proposed that the cones were formed by individual molecules or small aggregates attaching themselves to these spheres subsequent to their deposition. If structurally the spheres are isotropic and the growth cones exhibit a degree of anisotropy, their relative volume fractions within a layer will explain the observed variation with deposition rate of its overall anisotropy.

A comprehensive model, designed to explain the structures of PyC coatings as a function of a number of the coating variables has been put forward by Lefevre and Price (1977). They point out that one area of confusion in the development of models is knowledge of the reaction zone temperature. Too often the temperatures that are quoted by experimenters do not refer to this important parameter, but rather to some other, arbitrarily chosen point within the furnace. Amongst the simplifications incorporated into their model is the assumption of a constant reaction zone temperature.

Their model assumes that liquid, incompletely polymerised droplets, referred to below as sub-aggregates, with a low enough viscosity to allow for deformation, are produced in the gas phase, but that after a period of time further polymerisation makes them sufficiently solid for them to be no longer capable of deformation. In addition, while still in the gas phase it is possible for these sub-aggregates to collide with each other to form aggregates. Three times associated with these processes are identified, namely the times that individual sub-aggregates and aggregates survive, and also the time taken for solidification to occur. The relative values of these three times, determined by the various coating parameters, affect the packing of carbonaceous material, both just before deposition and also on the substrate, and hence the PyC structure that is eventually obtained. This model is able to account for a number of the structures that have been obtained in a fluidised bed.

A not completely unrelated model, which concentrates on the structure of the gaseous aggregates just before their deposition onto surfaces, has been put forward by Linke *et al* (1977). The growth rate of these aggregates is considered quantitatively, but in addition evaporation is also assumed to be a significant process, implying that aggregates may not exceed some limiting size. Four different regimes are considered, namely combinations of high/low hydrocarbon partial pressures and high/low evaporation rates. (Higher evaporation rates occur at more elevated temperatures, when there is a correspondingly higher rate of carbonisation of

aggregates.) The four different aggregate structures may be correlated with the PyC properties corresponding to the four extremities of the three-dimensional plots shown in Figs 7.4 and 7.5.

In summary, while a variety of models to account for the structures obtained during deposition has been proposed, nevertheless a number of common features are apparent. For example, all agree that under certain conditions spherical 'droplets' can be formed in the gas phase and that their existence is the underlying reason why isotropic deposits can be formed. While there may be differences between them, some at least may reflect that individual models relate only to some specific observations, which do not embrace the whole range of possible experimental variables. Therefore, while we now possess a qualitative understanding of how structures depend on the coating conditions, an ability to make any quantitative predictions is still some way off.

7.3. As-Manufactured Physical Properties

Section 7.2 described some measurements on PyC layers which gave an indication of their structures. In this section measurements on other physical, and also mechanical properties are reported.

The thermal conductivity of a number of PyC coatings with different structures, measured at room temperature, normal to the plane of deposition, has been reported by Bokros *et al* (1966). Their results are shown in Table 7.1.

Table 7.1 indicates that the highly anisotropic laminar pyrocarbons exhibit relatively lower thermal conductivity values; this is in keeping with our knowledge that the thermal conductivity of pyrolytic graphite is considerably higher in the *a*, compared with the *c* direction (Kelly, 1981). Fig 7.7 is a graph of these thermal conductivity values versus BAF and illustrates the strong connection between the two variables. By contrast, comparable plots of conductivity versus density or L_c exhibit little or no correlation.

Turning next to thermal expansion measurements, Pellegrini (1972) has measured α_c, the X ray lattice coefficient of thermal expansion (c.t.e.) of PyC crystallites in the *c* direction over the temperature range 20–1200 °C. He observed an increase with L_c from about 18 to 23×10^{-6} K^{-1} as L_c rises from 2 to 15 nm. Doubtless this variation reflects on the differing amounts of restraint between crystallites with their size as the temperature is changed.

TABLE 7.1.ROOM TEMPERATURE THERMAL CONDUCTIVITY VALUES, MEASURED NORMAL TO THE DEPOSITION PLANE OF A NUMBER OF PYROCARBONS. AFTER BOKROS *ET AL* (1966).

Structure	Density	Anisotropy	L_c	Thermal Conductivity
	Mg. m^{-3}	BAF	nm	$W.m^{-1}.K^{-1}$
Laminar	2.11	3.4	4.3	0.50
Laminar	1.92	1.6	3.3	1.00
Laminar	1.94	1.6	7.3	2.76
Laminar	1.51	2.1	2.5	0.79
Granular	2.01	1.1	14.0	8.78
Isotropic	1.55	1.0	4.9	9.61
Isotropic	2.00	1.3	14.5	7.52
Isotropic	1.82	1.05	10.7	12.54

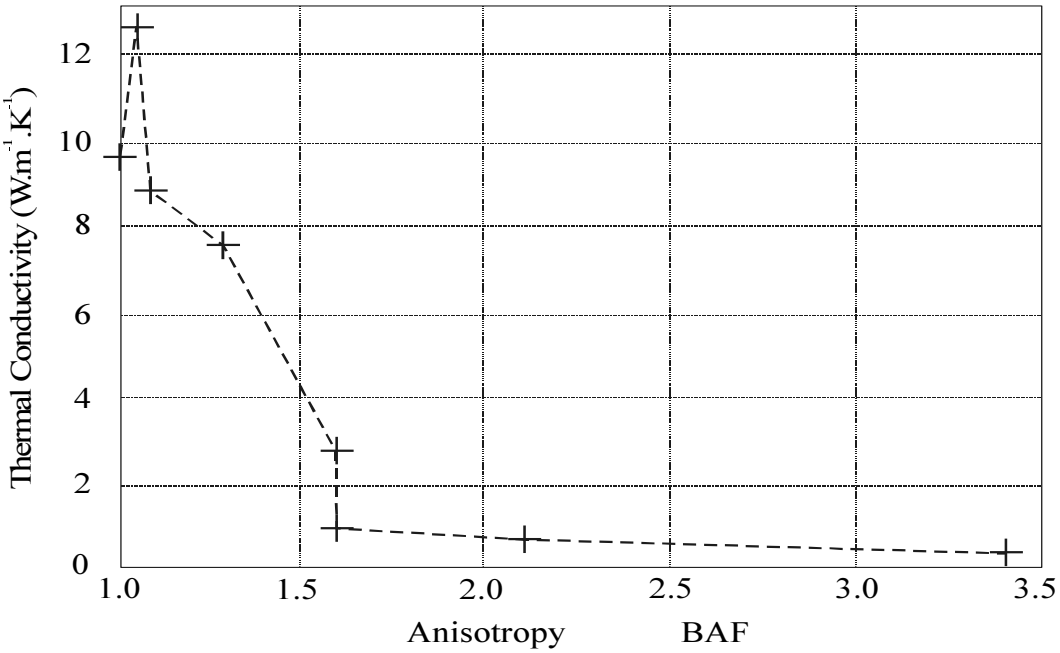

FIG. 7.7. Variation of thermal conductivity with anisotropy.

Matsuo (1988) has reported some measurements on the thermal expansion of a pyrolytic carbon. In the plane of deposition, a shrinkage was observed as the temperature was raised to 400 °C. Above this temperature an expansion occurred, its fractional value compared with the room temperature dimension being 8×10^{-4} at 900 °C. Normal to the plane of deposition the expansion was nearly linear with temperature, its fractional value at 900 °C being 20×10^{-3}. Unfortunately the BAF value of this sample was not given, but clearly, on the basis of the above expansions, it possessed a significant anisotropy.

Perhaps the thermal expansion measurements on PyC that are most relevant to HTR coated particle performance, because the material had been deposited onto particles, are those due to Pojur *et al* (1972). Three hollow hemispheres of isotropic PyC, which were prepared from layers extracted from coated particles, were employed to provide a gap between two optically flat plates nearly parallel to each other. Expansions as the temperature was raised were measured by observing the movement of interference fringes. As a result, such measurements yield values for the c.t.e. in the plane of deposition, the direction which is of special importance when the integrity of coated particles is being considered during the course of temperature changes (Martin, 1975). Linear thermal expansion coefficients were reported over the temperature range 300–800 K. Their experimental c.t.e. values are shown as data points in Fig 7.8, together with a curve that was fitted through them and given by the analytical relation

$$\text{c.t.e.}(\times 10^{-6}\,\text{K}^{-1}) = 2.5523 + 8.220 \times 10^{-3}\,T - 5.509 \times 10^{-6}\,T^2 \qquad (7.2)$$

where T is the temperature (K). Figure 7.8 indicates c.t.e. values in the region of $5.5 \times 10^{-6}\,\text{K}^{-1}$, which is rather less than one third Pellegrini's (1972) α_c value for crystallites, a figure which

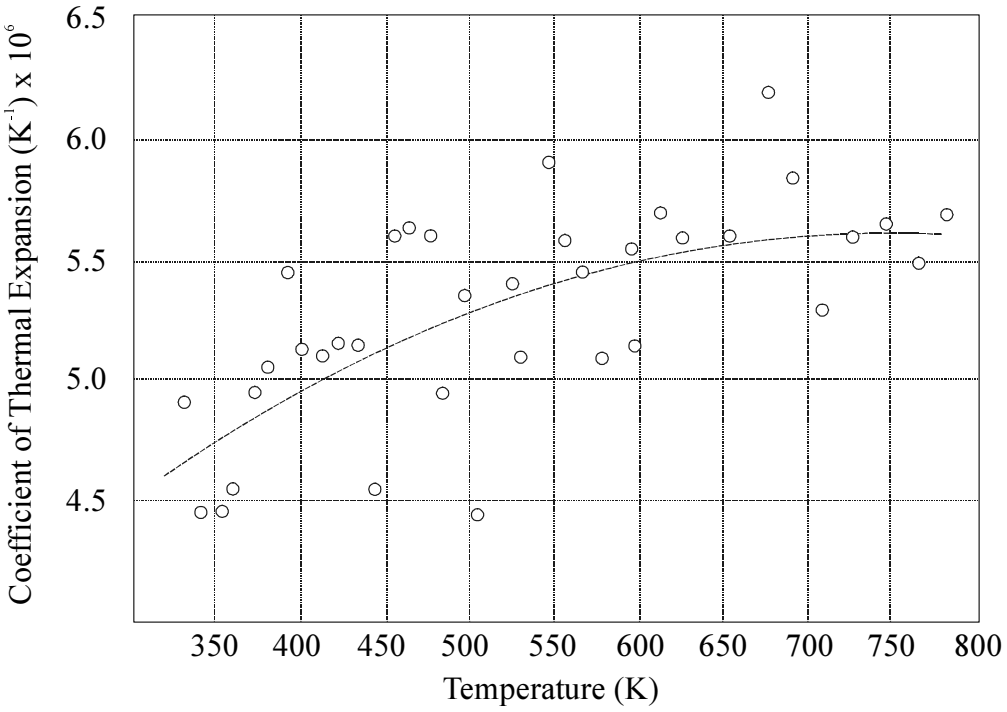

FIG. 7.8. Experimental and fitted coefficients of thermal expansion.

might be expected for an isotropic PyC since, (see Chapter 3), the corresponding value for α_a is at least an order of magnitude smaller. Doubtless this discrepancy is because the porosity that is present is able to accommodate some of the thermal expansion. This is in keeping with some c.t.e. values measured on coatings of varying anisotropies by Price *et al* (1967) which, when plotted against a preferred orientation parameter, tend to fall below the expected straight line that joins the α_c and α_a values on such a graph. It is noteworthy that their c.t.e. values for isotropic pyrocarbons, measured at 400 °C, are in keeping with those due to Pojur *et al* (1972).

There have been a number of studies relating to the mechanical properties of pyrocarbons. It appears that either within or outside an irradiation environment, failure of PyC layers occurs because a certain stress, rather than a total strain or total creep strain level has been exceeded (Kaae *et al*, 1972b). As a result, in general pyrocarbons may be treated as brittle materials whose fracture stress is determined by the flaws they contain. Because flaw sizes will exhibit a statistical distribution, the probability, *f*, that failure will occur when a stress σ is applied is often expressed in terms of the Weibull equation

$$f = 1 - \exp\left\{-\left(\frac{\sigma}{\sigma_0}\right)^m\right\}, \tag{7.3}$$

where σ_0 and *m* are constants whose values are determined from experiments. A more convenient representation of equation (7.3) is

$$f = 1 - \exp\left\{-\ln 2\left(\frac{\sigma}{\overline{\sigma}}\right)^m\right\} \tag{7.4}$$

where $\bar{\sigma}$ is the mean stress for failure to occur, i.e. the stress at which $f = 0.5$.

Almost without exception, fracture stress values relating to PyC coatings have been derived from bend test studies, from which elastic (or Young's) moduli may also be derived. As a result, values of both these parameters that have been derived from one particular set of measurements will be reported together.

Bokros and Price (1966) have measured values of $\bar{\sigma}$ and the elastic modulus, E, of a variety of PyC coatings that have been deposited onto discs from methane. The values they obtained for each structure are summarised in Table 7.2.

TABLE 7.2. SUMMARY OF ROOM TEMPERATURE MECHANICAL PROPERTIES OF PyCCOATINGS DEPOSITED FROM METHANE. AFTER BOKROS AND PRICE (1966).

Structure	Fracture stress MPa	Elastic modulus GPa
Laminar	310–620	31–48
Isotropic	200–380	12–19
Granular	100–140	8–9

Table 7.2 indicates that fracture stress and elastic modulus values of isotropic PyC coatings lie between the corresponding figures for laminar and granular structures. However Bokros and Price (1966) have also shown that for isotropic coatings the strain when failure occurs is relatively higher, being in the region of 2%, compared with values of about 1% for the other two structures.

Kaae (1971a) has performed bend test measurements on some isotropic coatings which had been deposited from propane at temperatures below 1600 °C. He found that as the density increased from 1.3 to 1.9 $Mg.m^{-3}$ the fracture stress rose from 340 to 520 MPa and the elastic modulus from 17 to 28 GPa. Both of these parameters tended to decrease as the value of L_c increased from 3 to 6 nm. Rather similar results have been obtained by Kaae (1971b) for coatings deposited from propane/acetylene mixtures.

Kaae *et al* (1977) have studied the mechanical properties of coatings derived from propylene. Unlike their results for coatings derived from propane, the elastic modulus was found to be independent of density, but instead was a function of the deposition rate. It fell from ~65 to 15 GPa as rates increased from 1 to 10 μm/min. One possible explanation for this trend is that samples prepared at a higher deposition rate contained a relatively higher amount of open porosity, bearing in mind that the quoted densities were derived from liquid immersion methods. In keeping with these results, Briggs *et al* (1976), by crushing particles containing PyC coats deposited from propylene at an unspecified rate, obtained a value for E of 18 GPa.

Kaae *et al*'s (1977) corresponding fracture studies obtained values for $\bar{\sigma}$ in the region of 400 MPa at deposition rates of ~1μm/min, decreasing to around 200 MPa at rates greater than ~10μm/min. Again, this decrease could be due to the presence of higher amounts of open porosity or surface flaws, since no clear trend in the values of $\bar{\sigma}$ with density was apparent. Values of m exhibited no clear correlation with either density or deposition rate, though for densities >1.85 $Mg.m^{-3}$ numbers in the region of 10 were obtained.

The above fracture stress results all suffer from one major deficiency if it is required to apply them to coated particles, namely they were derived directly from bend test measurements,

in which the high stresses causing fracture are located over a limited volume. In a coated particle fracture stresses are expected to be lower, since the volume over which the critical flaw size for failure to occur will be larger. Bongartz *et al* (1976) have addressed this problem in their brittle ring test, a technique which possesses the advantage of performing measurements on portions of PyC coatings taken from particles, unlike the above mentioned fracture stress results which were obtained from deposits on flat discs. Table 7.3 shows their results for coatings deposited from propylene in increasing order of density. In addition to values for $\overline{\sigma}$, m and E (each based on about 50 measurements), figures for the mean failure stress in a PyC particle coating, $\overline{\sigma}_p$, and the stress required to fail 1 in 10^4 coatings, $\sigma_{\text{E-04}}$, using a Weibull analysis, are shown.

TABLE 7.3.ELASTIC MODULUS AND FRACTURE STRESSES OF PROPYLENE DERIVED PYROCARBONS. AFTER BONGARTZ *ET AL* (1976).

Density	E	$\overline{\sigma}$	m	$\overline{\sigma}_p$	$\sigma_{\text{E-04}}$
Mg.m^{-3}	GPa	Mpa		MPa	MPa
1.28	11.0	180	3.3	40	2.7
1.28	15.0	260	3.7	58	5.3
1.31	15.0	300	5.1	84	15
1.36	13.0	240	4.2	62	7.5
1.45	11.5	210	3.3	50	3.4
1.73	20.8	460	7.0	190	54
1.74	26.0	490	5.6	180	37
1.95	47.0	640	5.2	220	40

It is noteworthy that in contrast with the results of Kaae *et al* (1977), values of E and $\overline{\sigma}$ in general increase with density, but cover the same range of values; also that the ratio $\overline{\sigma} / \overline{\sigma}_p$ lies between 2.4 and 4.5. Table VII.3 suggests that fracture stress values derived from bend tests cannot be used directly in assessing the stresses that PyC layers in coated particles can sustain, and also that isotropic coatings possessing as high a density as possible are desirable.

Finally, the only measurements of Poisson's ratio that appear to have been published are due to Price and Kaae (1969). They obtained values of 0.210 and 0.236 for respectively LTI and HTI coatings; these values refer to both the applied stress and resulting strain directions being in the deposition plane.

7.4. Effects of Irradiation

Fundamental to some of the changes in the physical properties of PyC during irradiation are the corresponding modifications to their structures. In particular, pyrocarbons that initially are isotropic become anisotropic. Kaae (1977) has shown that anisotropy can develop in unrestrained PyC but that, at a given neutron dose, its extent is greatly enhanced when the material is restrained. Figure 7.9 shows the increase in BAF when initially isotropic, propylene derived PyC of different initial densities is irradiated at 1400 °C to two neutron doses (Tempest, 1978)[1]. The PyC layers were deposited onto a silicon carbide coating so that, to a good approximation, the creep strain is the unrestrained dimensional change in the plane of deposition. Figure 7.9 illustrates the importance of limiting the creep strain if it is required to minimise the increase in anisotropy, and that this is best achieved by maximising the initial density.

[1] Neutron doses are quoted in the units given by the authors of papers cited. DNE stands for DIDO Nickel Equivalent dose. To convert from that scale to one expressed as neutron energies >29fJ, multiply by 1.5.

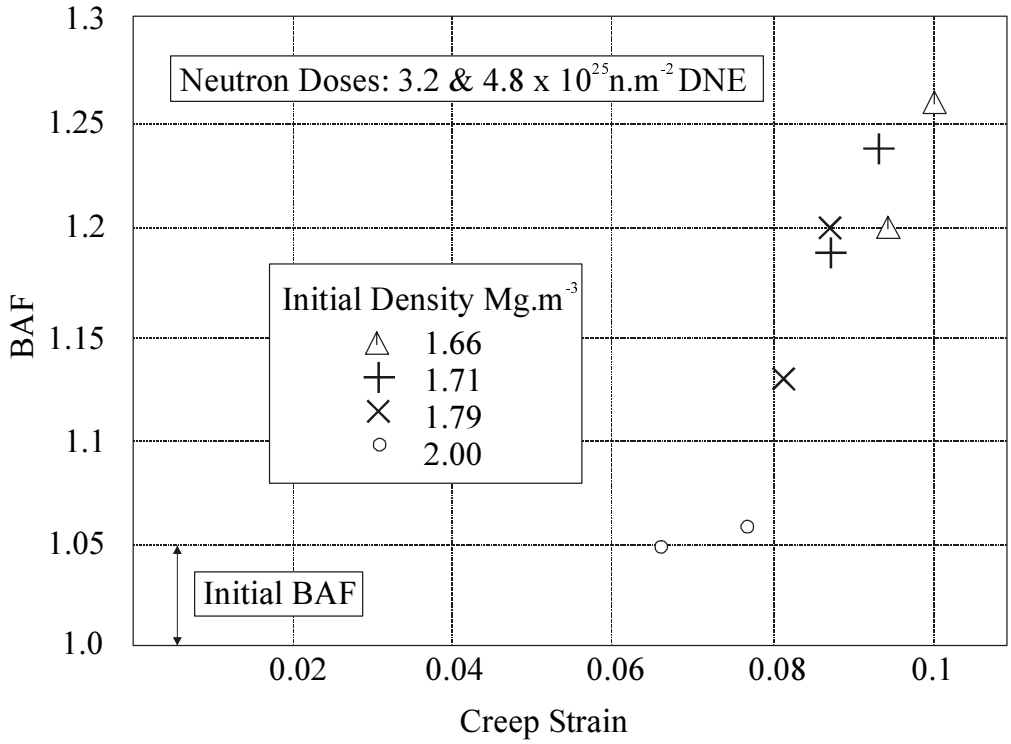

FIG. 7.9. Anisotropy changes following irradiation at two neutron doses.

The shrinkage of PyC with low initial densities has been accounted for by Kaae (1975) in terms of the elimination of irregularities in the twisted or distorted ribbons or fibres noted above. From pore size distribution measurements, Krautwasser and Nickel (1977) have identified an isotropic fibre component which acts as a buffer to the anisotropic changes in the dimensions of individual crystallites. However, too large a fibre component (presumably associated with low density material) is undesirable since its isotropic shrinkage rate is high. Again, Bokros *et al* (1966) have found that materials with L_c values that respectively are initially above or below 5 nm tend to approach this particular value during irradiation. Corresponding changes in the thermal resistivity follow a similar trend, since theoretically resistivity is believed to vary linearly with the reciprocal of the crystallite size.

Comparatively little information on the effect of irradiation on the c.t.e. has been published. The measurements by Matsuo (1988) on as-fabricated PyC reported above have included material that had been irradiated at ~1100 °C to a dose of 2.2×10^{25} n.m^{-2} (E >29 fJ). In the plane of deposition, the initial shrinkage as the temperature is raised from room temperature is now greater, while at 900 °C the fractional overall expansion is $\sim 3 \times 10^{-4}$, compared with the corresponding unirradiated value of 8×10^{-4}. By contrast, the fractional expansion at 900 °C normal to the plane of deposition had increased from 20 to 25×10^{-3}. These results suggest that the irradiation has increased the anisotropy of the material.

Yates and Pirgon (1974) have extended the studies reported above in Fig 7.8. They found that the c.t.e.'s of isotropic propylene and methane deposited pyrocarbons were the same after fabrication. However, following irradiation at 1100 °C to a dose of 1.5×10^{25} n.m^{-2} DNE, the c.t.e. of the coating from propylene had decreased by one third, suggesting that the irradiation had resulted in an increase in the anisotropy, whereas the c.t.e. of that derived from methane remained unchanged. On the other hand some methane deposited, isotropic coatings irradiated to

a dose in the region of 2×10^{25} n.m^{-2} (E > 29 fJ) exhibited c.t.e. values at 400 °C between 3.9 and 5.0×10^{-6} K^{-1} (Price and Bokros, 1967). Unfortunately the corresponding pre-irradiation values were not quoted, but since these particular figures are lower than the corresponding values shown in Fig 7.8, it would appear that the irradiation has introduced a certain amount of anisotropy.

Because of the importance in maintaining the integrity of PyC layers during the irradiation of coated particles, many studies have been performed of their dimensional changes as a function of neutron dose. In general terms, during irradiation individual crystallites will expand in the *c* and contract in the *a* direction, with their overall volume remaining nearly unchanged. However, the overall macroscopic dimensional changes will also be governed by the extent to which these microscopic changes are accommodated within the material; as a result, this will be determined, amongst other things, by the porosity and anisotropy. Some typical examples of dimensional changes as a function of neutron dose, both parallel and perpendicular to the plane of deposition, for three unrestrained pyrocarbon coatings are shown in Fig 7.10 (Kaae, 1977). Two of these, being initially isotropic, exhibit, at first, comparable dimensional changes in the two directions, but internal stresses generated within the coatings during irradiation introduce anisotropy which manifests itself in dimensional change differences. Overall, there is a greater densification in the case of the low density isotropic material, in which the higher porosity fraction is able to accommodate a correspondingly larger proportion of the crystallite *c* axis expansions. As might be expected, differences between the dimensional changes in the two directions are larger in the slightly anisotropic PyC. From the point of view of maintaining the integrity of the PyC layers of a coated particle during irradiation, it is important that shrinkage rates in the parallel direction should not be too high (Martin, 1973). As a result, Fig 7.10 suggests that isotropic coatings possessing not too low a density should be employed. Although not shown in Fig 7.10, the overall density of high density material can decrease during the course of irradiation at high neutron doses. Clearly (as a precautionary note) under these circumstances the resulting cracks and pores that are created to accommodate the crystallite strains should not be of such a nature that they affect deleteriously the layer's fission product retention capability. It should be emphasised that Fig 7.10 is a simplified summary of many dimensional change measurement changes that have been reported, and that these depend on a number of structural features relating to the material. For some specific examples see Bokros *et al* (1969), Kaae *et al* (1972a, 1972b) and Everett *et al* (1971). The low and high density isotropic material graphs shown in Fig 7.10 relate approximately to some published methane deposited PyC coatings of density 1.55 and 1.92 Mg.m^{-3} respectively, irradiated over the temperature range 880–950 °C (see Fig 2b of Bokros *et al*, 1969; Figs 2a–2c demonstrate that over the temperature range 520–1270 °C dimensional change rates increase with temperature).

Bokros and Schwartz (1967) have put forward a model to describe these dimensional changes. Essentially it consists of two components. The first represents an isotropic shrinkage, whose rate decreases monotonically with neutron dose. The second comprises an anisotropic component, whose contribution in the two principal directions are governed by the dimensional changes of the crystallites in respectively the *a* and *c* directions, together with an anisotropy factor. This part of the model is analogous to the one describing dimensional changes in graphite and discussed in Chapter 3.

Unfortunately, dimensional change measurements on unrestrained PyC are not a true indicator of the stresses that can be built up in particle coating layers because, as already shown in Fig 7.9, restraint can enhance the anisotropy, which in turn can increase shrinkage rates in the

deposition plane and hence stresses, and thereby further raise the anisotropy. Kaae (1974) interpreted some PyC layer failures on coated particles, which would not have been predicted on the basis of measured unrestrained dimensional change rates, in terms of such an enhancement in the anisotropy, and hence in the shrinkage rate in the plane of deposition.

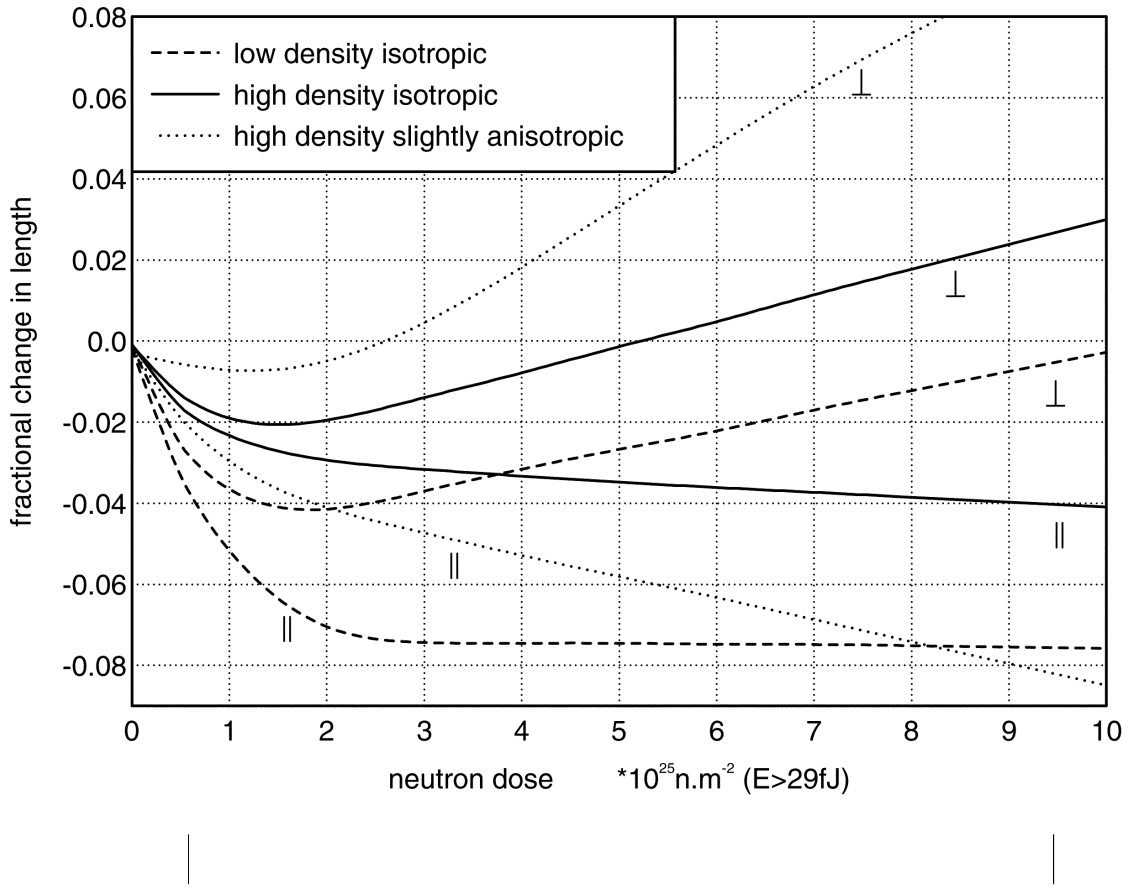

FIG. 7.10. Dimensional changes of unrestrained PyC parallel and perpendicular to the plane od deposition.

Kaae (1973,1977) has reported the change in Young's modulus of isotropic, poorly crystalline (L_c ~ 3 nm) PyC. He found that its value increased about linearly with neutron dose from ~ 20 to 60 GPa after an irradiation to 8.3×10^{25} n.m^{-2} (E > 29 fJ). This increase was independent of the irradiation temperature over the range 800–1250 °C, but was somewhat reduced at 1400 °C.

Price and Bokros (1967) have reported no significant change in the fracture stress of laminar PyC when irradiated to a dose of 2.4×10^{25} n.m^{-2} (E >29 fJ). However, comparable irradiations of isotropic and granular pyrocarbons produced increases of up to 60%; these materials were relatively crystalline, with L_c values in the region of 10 nm. By contrast, in the case of isotropic, poorly crystalline PyC (L_c ~3 nm), irradiation over the temperature range 650–1250 °C up to doses of 8.3×10^{25} n.m^{-2} (E >29 fJ) exhibited little change (Kaae, 1973). Because the as-deposited more crystalline material exhibited significantly lower strengths compared with those relating to poorly crystalline PyC, irradiation causes the fracture stresses of the two types of material to become more nearly equal to one another. Kaae (1974) has also measured the fracture stresses of irradiated pyrocarbons that had been respectively unrestrained and restrained during the course of the irradiation and shown that there are no significant differences between the two.

If the fracture stress of PyC obeys the Weibull relation (equations (7.3) or (7.4)), we would expect that, for a given structure, the PyC failure fraction of a batch of particles would increase the larger the coating radius. Irradiations of batches of dummy particles with different radii to a dose of 5.5×10^{25} n.m^{-2} (E >29 fJ) by Bullock (1981) have confirmed this and shown that, within the experimental uncertainty, failure fractions were in accord with the Weibull relationship.

A number of estimates has been made of the irradiation creep constant of PyC - a figure which is as important as dimensional change rate values in determining coating stresses, but which has received comparatively less attention. These all assume that the creep, ε, is given by

$$\varepsilon = K.\sigma.\Gamma \tag{7.5}$$

where K is the creep constant, σ the applied stress (assumed constant over the course of the irradiation) and Γ the neutron dose.

Estimates of the creep constant have been made by Price and Bokros (1967) and Kaae *et al* (1972b). They were obtained using measurements of flexure strengths, dimensional change rates and observations of whether or not specific restrained layers had failed during irradiation. Values of respectively 0.9 and 0.7×10^{-7} [psi. 10^{20} n.cm^{-2} (E > 29f J)]$^{-1}$ were quoted, which may be converted to 2.0 and 1.5×10^{-29} [MPa. n.m^{-2} (DNE)]$^{-1}$.

A not dissimilar analysis was performed by Buckley *et al* (1975). Stresses in the PyC layers of coated particles that had been observed to remain intact after irradiation were calculated, using appropriate known input data and a variety of postulated values for the creep constant. Since, throughout the lifetime of the particle, the known fracture stress had not been exceeded, a minimum value for the creep constant of 5×10^{-29} [MPa. n.m^{-2} (DNE)]$^{-1}$ was deduced, but with the proviso that a figure of 7.4×10^{-29} [MPa. n.m^{-2} (DNE)]$^{-1}$ could be a more realistic lower limit.

Three direct measurements of the creep constant of PyC have been reported. Morgand (1975) subjected massive samples (30×1×~5 mm) to uniaxial stresses in the range 13–20 MPa to a maximum dose of 1.6×10^{25} n.m^{-2} (DNE). A creep constant of 2×10^{-28} [MPa. n.m^{-2} (DNE)]$^{-1}$ was derived, a value appreciably higher than the above estimates or the other experimental figures reported below. Although this methane derived PyC was observed to possess structures that were similar to those found on coated particles, it should be noted that it was deposited in a rotating furnace rather than a fluidised bed. Perhaps more significantly, the samples exhibited a variation in density over their thickness and possessed a stratified structure. As a result, it is not impossible that these structural irregularities may enhance the creep above the values that would have been obtained, had the structure been more uniform, and so more similar to the layers on coated particles.

Buckley *et al* (1975) employed a high voltage electron microscope as the irradiation source to measure the creep of PyC at about 1000 °C. Split ring samples were prepared from coated particles and stressed by fitting them onto appropriately oversized copper spindles. Strains were assessed from measurements of the gap size at the split. After irradiation the spindle was dissolved and the gap size re-measured. The creep strain was found to be about 1.2 elastic deflections (as measured before irradiation) per 10^{24} n.m^{-2} (DNE). The derivation of K from this experiment, using equation (7.5), requires also a knowledge of the unirradiated elastic modulus,

a value which is unknown for this sample. As shown in Section 7.3, this can be rather variable; however, if we assume as a reasonable mean value that E = 20 GPa, a figure for K of 6×10^{-29} [MPa. n.m^{-2} (DNE)]$^{-1}$ is obtained (its value scaling inversely with the value assumed for the elastic constant). (Note however that, given the scatter in the published experimental results, this figure could be up to a factor of two lower if a small contribution due to primary creep were assumed.)

Brocklehurst and Gilchrist (1976) have measured the creep of PyC discs under a constant stress during reactor irradiation. The discs were supported around their rims and a dead weight applied at the centres. Deflections were measured before and after irradiations at 1000 °C up to a dose of 4×10^{24} n.m^{-2} (DNE). Isotropic PyC discs derived from propylene of density 1.64 and 1.95 Mg.m^{-3} were studied and creep rates of respectively 1.0 and 0.5 elastic deflections per 10^{24} n.m^{-2} (DNE) obtained. If, as before, we assume a figure of 20 GPa for the elastic modulus, then the corresponding creep constant values of 5 and 2.5×10^{-29} [MPa. n.m^{-2} (DNE)]$^{-1}$ are obtained. It is difficult to compare these figures with the K value obtained from the electron microscope irradiations because Buckley *et al* (1975) did not provide any specifications of their samples. In addition, it should be noted that because Brocklehurst and Gilchrist (1976) found that the elastic moduli of their higher density specimens were somewhat larger than that of the lower density materials, the difference between the two K values quoted above will be greater than a factor of two.

Very little appears to have been published on Poisson's ratio during creep. Buckley *et al* (1975) quote a value of 0.4, based on some unpublished work at Harwell by K.S.B. Rose and J. Williams.

It is generally assumed that, at irradiation temperatures considered here, thermal creep is negligible compared with the irradiation creep contribution. This is in keeping with measurements of creep during irradiation by Buckley *et al* (1975), who found that it was proportional to the irradiation dose, in accordance with equation (7.5), but independent of the dose rate.

7.5. Pyrocarbon alloys

So far the present chapter has been devoted entirely to PyC and its use as a coating material for the spherical fuel particles that are employed in an HTR. However, mention should be made of work on the development of two-phase mixtures of PyC and SiC, which can be deposited simultaneously under appropriate conditions in a fluidised bed. The hope was that such so-called alloys would exhibit a superior irradiation performance over, and therefore replace, the conventional PyC layers of coated particles. A useful review of this topic, together with numerous references to earlier work, has been provided by Bullock (1983). A brief summary of its findings is presented here.

Initial work suggested that these alloys possessed certain attractive features over PyC. For example, fission product diffusion coefficient values were relatively lower, radiation induced dimensional changes were also lower, and therefore more readily controlled, and the layers were stronger. On the other hand, the elastic modulus was higher, and it was not clear whether, for a given elastic strain, the enhanced stress was more than counterbalanced by its increased strength. Unfortunately, a more extensive irradiation programme did not indicate a significantly improved irradiation performance of alloyed particles, in terms of the fraction which had failed, compared

with those possessing conventional PyC coatings. This is believed to be due to the lower creep constant of the alloy layers which, to a first approximation, counterbalances the benefits of reduced dimensional changes. Again, it was found that the rate at which fission products diffuse through alloy coatings increases with fission product concentration, with the result that at high burnups the fission product retention ability of alloy material is not markedly different from that of PyC coatings. The one positive conclusion is that alloy coatings could be usefully employed in BISO particles containing fertile fuel for which the burnup is more limited compared with particles containing fissile fuel. This is because, given the comparatively lower concentration of fission products (in particular caesium), their rates of diffusion at a specific temperature will be significantly lower compared with those through a pure PyC layer. It should also be noted that BISO particles with alloy coatings can be reprocessed and the bred fuel separated.

7.6. Discussion and conclusions

This chapter has demonstrated, not only the great diversity of PyC structures that can be produced, but also that this variety is still considerable when one's attention is limited to approximately isotropic pyrocarbons that have been deposited in a fluidised bed. As a result, materials with a wide range of physical properties can be produced. From the point of view of depositing PyC layers onto coated particles so that they behave satisfactorily under irradiation, this is advantageous, since it means that the properties of these layers can be controlled, and hence optimised. However, because of the wide range of variables available in the coating process, a certain amount of trial and error over the deposition procedures will be required in order to achieve this optimisation. Also, careful quality control in the manufacturing process is required if many, reproducible batches of particles with acceptable low failure fractions are to be achieved.

As far as the various properties of PyC are concerned, it appears that the most important, from the point of view of particle endurance during irradiation, are the c.t.e., the irradiation creep constant and dimensional changes during irradiation. Comparatively little information on the first two of these properties is available, e.g. how they vary with density, anisotropy and direction. Another issue over which insufficient data are available is how the anisotropy of coatings changes with restraining stresses. For example, the effect of the as-deposited density and anisotropy on such changes is not known sufficiently. Thus, even though a significant literature exists on dimensional changes, most of it relates to unrestrained material, so that its application to PyC layers in TRISO particles is more problematical. Clearly the situation is even less satisfactory as far as the c.t.e. and irradiation creep constant are concerned.

It will be apparent, from the cited literature, that very little work relating to the properties of PyC that is relevant to the HTR reactor system has been performed in the last one or two decades. This is due, first to the waning interest in the HTR system, starting around the late 1970's, and secondly to the widespread perception that, at least during normal reactor operation, mechanical failure of particles due to the internal buildup of gas pressure is not a problem. As a result, more recent work has concentrated on the failure of particles during the course of accidents, due to gas pressure induced failures and various forms of chemical attack, together with the distribution of released fission products throughout the reactor (Verfondern, 1997). It is perhaps noteworthy that this particular reference, which is a large compendium of a world wide IAEA co-ordinated research programme on HTR fuel performance, makes hardly any reference to PyC. However two observations on this current state of affairs would appear to be relevant. Firstly, some of the stress models used to predict whether or not particles will fail during a specific accident scenario ignore entirely the effect of the PyC coatings on particle endurance;

however, they will certainly play a part due to differential PyC-SiC expansion effects as the temperature is raised, with perhaps some stress changes occurring due to thermal creep at extremely high temperatures. Secondly, with the renewed interest in a number of countries in the HTR reactor system, particle endurance considerations during normal operation are likely to become of greater concern compared with that at present. This is because any commercialisation of the HTR will inevitably lead, on economic grounds, to a desire to improve the irradiation performance of fuel particles. Such a requirement is highly likely to lead to a realisation that our current understanding and knowledge of PyC coatings and their behaviour during irradiation are inadequate, along the lines indicated above; this would then lead to a new programme of work to address these deficiencies.

REFERENCES

[7.1] ALLEN P.L., FORD L.H. and SHENNAN J.V. Nuclear Technology, **35**, 246 (1977).
[7.2] BARD R.J., BAXMAN H.R., BERTINO J.P. and O'ROURKE J.A. Carbon, **6**, 603 (1968).
[7.3] BEATTY R.L. USAEC Report ORNL-TM-1649 (1967).
[7.4] BOKROS J.C. Carbon, **3**, 17 (1965).
[7.5] BOKROS J.C. and PRICE R.J. Carbon, **3**, 503 (1966).
[7.6] BOKROS J.C., PRICE R.J. and KOYAMA K. Carbon, **4**, 293 (1966).
[7.7] BOKROS J.C. and SCHWARTZ A.S. Carbon, **5**, 481 (1967).
[7.8] BOKROS J.C. Chemistry and Physics of Carbon, **5** (Ed. P.L. Walker, Jr.), Marcel Dekker, New York, 1 (1969).
[7.9] BOKROS J.C., GUTHRIE G.L., DUNLAP R.W. and SCHWARTZ A.S. J. Nucl. Mater., **31**, 5 (1969).
[7.10] BONGARTZ K., GYARMATI E., SCHUSTER H. and TAÜBER K. J. Nucl. Mater., **62**, 123 (1976).
[7.11] BRIGGS A., DAVIDGE R.W., PADGETT C. and Quickenden S. J. Nucl. Mater., **61**, 233 (1976).
[7.12] BROCKLEHURST J.E. and GILCHRIST K.E. J. Nucl. Mater., **59**, 7 (1976).
[7.13] BUCKLEY S.N., MANTHORPE S.A. and Martin D.G. Ext. Abstr. 12th Conf. Carbon, p311 (1975).
[7.14] BULLOCK R.E. Carbon, **19**, 255 (1981).
[7.15] BULLOCK R.E. J. Nucl. Mater., **113**, 81 (1983).
[7.16] EVANS A.G., PADGETT C. and DAVIDGE R.W. J. Am. Ceram. Soc., **56**, 36 (1973).
[7.17] EVERETT M.R., GRAHAM L.W., MANZEL R. and BLACKSTONE R. Carbon, **9**, 417 (1971).
[7.18] FORD L.H., HIBBERT N.S. and MARTIN D.G. J. Nucl. Mater., **45**, 139 (1972/3).
[7.19] FORD L.H. and BILSBY C.F. J. Nucl. Mater., **60**, 79 (1976).
[7.20] HUSCHKA H. and VYGEN P. Nuclear Technology, **35**, 238 (1977).
[7.21] KAAE J.L. J. Nucl. Mater., **38**, 42 (1971a).
[7.22] KAAE J.L. Carbon, **9**, 291 (1971b).
[7.23] KAAE J.L., Stevens D.W. and Bokros J.C. Carbon, **10**, 561 (1972a).
[7.24] KAAE J.L., Bokros J.C. and Stevens D.W. Carbon, **10**, 571 (1972b).
[7.25] KAAE J.L. J. Nucl. Mater., **46**, 121 (1973).
[7.26] KAAE J.L. Carbon, **12**, 577 (1974).
[7.27] KAAE J.L. J. Nucl. Mater., **57**, 82 (1975).
[7.28] KAAE J.L. Nuclear Technology, **35**, 359 (1977).

[7.29] KAAE J.L., Bullock R.E., Scott C.B. and Harmon D.P. Nuclear Technology, **35**, 368 (1977).
[7.30] KAAE J.L. Carbon, **23**, 665 (1985).
[7.31] KELLY B.T. Physics of Graphite, Applied Science Publishers, London (1981).
[7.32] KOBAYASHI F., IKAWA K., IWAMOTO K. Carbon, **10**, 647 (1972).
[7.33] KOBAYASHI F., IKAWA K., IWAMOTO K. Carbon, **12**, 87 (1974).
[7.34] KRAUTWASSER P. and NICKEL H. Ext. Abstr. 12th Conf. Carbon, p155 (1975).
[7.35] KRAUTWASSER P. and NICKEL H. Nuclear Technology, **35**, 310 (1977).
[7.36] LACKEY W.J., STINTON D.P. and SEASE J.D. Nuclear Technology, **35**, 227 (1977).
[7.37] LEFEVRE R.L.R. and PRICE M.S.T. Nuclear Technology, **35**, 263 (1977).
[7.38] LINKE J., KOIZLIK K. and NICKEL H. Nuclear Technology, **35**, 257 (1977).
[7.39] MARTIN D.G. J. Nucl. Mater., **48**, 35 (1973).
[7.40] MARTIN D.G. 3rd Int. Conf. on Structural Mechanics in Reactor Technology, London, U.K., Paper C1/4 (1975).
[7.41] MATSUO H. High Temperatures High Pressures, **20**, 579 (1988).
[7.42] MORGAND P. J. Nucl. Mater., **58**, 47 (1975).
[7.43] PELLEGRINI G. Carbon, **10**, 487 (1972).
[7.44] PLUCHERY M. THESIS, University of Grenoble (1973).
[7.45] POJUR A.F., YATES B. and KELLY B.T. J. Phys. D: Appl. Phys., **5**, 1321 (1972).
[7.46] POLLMANN E., PELISSIER J., YUST C.S. and KAAE J.L. Nuclear Technology, **35**, 301 (1977).
[7.47] PRICE R.J. and BOKROS J.C. J. Nucl. Mater., **21**, 158 (1967).
[7.48] PRICE R.J., BOKROS J.C. and KOYAMA K. Carbon, **5**, 423 (1967).
[7.49] PRICE R.J. and KAAE J.L. Carbon, **7**, 706 (1969).
[7.50] PRICE M.S.T. and SHEPHERD L.R. Physics in Technology, **10**, 110 (1979).
[7.51] STANSFIELD O.M. Energy, **16**, 33 (1991).
[7.52] STEVENS D.W. Ext. Abstr. 12th Conf. Carbon, p111 (1975).
[7.53] TEMPEST P.A. Carbon, **16**, 171 (1978).
[7.54] VERFONDERN K (ED). Forschungszentrum Jülich Internal Report FZJ-ISR-IB-3/97 (1997).
[7.55] YATES B. and PIRGON O. UKAEA publication, TRG Report 2537 (1974).

APPENDIX 1

RADIOLYTIC OXIDATION IN GRAPHITE

Outline of gas-phase processes

The oxidation of graphite in radiolysed CO_2-based gas mixtures proceeds by a fundamentally different mechanism from thermal oxidation, and an understanding of the oxidation process requires some insight into the chemistry occurring in the gas phase. This section reviews the effect of irradiation on CO_2 and considers the effects of other species - CO, CH_4 and H_2O, maintained in the coolant of Magnox and AGR reactors.

Gaseous CO_2 is apparently stable under radiolysis, except at very high dose rates. Studies of isotope exchange between CO and CO_2 in gas mixtures, however, show clearly that this apparent stability is in fact the result of a dynamic process of decomposition and recombination; ionising radiation forms ion pairs in CO_2 which quickly interact to reform stable CO_2. The rate of formation of species under radiolysis is usually defined by the so-called G-value, the number of species produced per 100 eV of energy deposited. The G-value may vary with the nature of the radiation because the density of the ionisation produced can vary the probability of the fast recombination of the ion pairs. Values observed by various investigators are shown in Table AI.1, and vary between about 1 and 3. As noted by Wright and illustrated in Fig A1.1, the G-values bear a monotonic relation to the particle velocities.

TABLE AI.1 *G*-VALUES FOR VARIOUS IRRADIATING PARTICLES IN CO_2

Particle	*G* (ion pair)	Ref.
Electrons 18 keV	3.05	Jesse and Sadauskis (1955)
67 keV	3.04	
Protons 1.83 MeV	2.91	Larson (1958)
α-particles (Po^{210})	2.94	Widder and Huber (1958)
Recoil ions Th C 117 keV	0.98	Stone and Cochran (1957)
Th C 168 keV	1.01	
C^{13} 1.64-2.92 MeV	2.38	Leake (1967)
O^{16} and C^{12} 0.1-1.5 MeV	1.47-2.56	
O^{16} 30 keV	1.45	Boring and Woods (1968)
40 keV	1.52	
50 keV	1.58	

This variation is not a significant difficulty in interpreting data from AGR or Magnox reactors, because in each case the energy deposition is largely due to energetic photons, with a rather smaller component from neutron scattering.

The situation is, however, complicated by the fact that most of the oxidation in graphite is due to species activated in the open porosity; and in order to estimate the number of active species produced it is necessary to estimate the rate of energy deposition in the pores of the graphite. Whilst the rate of energy deposition may be straightforwardly estimated by calorimetry, the values thus obtained are not necessarily those appropriate to the graphite pores.

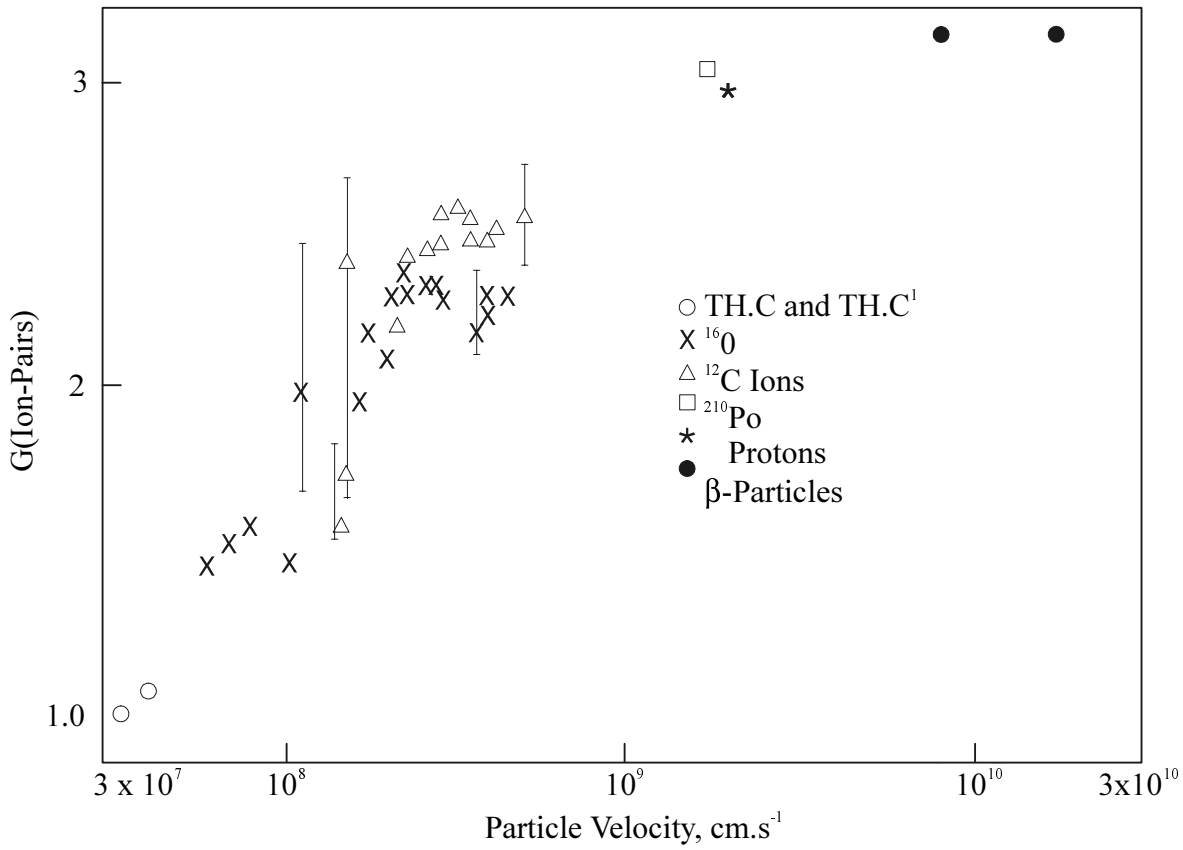

FIG. A1.1. Variation in ion-pair yield in CO_2 with particle velocity.

Given that a significant amount of the radiation yield is likely to be cause by secondary particles, if the volume of the pore is sufficiently small to allow some of the secondary particles to leave the pore unstopped the G-value will be modified. However, Linacre *et al* (1965) have concluded that for the spectrum of gamma energies found in reactors the pore sizes are large compared with the range of secondary particles, and that the gamma dose rates are close to those predicted by calorimetry. However, Wright has pointed out that for neutrons with energies up to 2 MeV this is not necessarily true for the recoil ions produced by neutron scattering. Nevertheless practical experience strongly suggests that taking the dose rate determined by calorimetry and using a G-value of 3 describes radiolysis of CO_2 in graphite pores satisfactorily.

The exact nature of the active species responsible for graphite oxidation has been extensively studied, but no firm conclusions have yet been reached. Most recent workers consider charged particles to be responsible rather than neutral species, but these ions could be more complex than the direct products of irradiation.

Mass spectrometer studies at the University of Liverpool, reported by Wood (1982), appear to indicate that clustered positive ions of the form $[CO_2]^+_n$ are the primary oxidising species. These experiments also produced data on the effect of CO, which have been interpreted by Wickham *et al* (1977) to indicate the successive replacement of CO_2 units in the ionic clusters by CO. Similarly, in the presence of small amounts of water replacement by H_2O is possible (Wickham, 1979). Thermodynamic studies reported by Wickham and Headley (1983) strongly suggest that over most of the temperature ranges encountered in Magnox and AGR stations, the dominant positively charged species should be $[CO_2]^+_2$. However, the effect of CO

on this species should be to produce $[CO]^{+}_{2}$, which is not capable of oxidising graphite. Similar difficulties are encountered if one considers the trimer $[CO_2]^{+}_{3}$. There is therefore some doubt as to the efficacy of positive ions in the graphite oxidation process.

The negative ion chemistry leads primarily to the formation of the CO_3^- ion. Whilst there has been some debate on whether the rate of reaction between this ion and CO is sufficiently fast to account for the observed inhibition by CO, recent studies on the range of active species have gone some way to resurrecting the possibility. Experimental data on negative ion clusters is poor, but estimates indicate that CO_3^- is likely to be important under most reactor conditions, although some doubt has been cast on this conclusion by Kummler *et al* (1977).

In the presence of methane the chemistry occurring in the gas-phase is considerably more complex, and the reader is referred to a paper by Norfolk *et al* (1983) for a fuller description than is possible or appropriate here. Essentially, however, CH_4 molecules react with activated CO_2 species, resulting in deactivation of the CO_2, with formation of radicals and ions from the CH_4, which may react with each other or with CO_2 or CO to form more complex organic species. Some of the reaction products migrate to, and interact with, the walls of the graphite pore.

The implications of gas-phase chemistry for graphite oxidation

As noted above, the nature of the oxidising species is still a matter of some debate, but whatever its nature it may suffer one of three possible fates:

(i) It may be deactivated by collision with CO_2 in the gas-phase.

(ii) It may be deactivated by collision with CO or CH_4 (or perhaps by collision with some other hydrocarbon species formed radiolytically from CH_4).

(iii) It may reach the pore walls and gasify a carbon atom, producing CO.

Graphite oxidation rates are therefore determined not only by the number of active species produced, but also by the distance they diffuse without being deactivated and hence the probability that they will reach the graphite surface. Johnson (1981) quotes an expression for mean diffusion length for the active species in terms of the diffusion coefficient, D, and the CO and CH_4 concentrations, $[CO]$ and $[CH_4]$:

$$L = \left\{ \frac{\Delta}{k_1[CO] + k_2[CH_4]} \right\}^{\frac{1}{2}} \qquad \text{(A1.1)}$$

Experimental evidence suggests that the effectiveness of CH_4 as a gas-phase inhibitor is some 10 times greater than that of CO for equal concentrations. These mechanisms for deactivating activated CO_2 species will reduce the rate of carbon gasification substantially below that expected in pure CO_2, and give rise to what is generally termed ‘gas-phase inhibition’.

As noted above, some of the products of CH_4 radiolysis may migrate to the surface of the pore wall. These species act to reduce the rate of graphite oxidation, although the mechanism is unclear. There are two main possibilities: either they act by blocking the access of oxidising

species to active sites on the graphite surface, thus preventing carbon gasification; or they form a sacrificial layer on the graphite surface which is oxidised preferentially, thus preserving the carbon substrate.

The rate of radiolytic oxidation of a graphite specimen will therefore be affected by the number of active species produced in the gas-phase, the fraction of these species reaching the graphite surface and gasifying carbon atoms, and the effects of surface protection mechanisms. The distance travelled by the active species before being deactivated by collision in the gas-phase is small; this means that the vast majority of the radiolytic oxidation occurs in-pore, as almost all the active species produced in the bulk gas are deactivated before reaching the graphite surface, and only the production of active species within the graphite porosity need be considered. The porous structure of the graphite will therefore be an important determinant of the oxidation rate. The relationship between porous structure and oxidation rate is complex, and is best approached by considering first the situation where all inhibition of the oxidation reaction takes place in the gas phase, and then extending the treatment to the situation where surface inhibition is also significant.

Gas-phase inhibition only

Consider the effects of porous structure in the situation where only gas-phase inhibition occurs. The rate of oxidation will be related to the number of active species reaching the pore wall. This will be dependent on the number of species produced, and hence the open pore volume of the graphite. Furthermore the rate will be affected by the fraction of these species reaching the graphite surface; this will depend upon the mean distance active species must travel to reach the walls of the pore and hence upon the pore dimensions.

In a situation where the fraction of the active species reaching the pore wall is almost the same throughout the porosity, as will be the case in pure CO_2, or CO_2 containing only very small amounts of CO, the rate of oxidation should be proportional to the open pore volume. Standring and Ashton (1965) quote oxidation rates at low weight loss for a number of graphites in CO_2 as a function of initial open pore volume. Fig A1.2 shows these rates normalised to that for PGA graphite, the material used to fabricate the cores of UK Magnox power stations; the relationship is clearly linear.

Taking this as a starting point, and assuming that radiolytic oxidation occurs uniformly throughout the porous structure, the initial rate of radiolytic oxidation can be expressed as

$$R_0 = k\varepsilon_0 G \qquad \text{(A1.2)}$$

where R_0 is the initial oxidation rate per unit dose, k a constant, and ε_0 the initial open pore volume. G is the effective G-value for production of oxidising species, that is the true G-value modified to allow for the fraction of species reaching the surface. To extend this expression to cover situations where the porous structure of the graphite has been modified by oxidation, it is necessary to account for two effects: the enlargement of open porosity by the oxidation process, and the accessing of initially closed porosity by oxidation. It is straightforward to determine the increase in open pore volume from the crystal density of graphite and the weight loss. Standring and Ashton investigated the change in closed porosity associated with oxidation; their data are consistent with a model where about 40% of the initially closed porosity is opened up at very

low weight losses and the remainder hardly at all, at least up to weight losses of 30%. This leads to a model for the evolution of porosity which can be expressed as

$$\varepsilon = \varepsilon_e + \alpha W \qquad \text{(A1.3)}$$

In this expression ε is the instantaneous open pore volume, α a constant and W the weight loss. The initial opening of closed porosity is accounted for by using an effective value for initial open pore volume, ε_e , rather than the true value, ε_0.

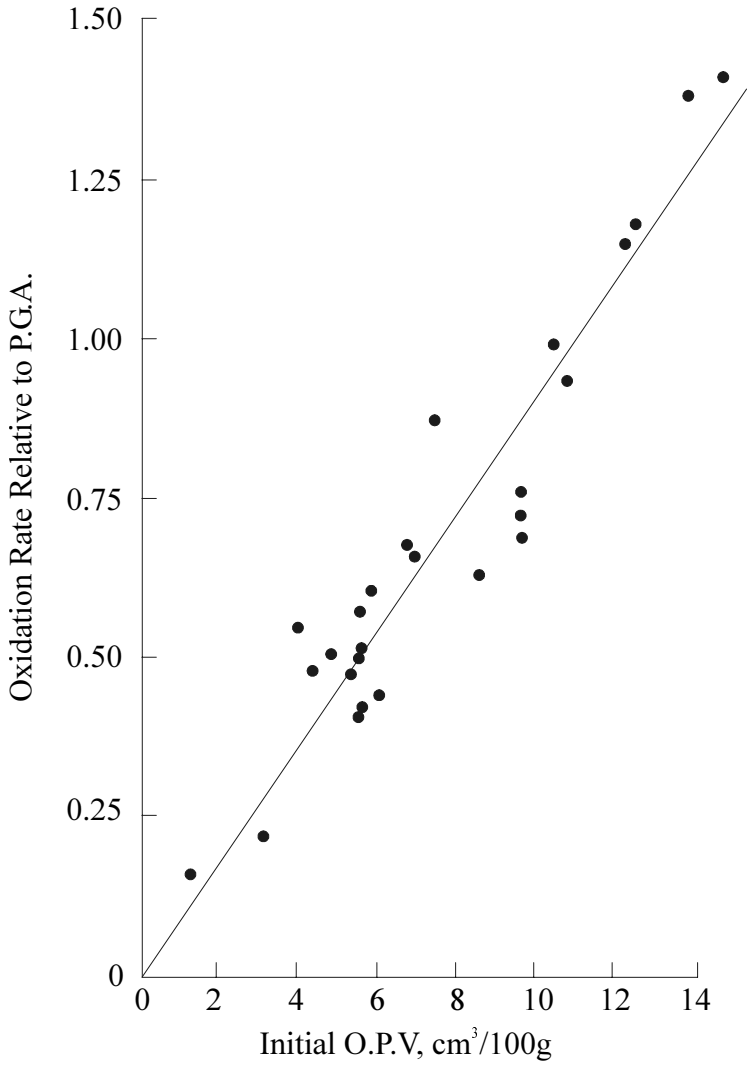

FIG. A1.2. Oxidation rate of graphites relative to PGA as a function of open pore volume.

Using these two expressions, Standring (1966) demonstrates that the weight loss, W, at any dose, D, is given by

$$W = \frac{\varepsilon_e}{\alpha}\left[\exp\left(\frac{\alpha R_0 D}{\varepsilon_e}\right) - 1\right] \qquad \text{(A1.4)}$$

Whilst this expression is effective for calculating weight loss as a function of dose at modest weight losses in the presence of small concentrations of relatively weak gas-phase inhibitors like CO, it suffers from the manifest shortcomings that the weight loss is not constrained to a maximum value of 100%, and that the rate of oxidation will increase indefinitely with weight loss. These difficulties are the result of the implicit assumption that the effective G-value does not vary with weight loss. In reality this cannot be so, as the increase in pore size will result in a smaller fraction of the active species reaching the surface of the graphite and hence a decreasing G-value. In the presence of more effective gas-phase inhibition this effect becomes important at weight losses of technological significance.

Graphite inhibition allowing for pore growth and surface inhibition

In an attempt to overcome the deficiencies described above, and also to account for the presence of surface inhibition by methane, the following empirical expressions, quoted by *inter alia* Kelly (1985) and based loosely on the Standring equation, have been widely used to calculate the rate of graphite oxidation in $CO_2/CO/CH_4$ gas mixtures:

$$W = d_1\left(\frac{dx}{dD}\right)_0\left[\exp\left(\frac{D}{d_1}\right) - 1\right] \qquad \text{for } D \le 1.1d_1$$

$$W = d_1\left(\frac{dx}{dD}\right)_0\left[3\left(\frac{D}{d_1}\right) - 1.296\right] \qquad \text{for } D \ge 1.1d_1 \qquad \text{(A1.5)}$$

where $(dx/dD)_0$ is the initial rate of graphite oxidation for the gas composition of interest, interpolated from the curves in Fig A1.3, and d_1 is a constant. The agreement of these equations with weight loss data obtained in MTR experiments is shown in Fig A1.4. It should be noted that the gas composition used to determine $(dx/dD)_0$ is not that in the bulk gas but that in the graphite porosity. This will differ from that in the bulk, as CO is generated by the oxidation process and methane destroyed by radiolysis.

As described above there are two possible mechanisms for surface inhibition: blocking access to active sites, or the formation of a sacrificial layer. The second of these two mechanisms has been modelled in some detail by Johnson (1981). If the number of oxidising species reaching the wall of a pore in unit time is J_{ox} then

$$J_{ox} = \xi\left(\frac{x}{L}\right)N_p \qquad \text{(A1.6)}$$

where N_p is the number of species produced in the pore in unit time, and $\xi(x/L)$ the probability that an oxidising species with mean diffusion length L will reach the wall of a pore with characteristic dimension x. The flux of depositing species, J_d, is given by

$$J_d = \left\{1 - \xi\left(\frac{x}{L}\right)\right\} N_p \left\{\frac{k_2[CH_4]}{k_1[CO] + k_2[CH_4]}\right\} \tag{A1.7}$$

where the term in the last set of braces represents f, the fraction of active species in the gas-phase deactivated by collision with methane. It is therefore straightforward to show that the net flux of oxidising species, J, is given by

$$J = N_p \left\{\xi\left(\frac{x}{L}\right) - \left[1 - \xi\left(\frac{x}{L}\right)\right]\right\} f \tag{A1.8}$$

It is clear from the model that, given that the value of the function $\xi(x/L)$ decreases with increasing x, there exists a pore with characteristic dimension x_t where the flux of oxidising species equals that of depositing species; that is

$$\xi\left(\frac{x_t}{L}\right)\{1 + f\} = f \tag{A1.9}$$

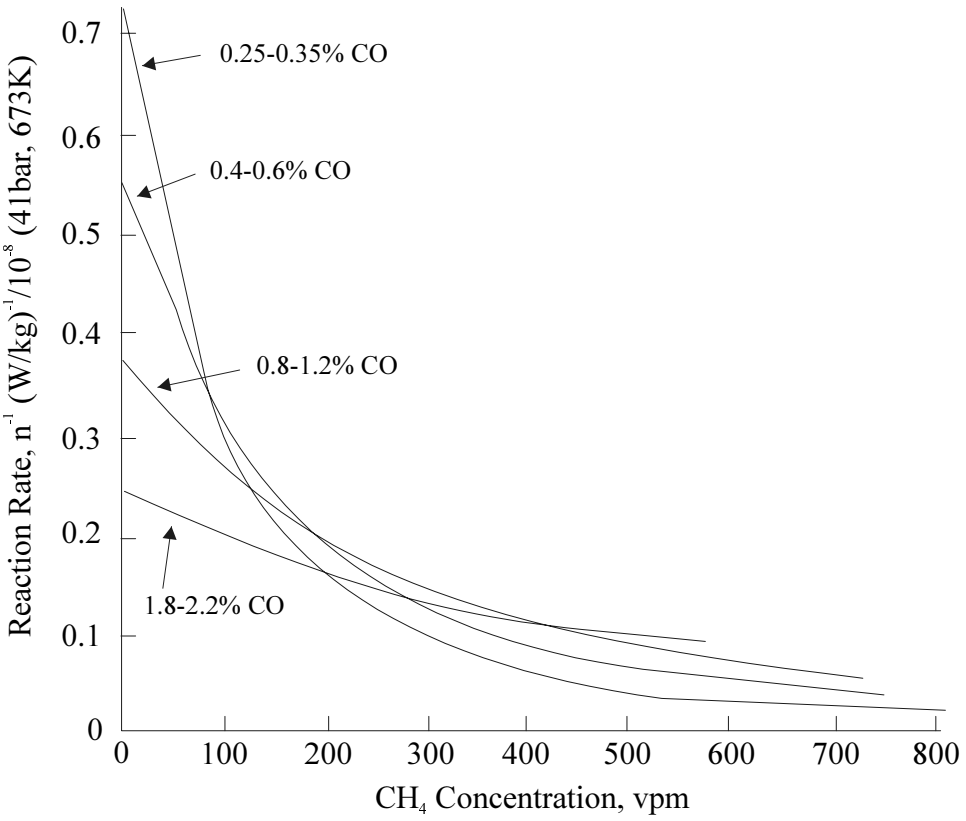

FIG. A1.3. Initial oxidation rates of moderator graphite in coolant gases of different composition.

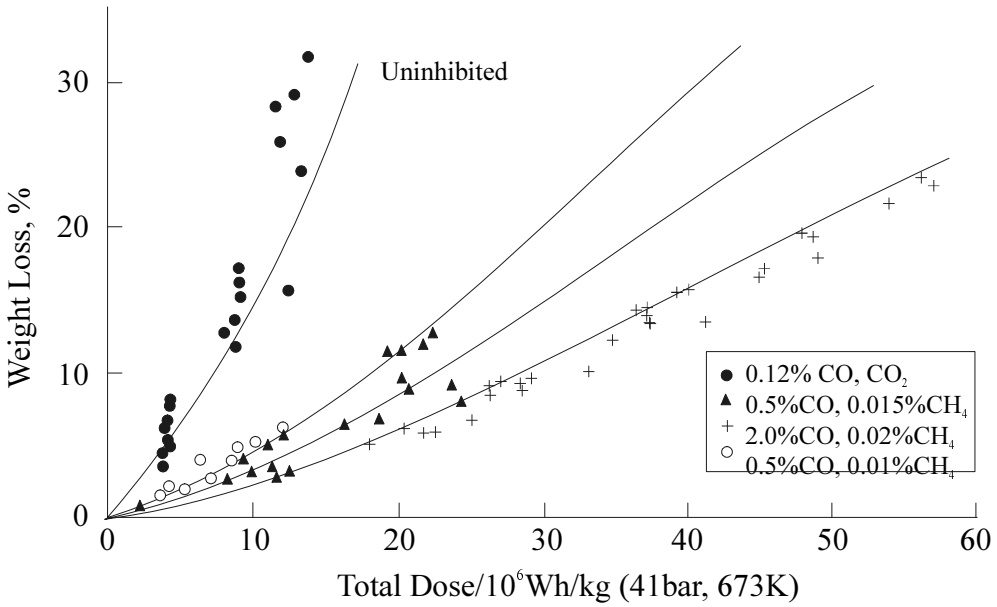

FIG. A1.4. Moderator weight loss against dose in different coolants.

Pores larger than x_t are net depositing and will shrink, pores smaller than this are net oxidising and will grow. In principle therefore, given the pore size distribution for the graphite, it is possible to calculate the weight loss by integrating the oxidising flux over the pores in the size range $x = 0$ to x_t. In practice there are a number of difficulties with this approach, not least of which is defining the shape of the pores, upon which the form of the function $\xi(x/L)$ depends. The theory has, however, been worked rigorously for pores in the form of cylinders, spheres and infinite slabs. This gives the following expressions, where the characteristic dimension x is the half-width of a slab pore, and the radius of a cylindrical or spherical pore, and I_0 and I_1 are zero and first order Bessel functions:

$$\text{Slab - shaped pore:} \quad \xi\left(\frac{x}{L}\right) = \frac{L}{x}\tanh\left(\frac{x}{L}\right)$$

$$\text{Cylindrical pore:} \quad \xi\left(\frac{x}{L}\right) = \frac{2L}{x}\frac{I_1(x/L)}{I_0(x/L)} \qquad \text{(A1.10)}$$

$$\text{Spherical pore:} \quad \xi\left(\frac{x}{L}\right) = \frac{3L}{x}\left[\coth\left(\frac{x}{L}\right) - \frac{L}{x}\right]$$

REFERENCES TO APPENDIX 1

BORING, J.W. AND WOODS, F.R. (1968), *Radiat. Res*., **35**, 472.
JESSE W.P. AND SADAUSKIS J. (1955), *Phys. Rev*., **97**, 1668.
JOHNSON, P.A.V. (1981), *J. Nucl. Energy*, **20**, 231.
KELLY, B.T. (1985), *Prog. Nucl. En*., **16**, 73.
KUMMLER R., LEFFERT C., IM K., PICIRELLI R., KEVAN L. AND WILLIS C. J. (1977), *Chem. Phys*., **81**, 2451.
LARSON, H.V. (1958), *Phys. Rev*., **112**, 1927.
LEAKE, J.W. (1967), *UKAEA Report* AERE-R-5130.
LINACRE, J.K., TAYLOR, N.K. AND THOMAS, R.B. (1965), *UKAEA Report* AERE-R-4806.
NORFOLK D.J., SKINNER R.F. AND WILLIAMS W.J. *Radiat. Phys. Chem*., **21(3)**, 307 (1983).
STANDRING, J. (1966), *J. Nucl. Energy*, **20**, 201.
STANDRING, J. AND ASHTON, B.W. (1965), *Carbon*, **3**, 157.
STONE, W.G. AND COCHRAN, L.W. (1957), *Phys. Rev*., **107**, 702.
WICKHAM, A.J., BEST, J.V. AND WOOD, C.J. (1977), *Radiat. Phys. Chem*., **10**, 107.
WICKHAM, A.J. (1979), *Chem. Br*., **15**, 286.
WICKHAM, A.J. AND HEADLEY, J.V. (1983), CEGB Report TRRD/B/0247/N83.
WIDDER, F. AND HUBER, P. (1958), *Helv. Phys. Acta*, **31**, 601.
WOOD C.J. (1982), *Annals of Nucl. Energy*, **9(4)**, 195.
WRIGHT, J., Personal communication.

APPENDIX 2

THE THERMAL OXIDATION OF GRAPHITE

A2.1. General

Graphite is used in a variety of nuclear reactor types; principally for moderator, reflector, fuel sleeve and fuel tube material. Since it is a form of carbon, like coal and charcoal, its oxidation behaviour might be expected to be of concern to the graphite chemist. The oxidising environments of particular interest are air (oxygen), carbon dioxide and steam (water).

A2.2. Reactions and thermodynamics

A2.2.1. *Reaction with oxygen*

$$\tfrac{1}{2}\ O_2 + C = CO \qquad \Delta H = -\ 110.5\ kJ.mol^{-1} \qquad (A2.1)$$

$$O_2 + C = CO_2 \qquad \Delta H = -\ 393.5\ kJ.mol^{-1} \qquad (A2.2)$$

where ΔH is the standard enthalpy of formation at 298 °C.

Reaction (A2.1) maximises the amount of carbon which may be removed by a given mass of oxygen (as carbon monoxide). Reaction (A2.2) maximises the amount of heat produced by oxidising a given mass of carbon (to carbon dioxide). Reaction (A2.2) may also be regarded as proceeding in stages, with reaction (A2.1) followed by

$$\tfrac{1}{2}\ O_2 + CO = CO_2 \qquad \Delta H = -\ 283.0\ kJ.mol^{-1} \qquad (A2.3)$$

(obtained by difference - Hess's law)

Reaction (A2.3) can take place wholly in the gas phase.

The above reactions are exothermic and favoured thermodynamically. Despite this fact, pure dense nuclear graphites do not readily react with air, so kinetic factors are obviously of importance.

A2.2.2. *Reaction with carbon dioxide*

This can be readily inferred by multiplying reaction (A2.1) by 2, including the ΔH term. The result is then added to reaction (A2.2) reversed. Overall, the (Boudouard) reaction is

$$C + CO_2 = 2CO \qquad \Delta H = +172.5\ kJ.mol^{-1} \qquad (A2.4)$$

A2.2.3. *Reaction with water (water gas reaction)*

$$C + H_2O = CO + H_2 \qquad \Delta H = +131.3\ kJ.mol^{-1} \qquad (A2.5)$$

also

$$C + 2H_2O = CO_2 + 2H_2 \qquad \Delta H = -82.4\ kJ.mol^{-1} \qquad (A2.6)$$

The hydrogen produced can then react with carbon:

$$C + 2H_2 = CH_4 \qquad \Delta H = -74.81 \text{ kJ.mol}^{-1} \qquad \text{(A2.7)}$$

Subtracting (A2.5) from (A2.6) gives

$$CO + H_2O = CO_2 + H_2 \qquad \Delta H = -213.7 \text{ kJ.mol}^{-1} \qquad \text{(A2.8)}$$

This is the water gas shift reaction which takes place in the gas phase.

In many practical cases, products from the above reactions are free to escape, such that thermodynamic equilibrium is not reached. The enthalpy changes are of importance, however, since they give a measure of the heat produced in exothermic reactions.

A2.3. Mechanisms, regimes and kinetics

A2.3.1. *Mechanisms*

The oxidation mechanisms consist of a series of physical and chemical steps. Non-catalysed oxidation typically follows the route:

(i) Transport of oxidant to the graphite surface.

(ii) Adsorption of oxidant onto the graphite surface (physisorption).

(iii) Formation of carbon-oxygen bonds (chemisorption).

(iv) Formation of carbon-hydrogen bonds in reaction (A2.7) (reduction).

(v) Breaking of the carbon-carbon bonds.

(vi) Desorption of carbon monoxide, or other product.

(vii) Transport of reaction product from the graphite surface.

Any of the above steps may be rate controlling, i.e. develop the major reactant concentration gradient.

A2.3.2. *Controlling factors*

Factors controlling the rate of oxidation may include the following:

(viii) The rate at which the oxidant is supplied to the surface.

(ix) The partial pressure of the oxidant.

(x) The reactive surface area available to the oxidant at the surface.

(xi) The amount and distribution of catalytic impurities in the graphite.

(xii) The temperature.

(xiii) The rate at which reaction products are removed.

(xiv) The fast neutron damage to the graphite.

(xv) The amount of pre-oxidation (radiolytic or thermal burn-off).

(xvi) The quantity of in-pore deposits.

(xvii) The effective diffusion coefficient.

A2.3.3. *Oxidation Regimes and Kinetics*

Regime 1

At low oxidation rates (generally at relatively low temperatures for the particular oxidation reaction) the oxidant may be at essentially the same concentration throughout the transport pores of the graphite. This 'chemical' regime is characterised by the fact that the reaction rate is largely determined by the intrinsic reactivity of the graphite (steps (ii) to (vi), above). Different parts of the structure may react at different rates; the binder being more reactive than the grist particles and edge atoms being more reactive than basal plane atoms, for example. It may also be the case that the gas composition varies in non-transport pores and that the effect of a given gas composition varies with pore shape (because of gas phase reactions).

Reaction between air and pure nuclear graphites is generally not measurable below about 350°C and only becomes significant in the region of 400°C. The rate of reaction is typically of the order of 3-8 $\times$ 10^{-10} $kg.kg^{-1}.s^{-1}$ at this temperature (historically expressed in μg/gh; 1μg/gh being 2.78 $\times$ 10^{-10} $kg.kg^{-1}.s^{-1}$). The chemical regime then extends typically up to 550-600°C.

The units for oxidation rate imply a rate law of the form

$$\frac{dm}{dt} = k\,m \qquad \text{(A2.9)}$$

where

m = graphite mass (kg)
t = time (s)
k = a (rate) constant (s^{-1})

However, for a solid reacting body, rate laws of the form shown below would be expected for reaction at the superficial surface (with some simple assumptions):

Slabs $$\frac{dm}{dt} = k \qquad \text{(A2.10)}$$

Cylinders $$\frac{dm}{dt} = k\, m^{1/2} \qquad \text{(A2.11)}$$

Spheres $$\frac{dm}{dt} = k\, m^{2/3} \qquad \text{(A2.12)}$$

The reaction is, of course, taking place within the porous body of the graphite. It cannot, however, be related to the initial open pore volume (which might be expected to be proportional to graphite mass) since the reaction must take place at the surface of the pores. The rate law is thus only superficially similar to a homogeneous first order gas phase expression and care must be taken in its use, particularly in describing the time dependence of graphite burn off.

The variation of reaction rate with temperature is of importance:

$$k = A e^{-\frac{E}{RT}} \qquad \text{(A2.13)}$$

where

A is a pre-exponential factor (s^{-1})
E is the apparent temperature coefficient of reaction ('activation energy') ($J.mol^{-1}$)
R is the gas constant ($J.mol^{-1}.K^{-1}$)

E has a typical value of 170 $kJ.mol^{-1}$.

Similar considerations apply to reaction with carbon dioxide and water vapour (H_2O). The reaction with CO_2 is of less importance, however, since it is negligible at 625°C (Thurlbeck, 1962) and does not pose a problem even at the highest AGR inner sleeve temperatures of 675°C (Prince, 1976). The reaction is also endothermic (equation (A2.4)) and so does not have the same safety implications as the reaction with air.

The reaction with H_2O is of particular importance in HTR reactors, because of the (generally small) inleakage from the steam side into the gas circuit, where it can react with hot graphite fuel tubes. Since the partial pressure of the water vapour is a variable in this system, rate equations of the form

$$r = A P^n \qquad \text{(A2.14)}$$

are applied, where
r = the specific reaction rate ($kg.kg^{-1}.s^{-1}$)
A = a (rate) constant ($(s^{-1}.(N.m^{-2})^{-1}$)
P = partial pressure of water vapour ($N.m^{-2}$)

The reaction with water vapour is generally insignificant below 800°C and approximately obeys equation (A2.14) with $n = 0.5$ over the temperature range 1000–1200°C. The kinetics can also be described by a Langmuir-Hinshelwood scheme (Walker *et al.*, 1959; Atkins, 1987; Stairmand, 1990).

Regime 2

In this regime, the reaction rate becomes high enough for access of the gas to the in-pore structure to be significantly limited by diffusion control (steps (i) and (vii), above). This can also arise from a particularly restrictive structure. For the air-graphite system, this occurs approximately in the range 600–900°C. The 'activation energy' is halved in this regime and the kinetic expressions involve the effective diffusion coefficient for the graphite (Walker *et al.*, 1959; Giberson and Walker, 1965).

Regime 3

This is the mass transfer regime (Burnette *et al.*, 1979; Raeder and Gulden, 1989), where reaction at the superficial surface of the graphite is so high that most of the oxidant is consumed there, the oxidant concentration gradient generally developing across the laminar sub-layer. The reaction rate is now expressed in terms of the superficial surface area of the graphite ($kg.m^{-2}.s^{-1}$) together with any oxidant partial pressure dependence. The change from one regime to another may be progressive and mode 2 may appear to be missing in some cases.

Two other 'regimes' appear trivial, but can usefully be distinguished:

Regime 4

If there is a fixed rate of ingress of oxidant to the system, for example as a known quantity of impurity in the make-up gas, the rate of oxidation cannot exceed the rate of supply of oxidant (rate balance). The preferred site of any resulting oxidation may not be known, however.

Regime 5

If the system contains a fixed amount of oxidant, for example that remaining after blowing down and recharging the coolant gas, the extent of oxidation is limited by the amount of oxidant available (mass balance). Neither the location, nor the rate of reaction, may be known in this case.

A2.3.4. *Catalysis*

The kinetics in the chemical regime may be further complicated by catalysis (McKee, 1981). The catalyst (impurity) particles act to increase the reaction rate by offering an alternative reaction pathway. This lowers the activation energy. Reaction rates are particularly increased at lower temperatures (this leads to a 'compensation' effect).

A simple catalytic model involves the oxidation of metal atoms (M) by oxygen, followed by reduction of the oxide by carbon:

$$\tfrac{1}{2}\, O_2 + M = MO \qquad \text{(A2.15)}$$

$$MO + C = CO + M \qquad \text{(A2.16)}$$

The reaction may proceed by a 'tunnelling' mechanism.

Reaction inhibitors are also known (McKee, 1991) and some substances are able to act to either promote or inhibit reaction, perhaps by competing for active sites (e.g. water/oxygen). Boron (with phosphorus) is known as an inhibitor for thermal oxidation, but when intercalated into the graphite structure will promote oxidation (Karra *et al.*, 1995) (perhaps by mimicking fast neutron damage).

A2.4. Requirements for the information

Early designs of graphite moderated reactor operated with air as the coolant and there was a requirement to understand both the likely ongoing oxidation behaviour of the graphite and its behaviour during a temperature excursion. As these reactors were superseded by carbon dioxide cooled designs, an understanding of the reaction of graphite with air remained important for the following reasons:

(i) Safety case information relevant to both major and minor ingresses of air to the system under fault or other conditions (Dodson, 1960; Nairn and Wilkinson, 1960; Blanchard and Fitzgerald, 1978).

(ii) The possible requirements to carry out deliberate oxidations to

  (a) Remove deposits from fuel.

  (b) Open up the structure of low diffusivity graphite to improve inhibitor (e.g. methane) access.

  (c) Remove deposits from fuel pin and heat exchanger surfaces to improve heat transfer.

  (d) Estimate the amount of deposit in graphite moderator and fuel sleeves by differential thermal oxidation (Welch, 1972; Oxley and Dymond, 1972; Baguley and Livesey, 1972) (so as to be able to correct the weight loss).

  (e) Alter the structure of experimental graphites in controlled ways to improve theoretical knowledge of the interaction between reactivity and structure.

A2.5. Essential measurements and knowledge

The complexity of graphite oxidation behaviour is such that the following are generally required:

(i) Good statistical data on the relevant oxidation rates for a range of blocks and heats.

(ii) An awareness of the relevant oxidation regime and the rate laws which are likely to apply.

(iii) Information on the temperature coefficient of reaction.

(iv) Information or measurement on the heat change on reaction.

(v) Theoretical or experimental information on factors affecting the oxidation rate, such as fast neutron damage, burn-up, deposition of potential catalysts, etc.

(vi) Modelling knowledge to extrapolate from small scale samples, or full scale tests.

As some graphite reactors are coming to the end of their lives, there is an increasing requirement to carry out assessments for long term storage or disposal (Wickham *et al.*, 1996). The potential oxidation behaviour is also of concern in this context.

ACKNOWLEDGEMENTS

In compiling this account, the author has been particularly grateful for reviews by J. Stairmand (Stairmand, 1990) and T. Wickham *et al.* (Wickham *et al.*, 1996) who in turn cite the pioneering work of P.L. Walker (Walker *et al.*, 1959) and Dubinin (Dubinin, 1966). Any important omissions are the author's own, however.

REFERENCES TO APPENDIX 2

ATKINS, P.W. (1987), *Physical Chemistry*, 3rd edition, Oxford University Press, 783.

BAGULEY, G. AND LIVESEY, J.N. (1972), *DTO Applied to Graphite/Carbon Deposit Systems – Paper 1, The Attack Rate of the underlying Graphite during Oxidation of In-pore Deposits*, Symposium on Differential Thermal Oxidation held at Berkeley Nuclear Laboratories.

BLANCHARD, A. AND FITZGERALD, B. *The Air Reactivity of WAGR Moderator and Sleeve Graphites*, UKAEA Report WAGR/TC/P(78)21 (1978).

BURNETTE, R.D., VELASQUEZ, C. AND HARRINGTON, R.O. (1979), *Studies of the Rate of Steam Oxidation of Graphite at High Gas Velocity*, 14th Biennial Conference on Carbon, Pennsylvania State University.

DODSON, M.H. (1960), *The Depth of Oxidation of Graphite: A Theoretical Approach*, UKAEA Report DEG 148 (CA).

DUBININ, M. (1966), *Chemistry and Physics of Carbon*, **2** (Ed. P.L. Walker, Jr), Marcel Dekker, NewYork, 51

GIBERSON, R.C. AND WALKER, J.P. (1965), *Reaction of Nuclear Graphite with Water Vapour - Part 1: Effect of Hydrogen and Water Vapour Partial Pressures*, Battelle Northwest Report, BNSA-181.

KARRA, M., ZALDIVAR, R.J, RELLICK, G.S., THROWER, P.A. AND RADOVIC, L.R. (1995), *Substitutional Boron in Carbon — Inhibitor or Catalyst?*, Proc. 22nd Biennial Conference on Carbon, San Diego

MCKEE, D.W. (1981), *Chemistry and Physics of Carbon*, **16** (Ed. P.L Walker, Jr), Marcel Dekker, New York, 1.

MCKEE, D.W. (1991), *Chemistry and Physics of Carbon*, **23** (Ed. P.L Walker, Jr), Marcel Dekker, New York, 173.

NAIRN, J.S. AND WILKINSON, V.J. (1960), *The Prediction of Conditions for Self-sustaining Graphite Combustion in Air*, Paper GCM/UK/11, US/UK Compatibility Conference.

OXLEY, E. AND DYMOND, B. (1972), *DTO Applied to Graphite/Carbon Deposit Systems - Paper 8, DTO Studies of Irradiated Graphite using Gas Chromatography*, Symposium on Differential Thermal Oxidation held at Berkeley Nuclear Laboratories.

PRINCE, N. (1976), *Experience in the Design of Graphite Moderator Structures*, Paper presented to the Nuclear Engineering Society

RAEDER, J. AND GULDEN, W. (1989), *Safety Analyses performed by NET*, IAEA Technical Committee Meeting on Fusion Reactor Safety, Jackson, Wyoming.

STAIRMAND, J.W. (1990), *Graphite Oxidation - A Literature Survey*, AEA Technology Report AEA-FUS-83.

THURLBECK, A. (1962), *Summarised Compatibility Review of Reactor Materials for CO_2 –cooled Graphite Moderated Reactors*, TRG Report 267(W).

WALKER, P.L., RUSINKO, F. AND AUSTIN, L.G. (1959), *Advances in Catalysis*, **11**, 123.

WELCH, E.E. (1972), *DTO Applied to Graphite/Carbon Deposit Systems - Paper 1, Principles and Problems*, Symposium on Differential Thermal Oxidation held at Berkeley Nuclear Laboratories.

WICKHAM, A.J., MARSDEN, B.J., PILKINGTON, N.J. AND HEATH, T.G. (1996), *The Possibility and Consequences of Graphite Core Degradation during 'Care and Maintenance' and'Safestore'*, AEA Technology Report AEA/16423595/R/001.

CONTRIBUTORS TO DRAFTING AND REVIEW

Arai, T.	Japan Atomic Energy Research Institute, Japan
Blanchard, A.	United Kingdom Atomic Energy Authority, United Kingdom
Burchell, T.	Oak Ridge National Laboratory, United States of America
Haag, G.	Forschungszentrum Jülich, Germany
Hall, K.	United Kingdom Atomic Energy Authority, United Kingdom
Harper, A.	United Kingdom Atomic Energy Authority, United Kingdom
Kelly, B.	United Kingdom Atomic Energy Authority, United Kingdom
Marsden, B.	United Kingdom Atomic Energy Authority, United Kingdom
Martin, D.	United Kingdom Atomic Energy Authority, United Kingdom
Shtrombakh, J.	Russian Research Centre Kurchatov Institute, Russian Federation

00-00798